PB 180 523T

U.S.S.R. LITERATURE ON AIR POLLUTION AND RELATED OCCUPATIONAL DISEASES, VOLUME 18. ACOUSTICAL COAGULATION AND PRECIPITATION OF AEROSOLS.

E.P. Mednikov

Levine (B.S)
Washington, D.C.

1968

PB 180523 T

U.S.S.R. LITERATURE ON AIR POLLUTION AND RELATED OCCUPATIONAL DISEASES

Volume 18

A SURVEY

by

B. S. Levine, Ph. D.

ACOUSTICAL COAGULATION AND PRECIPITATION OF AEROSOLS

Processed by
CLEARINGHOUSE FOR FEDERAL SCIENTIFIC AND
TECHNICAL INFORMATION
U. S. DEPARTMENT OF COMMERCE
Springfield, Virginia

Reproduced by the
CLEARINGHOUSE
for Federal Scientific & Technical
Information Springfield Va. 22151

193

The present English edition is a part of a survey conducted by
B. S. Levine, Ph. D.
of 3312 Northampton St., N. W.
Washington, D. C. 20015
supported by PHS Research Grant AP - 00176,
awarded by the Division of Air Pollution
of the U. S. P. H. Service

ACADEMY OF SCIENCES USSR

INSTITUTE OF FUEL RESOURCES

Ye. P. Mednikov

ACOUSTICAL COAGULATION AND PRECIPITATION OF AEROSOLS

IZD-VO AN USSR
MOSCOW

CONTENTS

Conducted by Editor In Chief
L. V. Radushkevich 1

Foreword 1

Chapter 1
Introduction
1. Special Properties of a High-Intensity Sound Field 4
2. Sources of High-Intensity Sound 21
3. A Brief Outline of the Development of Aerosol Acoustical Coagulation and Precipitation Problems 31

Chapter 2
Motion of Aerosol Particles in a Sound Field
4. Preliminary Information 41
5. Vibratory Motion of Aerosol Particles 45
6. Drift of Aerosol Particles 52
7. Circulating and Fluctuating Aerosol Particle Motions 65
8. Scattering and Absorption of Acoustical Energy by Aerosol Particles 68

Chapter 3
Aerosol Particle Interaction in a Sound Field
9. Preliminary Information 77
10. Orthokinetic Interaction of Aerosol Particles 83
11. Parakinetic Interaction of Aerosol Particles 90
12. Attractional Interaction of Aerosol Particles 102
13. Pulsation Interaction of Aerosol Particles 111

Chapter 4
Mechanism and General Principles of Acoustical Aerosol Coagulation
14. The Course Followed by Acoustical Aerosol Coagulation 118
15. Kinetic Equation of the Process 124
16. Effect of Aerosol and Acoustical Characteristics on the Kinetics of the Process 128
17. Some Earlier Hypotheses of Acoustical Aerosol Coagulation 136

Chapter 5
Practice of Acoustical Coagulation and Aerosols Precipitation
18. Acoustical Dispersion of Natural and Artificial Fogs 141

19. **Acousto-Gravitational Precipitation of Industrial Dusts, Smokes, and Fogs** 149
20. **Acousto-Inertial Precipitation of Industrial Dusts, Smokes, and Fogs** 156
21. **Acoustical Aerosol Separation and Filtration** 169

Appendix

1. **Evaporation and Condensation Droplet Growth During Fog Sonication** 174
2. **Sound Effect on the Processes of Combustion and Degasification of Fuel Droplets** 181
3. **Behavior of Precipitated Solid Particles in a Sound Field of an "Acoustical Dryer"** 183

This monograph deals with the physical fundamentals of coalescence and precipitation of aerosols in the acoustic field and with the basic problems of practical use of these processes as applied to purification of industrial smoke, dust, and vapors.

Brief consideration is given also to problems of evaporation, condensation, combustion, and degasification of vapor drops and desiccation of precipitated solids in the acoustical field. ( )

The monograph is intended for scientific and engineering personnel who come in contact with problems associated with precipitation and utilization of aerosols.

Editor in Chief
Doctor of Chemical Sciences
Professor L. V. Radushkevich

FOREWORD

Practically all natural and artificial gases which man encounters in the course of his activity, contain amounts of suspended admixtures of solid or liquid materials which constitute aero-dispersed systems or aerosols. The atmospheric air man breathes normally contains negligible gravimetric amounts of suspended admixtures although their content in dense fogs and clouds, and in mines at times attains several grams and more per m^3 of air. Considerable quantities of suspended admixtures are contained in natural gases, frequently kilograms/m^3 of the gas. A considerable amount of suspended admixtures is contained also in artificial gases, particularly in fuel gases. To this category belong the following: coke gas, blast furnace gas, producer gas, etc., smoke from industrial furnaces and ovens, exhaust gases of carbon black and similar plants, the ventilating air used in mining and fuel processing industries. Acid smogs, radioactive aerosols, camouflage smokes, etc., also contain particulate admixtures.

The presence of suspended admixtures in most of the above enumerated gases is undesirable, and it frequently becomes necessary to precipitate and remove same from the dispersed phase, to change it qualitatively, or to remove it partially or completely. One of the ways by which the first two problems can be solved is artificial coagulation of aerosols, i.e., aggregation by adhesion or coalescence of aerosol particles by physical means. Most effective among the latter is high-intensity sonic and ultrasonic oscillation which presents possibilities for application in many branches of science and technology. Consolidation of suspended particles occurring in the course of acoustic aerosol coagulation induces substantial changes in the physical characteristics of aerosols. The reduction of the total surface of a dispersed phase reduces light scattering. This in turn enhances the system transparency frequently to full visibility, while increases in the particle size and mass enhance the particulates' increased tendency to precipitate from the gaseous medium under the effect of natural gravity or the induced inertia, electric attraction, etc. All this is of great value and use to the technology of dust- and fine droplet-trapping in modern air and gas purification technology. Modern trapping devices, such as settling chambers, dust extractors, scrubbers, electrofilters, basically depend upon size of particulates and the effectiveness of their precipitation. The lower is the particulate dispersion the higher is the effectiveness of precipitation. The highest dispersed particles, several microns or less in diameter which are present in most industrial smokes, dusts, and vapors, precipitate particularly poorly. Preliminary acoustic coagulation of such particles offers means of substantially increasing the effectiveness of their precipitation in the dust-droplets trapping devices.

The acoustic coagulation principle was first applied in practice in the late 40's when powerful acoustic oscillations, acoustic sirens, had been developed. However, the new attempts failed to attain adequate acoustical intensification of gas purification. Therefore, more detailed study of the mechanism of the new process, its possibilities, development of more powerful sound generators was undertaken, often inopportunely, in the direction of introducing the new principle into different industries, urgently in need of improving their gas purification operations. Many technical and popular-science journals carried during those years, advertised articles which hailed the acoustical method of aerosol coagulation as the panacea for all mishaps associated with atmospheric pollution. Despite that, the acoustical method of aerosol coagulation failed to become universal, neither were other physical methods used in the dust- and droplet-trapping technology.

Acoustical coagulation is a special method. The extent of its application is comparatively narrow; yet within its area of application it is capable of attaining results unattainable by any other method. This became increasingly apparent during recent years. At the same time, it became clear that acoustical oscilliations could be used to intensify not only the coagulation of suspended particles, but also the process of their direct precipitation; this appeared to provide in some instances a more effective and economical solution of the intensive gas purification problems. This refers in particular to the recently discovered method of acoustical filtration of aerosols which seems to make possible the reduction of residual particle concentration to fractions of mg/m^3 of a gas at a moderate specific energy consumption for the sonification and extrusion of the gases. If future tests will support the early experimental conclusions, then the application of acoustical oscillation in the dust- and droplet-trapping technology will become widespread.

In considering processes of aerosol coagulation and precipitation in an acoustical field, the pertinent physical and physico-chemical processes should be considered. It has been established that accelerated condensation and degassing of droplets occurred during the sonification of vapors, while during the sonification of humid smokes and dusts and their precipitation products, there occurred drying of the solid dispersion phase. The above processes exhibit a distinct effect on the kinetics of aerosol coagulation and precipitation, which, in the case of coarsely dispersed systems, are suppressed. The above is of a highly practical value from the standpoint of a successful solution of the following important problems: dispersion of natural fogs, separation of natural gas condensates, extraction of incidental gases from crude oil, intensified combustion of atomized liquid and solid fuels, drying of thermosensitive powdered products, etc.

There exists at the present a considerable volume of theoretical and experimental material on acoustical aerosol coagulation and associated problems. However, such data appear extremely fragmentary and contradictory. This is associated, to a greater degree, with the uniqueness of the new method which calls for the knowledge of relatively independent scientific fields, such as hydrodynamics, acoustics, aerosol mechanics, physical chemistry, chemical engineering, and includes their lesser developed branches. Furthermore, it could be associated with exceptional experimental difficulties in a given field due to lack of essential acoustical equipment on the one hand and, on the other hand, an unusual motion of aerosols in the sound field which impedes direct observation of the primary events. It is not surprising that, under these conditions, numerous investigators arrived at erroneous conclusions concerning the mechanism of the processes under consideration, their effectiveness, areas of application, etc.

An attempt was made in the present monograph to systematize and generalize the accumulated materials on acoustical coagulation and precipitation of aerosols. Moreover, particular attention has been given to the physical aspects of the processes and to their practical applications in technology. Additional brief consideration has been given to the processes of evaporation, condensation, combustion, and decontamination of a dispersed liquid phase and the drying of the precipitated solid-state products in the sound field.

The author considers it his pleasant duty to express gratitude to Doctor of Chemical Sciences, B. B. Kudryavtsev, Doctors of Physico-Mathematical Sciences, V. F. Nozdrev and S. N. Rzhevkin, and Candidate of Chemical Sciences, I. F. Bogdanov, for their moral support and useful advice. The author is grateful to Doctor of Chemical Sciences, L. V. Radushkevich, for reading and editing the manuscript. The author also expresses his thanks to Z. V. Grigor'eva and A. M. Timoshenko for their help in the graphical illustrations.

CHAPTER 1

INTRODUCTION

1. SPECIAL PROPERTIES OF A HIGH-INTENSITY SOUND FIELD.

The coagulating action which sound can exert on aerosols and other physical and biological effects of sonification in gaseous media can be observed only in connection with very high-intensity sound, the power level of which exceeded considerably the pain threshold of the human ear. Such high-intensity acoustical vibrations are characterized by a number of specific properties which distinguish them from acoustical vibrations at the normal level. Acoustical vibrations, or simply sound in the physical sense, implies compressional and rarefactional displacements of the elastic medium, in the present case a gas, propagating in a wave-like motion from the sound source. The sound source is usually a vibrating or pulsating solid, liquid, or gaseous body which is excited by aerohydrodynamic or electromechanical means. The vibrations and pulsations of this body cause alternating compression and rarefication of the adjoining gas layer and this, in turn, induces advancing and regressing displacement of the adjoining gas particles. The latter causes pressure to change its sign in the layer, resulting in an oscillatory displacement of particles in the subsequent gas layer; in this manner, vibrations propagate from one layer to the next, farther and farther from the sound source with a velocity, called sound velocity. If the origin (t=0) corresponds to an instant at which the medium assumes an equilibrium and its particles begin to oscillate according to the wave motion at an observation point, assuming a sinusoidal sound source, the particle displacement x_g, vibrations velocity u_g, and sound (i.e., excess) pressure p_g vary with time according to the following equations:

$$x_g = A_g \sin \omega t, \tag{1.1}$$

$$u_g = U_g \cos \omega t, \tag{1.2}$$

$$p_g = P_g \cos \omega t, \tag{1.3}$$

where A_g, U_g, and P_g represent displacement amplitude, velocity, and pressure, respectively; ω is the angular velocity equal to $2\pi f$ (where f is the oscillation frequency in H_z *).

---

* 1 Hertz (H_z) = 1 vibration per second; 1,000 H_z = 1 kilohertz (kH_z).

The sound velocity and pressure are, thus, shifted in time with respect to the particle displacement by 1/4T, where T is the period of vibrations.

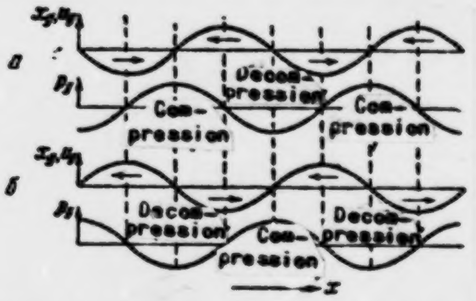

Fig. 1. Distribution of sound pressure of oscillatory velocity and dislocation in static sound waves.
a - b At time t; b - c At time t + $\frac{1}{2}$ T

When the sound wave meets an obstacle of dimensions greater than acoustical wavelength λ, it is first reflected from the obstacle according to the laws of geometric optics and, subsequently, interacts with the direct wave. As a result of interference, the vibration amplitudes increase at some points and decrease at others. If the obstacle consists of a plane surface perpendicular to the direction of the sound wave propagation and is located at a distance from the sound source equal to the multiples of λ/2, a so-called standing wave is formed as a result of interference of the direct and reflected waves (Fig. 1). In this case, changes in x_g, u_g, and p_g are defined by the following equations:

$$x_g = 2A_g \sin kx_0 \sin \omega t, \tag{1.4}$$

$$u_g = 2U_g \sin kx_0 \cos \omega t, \tag{1.5}$$

$$p_g = 2P_g \cos kx_0 \cos \omega t, \tag{1.6}$$

where $\underline{k}$ is the wave number equal to $\frac{\omega}{c_g} = \frac{2\pi}{\lambda}$, and x_0 is the distance to the closest node, i. e., a point where the particle displacement and velocity are fixed and are equal to zero (the point where the same quantities attain a maximum is called an antinode).

In contrast to the previously described travelling wave, the particle displacement, velocity, and the sound pressure are functions not only of time but also of space. In high-intensity sound, the above described wave propagation is supplemented by a series of new phenomena, the so-called, second order effects [133, 7, 10, 46, 72, 205]. These effects are associated with the following circumstances: the sound pressure together with the vibration velocity and displacement in a given medium increase to high values for which new rules hold which are outside the scope of classical acoustics (acoustics of small amplitudes). The latter describes most cases of sound radiation and propagation by an equation of vibrational medium motion, known as the wave equation; for the case of a plane wave, the equation has the following form [7, 62, 105]:

$$\frac{\partial^2 u_g}{\partial t^2} = c_g^2 \frac{\partial^2 u_g}{\partial x^2}, \tag{1.7}$$

where x is the distance from the sound source, c_g is the sound velocity which for a gas is determined by the following expression:

$$c_g = \sqrt{\frac{P_{ст}}{\rho_g}\gamma} \qquad (1.8)$$

P_{st} is the static pressure of the medium, ρ_g is the gas density, and γ is the ratio of specific heats, C_p/C_v). The wave equation is derived from the motion equation of an ideal fluid combined with the continuate equation and equation of state of the gas, all equations being linearized, i.e., only the first order terms are considered, and the second order terms are disregarded [105]. This can be done if the sound pressure is neglibily small in comparison with the static pressure of the medium, and, therefore, the difference in the medium density in the compression and rarefaction regions may not be accounted for. The assumption is equivalent to saying that, 1) the vibration velocity is negligibly small in comparison with the sound velocity (the difference in the propagation velocity of disturbances in the compression and rarefaction regions can be neglected), or 2) the particle displacement is negligible in comparison with wavelength, i.e., the displacement is directly proportional to the sound pressure as in Hook's Law.

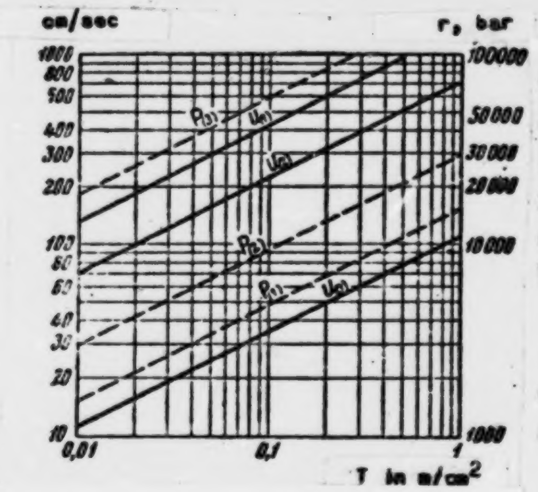

Fig. 2. Amplitude values of oscillatory velocity and sound pressure for some gases at high sound intensity. 1 - Hydrogen at 760 mm and 20° C. ($\rho_g c_g = 11.5$ г·cc^{-1-2}); 2 - Air at 760 mm and 20° C. ($\rho_g c_g = 41{,}3$ г·сек$^{-1}$ см$^{-2}$); 3 - Methane at 50 ата and 20° C ($\rho_g c_g = 1550$ г·сек$^{-1}$см$^{-2}$)

Figure 2 shows amplitude of vibration velocity U_g and the corresponding amplitudes of sound pressure P_g for a high-intensity sound J* in the following gases, the acoustic impedances $\rho_g c_g$ of which differ sharply: hydrogen, air, and compressed methane (the basic component of natural gas).

Vibration velocity amplitudes were calculated according to a well known formula for a plane wave [7]:

$$U_g = \sqrt{\frac{2J}{\rho_g c_g}}, \qquad (1.9)$$

and sound pressure amplitudes were calculated from the following formula:**

$$P_g = \rho_g c_g U_g. \qquad (1.10)$$

---

* The sound force, or intensity J (or I) is defined as the flow of sound energy through a 1 cm^2 area of the sound wave front per second. In the CGS system, the unit for the sound intensity, is 1 erg/cm^2/sec; in practice, the unit is 1 watt/cm^2, equal to 10^7 erg/cm^2/sec.

** The sound pressure is measured in acoustical bars (1 bar=dyne/cm^2); it is related to the sound intensity by the following expression $J = p_g^2/\rho_g c_g$, in the experimental measurement of the sound field by means of acoustic probes (subscript $_g$ will not be shown subsequently).

The effective values of vibration velocity u_g and the sound pressure p_g are obtained by dividing quantities U_g and P_g by $\sqrt{2}$.

It can be seen from Figure 2 that in the range of sound intensity $J = 0.1 - 1.0$ watt/cm², where a rapid coagulation of aerosols is observed, the amplitude of vibration velocity U_g attained values of 2.2 - 7.0 m/sec in air, which amounts to 0.65 - 2.1% of the sound velocity; the sound pressure amplitude attains values of 9,000 - 29,000 bar, which amounts to 0.9 - 3.0% of the atmospheric pressure.

Figure 3 shows that the magnitude of particle displacement A_g also attained extraordinarily high values for a given sound intensity. The values of A_g can be calculated from the following known relationship [7]:

$$A_g = \frac{U_g}{\omega} = \frac{1}{2\pi f}\sqrt{\frac{2J}{\rho_g c_g}}. \qquad (1.11)$$

In the 1,000 - 5,000 range, which is very often used for particle coagulation by acoustical means, A_g for $J = 0.1 - 1.0$ watt/cm² lies in the 70 - 1,100μ range. The latter considerably exceeds aerosol dimensions and is of the same order of magnitude as the average distance between particles (see # 9).

Higher- order terms cannot be neglected for the indicated values of sound pressure, particle velocity, and displacement, and their presence sharply intensified some existing acoustical effects, inducing a series of new effects, which include the following:

1) strong heterogeneity of the sound field - presence of high sound pressure and particle velocity gradients, especially near the sound source;

2) distortion of the sound waveform during propagation and the resultant appearance of harmonics;

3) increased sound absorption;

4) intensification of the radiation pressure, up to the threshold of feeling;

5) appearance of a strong incident flow (or a series of closed vortexes) called the acoustical ("sonic") wind or current;

6) medium turbulence.

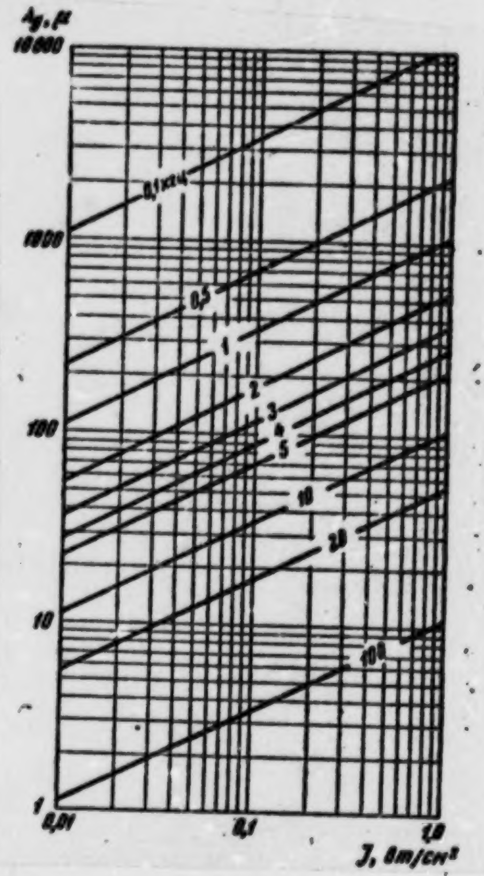

Fig. 3. Amplitudes of air particle oscillations at high sound intensity

Examine briefly the enumerated acoustical effects.

1) The heterogeneity of the sound field. In the analysis of many acoustical problems the sonic field is idealized, namely, the wavefront is assumed to be an absolute plane. The assumption simplifies the solution of problems, but in most cases such solutions are unreal.

It was established in [72, 105] that even in the case of assumed ideally flat radiators, the near field is exceptionally heterogeneous and is unrelated to the common plane wave. As an illustration, Figure 4 shows the distribution of sound pressure in the vicinity of a piston-type radiator calculated by Shtentsel'. Using Huygen's principle, he summed up the spherical waves radiated at each point in space from each point of the piston surface. As can be seen, the near field was heterogeneous in the transverse and longitudinal directions, and the heterogeneity increased with increasing acoustical frequency. Admittedly, the average pressure in the transverse direction was equal for all cross-sections, illustrating the possibility of standing waves formation.

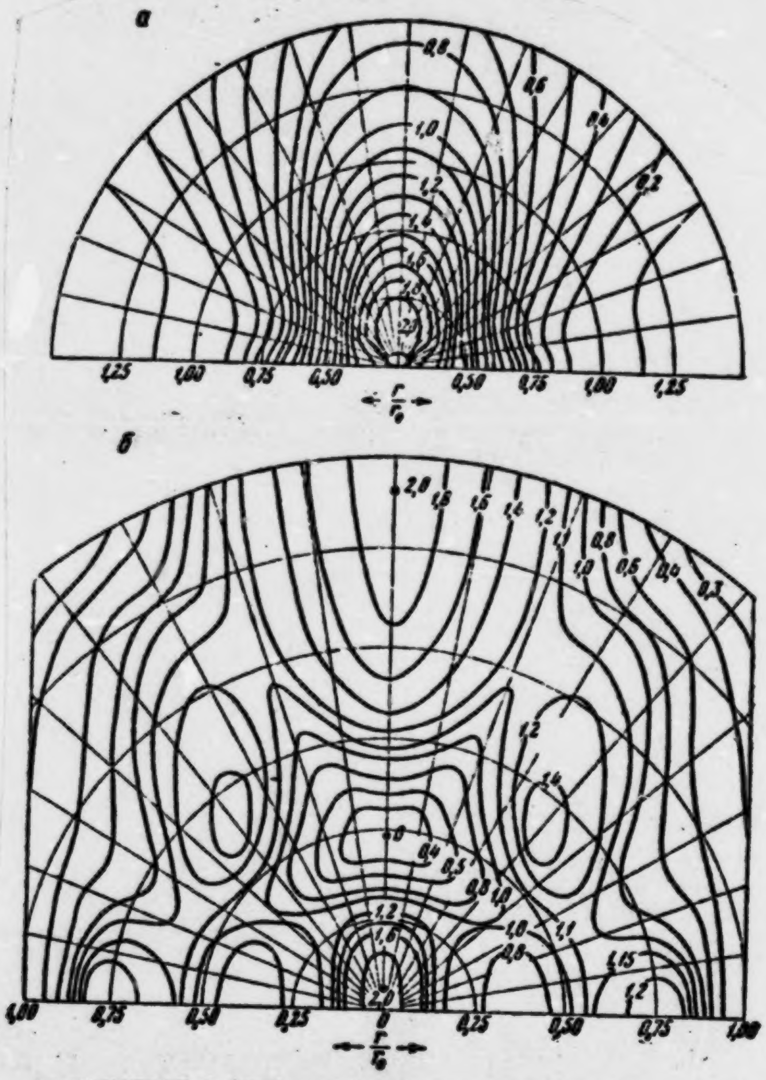

Fig. 4. Sound pressure distribution in the proximity of a piston eradiator, according to Shtentsel.

OK > $a - D/\lambda = \frac{4}{\pi}$; $б - D/\lambda = \frac{10}{\pi}$

Moving away from the sound source, the sound wavefront gradually smoothes out. However, it remains partly heterogeneous, and can be considered plain only at one small central point. As an illustration of this Figure 5 shows the so-called radiation patterns of piston-type radiators indicating the sound pressure distribution in the case of radiation into free space. Figure 5 also shows that the sonic beam narrows with an increase in frequency (at a constant radiator diameter D), although the sound wavefront heterogeneity fails to decrease. Its heterogeneity is more pronounced when the wavefront propagated in a confined space, as in a tube. In such a case, the plane sound wave arises only on rare occasions, when the tube diameter D is small in comparison with the wavelength λ. Otherwise, transverse modes appear. The following inequality serves as a criterion for the transverse mode formation [105]:

$$f_0 > \frac{1{,}84}{\pi}\frac{c_g}{D}. \qquad (1.12)$$

Figure 6 shows the distribution of sound pressure along the transverse cross-section of the coagulation chamber with a diameter D=20 cm [85]. A highly pronounced sound pressure peak is seen at the center of the chamber which slightly decreases with the distance from the sound source. In view of the oblique sound wave reflection from the tube walls and their interference with direct waves, sound pressure decreases along the tube, and subsequently increases and decreases periodically [97, 126, 298]. All above phenomena occur at any sound intensity; however, the sound pressure gradients and, consequently, the particle velocity, attain enormous values at high intensity levels affecting the hydrodynamic stability of the total sound field.

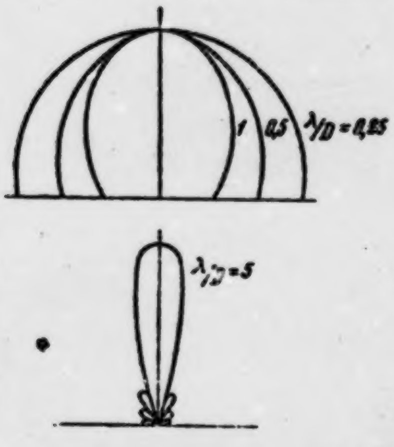

Fig. 5. Direction of piston sound transmitters at different D/λ ratios

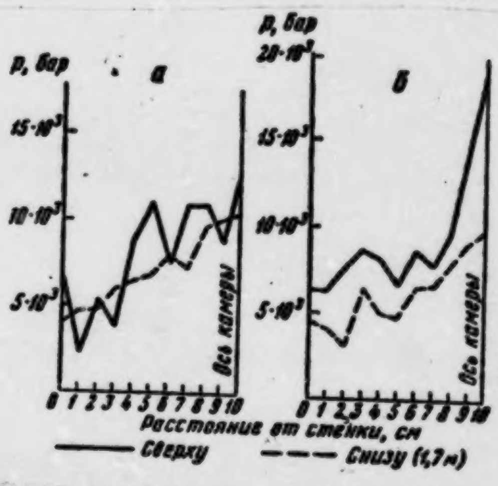

Fig. 6. Distribution of sound pressure in the coagulation chamber. a – At 3.6 k Hertz frequency. b – At 6.0 k.

2) Distortion of the sound wavefront. In the process of its propagation, a sound wave generated by a sinusoidal source transformed gradually from the sinusoidal into a sawtooth "shock" wave (Figure 7a). This may be due to the fact that in the case of large sound pressure amplitudes, different portions of a wave propagate at different velocities. Regions of increased pressure (compression), where the medium particles move in the direction of wave propagation, propagate at an increased velocity. Conversely, regions of decreased pressure (rarefaction), where particles move in the opposite direction, propagate at a decreased velocity, causing the wave profile in the interval between the greatest compression and rarefaction regions to become increasingly steeper; as a result the wave "overflows," generating an explosion [46, 124, 133]. The onset of this event is retarded to some extent by the inevitable decrease in the medium particle velocity. The non-sinusoidal sawtooth wave may be represented as a Fourier series [11] comprising a sinusoidal wave with a fundamental frequency ω_0 (first harmonic) and higher order harmonics with frequencies of 2 ω_0, 3 ω_0, etc. Figure 7b is a graphical representation of a wave distorted by the second harmonic.

Thus it may be concluded that the sound wave distortion is accompanied by the appearance of significant harmonics.

According to Riemann, the relative magnitude of pressure of the second harmonic P_2/P_1, which represents the degree of wave distortion, may be expressed by the following formula [46, 124, 6]:

$$\frac{P_2}{P_1} = \frac{\gamma+1}{2\sqrt{2}\,\rho_g c_g^3}\,\omega_0\,Px. \qquad (1.13)$$

It may be concluded from this equation that the degree of waveform distortion increased linearly with frequency ω_0, sound pressure at a fundamental frequency P_1, and distance x traveled by the wave.

Figure 8 presents oscillograms which illustrate variations in the waveform (f_0=15 kHz) in air as (a) functions of sound intensity level for a fixed distance from the sound source and (b) functions of distance for a fixed sound intensity level equal to 156 db* (time sweep) [205].

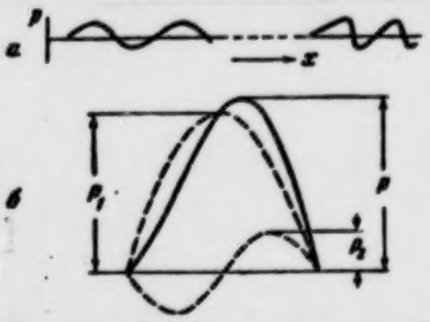

Fig. 7. Sound wave form distortion in the process of extension.
a - General plan; b - Breaking down of the distorted waves into two harmonics

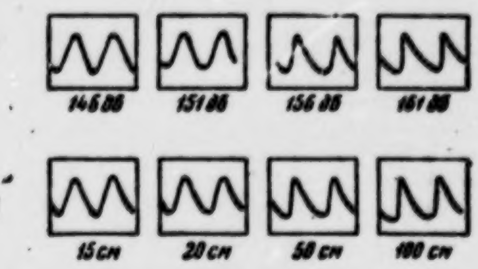

Fig. 8. Changes in the sound wave form. (f_0 = 15 кгц)
a - at high level intensity sound origin and at constant distance of 50 cm; -
b - at receding sound source and sound intensity of 156 db.

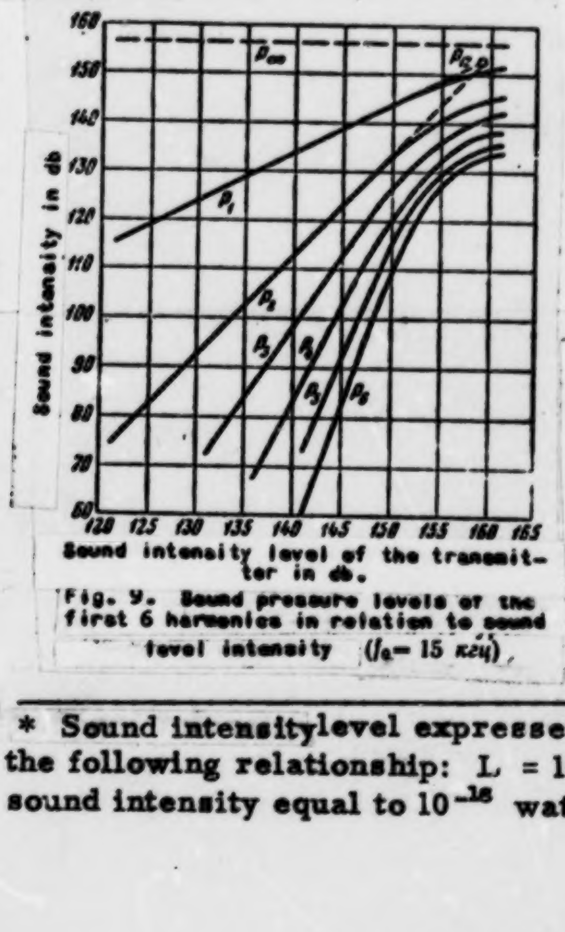

Fig. 9. Sound pressure levels of the first 6 harmonics in relation to sound level intensity (f_0 = 15 кгц)

Figure 9 shows sound pressure levels of the first six harmonics of a 15 kHz sound wave as a function of source intensity level [205]. Nomogram in Figure 9 and equation (1.13) can be used in finding pressure levels of any of the first six harmonics at an arbitrary pressure level and frequency of and distance from the sound source.

The condition for the existence of a discontinuity in air is, according to A. A. Goldberg [25], the inequality $p_{bar} \geq 2\pi f(_{kHz})$ which is always satisfied for gases. The distance from source to discontinuity is determined by the following expression [25, 88]:

$$x_{кр} \leqslant \frac{2\rho_g c_g^3}{(\gamma+1)\,\omega_0 P_x}. \qquad (1.14)$$

---

* Sound intensitylevel expressed in decibels (db) is related to intensity by the following relationship: L = 10 lg J/J_0 (or I/I_0, where J_0 is the standard sound intensity equal to 10^{-16} watts/cm^2.

The distorted waveform of an acoustical standing wave varies with time [133] and, therefore, the sound pressure had a given finite value at antinodes. The number which indicates by how much the above quantity was smaller at the nodes is called the standing wave ratio.

3) Increased medium sound absorption. If a sound wave possessed a small initial oscillation amplitude A_{g0}, or pressure P_0, it decreased exponentially with propagation along the x axis [7, 72]:

$$A_g = A_{g0}e^{-\alpha_g x},$$
$$P = P_0 e^{-\alpha_g x}, \qquad (1.15)$$

where α_g is the so-called sound absorption coefficient of a gas in cm^{-1} (if the absorption coefficient is expressed in db/m), the number expressing α_g in cm^{-1} must be multiplied by 868.6, if conversion is desired.

The sound intensity decreased with distance according to the following equation:

$$J = J_0 e^{-\alpha'_g x}. \qquad (1.15')$$

The above equation is based on an assumption that a portion of the input energy lost in a layer was proportional to its thickness: $dJ/J = \alpha'_g dx$. The sound absorption coefficient α'_g represents the portion of acoustical energy lost in the interval x = 1. Clearly, $\alpha'_g = 2\alpha_g$.

The absorption of acoustical energy by the gaseous medium may be explained, under small amplitude conditions, by the internal friction or the viscosity and thermal conductivity of the medium (heat transfer existed between the compressed and rarefied portions of the medium). According to the sonic theory this assumption leads to the following expression for the abosrption coefficient [7, 46, 233]:

$$\alpha_{g0} = \alpha_g^{\eta} + \alpha_g^{\lambda} + \alpha_g^{\eta'} = \frac{b\omega^2}{2\rho c_g^3}, \qquad (1.16)$$

where

$$b = \frac{4}{3}\eta + \frac{\gamma - 1}{C_p}\lambda_g + \eta' \qquad (1.17)$$

(η is the dynamic viscosity, λ_g is the coefficient of thermal conductivity, and η' is the second viscosity). The second term in (1.17) is equal to 0.554 for air and, therefore $b \approx 2\eta + \eta'$. For all practical purposes $B \approx 2.5\eta$ for air [233]. According to equation (1.16), the absorption coefficient for dry air is negligibly small under normal conditions; in the 3 - 10 kHz range $\alpha_{g0} = 10^{-3} \div 10^{-2}$ db/m. Measurements yield considerably greater values under atmospheric conditions due to the presence of water vapor in the air [6, 7, 46, 267]. Knudsen checked this for frequencies of 1.5, 3, 6, and 10 kHz and established that the sound absorption coefficient was lowest in dry air; subsequently, it rises abruptly attaining a maximum at a relative humidity of 12-20%, after which it decreases again. The maximum value of the sound adsorption coefficient in the 3 - 10 kHz range is $\alpha^{\varepsilon}_{g0}$ = 0.17 - 0.56 db/m. The presence of boundaries causes additional viscous and thermal losses in acoustic energy.

In the case of a tube with radius R, the additional absorption coefficient according to Kirchkoff [6, 7] is:

$$\alpha_{\text{ст}} = \frac{1,1}{c_g R}\sqrt{f}. \tag{1.18}$$

It is thus seen that as the port dimensions decrease, sound absorption increases rapidly. The absorption coefficient in a high-intensity acoustic field is greater than α_{g0} by several orders of magnitude. This can be basically explained by the appearance of harmonics which, according to (1.16), are absorbed much more readily than the fundamental frequency. In accordance with the theory formulated by Z. A. Goldberg [25], the local sound absorption coefficient for a sawtooth wave is expressed by the following formula:

$$\alpha_g = \alpha_{g0}\frac{\gamma+1}{\pi}\frac{P_x}{b\omega_0}, \tag{1.19}$$

where P_x is the pressure amplitude at point x. Thus, at high intensities, the absorption coefficient is directly proportional to the vibration frequency if (1.16) is included and to the local sound pressure. In the case of air, equation (1.19) acquires the following form:

$$\alpha_g = 3,6\cdot 10^{-8} f P_x (\partial б/м), \tag{1.19'}$$

which in the 1 - 10 kHz range yields:

α_g = 0.23 - 2.3 db/m for J (or I) = 0.1 w/cm^2.
α_g = 0.73 - 7.3 db/m for J (or I) = 1.0 w/cm^2.

The linear dependence of α_g on p was confirmed experimentally in [97]; the result of that work is illustrated graphically in Figure 10 (f = 13 kHz, R = 6 cm). The experimental data can be formulated by the following linear equation:

$$\alpha_g^{\text{э}} = \alpha_{g0}^{\text{э}} + m p_x, \tag{1.20}$$

where $\alpha^{\varepsilon}_{g0}$ is the experimental value of the sound absorption coefficient at zero sound pressure and includes losses at the vessel walls in addition to losses in gas; m is the proportionality factor.

However, the absolute value of mp_x is 6- to 7-fold lower than theoretical values of α_g obtained from (1.19); this cannot be explained by poor measurements alone. In view of sound absorption, coefficient dependence on sound pressure, sound attenuation with distance is no longer exponential, and can be determined from the following formula [98]:

$$p = p_0 \frac{\alpha_{g0}}{\alpha_{g0} e^{\alpha_{g0} x} - m p_0 (1 - e^{\alpha_{g0} x})}, \qquad (1.21)$$

applicable to plane acoustical waves only. In conclusion, it is to be noted that sound attenuation in free space with distance from the source depends not only on the acoustical energy absorption by the medium, but also on certain geometric factors, such as divergence of the acoustical beam (see Fig. 5), the intensity of which decreased with its cross section area.

4) The acoustical radiation pressure. When acoustical waves meet an obstacle, a definite force is exerted on the latter. The force of radiation pressure is directed along the wave propagation in the case of a traveling wave and from a node to antinode (where the acoustical pressure approaches zero) in the case of a standing wave. This phenomenon cannot be described graphically. V.A. Krasilnikov offered the following explanation in his popular monograph "Sonic and Ultrasonic Waves" [46]:

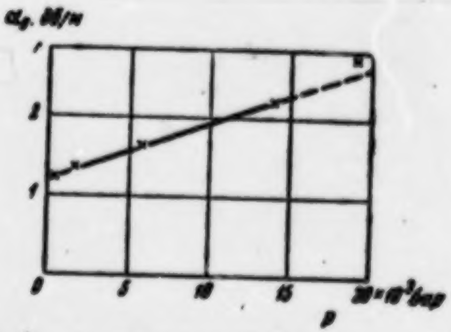

Fig. 10. Functional relation between sound attenuation coefficient and sound pressure (f = 13 Hz.)

> "Particle velocity in compression regions is in the direction of wave propagation, while in rarefaction regions, it is in the opposite direction. Thus, resistance to particles' motion is smaller when the particles travel from the compression zone to the rarefaction zone than when the converse occurs. Since the pressure is determined by the product of particle velocity and the resistivity of the medium, as shown in (1.10), pressure along the wave propagation direction is slightly greater than that in the opposite direction. In this manner, a constant pressure is generated in the direction of sound propagation."

The solution of a wave equation including quadratic terms (second order approximation) shows that sound pressure at the obstacle is not sinusoidal. Its average temporal value is not equal to zero as it is assumed in small amplitude acoustics, the proof of which was presented in detail in [72, 205]. Radiation pressure is the average pressure developed by the acoustic wave at the obstacle, accounting for the interaction between the sound field and the unperturbed medium. Magnitude of radiation pressure is obtained readily using the reasoning of Pol' [100], who writes:

> "Let two straight lines mark the boundaries of a parallel beam. The particles in the beam vibrate sinusoidally in the direction of double arrows with maximum velocity of U_s (the designations here and below are the author's - Ye. M.). Consequently, the static pressure P_{st} inside

the beam decreased according to Bernoulli's equation by a quantity equal to 1/2 $p_g U^2_g$. This causes outside air to penetrate the beam which strikes the right-hand side boundary. Moreover, its velocity decreases to zero and the pressure increases by an amount equal to $p = 1/2\, p_g U^2_g$. This is exactly the radiation pressure. The quantity 1/2 $p_g U^2_g$ is at the same time equal to the ratio

$$\frac{\text{Kinetic energy in sound field volume V,}}{\text{sound field volume V}}$$

i.e., it is equal to density $\overline{E}$ of the acoustic energy. For the same reason, sound pressure p_r equals volume density $\overline{E}$ of the same radiated energy:"

$$p_R = \overline{E} = \frac{J}{c_g}. \qquad (1.22)$$

Similarly, the magnitude of radiation pressure at the totally absorbing obstacle, dimensions of which considerably exceed the wavelength, likewise equals the above magnitude. In the case of total sound reflection, the radiation pressure is twice as great:

$$p_R = 2\overline{E} = \frac{2J}{c_g}. \qquad (1.22')$$

In a general case of an obstacle with a reflection coefficient β, the radiation pressure magnitude is determined by the following equation:

$$p_R = (1+\beta^2)\overline{E} = (1+\beta^2)\frac{J}{c_g}. \qquad (1.23)$$

The force on the obstacle generated by the radiation pressure depends, on the one hand, on the kinetic energy density of vibrational motion averaged over the time and space, and, on the other hand, on the shape, dimensions, and the reflectivity of the obstacle. In a field of high-intensity sound having a considerable energy density (at J (or I) = 0.1 - 1.0 w/cm^2 in the air E = 30 - 300 erg/cm^3), forces generated by radiation pressure on normal size objects acquire appreciable magnitudes. This is evidenced by the "levitation" of glass balls, coins, and similar objects observable in a high-intensity field of a standing wave [137, 179].

5) The acoustical wind. The vibrational motion in a high-intensity sound is accompanied by a progressive (non-periodic) acoustical mass flow.

The gas flow in a traveling wave is directed away from the sound source in the beam center, and in the opposite direction on the beam circumference (see Fig. 11a). A series of closed (toroidally closed in a cylinder) vortexes may be observed in a standing wave bounded by the longitudinal walls. These are directed from antinodes to nodes near the walls, as can be seen in Fig. 11b.

It is generally accepted that acoustical winds are the result of a drop in radiation pressure caused by absorption of acoustical waves by a medium. It should be noted that acoustical wind phenomena were initially discovered with the aid of aerosols by Kundt while he was observing dust patterns (Dvorak, 1887). Shortly thereafter, Rayleigh also noted this phenomenon and, by including medium viscosity, derived the following equations for non-periodic components in a standing wave [107]:

for velocity parallel to a plane surface (axes x),

$$u_2 = -\frac{3U_g^2 \sin 2kx}{16c_g}\left[1 - \frac{3(y_1 - y)^2}{y_1^2}\right]; \qquad (1.24)$$

for velocity perpendicular to a plane surface,

$$v_2 = -\frac{3U_g^2\, 2k \cos 2kx}{16c_g}\left[y_1 - y - \frac{(y_1 - y)^3}{y_1^2}\right], \qquad (1.25)$$

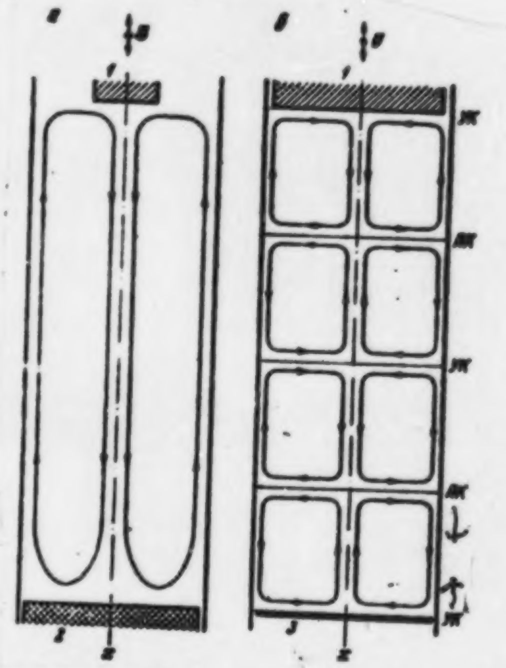

Fig. 11. Accoustical flow (sound wind) which arises in the sound field. a - b in travelling waves; b - c static wave - 1 - sound transmitter; 2 - sound absorbing substance (reflector). Arrow marked section equals λ/4.

where x and y are distances from the antinodes measured respectively parallel and perpendicular to the surface; y_1 is the distance measured from the wall to the symmetry plane.

The acoustical vortex streamlines may be calculated by means of the following stream function [73]:

$$\psi = \sin 2kx - \frac{1}{y^3 - 3y_1y^2 + 2y_1^2y}. \qquad (1.26)$$

Velocity curves and acoustical vortex streamlines given by equations (1.24), (1.25), and (1.26) can be found in [73]. It should be noted, however, that a considerable disagreement existed in a high-intensity sound between the theory and experiment. Experimentally obtained streamlines are less angular, i. e., they have a more continuous rounded shape; moreover, the greater the curvature the higher is the intensity [140]. According to Eckart [187], direct acoustical flow velocity along the axis of a cylindrical vessel for the case of a traveling wave is:

$$(u_2)_{\text{макс}} = \frac{\omega^2 J_0 R^2}{\rho_g c_g^4}\left(2 + \frac{\eta'}{\eta}\right)\Phi(R_{\text{пр}}). \qquad (1.27)$$

where J_0 (I_0) is the sound intensity directly at the source, $\Phi(R_4)$ is a factor which is a function of the ratio of acoustical beam radius R and the tube radius R_0.

$$\Phi(R_{np}) = \frac{1}{2}\left(\frac{R^2}{R_0^2} - 1\right) - \log\frac{R}{R_0}.$$

Eckart's and Rayleigh's equations are applicable only in the case of infinitesimal sound absorption when the sound absorption coefficient is independent of intensity. The equations are also inapplicable at low acoustical frequencies, since they were derived on the assumption that the wavelength was of considerably lesser dimensions than the vessel. In this connection, new theoretical studies of the acoustical wind were conducted recently. Among these the work of Westervelt deserves special notice [287]. A. I. Ivanovskii [36] recently conducted a detailed theoretical study of the problem of acoustical flow; he found a general solution which gave velocity values for any sound absorption coefficient α_g and vessel length L with an accuracy up to the factor $\Phi(R_d)$.

For $\alpha_g L \ll 1$, the acoustical wind velocity is:

$$u_2 = \frac{2\alpha_{g0} J_0}{c_g \eta} R^2 \Phi(R_{np}). \qquad (1.28)$$

The above expression coincides with Eckart's formula (1.27) providing it included the value of α_{g0} from (1.16), and (1.17), in which $b \approx 2\eta + \eta'$.

For $\alpha_g L \approx 1$, the acoustical wind velocity is:

$$u_2 = \frac{2J_0}{c_g \eta} \cdot \frac{1 - e^{-\alpha_g L}}{L} R^2 \Phi(R_{np}). \qquad (1.29)$$

For $\alpha L \gg 1$ [sic]*, i.e., when the sound is totally absorbed in the vessel, velocity of the acoustic wind is:

$$u_2 = \frac{2J_0}{c_g \eta} \frac{1}{L} R^2 \Phi(R_{np}). \qquad (1.30)$$

The above equations indicate that the acoustical wind velocity was proportional to that portion of acoustical energy which remained in the vessel after its absorption by the medium (in the case of aerosols, it is necessary to include the absorption of acoustical energy by the aerosols, as it is discussed in Paragraph 8 below). Experimental verification of the above formulas applied to gases, is at present unavailable. Moreover, there is a complete lack of concrete data on the magnitude of the acoustical wind velocities in gases. An exception to this is paper [233], although experiments reported in it had been conducted unfortunately at a very high frequency (f = 185 khz). Furthermore, no absolute measurements of sound intensity were taken. However, it is known that the acoustical wind velocity in gases is considerably greater than in fluids, and in the very high-intensity fields it attains few meters/sec [137].

---

* should read $\alpha_g L \gg 1$ [B.S.L.]

6) Acoustical turbulence. Observation of aerosol behavior under intense sonication leads to the conclusion that a gaseous medium is in the state of turbulence. This is clearly manifested when a narrow stream of smoke is injected into the sonicated gaseous medium. As it penetrates the regular acoustical stream, it immediately spreads in all directions. The turbulent acoustical flow may be the result of superposition of the continuous spectrum of pulsations of different magnitudes and directions on the advancing-regressing medium flow. Acoustical turbulence formation is connected with the above described unusual heterogeneity of the near field [10, 46] which, under high acoustical intensities, generated vortexes carried further by the acoustical wind. In addition, interaction takes place between the direct and retrogressive streams [36] in traveling waves, on the boundaries of which, as Kwick has shown [219], rotational motion is generated. In the case of standing waves, this is assisted by 1), the circulatory motion in the regions between the nodes and antinodes, and 2), the aerodynamic mixing discovered by Mickelson and Baldwin [236]. All above effects are sustained by the medium vibrational energy. Therefore, Reynolds number, which reflected the process of sound propagation in a gaseous medium, may be expressed according to V. A. Krasil'nikov [46] as follows:

$$\mathrm{Re}^{\text{ак}} = \frac{u_g \lambda}{b/\rho_g}. \tag{1.31}$$

The effective oscillatory velocity u_g stands for average flow velocity, the wavelength λ — scale of motion, and the constant b [see (1.17)] divided by the medium density ρ_g — kinematic viscosity. By considering relationship $\lambda = c_g/f$ and equation (1.11), the expression for Re^{ac} may be represented in the following form:

$$\mathrm{Re}^{\text{ак}} = \pi\sqrt{2}\,\frac{\rho_g c_g}{b}A_g, \tag{1.31'}$$

whence, Reynolds number is directly proportional to the acoustical impedance and the medium vibration amplitude and indirectly proportional to the medium viscosity. If A_g is expressed in terms of parameters J (or I) and f, the expression (1.31) can be rewritten as follows:

$$\mathrm{Re}^{\text{ак}} = \frac{(\rho_g c_g)^{1/2}}{b}\,\frac{J^{1/2}}{f}. \tag{1.31''}$$

No experimental data were found on Reynolds critical number Re^{ac}_{cr}, for which the acoustical flow loses its hydrodynamic stability and becomes turbulent. The only work conducted in this direction by Kastner and Shih [209] is applicable to low frequencies (up to 30 hz), and cannot be used to determine the behavior of Re_{cr}^{ac} at higher frequencies. Supported by his experience with fluid sonication, V. A. Krasil'nikov [46] assumed that Re_{cr}^{ac} was approximately one order of magnitude lower than that in the tube flow (where $Re_{cr} = 2300$); likewise, no information was found on the internal structure of acoustical turbulence. Without such information, it is impossible to evaluate the effect of this phenomenon on the physico-chemical processes enhanced by sounds. This author is of the belief [83] that if acoustical turbulence is developed sufficiently, the knowledge about its microstructure at a considerable distance from the sound source and boundary surfaces may be obtained from the isotropic turbulence theory developed by A. N. Kolmogorov, according to which, energy of primary large-scale vortexes was gradually transformed into energy of small-scale eddys (according to the 2/3 power law). Upon reaching the so-called "internal" range l_0, in which the viscous forces predominated ($Re<1$), the energy became dissipated (converted into heat). The interaction between pulsations is terminated within this subrange, and all medium properties become isotropic, i. e., independent of the flow direction. In particular, the pulsation frequency becomes independent of the scale of motion and equal to a constant maximum value. The isotropic turbulence theory fails to stipulate the vortex formation and transformation mechanisms; therefore, its results may be applied to acoustical turbulence provided the medium compressibility was considered (1.17). A. N. Kolmogorov postulated [44] that properties of turbulent motion in regions small in comparison with the "internal" range l_0, are determined by two quantities: the energy dissipation Σ and the medium viscosity γ (which in the case of acoustical fields is b/p).

According to dimensional analysis [62], the expression for the energy dissipation is:

$$\varepsilon \sim \frac{u_g^3}{\lambda} \sim \frac{J^{3/2} f}{\rho_g^{3/2} c_g^{5/2}} \left[\frac{\text{эрг}}{\text{г.сек}}\right]. \qquad (1.32)$$

On the other hand, energy dissipation may be determined from data on sound attenuation in a gaseous medium by means of a simple formula:

$$\varepsilon = \frac{\alpha_g' J}{\rho_g}, \qquad (1.33)$$

where α'_g is the sound absorption coefficient, less the molecular absorption which ensues turbulence indirectly.

If Z. A. Gol'dberg's expression for sound absorption coefficient is substituted into the above equation for the case of finite amplitude vibrations (1.19) and, in addition to equations (1.16) and (1.17), we get:

$$\varepsilon = 2\sqrt{2}(\gamma + 1)\frac{u_g^3}{\lambda} = 2\sqrt{2}(\gamma + 1)\frac{J_g^{3/2} f}{\rho_g^{3/2} c_g^{5/2}}. \qquad (1.34)$$

It can be seen that the above equation and (1.32) are identical, indicating that the initial characteristics of acoustical turbulence were properly selected and the dimensional analysis was applicable, if factor $\xi = 2\sqrt{2}\,(\gamma + 1)$, which equals 6.8 for air, was included in the derived equation (1.32).

A comparison of theoretical and experimental energy dissipation values such as was done in [99] and shown in Figure 10, leads to the conclusion that a better agreement can be obtained for very small values of ξ, which is evidently due to the insufficient development of acoustical turbulence and, consequently, its incomplete isotropy for similar acoustical parameters.

Nevertheless, for the purposes of subsequent calculations for establishing the order of magnitudes of the local acoustical turbulence characteristics, the above considerations are not essential, since quantity ξ has a fractional power in all subsequent formulas. As a result, the effect of the magnitude of ξ is well concealed. According to equation (1.34), the following values of the energy dissipation are obtained in the 1 - 10 khz frequency range:

at J (or I) = 0.1 w/cm^2, $\epsilon = 7.3 \times 10^5 - 7.3 \times 10^6$,
at J = 1.0 w/cm^2, $\epsilon = 2.3 \times 10^7 - 2.3 \times 10^8$.

Therefore, it may be concluded that acoustical turbulence was not characterized by an exceptionally high intensity; rather, it was equal to the standard turbulence occurring in the tube with a diameter $D = \lambda/\xi$ at flow velocities equal to the oscillatory velocity of a gas ($w_r = u_g$). According to dimensional analysis [62], acoustical turbulence "subrange" was equivalent to the following expression:

$$l_0 \sim \left[\frac{(b/\rho_g)^3}{\varepsilon}\right]^{1/4} \sim \frac{b^{3/4} c_g^{5/8}}{\xi^{1/4} \rho_g^{3/8}} J^{-\frac{3}{8}} f^{-\frac{1}{4}}. \qquad (1.35)$$

The above indicated that the dependence of l_0 on the acoustical intensity J (or I) and especially on the frequency of oscillation f was very weak. In the f = 1 - 10 khz range, at J = 0.1 w/cm^2 we have the following: $l_0 \approx 180 - 100\mu$, and at J = 1.0 w/cm^2, $l_0 \approx 75 - 45\mu$. The relative oscillatory velocity of gas particles at distance l apart within the limits of the turbulence subrange ($l < l_0$) is:

$$v_l = \sigma_1 \left(\frac{\varepsilon}{b/\rho_g}\right)^{1/2} l \approx \frac{1}{4} \frac{\xi^{1/2} J^{3/4} f^{1/2}}{b^{1/2} \rho_g^{1/4} c_g^{5/4}} l, \qquad (1.36)$$

and outside the subrange ($l > l_0$) it is:

$$v_l = \sigma_2 (\varepsilon l)^{1/3} = \frac{\xi^{1/3} J^{1/2} f^{1/3}}{\rho_g^{1/2} c_g^{5/6}} l^{1/3}, \qquad (1.37)$$

where σ_1 and σ_2 are coefficients of proportionality, usually taken as $1/\sqrt{15} \approx \frac{1}{4}$ and 1, respectively.

The rate of relative oscillatory particle velocity is independent of the wavelike flow character, since it is assumed that $l \ll \lambda$, and accordingly, both medium particles are practically in the same oscillatory velocity phase. The maximum oscillatory velocity within the $l < l_o$ subrange is found. At $l = l_o$, J = 0.1 w/cm², and f = 1 - 10 khz, it lies in the range of v_l = 5.8 – 10.4 cm/sec. which constitutes 3.7 – 6.6% of the oscillatory gas velocity. The lower frequency limit of turbulent pulsations which originate inside the acoustical flow, is given by the following relationship:

$$\omega_\lambda \sim \frac{u_g}{\lambda} \sim \frac{J^{1/2} f}{\rho_g^{1/2} c_g^{3/2}}, \tag{1.38}$$

The order of magnitude of the upper limit of the turbulent pulsation frequency spectrum which lies within the l_o "subrange" is:

$$\omega_{l_o} \sim \frac{v_{l_o}}{l_o} \approx \sigma_1 \left(\frac{\varepsilon}{b/\rho_g}\right)^{1/2} \approx \frac{1}{4} \frac{\xi^{1/2} J^{3/4} f^{1/2}}{b^{1/2} \rho_g^{1/4} c_g^{5/4}}. \tag{1.39}$$

At a normal acoustical intensity, J (or I) = 0.1 w/cm², the frequency spectrum of turbulent pulsations is as follows:

at f = 1 khz, f_1 = 1.5 - 60 hz,
at f = 10 khz, f_1 = 15 - 190 hz.

At increased acoustical intensity, J (or I) = 1 w/cm², the frequency spectrum is somewhat broader:

at f = 1 khz, f_1 = 5.0 - 340 hz,
at f = 10 khz, f_1 = 50 - 1050 hz.

Thus, it may be stated that the frequency spectrum of turbulent pulsations is comparatively narrow and always lies in the low frequency range below the fundamental frequency. In conclusion, some data on the nature of motion in the boundary layer of large obstacles and walls are introduced here.

Assuming that $A_g \ll L$ (where L is the surface length), the boundary layer thickness in the case of the medium oscillatory motion is equal to the "depth of penetration" determined with the aid of the following expression [62]:

$$\delta \sim \sqrt{\frac{2\nu}{\omega}} \approx \sqrt{\frac{\nu}{\pi f}}. \tag{1.40}$$

which in the 1 - 10 khz frequency range is δ = 70 - 22μ. The energy dissipation in this layer is a few orders of magnitude greater than in the remaining volume and, according to [62], may be calculated using the following formula:

$$\varepsilon_{\text{norp}} = \frac{1}{4} \omega U_g^2. \tag{1.41}$$

Table 1

Effect	Required sound J intensity, vt/cm^2	Corresponding force level of sound L, db
Threshold of human ear pain sensation (110)	0,00001—0,001	110—130
Beginning of aerosol coagulation effect by sound (156)	0,003—0,01	135—140
Beginning of sound intensification effect on the drying process of fibrous granular, and powder substances (8)	0,01—0,03	140—145
Rapid aerosol coagulation (184); enhanced rate of fibrous and powdered substance drying (8); foam disintegration (157); aerosol filtration (301)	0,1—1,0	150—160
Gradual warming of sound absorbing materials, such as cotton and the like (137, 253);	1,0	160
Burning sensation between touching fingers. Death of animals and insects. (157, 252, 253)	1—3	160—165
Strong acoustical winds of several m/sec velocity (137)	3—10	165—170
Swimming under pressure of glass sound spheres, coins and other object present in the field of a static wave (137, 179)	3—30*	165—175
Rapid burning of sound absorbing materials for several seconds (137)	10—30	170—175
Maximum sound intensity reached according to calculations in the throat of sound siren (208)	300—1000	185—190

In the field of static sound wave the concept of "intensity sound" loses its force, since under such conditions the current of acoustical energy is totally absent. Uncer such conditions it is more appropriate to operate with sound intensity values. However, under practical conditions units measuring sound intensity are frequently used conditionally.

However, in contrast to the acoustical turbulence which occurs in the entire sound field, the phenomenon is limited to the eddy motion only in the boundary layer. The pulsations cannot be isotropic, since the thickness of the boundary layer is of the same order of magnitude as the turbulence subrange determined from (1.35) for $\epsilon = \epsilon$ boundary. The above specific properties of high-intensity acoustical vibrations gave rise to a whole series of physical and biological effects observed in sonicated gaseous media. The most significant of these are shown in Table 1 above.

2. SOURCES OF HIGH-INTENSITY SOUND.

Special sound sources are used to generate high-intensity acoustic vibrations in gaseous media. Pneumatic sound radiators, such as sirens, have found applications in industrial installations. In laboratory practice, whistles, such as the electrodynamic and, occasionally, magnetostrictive sound radiators, have also been used. Two types of sirens are known: dynamic (rotary) and static (whistle-type). Mainly dynamic sirens have been utilized in industrial practice, heretofore. They cover a wide frequency range and offer a continuous coverage, have a high factor of energy conversion of compressed air (gas, steam) into acoustical vibrations (i.e., acoustical efficiency) with practically unlimited acoustical power radiation.

The dynamic siren consists of a circular stator (main body), with ports located on its circumference, and a rotor with teeth in the form of a perforated disk or cylinder. The compressed air (steam, gas) is introduced into the stator housing from a special compressor. During rotor rotation the teeth interrupt periodically the flow of compressed air which escapes from the stator ports. This gives rise to pulsations of air pressure which cause the gaseous medium to oscillate.

Two types of dynamic sirens of different construction are known: axial and radial. The axial siren (see Fig. 12a) ports through which the pulsating air stream flows are axially distributed, and the sound is directed to the object by special horns (usually exponential). The radial siren (Fig. 12b) ports are radially distributed and the sound is directed to the object by means of a special, usually parabolic reflector. Axial sirens are easily designed when they are to be small; the radial, on the other hand, are easy to design when they are to be large. The fundamental frequency of the radiated sonic vibrations is:

$$f_0 = \frac{zn_c}{60}. \qquad (2.1)$$

where z is the number of teeth in the rotor, and n_c is the rotor rpm. In addition to this frequency, dynamic sirens radiate (unless special measures are taken) moderately strong harmonics. Methods for their calculations are cited in a paper by Inone [37]. The acoustical power generated by a dynamic siren may be calculated by the following formula:

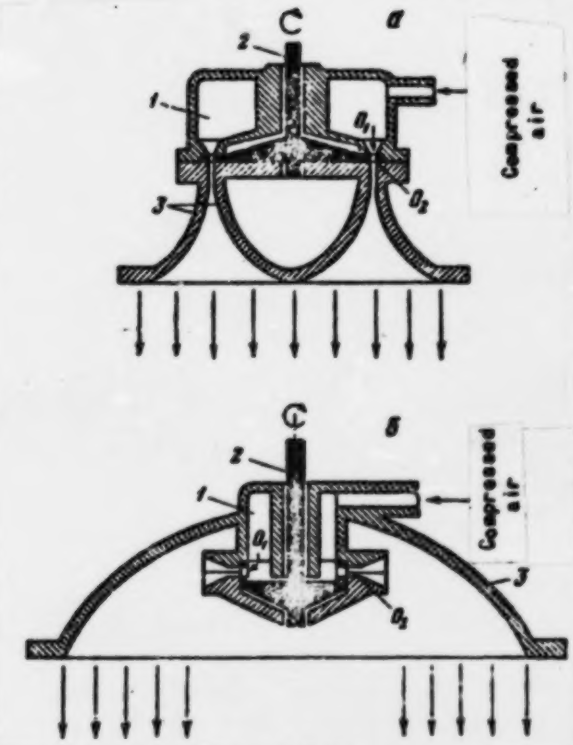

Fig. 12. Schematic presentation of sound emitting dynamic sirens.
a – axial type (1 – stator with perforations C_1; 2 – rotor with perforations O_2; 3 – Mouthpiece); b – radial type (1–stator with funnel-shaped perforation s O_2; 2 – Rotor with perforations O_1; 3 – Reflector.)

$$W_{ак} = \alpha_c(1+\delta)\frac{'Q_m L_{ак}}{102}\eta_{ак} \quad квт. \qquad (2.2)$$

where Q_m is the theoretical discharge rate of air through the siren ports in m/sec; α_c is the constriction factor for the air stream blocked by a tooth; δ is a coefficient which recorded that portion of air which escaped through the gap between the stator and rotor; the product α_0 $(1+\delta)$ lies in the range between 0.7 - 1.4 [247]; L_{ad} is the theoretical work performed by the adiabatic expansion of $1m^3$ of compressed air (in kg/m^3); η_{ac} is the siren acoustical efficiency. Quantities Q_s and L_{ad} are calculated by the following formulas:

$$Q_{\text{м}}=(\varepsilon_0 S_0)w, \qquad (2.3)$$

$$L_{\text{ад}}=\frac{\gamma_{\text{к}}}{2g}w^2, \qquad (2.4)$$

where S_0 is the total cross section of siren ports (in m^2); ϵ_0 is the overlap factor for teeth and ports (equal approximately to 0.5); γk is the specific weight of air at pressure equal to p_k (in kg/m^3); w is the velocity of air discharge determined by the following formula:

$$w=\sqrt{2g\frac{\gamma}{\gamma-1}\frac{p_c}{\gamma_c}\left[1-\left(\frac{p_{\text{к}}}{p_c}\right)^{\frac{\gamma-1}{\gamma}}\right]}\ \text{м/сек} \qquad (2.5)$$

[p_s is the absolute pressure of air compressed in the stator body (in kg/m^2); p_k is the absolute pressure of the surrounding medium (in kg/m^2); γ_s is the specific weight of compressed air (in kg/m^3); γ is the adiabatic curve index c_p/c_v which is equal to 1.4 for air, and 1.3 for natural gas and steam.] When the difference $\Delta p = p_s - p_k$ is small in comparison with p_k, the velocity is $w \approx \sqrt{2g\ \Delta p/\gamma_s}$ and $L_{ad} \approx \Delta p$. The acoustical efficiency of a siren η_{ac} depends on the following: 1) geometry and ratio of stator ports and rotor teeth sizes which determine the form of the radiated pressure pulses; 2) the compressed air pressure; 3) frequency of oscillations; 4) the presence or absence of a horn and its shape; and 5) siren design factors (clearance between the stator and rotor at the points where the ports are located, the rotor play, etc.). The method for determining the efficiency of the horn-equipped sirens was presented by Jones [208] as an electromechanical model. His method was given a brief treatment in a book by Heuter and Bolt [205]. In the case of rectangular pressure pulses generated when the ports and teeth are rectangular and when the tooth width is slightly greater than the port width, the acoustical siren efficiency is equal approximately to [208, 205]:

$$\eta_{\text{ак}} \approx \varphi(y)=\frac{(1+2y)^{1/2}-1}{y}, \qquad (2.6)$$

where y is a parameter approximately equal to $4\Delta_p/\gamma p_k$. A different formula is proposed in [205]:

$$\eta_{\text{ак}} \approx \frac{\varphi(y)}{1+0{,}5(ka)^2+0{,}42\beta a} \qquad (2.6')$$

(where k is the wave number $2\pi/\lambda$; a is the port width; β is the flare constant for the siren exponential horn). This formula is in a better agreement with the experiment. Values of function φ (y) for air are listed in Table 2; they show an approximate acoustical efficiency for sirens with rectangular compressed air pulses. It can be seen that high efficiency of a siren

($\eta_{ae} \geq 75\%$) can be achieved only under low air pressures ($p_0 \leq 0.3$ gage atm), the exception being only sirens with ports in the form of [de] Lavale [17] nozzles.

Table 2

Δp	y	$\varphi(y)$	Δp	y	$\varphi(y)$
0,00	0	1,000	0,90	2,570	0,577
0,10	0,286	0,888	1,00	2,880	0,556
0,20	0,572	0,813	1,25	3,570	0,518
0,30	0,858	0,758	1,50	4,285	0,488
0,40	1,144	0,712	1,75	5,000	0,463
0,50	1,430	0,675	2,00	5,720	0,442
0,60	1,714	0,642	3,00	8,575	0,380
0,70	2,000	0,618	4,00	11,420	0,340
0,80	2,288	0,595	5,00	14,300	0,309

Formula (2.6') shows that the acoustical efficiency of sirens also decreases with the increase in radiated sound frequency. Moreover, the fundamental frequency contained no more than 81% of the radiated power. When the radiated pressure pulsation is sinusoidal, such as is the case (96% of all cases) when ports are round and teeth are rectangular and the widths of both are identical, the siren acoustical efficiency is equal to only one half the value calculated by formulas (2.6) or (2.6'), and as shown in Table 2. Therefore, the maximum efficiency of sirens with sinusoidal pressure modulation never exceeded 50%. In practice the attainable value was $\eta_{ae} = 35 - 40\%$, since the use of pressures below 0.2 - 0.3 gage atm was related directly to design difficulties. Most widely used sirens are equipped with circular rotor and stator ports. When the port diameters are equal, the fundamental frequency radiates approximately 82% of the acoustical energy.

It should be stated that the above cited figures for acoustical efficiency pertain to dynamic sirens equipped exponential horns (conical horn design is difficult), i.e., horns, the cross sectional area of which increased according to the following expression [124]:

$$S_x = S_0 e^{\beta x}, \qquad (2.7)$$

where S_0 is the initial cross sectional area of the horn, x is the distance between a given plane and the initial plane, and β is the horn flare factor.

In the absence of an exponential horn, the siren acoustical efficiency falls abruptly, especially at low frequencies [137]. The theory and design of hornless sirens, used for signaling, is presented in [91, 92] by M. I. Karnovskii. The acoustical efficiency of these sirens fails to exceed 1 - 2% as a result of failure to match between sound source and sonicated medium.

Every exponential horn has its critical frequency below which the sound is cut off. This frequency depends on the horn flare factor [124]:

$$f_{кр} = \frac{\beta c_g}{4\pi}. \qquad (2.8)$$

This fact may be useful when the sound is to be cut off without discontinuing the delivery of the compressed air to the siren. In this case it is only necessary to lower n_c below n_r [sic]. *

The rotor in dynamic sirens is rotated by an electric motor or a pneumatic turbine. The power consumption of the drive mechanism is small and approaches 100 - 400 watts for experimental sirens and 1 - 2 kwatt for industrial (the lower values refer to low frequencies and higher values to higher frequencies). In comparison with air compressor power, this power is negligible.

Up to now, only the Ultrasonics Corporation of the USA was engaged in mass production of dynamic siren models. According to specification sheets [6, 7, 47, 184, 240, 254, 272, 291], the U-1, U-2, U-3, U-4, and other models had acoustical efficiencies up to 50 -70%, which appears as an overrated evaluation.

Dynamic sirens designed for laboratory use and experimental - industrial investigation have been described in the foreign literature [1, 6, 7, 92, 137, 227, 229, 246, 252, 253, 259, 274, 291]. Dynamic sirens had been developed also in the Soviet Union. The first working models were the LIOT and MEI sirens [73, 74, 75]. Later, sirens were developed at the IGI AN SSSR [60, 75], UNITI [17, 18], Gintsvetmet [126], Promenergo[299], Institute of Applied Geophysics An SSSR [20], and other institutions. In recent years, "static sirens" became the subject of extensive research. Static sirens are characterized by their simplicity and lack of rotating parts and special drive mechanisms. Static siren consists of series of whistles distributed radially in a single annular resonant chamber equipped with an exponential horn at its output (if one whistle is sufficient, the annular chamber may be replaced by a parabolic reflector). Five types of whistles are known capable of generating high acoustical power (Fig. 13):**

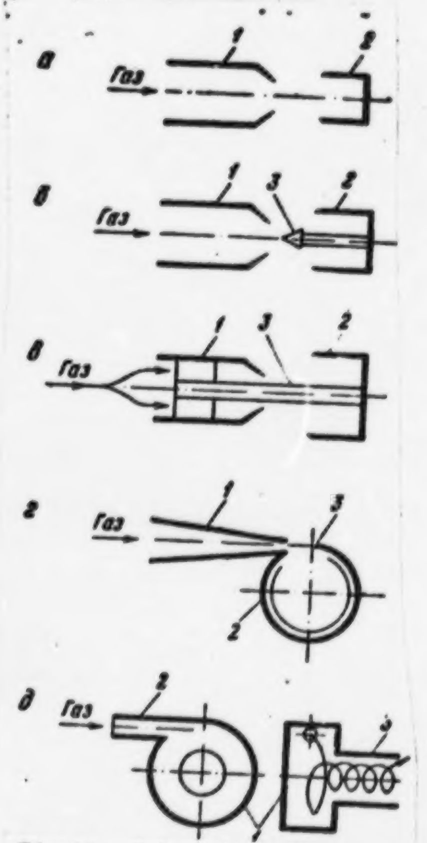

Fig 13. Schematic presentation of gas flowing (whistling) sound transmitters.
a - the Hartman whistle type (1 - nozzle; 2 - resonator); b - the Kurkin whistle type (1 - nozzle; 2 - Resonator; 3 - conical device); c - rod-shaped whistle (1 - nozzle; 2 - resonator; 3 - rod-shaped device); d - flow vibrating whistle (1 - slit-shaped nozzle; 2 - cylindrical or toroidal resonator with a blade-shaped contrivance 3); e - the vortex type whistle (1 - cylindrical chamber; 2 - tangential inflow type; 3-out-flow cylinder).

---

* Should read n_{cr}. B.S.L.

** The terminology below differs from the one used in the literature. The latter frequently gives insufficiently indicative nomenclature. For example, the Hartman shock wave whistle is called the "gas-jet-type" sonic radiator; this may stand also for the vibrating jet whistle which, in foreign literature, is called the "police" or "mouth" whistle [190].

a) the Hartman shock wave whistle [199, 7] in which the sonic vibrations are generated by shock waves set up by the impact of a supersonic gas jet onto a cylindrical resonator; moreover, regular shock waves are generated in the jet stream;

b) the shock wave whistle designed by Kurkin [53, 55, 56] differs from the preceding whistle by the presence of a conical pin which, in Kurkin's opinion, gives rise to oblique shock waves;

c) the stem-jet whistle [221] differs from the Hartman whistle by the presence of a concentric rod which eliminates an ineffective central region of the gas jet;

d) the vibrating jet whistle [190] in which sonic vibrations are generated by means of directing a plane gas jet onto the edge of a cylindrical (or toroidal) resonator wall. The feedback from the resonator cavity acting on the gas jet causes the jet to vibrate, if the jet is sufficiently thin;

e) the vortex whistle [282, 47] in which the sonic vibrations are generated by the moving vortex spiral, creating a rarefaction in the center of the chamber. This is periodically disturbed by the backward gas thrust as a result of which an obliquely-pulsating gas stream is established at its output.

The acoustical and geometric parameters of the Hartman shock wave whistles activated by the compressed air can be determined by eight empirical formulas which follow (d_c is the nozzle diameter in cm, p_c is the excess pressure in gage atm).

I. Maximum attainable frequency

$$f_0^{\text{макс}} = \frac{5860}{d_c} \text{ гц.} \qquad (2.9)$$

II. Relative range of frequency variation

$$R = \frac{f_0^{\text{макс}} - f_0^{\text{мин}}}{f_0^{\text{макс}}} 100 = 8{,}85\,(p_c - 0{,}93)\%. \qquad (2.10)$$

III. Distance between the nozzle and the edge of the first instability region (where the resonator is placed)

$$a_1 = [1 + 0{,}04\,(p_c - 0{,}93)^2]\,d_c \text{ см.} \qquad (2.11)$$

IV. Length of the first instability region

$$a_2 - a_1 = 0{,}43\,d_c \sqrt{p_c - 1{,}86} \text{ см.} \qquad (2.12)$$

V. Total acoustical power (including harmonics)

$$W_{\text{ак}} = (295 \sqrt{p_c - 0{,}93}\,d_c^2 \text{ вт.} \qquad (2.13)$$

VI. Power necessary to maintain the air stream

$$W_e = 5250\,(p_c + 1{,}033)\,[(p_c + 1{,}033)^{0{,}281} - 1{,}01]\,d_c^2\ \text{вт.} \quad (2.14)$$

VII. Efficiency of a single whistle

$$\eta_{ак} = \frac{W_{ак}}{W_e}\,100\ \%. \quad (2.15)$$

VIII. Volume of air consumed by the whistle

$$Q = 0{,}852\,(p_c + 1{,}033)\,d_c^2\ \ м^3/мин. \quad (2.16)$$

Table 3

d_c, мм	p_c, ати	λ, мм	f, кгц	W_e, вт	$W_{ак}$, вт	$\eta_{ак}$, %
2	2,61	11,7	28,2	335	13,4	3,99
3	2,61	18,2	16,3	694	38,2	5,40
4	2,74	24,6	13,4	1380	73,1	5,29
5	3,44	32,7	10,0	2920	103,0	3,52
6	3,16	37,0	8,9	3570	145,0	4,00

Table 3 shows the experimental data for shock wave whistles of different sizes with the following relationship: $d_p = d_c = 1$ (1 is the resonator depth). It may be concluded from data shown in Table 3 that the acoustical efficiency of shock wave whistles was low (4 -5%), and that the radiated acoustical power was relatively low, especially at higher frequencies (this is not due to frequency increase; it is due to a decrease in the nozzle cross section, and a proportional decrease in the air flow). Because of the above reasons, utilization of whistles without resonant chambers and horns is confined principally to laboratory setups. It should be noted that because the gas jet expanded beyond the nozzle, it has been currently recommended that the resonator diameter d be slightly larger than the nozzle diameter d_c, namely $d_p = (1.25 - 1.33)\ d_c$ [158, 172]. Moreover, to avoid rapid wear of the resonator rims it was recommended to increase d_p up to 1.65 d_c. The whistle efficiency, thus, increases by a factor of three and higher.

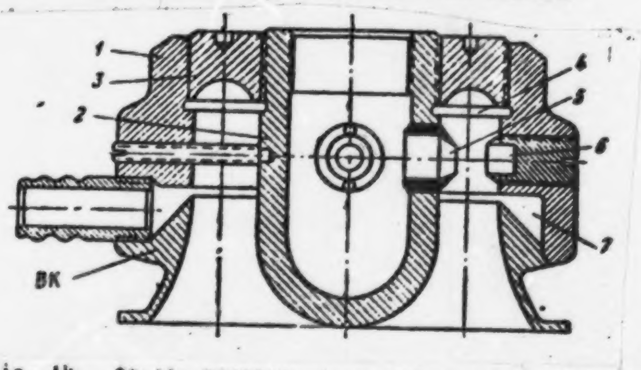

Fig. 14. Static NIIOGAZ siren with an accoustical collector

1 - Siren body with an outside dome-shaped horn, BK; 2 - inside dome-shaped horn equipped with an inflow pipe 3 - A movable butt; 4 - Circular resonating chamber; 5 - Nozzle and 6 - resonator (several complexes) 7 - Ring shaped slit for air auctioning off

Figure 14 shows a static siren designed at the Scientific Research Institute for Gas Purification in Industry and Sanitation (NIIOGAZ). It is equipped with Hartman whistles. It differs from an analogous Boucher whistle [148, 149, 150, 151, 158, 172] with respect to the presence of a movable threaded end section, which permitted adjustments to be made in the depth and volume of the resonant chamber, and an annular aperture

for air exhaust [52]. The acoustical efficiency of this siren at a frequency of 4.5 khz is approximately 10%. Data on Kurkin-designed shock wave whistles, which are more efficient than the Hartman whistles, are very scarce. In contrast to the Hartman whistles, Kurkin-type whistles operated with relatively small excess pressures of the order of 1 gage atm and lower. The resonator diameter is equal to or greater than the nozzle diameter. For equal diameters the frequency radiated by the Kurkin whistles is noticeably lower than the frequency of the Hartman whistles. The whistle is mounted at the throat of a special horn with an elliptical or circular cross section and an exponential taper.

In this siren, as in the static NIIOGAZ type, a vacuum accumulator is provided to expel air from the siren after its kinetic energy is transformed into acoustical vibrations. Results obtained by the Kurkin shock wave whistle with nozzle diameter equal to 10 mm are shown in Table 4.

Table 4

Angle of rod opening 2β, degrees	Pressure p in atm.u.	Rate of air consumption Q in $m^3/hr.$	Sound frequency f, in khz	Acoustical force	Acoustical eff. coef. η_{ac} in %
Without the rod	3,8	255	5,3	1,410	10,4
20	1,0	177	3,5	1,380	38,9
40	1,0	177	3,4	0,473	13,3
44	1,0	177	3,5	1,005	28,2
44,5	1,0	177	4,0	0,670	18,8
47,0	1,0	177	4,0	0,734	20,7
51,0	1,0	177	4,0	0,667	18,7
80,6	1,0	177	3,8	0,915	25,7

Rod type whistle sirens were first tried out by Sevori [47]. They were used as high intensity sound sources only recently as a result of research conducted by the Demister Co. of Sweden [221]. These whistles work effectively at low gas pressures, down to 0.3 - 0.5 gage atm, so that the velocity of the exhaust gas jet is below the speed of sound. The resonator diameter is much larger than the nozzle diameter, $d_p = 2.5\, d_s$. The effective frequency range is from 6 to 15 khz. At low frequencies the amount of air used is approximately one third that used by the Hartman whistles. The Swedish whistles are easily manufactured and adjusted, since they are less sensitive with respect to accuracy of distance between the nozzle and resonator.

Vibrating jet whistles had been known for a long time; they present essentially an extension of the Galton whistle design, although their theory has been developed only recently [190]. The fundamental frequency of the vibrating jet whistle is determined by a formula derived from a well-known formula by Helmholtz for natural frequency of a resonator, as derived by Rayleigh [107]:

$$f_0 = \frac{c_g}{2\pi}\sqrt{\frac{Kb}{V}}, \qquad (2.17)$$

where b is the resonator port length measured along the cylinder axis; K is a constant which depends on the width δ of the above port (when $\delta = 7.3$ mm, K = 0.713); V is the volume of the resonator. SinceV/b is the resonator cross section, the whistle frequency is determined by the cross section area.

According to Gavreau [190], the acoustical efficiency of the vibrating jet whistle is determined by the following expression:

$$\eta_{\text{aк}} = \frac{p_c^3}{\rho_g c_g} \frac{a^2 b^2 \delta}{q_0^3} \left[\frac{(V + 2q_0/\omega_n)^\gamma - V^\gamma}{(V + 2q_0/\omega_0)^\gamma + V^\gamma} \right]^2, \qquad (2.18)$$

where a is the jet width in m, q_0 is the air discharge rate per second in nm^3/sec, and p_0 is the air pressure in kg/m^2. The principle of the vibrating jet whistle is incorporated in the multiwhistle Gavreau siren [190, 150], the toroidal Lavavasseur siren [224, 7], and Jahn's siren [206, 150, 151].

Vortex sirens have been described by Vonnegut [282]. Greguss [28, 196] showed that to work effectively, the vortex whistle chamber radius R_k, the nozzle radius r_e, and the cylinder radius r_t must operate on the basis of the following relationship:

$$R_\text{к} = \frac{r_c^3 r_m}{r_\text{к}^3 z} + r_c, \qquad (2.19)$$

where α_s is the internal radius of the quasi-rigid cylinder produced by the gas motion ($r_s \approx r - 0.07$ cm) and z is a constant which depended on the coefficient of friction between the gas and the cylinder wall and the kinematic gas viscosity ($z \simeq 0.1$). The basic frequency of the vortex whistle is determined by the following formula [282, 235, 47]:

$$f_0 = \frac{\alpha_{\text{тр}} c_g}{\pi D} \left(\frac{p_c - p_\text{к}}{p_c} \right)^{1/2}, \qquad (2.20)$$

where α_{tr} is a constant accounting for the reduction in the vortex rotational velocity caused by friction against the resonator wall. In contrast to all previously discussed sound sources, the vortex whistle radiation pattern has two lobes; radiation is practically nonexistent along the whistle axis. Acoustical efficiency of static whistles attained same values as were cited above for the dynamic sirens with sinusoidal pressure modulation, i.e., the acoustical efficiency is equal to one half of function φ(y) shown in Table 2. Thus, on the one hand, the maximum acoustical efficiency of sirens equipped with Hartman shock wave whistles, which exhibit stable operation only at air pressures of the order of 2.5 - 3 gage atm, is equal to η_{ac} = 19 - 20%. On the other hand, the maximum efficiency sirens, equipped with Kurkin whistles, with stable operation under pressures of 1 gage atm and lower, was greater than η_{ac} = 28 - 29%. The maximum efficiency of sirens based on the vibrating jet or vortex whistles, which also work at low pressures, can attain 35 - 38%. Therefore, it can be concluded that, in comparison with high-efficiency dynamic sirens, the acoustical efficiency of static sirens was lower by a factor between 2 and 3. Other deficiencies of static sirens are the following: 1) need of adjustment; 2) lack of frequency regulation; and 3) intensified wear of working parts. Thus, application of static sirens can be justified when excess-pressure gas or steam was available, and a small-size setup was desired, etc. A common deficiency found in dynamic and static sirens up to now has been the presence of air flowing from the siren to the sonicated medium, i.e., unless a special membrane isolating the air flow and simultaneously reducing the sound intensity, was used. However, a method has been found recently which eliminates this deficiency by providing a suction system which draws off the air directly at the jet exhaust. This method was proposed and patented by Schaufler [260] and Lavavasseur [225]. In the Soviet Union this principle was incorporated in double-chamber sirens made at the UNITI [18] and in static sirens with a vacuum pump designed at the NIIOGAZ as shown in Figure 14.

In laboratory practice, aside from the sirens, applications were found for the high-power electrodynamic loud speakers and special electrodynamic radiators with resonating cores developed by St. Clair [178, 47]. The former provide low acoustical power at frequencies less than 1 - 2 khz; conversely, the latter exhibit high acoustical efficiencies (20 - 30%) and higher power output only at frequencies of 10 khz and up. Both differ from acoustical sirens with respect to high fidelity and stability of the tone essential to laboratory research. The, so-called, electro-pneumatic sound radiators were also developed [157] in which the sound vibrations are generated with the aid of electrically-modulated air stream. An ER 6786 electropneumatic radiator yielded 2.5 khz and 1 kwatt at 1 khz (with $p_e = 1.75$ gage atm, and $Q = 4.3$ nm^3/min) with a negligible consumption of electrical power for 20 watt vibration modulation.

In conclusion, acoustical measurement methods will be described. The fundamental frequency of acoustical vibrations radiated by a dynamic siren has been usually determined by measuring the siren motor rpm. This was done with the aid of a stationary or portable tachometer with subsequent conversion of the obtained value into frequency, using formula (2.1). The frequency of vibrations radiated by a static siren was determined by means of an acoustical analyzer, e.g., a harmonic analyzer, such as the AN-1-50, or the AS-3 or AS Ch Kh - 1 spectrum analyzers [113]. Equipment of this type is also necessary for the determination of audio harmonics of dynamic sirens. The I Ch type frequency meters are not suitable for these measurements. To determine the audio spectrum, an oscilloscope of type EO-7 and others may also be used. In addition to the test vibrations, an audio generator, such as 3G-12 and others, reference output is fed to the scope input. The analysis is carried out by means of Lissajou figures. Acoustical pressure is measured by calibrated microphone receivers coupled to a vacuum tube amplifier. The sound intensity is calculated from the formula on page 6.

The condenser microphones, with a titanium diaphragm and piezoelectrical sound receivers, are used at sound intensity levels above 130 - 140 db. The miniature ceramic barium titanate receivers, built in the form of small hollow cylinders or spheres, are especially convenient. In this case the amplifier is not needed frequently, and the electrical oscillations are applied directly to the input of a vacuum tube millivoltmeter of type MVL-2 and others. It should be noted, however, that the sensitivity of these receivers strongly depended on the ambient temperature. Therefore, in order to measure acoustical pressure in a high-temperature environment, it is necessary to use a specially-cooled or ventilated probe. Recently, piezoelectric receivers were made from a special ceramic material of type TsTS and others. These are useful at high temperatures of the order of 200° C and above. The receiver calibration consists of determining its sensitivity (µv/bar) at different frequencies. The most reliable method was described by N. N. Pisarevskii and T. V. Smyshlyayeva [19].

Since piezoelectrical receivers are highly independent of frequency, and since strong harmonics are present in the high-intensity acoustical fields, causing distortion of acoustical pressure measurements, their utilization has been favored over the condenser-type and other receivers. More detailed data on the acoustical measurement techniques may be found in a monograph by Beranek [6] and in selective articles published in the Acoustical Journal of the Academy of Sciences, USSR.

3. A BRIEF OUTLINE OF THE DEVELOPMENT OF AEROSOL ACOUSTICAL COAGULATION AND PRECIPITATION PROBLEMS

In 1926-1927 the famous physicist R. Wood and a rich patron of arts, Loomis, conducted experiments on the properties of powerful ultrasonic vibrations in liquids. They discovered several curious physical and biological effects which evoked a considerable interest in the world of science. Those experiments stimulated similar studies in gaseous media. Shortly thereafter, Patterson and Cawood [249] established that, when aerodispersed systems were exposed to ultrasonic vibrations, aggregation of suspended particles and their local accumulation had been observed at nodes of standing waves, similar to dust figures in the famous Kundt experiments [218]. This phenomenon, called the acoustical or sonic coagulation of aerosols, attracted the attention of investigators and, in the following years, special experiments had been conducted in England, Germany, and the Soviet Union.

Andrade conducted an experimental study of suspended particles' behavior in sound fields and established that the smallest particles actively participated in the vibrating motion of the gaseous medium [141]. Conversely, gas flowing around larger particles became turbulence centers of the medium, spiralled and zigzagged in the coagulation vessel. At the same time, aerosol particles participated in the circulating motion of the gas medium in the node-antinode region. Moreover, local particle concentration was observed not only at the nodes near the vessel walls, but also at the antinodes where the particles concentrated in the form of special discs [142]. The author concluded that the prime force behind the acoustical coagulation of aerosols was the hydrodynamic attraction of particles, which König [215] previously investigated theoretically, and which Rayleigh [107] noted as one of the reasons for the dust "ridges" formation in Kundt's tube. Using König's attraction force equations, derived on the assumption of the potential flow of acoustical current around a sphere, and on the experimental study of the kinetics of acoustical coagulation of magnesium oxide aerosols at high ultrasonic frequencies carried out by Parker [90], Andrade [2] postulated a mathematical theory of the process of acoustical aerosols coagulation. However, in so doing he made serious basic errors, which caused his theory to be rejected immediately after its appearance [34].

The most thorough investigations were made by Brandt, Freund, and Hiedemann [1, 9, 163, 167, 168, 170, 200]. These authors studied experimentally coagulation of aerosols (tobacco smoke, ammonium chloride, paraffin oil vapor) under static and dynamic conditions at different acoustical frequencies. They established that coagulation of these occurred more readily at audio frequencies than at high ultrasonic frequencies, which Andrade and Parker used in their experiments.

The authors confirmed the relationship between the amplitude of vibrating particles and their size by means of a movie camera, and theoretically derived an approximate equation for the degree of particle entrainment in the medium vibration, having established by calculation that the flow around aerosols in the sound field was predominantly viscous.

Being more descriptive than the corresponding König's equation [214], the new equation revealed the dependence of the particle vibration amplitude and phase displacement on their size and density and on the medium viscosity and vibration frequency. This enabled the authors to show another effect which enhanced aerosol coagulation, namely, the collision of small, actively vibrating particles with the larger but slower ones (orthokinetic effect). The authors assumed that precisely this effect played the leading role in the process, and introduced their theory of orthokinetic coagulation of aerosols in the sound field [1, 167].

In his dissertation [161], one of the authors, Brandt, demonstrated that the rate of acoustical aerosol coagulation was a linear function of the calculated particle concentration, thus advancing a strong argument in favor of the orthokinetic theory. Soviet scientists S. V. Garbachev and A. V. Severnyi [26, 195] conducted original studies on the elementary process of hydrodynamic interaction of water droplets suspended on glass threads in a sound field. The authors established that ponderomotive forces of attraction or repulsion developed between the droplets under the effect of sound which were similar to those arising in the flow. The ponderomotive effect of sound waves on large bodies in liquids was previously investigated by P. N. Lebedev [64]. A. B. Severnyi [109] tried to calculate ponderomotive interaction of droplets in sound fields on the basis of the hydrodynamic theory advanced by

Bjerkness [146], which allowed for their virtual pulsations. However, Severnyi failed to account for all parameters of the problem. As a result, his equation, derived for the time required for the drops to coalesce, proved to be theoretically and practically worthless.

Following experiments conducted in the 30's, which contributed considerably to the theory of acoustical coagulation of aerosols and which demonstrated the high effectiveness of the process, interest towards theoretical studies abated and attention of investigators turned to the clarification of practical possibilities for the utilization of discovered phenomenon. The first possibility, to utilize the coagulating action of sound in the dispersion of natural water mists, was demonstrated by Amy in 1931, and patented in the USA in 1934 [139]. The following years, the second possibility - utilization of the coagulating action of sound for the intensified purification of industrial smokes, dust, and fogs [164, 165, 166, 169, 177, 204], was secured by the corresponding patents.

In 1938, Gies (Lurgi Co., Germany) conducted unsuccessful experiments on the purification of dust-containing industrial gases [193], using whistles and a magnetostrictive projector as the sound sources. The specific power consumption used in the aerosol sonication was a hundred times as great as the power consumed in purifying the gases by other known methods. The main reason for the low efficiency of the process rested in the extremely low acoustical efficiency of sound sources used in the experiments (several percent). In the meantime, St. Clair (U.S. Bureau of Mines) while investigating acoustical coagulation of aerosols, mainly ammonium chloride [179, 181], developed a new electrodynamic acoustical generator (with a resonating core) with which efficiencies of the order of 20 - 30% could be obtained at high frequencies [178]. However, his acoustical generator was of little use for industrial purposes, since its effectiveness at lower frequencies was lowered sharply; other shortcomings confined its use to the laboratory only.

During the following years, which coincided with World War II, vigorous attempts had been made in the USA to build a powerful, highly efficient siren-type sound generator for special purposes specified by the U.S. Navy for the dispersion of fog on airfields. Using the electromechanical analog method, Jones developed the dynamic siren theory [208], which had the possibility of attaining high acoustical efficiencies. Unfortunately, the value of Jones' work was not fully appreciated in other countries and, therefore, many siren models built during subsequent years were frequently beyond criticism with respect to their efficiency.

Based on Jones' theory and calculations, Chrysler Corporation built the "Victory" sirens, having a sound power which attained 50 hp at acoustical efficiency of 70 - 90% [208]. With these sirens Lamer and Sinclair [266, 156*] conducted experiments in 1943 on the acoustical dispersion of natural fog at the Lanken airport in Cincinnati, Ohio. Positive results were obtained under calm weather conditions when the runways were sonicated for approximately one minute. The same investigators conducted previously a series of experiments on the dispersion of artificial water vapor. Experiments conducted on laboratory and larger scales brought positive and negative results, the latter due to the inappropriate selection of sound frequencies. Loudspeakers and small sirens made by the Federal Electric Company were used as sound sources. The same year Lamer, Sinclair, and Brescie [156]* conducted experiments on the acoustical dispersion of sea fog in Sandburg, California at high wind velocities (5 - 6 m/sec). However, the acoustical power of eight "Victory" sirens was insufficient to attain the desired visibility under such unfavorable conditions.

During post-war years, the USA Ultrasonics Corporation introduced series of siren models with efficiencies of 40 - 60%. This turned investigators to experimental work on the intensification of industrial gas purification. In 1947 the same firm built the first experimental unit for the recovery of highly dispersed carbon black [254, 184, 272]. It consisted of an acoustical coagulation chamber and two series-connected inertial precipitators - cyclones. This kind of combined dust-droplet trapping units will be referred to henceforth as acousto-inertial.

Experimental data on the first acousto-inertial unit proved to be very encouraging, which enhanced further experiments on recovering other industrial byproducts such as: sulfuric acid vapors, anhydrous sodium carbonate, molybdenum sulfite, cement dust, open-hearth furnace dust, flying cinders, and others [183, 184, 186, 216, 240, 241, 269, 273, 281]. Acoustical parameters, such as sound intensity, frequency of vibrations, sonication time, which determine the effectiveness of acoustical coagulation of different industrial aerosols, had been established during these experiments. In particular, it became apparent that there existed an optimal vibration frequency for each aerosol at which the process proceeded most efficiently. A strong dependence of the effectiveness of acousto-inertial precipitation on the physical characteristics of aerosols, such as degree of dispersion, gravimetric concentration of particles, etc., was discovered. It became clear that 1) highly dispersed aerosols possessed the best acoustical coagulability, even though they required higher sound intensities in order to effect consolidation of original particles in a short time to a size which could be effectively precipitated by inertial precipitators; 2) weakly concentrated aerosols possessed a lower acoustical coagulability, despite the fact that a highly intensifying action could be attained in this case by injecting atomized water ("sprinkling") which was not always applicable; 3) residual concentration of particles was considerable; etc.

---

* Reference [156] does not correspond to these authors [B.S.L.]

These conditions considerably narrowed the field of industrial application of the acousto-inertial method of aerosol precipitation. However, no serious attempts had been made to develop the process [203, 204, 264]. This may have been due to the fact that investigation was limited to practical applications only. Theoretical studies, without which planned development of technological processes is unthinkable, were completely neglected. Almost no experiments had been conducted during that period in the USA on the theory of acoustical coagulation of aerosols. The one exception was a study by St. Clair and his co-workers on the drifting of aerosol particles under the effect of radiational sound pressure [179, 181]. Using King's equation for the radiational pressure on a sphere immersed in a non-viscous medium [212], St. Clair derived the equation of a sphere motion in the direction of nearest antinode. St. Clair concluded that the radiational sound pressure was, indeed, the decisive factor in the intensive coagulation of aerosols in a sound field [179]. However, elementary calculations failed to corroborate the case in question [73]. Moreover, Westervelt's work, which appeared shortly thereafter, and which dealt with non-periodic ("constant") forces acting on particles suspended in the sound field [286], cast a doubt on St. Clair's equation. Westervelt showed that in addition to the radiational pressure, much more significant viscous forces acted upon suspended particles. These depended on periodic variations in the medium temperature. Also attendant were forces associated with unavoidable waveform distortion of finite-amplitude waves.

In view of the significant limitations imposed on the application of the acousto-inertial method of aerosol precipitation, which became apparent in the course of experimental work, the proposed method received industrial acceptance only in isolated cases, such as sulfuric acid vapor, anhydrous sodium ashes, sodium carbonate, molybdenum sulfide, etc. This greatly reduced the interest among the U.S. industrialists in the organization of experimental works, and, after 1951 - 1952, experiments in this direction were almost completely discontinued.

However, in other countries, the interest in the new method gradually increased from year to year. Experiments had been conducted in the Soviet Union, Hungary, German Federal Republic, Japan, Poland, Austria, France, and Czechoslovakia. The first study of the acousto-inertial precipitation of industrial aerosols was conducted in the USSR by P. A. Kouzov at the Leningrad Institute of Labor Protection (LIOT) in 1950 - 1951. Experiments had been conducted on the precipitation of aggregated light ashes trapped by means of electrofilters of power-plant boilers and emitted into the air by mechanical atomization. These, and other [193, 73] experiments, had indicated that aggregated aerosols possessed infinitesimal acoustical coagulability. As a result of this it is suggested that investigation of the coagulating effect of sound should be conducted with natural aerosols only. It must not be accepted that Schnitzler's (Lurgi Co., GFR) clearly negative conclusions about the method [262], which were based on experiments with the acousto -inertial precipitation of aggregated magnesium- and aluminum-oxide aerosols were well founded. Following the unsuccessful Baker soot coagulation experiments conducted at the VNIIGAZ (Kh. Grigoryan [29]), the present author obtained positive experimental results with acousto-inertial precipitation of artificial oil vapor [73, 74], conducted at the Moscow Institute of Energetics during 1953-1955.

The coagulating effect of sound was tested in Hungary in connection with the intensification of gravitational precipitation of cement dust directly in the smoke stack (Tarnoczy and Greguss [275]). Extensive experiments on the acousto-inertial method of precipitation of industrial aerosols had been conducted in Japan in 1950-1954 (Oyama, Inoue, Sawahata, and Okada [246, 38]). Japanese investigators experimented with the acousto-inertial precipitation of zinc, carbon black, coal tar, cracking-gas condensate, and obtained positive results for the last two aerosols. As a result of their experiments the authors established some empirical relations characteristic of said process. In particular, exponential dependence of final particles' concentration on the specific power consumption and the sonication time had been established. The authors participated in the construction of an industrial acousto-inertial plant for purification of cracking gas in Tokyo in 1952 [259].

Considerable interest was aroused by a study of the acousto-inertial precipitation of zinc oxide sublimates, conducted during the same period in Poland at a metallurgical plant in Szopenice (Maczewski, Rowinski and others [227, 228, 229, 92]. The experiments yielded good acoustical coagulability of zinc oxide sublimates. However, they also revealed that, as a result of the periodic decrease in their concentration in furnace gases, the final average particle concentration exceeded the allowable limits for toxic aerosols.

Experiments had been conducted in Austria on the acousto-inertial precipitation of ferric and cobalt oxides and others (Jahn [206]). Experiments indicated the need to maintain a given critical precipitators' velocity, above which an intensive disintegration of dry aggregated particles began. Subsequently, experiments had been conducted in France on the acoustical dispersion of artificial water vapors and the acousto-inertial precipitation of smoke. A positive effect of aerosol sonication by sound waves of different frequencies (produced by a static siren of the "Multiwhistle" type built by Boucher [148, 149, 150, 151]) was demonstrated by experiments in acousto-inertial precipitation of smoke from carbide furnaces (Boucher [150, 151]). Flue gases, artificial water vapor, etc., had been subjected to acousto-inertial precipitation in Taraba, Brzica [274], Czechoslovakia.

The above cited experimental studies helped to advance the knowledge in the field of acoustical coagulability of industrial aerosols; they also increased the uncertainty concerning the commercial capacity of the process due to low efficiency of the sirens used. Moreover, the same studies had been conducted for practical purposes in most cases. Nonetheless, the mechanism of the process of acoustical aerosol coagulation remained unexplained as before, and this inhibited further development of the process.

In the course of following years, Soviet scientists attained definite progress in clarifying that mechanism. During 1954-1955, the present author conducted a critical analysis of theoretical hypotheses on the mechanism of aerosol coagulation. The analysis was based on materials available at that time; it was concluded [73, 74] that none of the available materials offered a satisfactory explanation of the phenomenon. The orthokinetic interaction associated with irregular motion of particles was acknowledged as the only viable coagulation system. This system is still valid today in spite of the fact that many previous ideas about the behavioral rules governing aerosols in a sound field lost their validity.

S. V. Pshenai-Severin showed [103] that if aerosol interaction in a sound field was considered, it became necessary to proceed from the viscous flow concept described in terms of Oseen's hydrodynamic theory, which partially takes into account the inertial terms of the equation of the medium motion. In view of this, Bjerkness' and König's formulas, which were introduced into the potential flow assumptions and which were used earlier to describe the hydrodynamic interaction forces acting on spheres, were found unsuitable for the calculation of attraction forces between aerosols present in a sound field. Pshenai-Severin established that a longitudinal attraction occurred between aerosols in a sound field which was similar to the hydrodynamic attraction between cloud droplets [101, 102, 104, 250]. This form of interaction will be referred to henceforth as the attractional interaction.

Using Oseen's concept of flow around aerosols in a sound field, the author of the present monograph found that hysteresis came into action in the case of small obstacles [81]. As a result, particles of the vibrating medium assumed a zigzag motion with respect to particles around which the flow occurred. Moreover, a special acoustical flow occurred around each aerosol. In another treatise [82], the present author showed that in the case of orthokinetic aerosol interaction in the sound field selfcentering of aerosols took place, as a result of which trapping probability increased. Parallel to selfcentering, a reverse effect appeared possible for a given aerosol distribution. This effect will be referred to as the self-decentering of aerosols. Both phenomena represent a new form of aerosol interaction in a sound field. The effect, referred to in this book as the parakinetic aerosol interaction depended on the flow hysteresis of the medium around the particles, and on the particle inertia. A high-speed microfilm of the aerosol behavior in a sound field was taken recently by O. K. Eknadiosyants and L. I. Buravyi at the Acoustics Institute of the Soviet Academy of Sciences [12]. The study revealed the formation of spatial aerosol aggregates, which proved implicitly the existence of parakinetic interaction.

Podoshevnikov's experimental study of acoustical coagulation of highly dispersed dioctylphthalate is of interest [94]. He established the existence of an exponential relationship between the quantitative concentration of droplets and the sound pressure exerted during sonication time. This agreed with Inoue's conclusions [37] based on his experimental study of acoustical coagulation of tobacco smoke conducted by Brandt, Freund, and Hiedemann. Transformation of the dispersed composition of droplets, which occurred during acoustical coagulation of a fog, was investigated [95]. In collaboration with V. A. Gudemchuk and B. D. Tartakovskii, the author established [30] the existence of a negative effect of longitudinal partitions in the coagulation chamber on the rate of acoustical coagulation of the fog, which the authors associated with the observed attendant decrease in the medium turbulence. This observation definitely refuted P. N. Kubanskii's concept concerning the expediency of developing precipitational surfaces in the coagulation chambers [48, 49]. The same was theoretically disproved earlier in the work of this author [73]. However, contrary to assertions in [30, 93], there appeared no doubt that orthokinetic particle interaction played a leading role in the process of acoustical aerosol coagulation. In view of differences in the phase displacement angles of particle vibration with respect to the medium, instantaneous aerosol velocities became discernible even at insignificant differences in the degree of particle entrainment by the vibrating medium. Since all aerosols were polydispersed to a degree, ortho- and parakinetic interactions in a sound field were not an exception but a rule.

In an earlier work [83], in which the acoustical turbulence theory was developed, the present author showed that turbulent pulsations which occurred in the sound field were capable of rapidly drawing aerosol particles to distances at which self-centering and, subsequently, orthokinetic effects took place (a concept that Brownian motion was a leading factor of diffusion in the aggregated volume of particles, was refuted by this author earlier [76].

For better understanding of aerosol behavior in a sound field, the work by S. S. Dukhin [35] may be of interest. Dukhin presented a theory of aerosol drift into the node of a standing wave, which depended on the attendant asymmetry of vibrating motion of the medium particles. This problem was approximately solved earlier by A. D. Bagrinovskii [4], who unfoundedly considered this effect as the leading factor in acoustical aerosol coagulation.

In addition to the above cited theoretical works, many experiments had been conducted in the Soviet Union during recent years on the acoustical coagulation and precipitation of industrial aerosols, in which new systems had been tested. One of these consisted of a combination of an acoustical coagulator and a fabric filter, which permitted to obtain low residual particle concentrations at an increased rate of gas filtration. The system was first tested in the precipitation of borehole dust by P. Sh. Shkol'nikova ("Gipronikel'," Leningrad) [130, 131, 132, 300] and was received favorably by industry.

V. P. Kurkin (NIIOGAZ), while working on acoustical coagulation of highly-dispersed oil burner soot, investigated the following system: acoustical coagulator followed by two cyclones and a glass-fiber filter [54, 57, 298]. Kurkin established that the system was more efficient than the known "Canadian" system. In the course of investigation, the author designed a new gas jet radiator [53, 55, 56], the acoustical efficiency of which was higher than that of similar radiators built earlier. At the present time, installation of an experimental-industrial unit, of similar design, is being completed at one of the Soviet carbon black plants. The system had been tested on the "Promenergo" equipment built at a bronze-brass plant for the extraction of zinc oxide sublimates [23, 299].

It is now proposed to classify the acoustical coagulators as a class of dust catching devices which might also include turbulent, condensating, and electrical coagulators [59]. Acoustical gas separators for low temperature separation of natural gas condensate, now being tested experimentally, are of great interest [79, 84]. A portion of the natural gas excess pressure is being used in generating sound, and, therefore, the question of economy is of no importance. This idea had been tested first at one of the natural gas deposits in the Volgograd region [86]. The prospect of applying the acoustical method in the gas industry is favorable; however, serious efforts are required to overcome different problems. Interesting possibilities are being opened by the graduated method of acoustical aerosol coagulation [77, 78]. According to this method, coagulable aerosols are passed through series of coagulation chambers in which they are exposed to the action of acoustical vibrations with a gradually diminishing frequency optimal for each stage of particle coagulation.

Another method, described in [76], is also of great interest. In this method, aerosols are sonicated in an electric chamber, into which charged droplets of water or other liquid have been previously introduced. The droplets convey the dust settled on them toward the precipitating electrodes. The method, called the electrostatic, combines the coagulation and precipitation of aerosols.

Original experiments on the application of acoustic coagulation for the purpose of rain-making had been conducted by the El'brus Combined High-Altitude Expedition [32]. A series of additional experiments on the problem in question had been conducted in the USSR [13, 14, 15, 33, 89]. Among foreign works on the acoustical coagulation of aerosols, two proposals are of specific practical interest: 1) a patent granted to Smith [268] for a method of catalytic hydrocarbon pyrolysis in which the recovery of suspended catalysts was attained by means of acoustical coagulation, and 2) Slavik's proposal [24] to extract harmful gaseous chemical impurities by means of chemical reagents which first combined with the impurities to form suspended solid or liquid substances and, subsequently, could be precipitated by acoustical coagulation.

Recent attempts to utilize acoustical vibrations for the direct intensification of aerosol precipitation, are of great practical interest. The first proposal in this direction was patented by Westervelt and Sieck [290]. The proponents described a method of aerosol separation by specially profiled sirens which generated distorted waveforms, for which the maximum particle drift velocity was attained. Asklöf proposed a sonic droplet trap [301], in which the process of mist filtration through a porous cap was intensified by means of sonication. Asklöf's proposal opened a new phase in the acoustical dust-droplet trapping history, since it enabled to lower the residual aerosol concentration to a fractional part of mg/m^3 of a gas at a reasonable energy consumption. Boucher [147, 157] proposed to intensify the process of aerosol precipitation in the existing dust-droplet trapping devices - the Venturi scrubber and the cyclone. Sonication may be applied also to sleeve filters; Abboud [135, 157] presented a method of cleaning these by means of acoustical waves.

Interesting ideas appeared abroad also in the field of acoustical dispersion of natural mists. Boucher presented a new, so-called, thermo-acoustical method of fog dispersion from airfields [152]. His proposal consisted of a combined sonication and fog heating. He also proposed an acousto-chemical method for fog dispersion, which was a combination of sonication and atomization of hygroscopic substances in the fog [156]. This method is now being tested in France, England, Sweden, USA, and other countries. Both methods represent examples of sound utilization in the intensification of an evaporation process of a dispersed liquid phase. This possibility had been demonstrated during 1938-1942 and was based on the assumption that sound and turbulent pulsations flowed around the aerosols.

With the above in mind, Horsley and Danser [202] proposed in 1947 a method of spray drying of wet products, such as soap solution, in a sound field which, as far as is known, remained unadapted by the industry. However, stimulated by Greguss (1955), the process of sonicated drying of damp powdered materials had been developed. In this field, Boucher carried out interesting experiments [172, 153, 154, 155, 157], which are being continued by the Acoustics Institute of the Soviet Academy of Sciences [8], and other domestic and foreign scientific-research institutions. The special feature of the new method is the fact that drying was attained by a "cold" process without increasing the material temperature. This is invaluable in a case of drying heat-sensitive materials.

Up to now, sonicated drying had been tested on the following hard-drying materials: cellulose, carboxyl-methyl, titanium dioxide, colloidal zirconium hydroxide, silica gel, heat-sensitive ferments and hormones, cellulose ethyl, etc. In view of the excellent results obtained with acoustical drying of materials, this method can be recommended now for industrial application.

Greguss [28, 196] conducted interesting experiments on the combustion intensification of atomized liquid fuels in metallurgical furnaces used for smelting malleable cast iron; he used in the process a combination whistle-atomizer of his own design and obtained satisfactory results.

Intensification of other physicochemical processes taking place between dispersed and gaseous phases had also been tried. Thus, as early as 1947, Richardson [256] proposed the use of ultrasonic vibrations for the intensification of ammonia synthesis in the presence of suspended iron catalyst. Carlström [7] pointed out the possibility of intensification of the amalgamate condensation process used in dentistry. Investigations at the Universal Aniline Company (USA) proposed a process of forming finely dispersed carbonyl iron in the course of thermal decomposition of pentacarbonyl iron in the sound field. However, as far as known, their proposal failed to find practical applications.

Experiments on fluidization of powdered products (gypsum and others) [237, 217] and the generation of aerosols [134, 207, 270] by sonic and ultrasonic vibrations had been conducted. However, the above processes are based on entirely different physical effects and, therefore, will be considered briefly.

For the same reason the practical use of aerosol sonication will not be discussed. The latter had been used to determine the following: vibration amplitude of a gaseous medium [226, 173, 140, 141, 143, 263], acoustical waveform [191], acoustical currents [140], sound field near an absorbing surface [234], dispersed aerosol composition [174, 198], aerosol concentration, and many other parameters.

CHAPTER 2

MOTION OF AEROSOL PARTICLES IN A SOUND FIELD

4. PRELIMINARY INFORMATION

Solid or liquid particles suspended in a gaseous medium are characterized by high mobility. Sufficiently small particles ($r < 1\mu$) give rise to intensive Brownian motion; larger particles settle down to different degrees by their own force of gravity. In the presence of temperature gradients in the medium, generally occurring in large volumes, the suspended particles are carried off by the convectional flow of the medium. In addition, particles are absorbed in the turbulent flow by the medium's turbulent pulsations. In long cylindrical gas pipes, the particles spiral out toward the circumference [121]. In addition to the enumerated motion forms, particles of a sonicated gaseous medium migrate in series of movements of more complex and intensive nature, due to the following: 1) in one way or another, particles participate in oscillatory motion of a gas; 2) they propagate forward and drift under the influence of secondary effects, such as radiation pressure, asymmetry of the acoustical waveform, etc.; 3) they are carried off by the advancing circulating motion of the sonicated medium, the so-called acoustical wind, and, at the same time, participate in its turbulent pulsations; and 4) they perform complex motions which depend on the hydrodynamic parakinetic and attractional interaction with the neighboring particles. In addition, the suspended particles have a rotational motion, although this phenomenon is disregarded here, because it lies outside the scope of the problem at hand.

The relationships for the first three types of aerosol motion in an acoustical field will be analyzed in the succeeding paragraphs of this chapter. Particle motion caused by their mutual interaction will be examined separately in paragraphs 10 and 11 of Chapter 3. Only those types of aerosol motion in the acoustic field will be examined first which are not constrained by the presence of other particles. For all practical purposes, this occurred only in the infinitely rarefied, i.e., loosely concentrated, aerosols.

Before proceeding with the concrete analysis of each type of aerosol motion in an acoustical field, the following is noted: the aim of the subsequent sections of this chapter is to derive and analyze equations which corresponded to a type of aerosol motion and which determined their spatial and temporal displacement as a function of the physical parameters of the particles and the medium. In all such cases, as also in the entire field of hydrodynamics, analysis is based on Newton's second law:

$$m_p \frac{d^2 x_p}{dt^2} = F' + F'', \tag{4.1}$$

where m_p, x_p, and t are, correspondingly, mass, absolute displacement, and time necessary for particle displacement; F' is the "static" force acting on the particle which exists independently of particle displacement (this force owes its origin to the presence of pressure gradients in the acoustical field, the forces due to radiation pressure, etc.); F" is the "kinematic" force associated with the occurrence of a relative motion between particles and medium, i.e., the leading or lagging particle motion with respect to the medium. This force depended mainly on the nature of the medium flow around the particles. The flow, as is known, determined the Reynolds number $Re = 2ru_{gp}/\nu$, which described the relationship between the inertial (numerator) and the viscous (denominator) forces (see [100], p. 209). For small Reynolds numbers ($Re<1$), when the inertial forces are small in comparison with the viscous forces, the braking action of the streamlined body surface penetrated the medium to a considerable depth. A unique envelope formed around the body from the retarded boundary layer of a gas, the thickness of which, as it will be shown in Section 9, may exceed the aerosol size considerably. Such is the physical picture of the so-called viscous body flow. When the Reynolds number is increased, the inertial forces begin to prevail over the viscous forces of the medium, and the described picture changes; the gas boundary layer becomes progressively thinner, until it finally disappears completely. In this case, the viscous losses and the related effects of turbulence can be disregarded. A, so-called, potential body flow regime sets in. The difference between the viscous and potential states of a streamline flow around spherical objects is well illustrated in Figure 45 of the well-known N. A. Fuchs monograph [121].

The state of a streamline flow around aerosols developed in oscillatory medium under the normally applicable sound field parameters will be determined first. The maximum possible velocity of flow around aerosols in a sound field represented the peak value of the medium's oscillatory velocity. All other motion forms have velocities known to be smaller, since they have been produced by secondary effects, "sustained" by oscillatory motion energy. The amplitude of oscillatory velocity U for a "normal" sound intensity of the order of 0.1 watt/cm^2 is equal to 220 cm/sec. The maximum particle radius which corresponded to this velocity, for which Re = 1, equals $r \approx 3.5\mu$ for air ($\gamma = 0.15$). The radius of aerosols which tend to coagulate is usually less than $r = 3 - 5\mu$. For the greater portion of the oscillation period this corresponded to Re<1. Therefore, in order to evaluate all forms of aerosol motion in a sound field, it is usually possible to proceed from the viscous flow. Only in the high-intensity sound field is it necessary to take into consideration the streamlined flow around large aerosols, approaching the potential flow.

Generally speaking, all forms of aerosol motion examined below are irregular in nature. In this case, the hydrodynamic theory provided the following general expression for the force F" caused by the relative motion of the spherical particle in a viscous medium with an arbitrarily variable velocity u_{gp} ([160], p. 224; [61], p. 121; [111], p. 349; [121], p. 76; [108]:

$$F'' = \frac{2}{3}\pi r^3 \rho_g \frac{du_{gp}}{dt} + 6\pi\eta r u_{gp} + 6\sqrt{\pi\eta\rho_g}\, r^2 \int_{-\infty}^{t} \frac{du_{gp}}{dt_1} \frac{dt_1}{\sqrt{t - t_1}} \,. \quad (4.2)$$

In this equation, the first term contains that portion of the total force which is caused by direct transfer of momentum between the particles and the medium, achieved without the participation of viscous forces, i.e., in the same manner as in an ideal medium. This term is equal in magnitude to one half of the inertia force of the medium mass displaced by the particle ([61], p.52 - 53). This term may be disregarded as a rule because of the low gas density in relation to the particle density (an exception is an aerosol under very high pressure, natural gas, for example).

The second term in (4.2) represents the force caused by the relative motion of the viscous medium with a velocity equal to its velocity at time t. This constituted usually the main component of the force F". The third integral term in (4.2) expressed the inertial portion of force F", which is caused by the nonuniform motion of the viscous medium. Its value depended essentially on the prior motion of the particle, namely, on the acceleration at prior times t_1. When the velocity varied slowly, i.e., when the acceleration du_{gp}/dt was small, the integral term may be disregarded. In this case, the expression for the kinematic force acting on the particle was as follows:

$$F'' = 6\pi\eta r u_{gp}, \tag{4.3}$$

which is the well-known Stoke formula derived on the assumption of stationary flow of the viscous medium around a sphere. When Reynolds number is increased (Re>1), a correction factor by Oseen (1+3/16 Re) must be added to the formula. This, however, should be avoided, if possible, since it introduces a square velocity term which makes the solution of the differential equation for the particle motion difficult. The term "slow" variation of the acting force implied that variation of duration T was longer than the particle relaxation time τ, given by the following expression:

$$\tau = \frac{2}{9}\frac{\rho_p}{\eta} r^2. \tag{4.4}$$

This parameter, widely used in aerosol mechanics, characterized the rate at which equilibrium in the system "particle-medium" was reestablished, and it determined the particle sensitivity to variations in the forces acting on the particle. This is not surprising, since the given expression was the result of dividing the momentum acquired by the particle $m_p u_{gp}$ by the Stokes' force $F_{st} = 6\pi\eta r u_{gp}$.

Relaxation time of coagulating aerosols is very short. For a unit density ($\rho_p = 1$) in the atmospheric air ($\eta = 1.85 \times 10^{-4}$) it takes on the following values:

for $r = 0.1\mu$ $\tau = 1.2 \times 10^{-7}$ sec
for $r = 1.0\mu$ $\tau = 1.2 \times 10^{-5}$ sec
for $r = 10\mu$ $\tau = 1.2 \times 10^{-3}$ sec

It follows that the shorter was the particle relaxation time, the faster the particle acquired the new velocity value in relation to the medium. The new value corresponds to the instantaneous magnitude of the force acting on the particle.

If the relaxation time was small as compared with the medium velocity period, the particle barely departed from instantaneous medium velocity values which corresponded to the time-varying acting force. In hydrodynamics, this motion is referred to as quasistationary.

A general solution of the integro-differential equation for the nonuniform motion of spherical particles in an irregularly moving medium, obtained by substituting the expressions for F' and F" into (4.1), has been derived by Tchen [175, 122*] only recently.

---

* Reference does not correspond to Author [B.S.L.]

5. VIBRATORY MOTION OF AEROSOL PARTICLES

Particles suspended in a vibratory gaseous medium are carried away by the medium's motion, if they are sufficiently small. The degree of each particle entrainment, i. e., the ratio between the particle and medium displacements (or velocities), depended to a great degree, on the physical parameters of the particle and the medium. The exact theoretical solution of this problem was offered by König [214]. Later, this problem was given a brief treatment by Sewell in [265]. The same problem was also examined by S. M. Rytov, V. V. Vladimirskii, and M. D. Galanin [108]. The problem applicable to real aerosols coagulated in a sound field was reanalyzed by Brandt, Freund, and Hiedemann [167]. A thorough analysis of the problem of vibratory aerosol motion in a sound field was presented by N. A. Fuchs [121] in a monograph with supplements and correction presented in a subsequent review [122]. The corresponding equations for aerosol motion will now be formulated.

A "static" force acting on a particle in a given case is caused by the presence of a medium pressure gradient. It can be easily understood that the magnitude of this force was entirely independent of the particle density. Assume that the latter was exactly equal to the medium density. In this case, the particle with the velocity u_g must move together with the medium. The force capable of bringing about this type of particle motion is equal to the product of the particle mass and its acceleration. The mass of this particle is equal to the mass of the displaced medium m_g, and its acceleration is equal to the acceleration of the medium du_g/dt. The corresponding "static" force is

$$F' = m_g \frac{du_g}{dt} \tag{5.1}$$

The "kinematic" force, which varies periodically with frequency ω, instead of being expressed by the general equation (4.2), may be expressed by the following equation derived by Stokes ([61], p. 811; [121], p. 85):

$$F'' = -m_g\left(\frac{1}{2}+\frac{9}{4}b\right)\left(\frac{du_p}{dt}-\frac{du_g}{dt}\right)-\frac{9}{4}\,m_g\omega b(1+b)(u_p-u_g), \tag{5.2}$$

$$b = \frac{1}{r}\sqrt{\frac{2\nu}{\omega}} = \frac{\delta_{\text{погр}}}{r}.$$

(where only the relative velocity between the particle and medium is used instead of the absolute velocity of the particle as set in [61] and [121]).

The equation of motion for the particle in the oscillatory medium including (5.1) and (5.2) is as follows:

$$m_p \frac{du_p}{dt} = \frac{3}{2} m_g \frac{du_g}{dt} - \frac{1}{2} m_g \frac{du_p}{dt} - \frac{9}{4} m_g \omega b (1 + b)(u_p - u_g) -$$

$$- \frac{9}{4} m_g b \left(\frac{du_p}{t} - \frac{du_g}{dt} \right). \qquad (5.3)$$

Assume:

$M = m_p + \frac{9}{4} m_g b$ **(M - "reference mass"),**

$\frac{1}{B} = \frac{9}{4} m_g \omega b (1 + b) = \frac{9}{4} m_g \omega b + 6\pi\eta r$ **(B - "reference mobility"). Substituting these notations and disregarding the term $\frac{1}{2} m_g \frac{du_p}{dt}$, we obtain:**

$$M \frac{du_p}{dt} + \frac{u_p}{B} = \frac{9}{4} m_g \omega b (1 + b) u_g + \left(\frac{9}{4} m_g b + \frac{3}{2} m_g \right) \frac{du_g}{dt}. \qquad (5.4)$$

If the medium vibratory motion is expressed by the following equation:

$$u_g = U_g \sin \omega t, \qquad (5.5)$$

Then, after some transformations, equation (5.4) becomes as follows:

$$M \frac{du_p}{dt} + \frac{u_p}{B} = \frac{3}{2} m_g \omega U_g \sqrt{1 + 3b + \frac{9}{2} b^2 + \frac{9}{2} b^3 + \frac{9}{4} b^4} \sin (\omega t + \theta), \qquad (5.6)$$

where

$$\theta = \operatorname{arc\,tg} \frac{2/3 + b}{b (1 + b)}. \qquad (5.7)$$

The solution of this equation is as follows [39]:

$$u_p = U_g \sqrt{\frac{1 + 3b + \frac{9}{2} b^2 + \frac{9}{2} b^3 + \frac{9}{4} b^4}{a^2 + 3ab + \frac{9}{2} b^2 + \frac{9}{2} b^3 + \frac{9}{4} b^4}} \sin [\omega t - (\varphi - \theta)], \qquad (5.8)$$

where

$$a = \frac{2}{3} \frac{m_p}{m_g} + \frac{1}{3} \approx \frac{2}{3} \frac{\rho_p}{\rho_g}.$$

For sin [ωt - (φ - θ) = 1, the particle velocity attains its peak value $u_p = U_p$; whence, the degree of particle entrainment is determined by the following formula:

$$\mu_p = \frac{U_p}{U_g} = \sqrt{\frac{1 + 3b + \frac{9}{2} b^2 + \frac{9}{2} b^3 + \frac{9}{4} b^4}{a^2 + 3ab + \frac{9}{2} b^2 + \frac{9}{2} b^3 + \frac{9}{4} b^4}}. \qquad (5.9)$$

The phase shift between the particle and medium vibrations is equal to:

$$\operatorname{tg}(\varphi-\theta)=\frac{\frac{3}{2}(a-1)(b+b^2)}{a\left(1+\frac{3}{2}b\right)+\frac{3}{2}b+\frac{9}{2}b^2+\frac{9}{2}b^3+\frac{9}{4}b^4}. \qquad (5.10)$$

It is, thus, seen that expressions obtained by the exact solution of the aerosol motion problem become complex and involved; as a result, the relationship between the degree of particle entrainment and the phase shift of vibrations, and the physical parameters of the particle and medium, remain unclear. Thus, the approximate solution of the problem given by Brandt, Freund, and Hiedemann appears to be very useful and, at the same time, it provided a degree of accuracy sufficient for all practical purposes. The approximate solution of the problem needs to include only the viscous forces given by Stokes' equation (4.3):

$$m_p\frac{du_p}{dt}=6\pi\eta r(u_g-u_p). \qquad (5.11)$$

Include equations (5.5) and (4.4) and obtain the following equation:

$$\tau\frac{du_p}{dt}+u_p=U_g\sin\omega t. \qquad (5.12)$$

The general solution of this equation has the following form [36]:

$$u_p=\frac{U_g\sin(\omega t-\varphi)}{\sqrt{1+\omega^2\tau^2}}+\frac{\omega\tau U_g}{1+\omega^2\tau^2}e^{-\frac{t}{\tau}}, \qquad (5.13)$$

where the phase shift φ is determined by equation:

$$\operatorname{tg}\varphi=\omega\tau. \qquad (5.14)$$

The phase shift angle between the medium vibrations and the entrained particle can be explained by the fact that each particle had inertia which caused it to be entrained into the medium's motion with a certain delay characterized by angle φ. The second non-periodic term in equation (5.13) corresponded to the initial transient stage of vibration which rapidly approached zero. Therefore, the vibratory particle motion was governed by the following equation:

$$u_p=\frac{U_g}{\sqrt{1+\omega^2\tau^2}}\sin(\omega t-\varphi). \qquad (5.15)$$

Whence, it can be seen that the degree (or the coefficient) of particle entrainment into the vibratory medium flow had the following expression*:

$$\mu_p=\frac{U_p}{U_g}=\frac{A_p}{A_g}=\frac{1}{\sqrt{1+\omega^2\tau^2}}. \qquad (5.16)$$

---

* According to the authors, this expression and (5.19) may also be derived from König's (5.9), provided some terms were disregarded. Thus, all terms in the equation may be disregarded in relation to b^4, so long as magnitude of μ_p was close to unity. When $\mu_p<1$, the magnitude of b^2 approached the order (See footnote, page 48)

In this case, the equation of the vibratory particle motion had the following form:

$$u_p = \mu_p U_g \sin(\omega t - \varphi). \qquad (5.17)$$

It should be noted that parameter μ_p is merely the cosine of the phase shift angle between the oscillations of particles and the medium

$$\mu_p = \cos\varphi, \qquad (5.18)$$

which can be seen easily if (5.14) were taken into account. If equation (4.4) were substituted into equations (5.16) and (5.14), and if $\omega = 2\pi f$, the following equations are obtained:

$$\mu_p^{\circ} = \frac{1}{\sqrt{1+\left(\frac{4\pi\rho_p r^2 f}{9\eta}\right)^2}}. \qquad (5.19)$$

$$\mathrm{tg}\,\varphi = \frac{4\pi\rho_p r^2 f}{9\eta}. \qquad (5.20)$$

If the particles were very small ($r<1\mu$), η should be replaced by factor η/Cu, where Cu is the Cunningham correction factor for the medium discreteness, $Cu = (1 + Al_g/r)$ (where A is a factor, and l_g is the mean path of gas molecules [121]). For droplets with $r = 1\mu$, $Cu = 1.086$; when $r = 0.1\mu$, $Cu = 1.86$ (Cunningham's formula did not apply to smaller values of r).

From equation (5.19) derived by Brandt, Freund, and Hiedemann, it follows that particles suspended in a sonicated gaseous medium followed the medium vibrations more accurately if their radius and density were smaller, the medium viscosity greater, and the frequency of oscillations lower. If the physical parameters of the particles and the medium were invariable (p_p and μ = coust.), the degree of particle entrainment could be determined by the product r^2f.

Figure 15 illustrates graphically the relationship between degree of particle entrainment and the particle radius in air for different frequencies

---

of a. In the first approximation all terms, with the exception of a^2 and b^4, may be disregarded. Moreover, König's formula takes on the form of equation (5.16) or (5.19). The same formula remained valid up to $\mu_p \approx 0.5$, when the disregard of term 3ab introduced significant errors.

In the present authors' opinion, the theoretical basis for König's formula becomes questionable below this boundary. It has been observed during coagulation that as soon as the vibration amplitude of enlarged particles decreased to several tenths of the amplitude of gas vibrations, the particles suddenly ceased to vibrate and often moved along highly curved trajectories, the spherical particles exhibiting zigzag trajectories, and all others - spiral.

particle density p_p = 1 gm/cm^3). It is, thus, seen that at every frequency there existed small particles which followed the medium vibrations almost exactly ($\mu_p \approx 1$), and large particles which remained almost completely unentrained by the vibrating medium ($\mu_p \to 0$). The complete entrainment of suspended particles into the vibratory medium motion was impossible, since the particles become entrained mainly by action of the viscous forces which arise only in the presence of the relative medium motion.

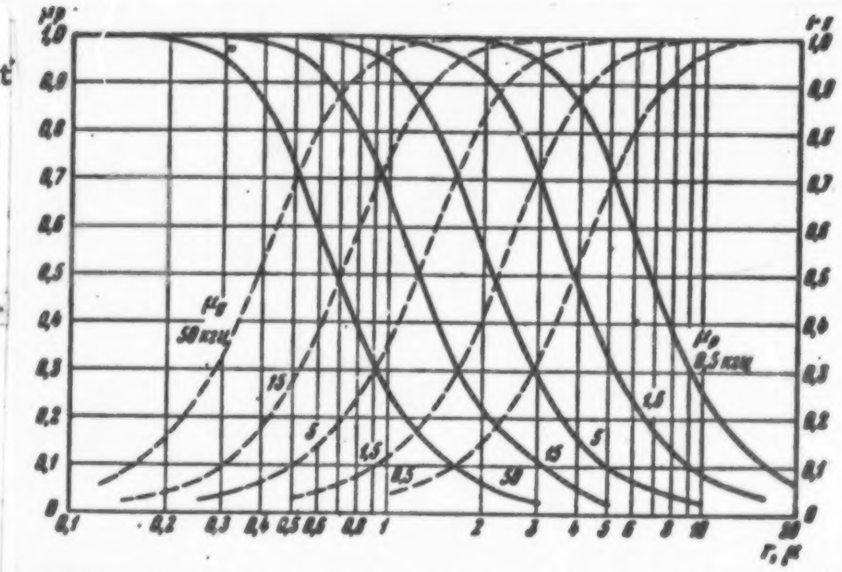

Fig. 15. Degree of μ_p involvement & degree of μ_g flow around aerosol particles in the air at different frequencies ($\rho_p = 1$ g/cm^3)

Normally, no large disagreement appeared between the degree of particle entrainment calculated from the simplified formula (5.19), and results obtained by using the exact equation (5.9). This is illustrated in Figure 16, copied from the monograph by N. A. Füchs [121], in which the solid line 1 expressed the functional dependence of the degree of entrainment μ_p on the ratio τ/T, obtained from the exact formula (5.9), and the broken line - from the simplified formula (5.19). The graph also shows the same functional dependence for the degree of streamline flow μ_g (see below). Values of $r\sqrt{\omega}$ which correspond to τ/T are given at the bottom. In both cases, the maximum range deviation $\tau/T = 0.2 - 2$ did not exceed 4%.

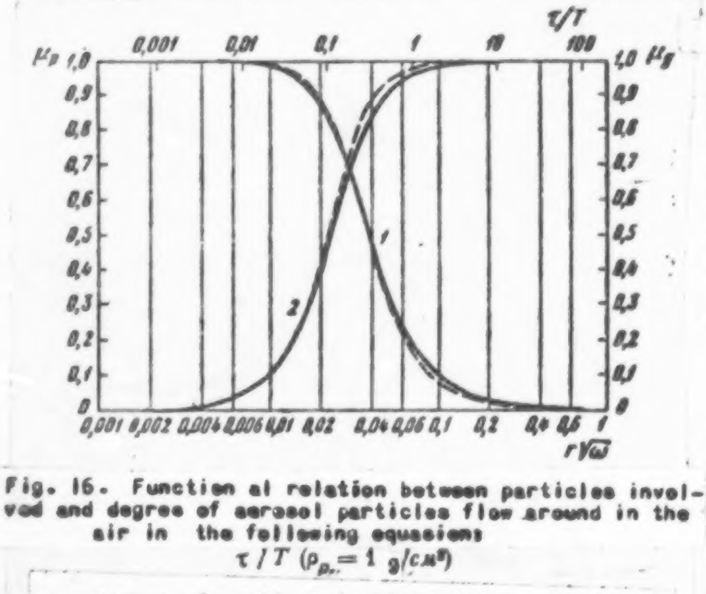

Fig. 16. Function al relation between particles involved and degree of aerosol particles flow around in the air in the following equasions

τ / T ($\rho_p = 1$ g/cm^3)

1 - Degree of particle involvement; 2 - Degree of particle flow-around

Figure 17 shows the functional dependence of phase shift angle (delay) of particle vibrations on the vibrations of air at identical frequencies. Particles totally entrained by the vibratory medium motion had a zero phase angle, and the remaining particles - $\pi/2$.

Since there is a phase shift between the particle and medium vibrations, the streamline velocity of the medium around the particles u_{gp} at any time instant t is expressed as follows:

$$u_{gp} = U_g \cdot \sin \omega t - U_g \mu_p \sin(\omega t - \varphi). \qquad (5.21)$$

Include (5.18) and perform simple transformations and get:

$$u_{gp} = \mu_g U_g \cos(\omega t - \varphi), \quad (5.22)$$

where μ_g is the streamline factor of the medium's flow around the particle which equals:

$$\mu_g = \sin\varphi = \frac{\omega\tau}{\sqrt{1+\omega^2\tau^2}}. \quad (5.23)$$

The amplitude of the streamline velocity equals:

$$U_{gp} = \mu_g U_g. \quad (5.24)$$

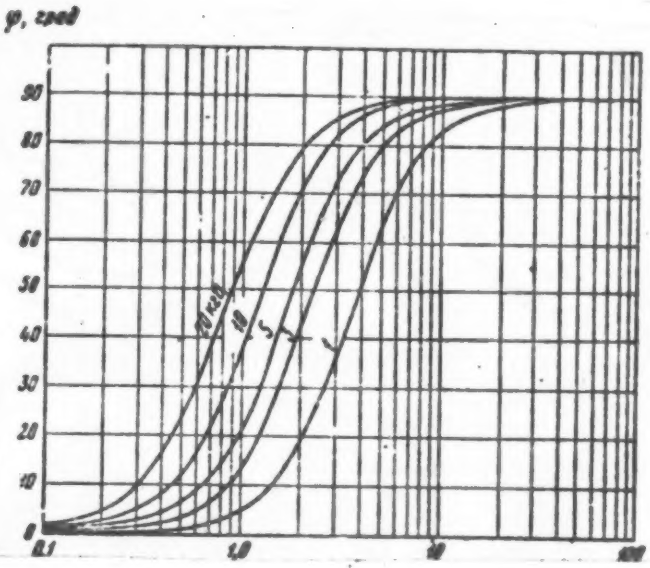

Fig. 17 Shift angle of aerosol particles φ in the air at different frequencies ($\rho_p = 1$ g/cm³).

Values of μ_g are indicated by dotted lines in Figure 15 for different frequencies. Attention should be drawn to the fact that μ_g was appreciable even for the smallest particles, for which the entrainment factor $\mu_p \to 1$. When $\omega\tau \ll 1$, μ_g equals:

$$\mu_g \approx \omega\tau. \quad (5.25)$$

It can be shown that the large particles, for which $\omega\tau \gg 1$, were not fully at rest and were drawn into the vibratory medium motion as follows:

$$\mu_p \approx (\omega\tau)^{-1}. \quad (5.26)$$

A simple relationship existed between μ_p and μ_g:

$$\mu_g = \omega\tau\mu_p, \quad (5.27)$$

$$\mu_p^2 + \mu_g^2 = 1. \quad (5.28)$$

The above is conveniently illustrated in Figure 18. The boldface line represents the sinusoidal velocity of the vibrating air (motion of the smallest particles, for which $\mu_p = 1$, coincided with this line). The fine line represents the vibratory motion of a suspended droplet having a degree of entrainment equal to $\mu_p = 0.8$. It lags the vibratory medium motion by an angle $\varphi = \text{Arccos}\ \mu_p \approx 34.4°$. The dotted curve represents the relative medium velocity flowing around the droplet, for which

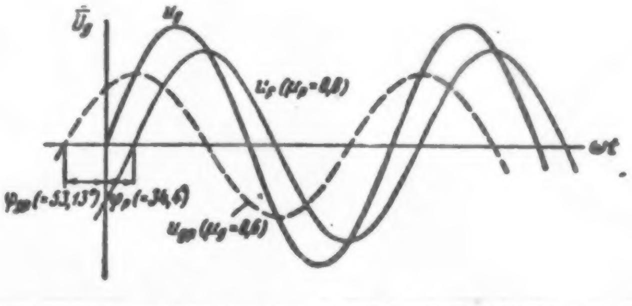

Fig. 18. Schematic drawing illustrating difference in phases of absolute medium oscillation rate (μ_g) of absolute aerosol particle oscillation velocity (μ_p) and of the relative oscillation velocities of particles in the medium.

$\mu_g = \sqrt{1 - \mu_p^2} = 0.6$. This velocity leads the particle velocity by an angle of 90° so that the phase shift angle relative to the vibratory motion of the medium is $\varphi - 90° - 53.13°$.

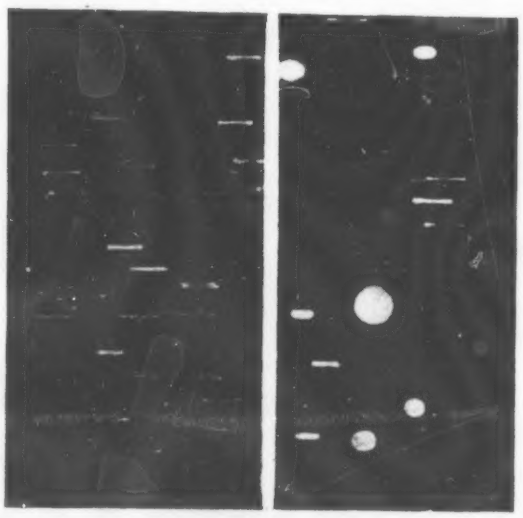

Fig. 19. Photographs illustrating difference in the degree of aerosol particles increase (droplets of paraffin fog) in oscillating medium movement (f = 10 khz; exposure time 1/250 sec; × 80)

a - Particle radii 0.3 - 0.6μ; b - particle radii from 0.3 to 4.5μ.

Equations (5.9) and (5.19) had been verified experimentally repeatedly and qualitative confirmation had been obtained by many tests. Figure 19 shows photographs taken by Brandt, Freund, and Hiedemann [9, 168], using exposure time longer than the period of gaseous medium vibration. The photographs show droplets of a paraffin oil vapor sonicated at a frequency of 10 khz. It can be seen that the largest particles remained at rest ($\mu_p = 0$) during sonication, and conversely, the small particles ($r < 1\mu$) actively participated in the vibratory medium motion. This is evident from the longitudinal traces (tracks) the lengths of which were twice that of the vibration amplitude.

The first quantitative, although considerably crude, verification of formulas (5.9) and (5.19), was attempted by Wagenschein [283], who measured the vibration amplitudes of lycopodium spores ($r = 15.85\mu$, $p_p = 1.1$) at a frequency of 85 hz and vibration amplitudes from 0.58 to 2.40 mm. The medium vibrations were set up by the Zernov method, i.e., a lightweight hermetically sealed vessel containing aerosols was fastened to the electromagnetically excited tuning fork. The vibration amplitudes of the vessel, gas, and particles were photographed through a microscope. The choice of lycopodium spores as the object of observation was unfortunate due to the presence of small fins on their surfaces which distorted the particle mobility. Because of this, the initial divergence of 20 to 30% between the experimental and the theoretical data followed. However, this was reduced to 5% after correcting the particle mobility by the rate of their fall.

In recent years, experiments had been conducted to determine the degree of particle entrainment at higher frequencies closer to those which had been used in the acoustical aerosol coagulation. The purpose of these tests was to develop a method for determining aerosol dispersion content. Among these were preliminary experiments by Cassel and Schultz [174] and the recent detailed experiments by Gucker and Doyle [198].

Figure 20 shows a comparison of the experimental results of Gucker and Doyle with theoretical data. The results were obtained in experiments with dioctyl phthalate vapor droplets ("Flexol" DOP and 39 H) with radii varying from 0.8 to 3.9μ at a frequency of 4.85 khz generated by St. Clair's electrodynamic vibrator. Particle vibration amplitudes were measured microphotographically at the nodes of a standing wave. Particle size was determined from microphotographic measurements of the fall velocity and from subsequent calculations using Stokes' formula and Cunningham's correction factor. Figure 20 shows that experimental and theoretical data were in close agreement.

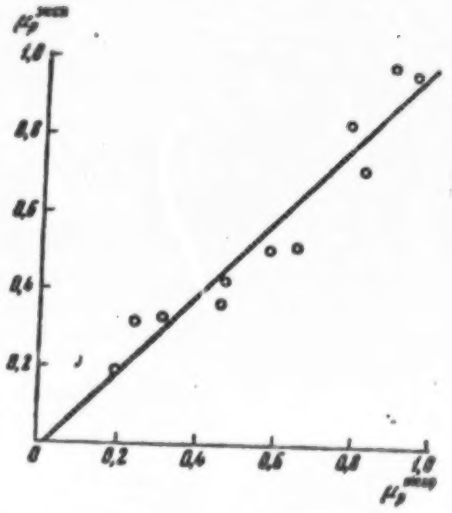

Fig. 20. Experimental data on degree of fog particles increase of diectylphthalate according to Haker and Doyle

In conclusion, the problem of aerosol stability in a vibrating gaseous medium will be briefly analyzed. It has been known that a system of vortexes was generated behind some streamlined obstacles, bars, and wedges in particular. The vortexes broke away from each side of the obstacle and, under certain conditions, caused a loss in stability and appearance of transverse body vibrations. A similar phenomenon, having a self-oscillatory character [125], had been observed while blowing past spherical obstacles [114] behind which, as assumed, a vortex formed. It was noted previously in the footnote on pages 47 - 48 that highly streamed aerosols executed chaotic motions in the sound field due to transverse velocity components. In this connection, the following guestion arises: is this caused by loss in the stability of particles suspended in the sound field?

The theory indicates [111] that the loss in stability in the advancing flow, which is characterized by the Reynolds number Re, begins to appear when:

$$\mathrm{Re} > \frac{9}{2}\left(\frac{h}{r}\right)^{2}\frac{1}{\sqrt{k_2(1-k_2)}}. \tag{5.29}$$

where h is the flow width k_2 is a non-dimensional coefficient and $k_2 \leq 1$.

It will be shown in Section 9 that aerosol streaming in a sound field had a quasistationary character, meaning that the inequality (5.29) is applicable here. It can be concluded from (5.29) that the stability of suspended particles was disturbed only when $\mathrm{Re} \gtrsim 10^7$, an occurrence which did not apply to sound fields. Therefore, it follows that the chaotic aerosol motion can be caused in a sound field by other phenomena which will be examined appropriately.

6. DRIFT OF AEROSOL PARTICLES

In the course of their vibratory motion, particles suspended in a gaseous medium underwent a progressive transfer or "drift," in the longitudinal direction in relation to the medium. There are at least four factors which enhanced drift of aerosol particles in a sound field:

1) acoustical radiation pressure exerted on the particles;
2) periodical variation in the vibrating medium viscosity;
3) distortion (asymmetry) of the acoustical waveform;
4) asymmetry in the oscillatory medium motion in a standing sound wave. In addition, the aerosol particle drift in an acoustical field was enhanced by the presence of other particles with developed boundary layers. This effect, however, is not comparable and will not be examined here.

Drift induced by acoustical radiation pressure. This type of particle drift has been known for a long time. It can be estimated quantitatively from King's equation for radiation pressure exerted on a stationary spherical obstacle of arbitrary density having a radius considerably smaller than the wavelength: kr<< 1. According to King [212], it is:

$$F_R = 4\,(kr)^4\,(\pi r^2)\,G\,(\rho_g/\rho_p)\,E, \tag{6.1}$$

in a traveling wave, and

$$F_R = 2\,(kr)\,(\pi r^2)\,G\,(\rho_g/\rho_p)\,E \sin 2kx_0, \tag{6.2}$$

in a standing wave, where k is the wave number, $G(p_g/p_g)$ is the density factor given by the following equation:

$$G\,(\rho_g/\rho_p) = \left[1 + \frac{2}{3}\,(1 - \rho_g/\rho_p)\right] \Big/ (2 + \rho_g/\rho_p)$$

(in the case of aerosol particles with $\rho_p \gg \rho_g$, $G\,(\rho_g/\rho_p) \simeq {}^5/_6$); x_0 is the distance to the closest standing wave node.

The derivation method for these equations consisted of the exact solution of the streamline problem for the case of a spherical object in a sound field. Viscosity and the heat transfer capability of the medium were disregarded.

A simpler and more convenient method was applied subsequently by Westervelt [286], and by L. D. Landau and E. M. Lifshits [62]. The essence of this method is contained in the following: if an object were placed in the path of a propagating sound wave, the wave became reflected and scattered in all directions upon incidence with the object. The scattered wave can be visualized as a wave radiated by the object itself. The impulse imparted by the wave to the object was greater than the impulse scattered by the object in the direction of the incident wave propagation. This gave rise to an excess force in relation to the forces of radiation pressure in a sound wave. The energy flux equal to $\pi_s c_s E$ was lost (scattered) by the incident sound wave. Quantity π_s was the total effective cross-section defined as the ratio of the total scattered flux to the incident energy flux density which, for the case of particles entrained into the oscillatory medium flow, was defined by the quantity $E_{s,} = \frac{1}{2}\rho_s U^2{}_{s,} = \mu_s^2\,\bar{\vec{E}}$ ($\bar{\vec{E}}$ is the absolute energy flux density equal to J/c_s).

The impulse flux in the incident sound wave is $\pi_s E_{gp}$, and in the region bounded by the solid angle d θ in the scattered wave, it is $E_s r^2 d\theta = E_{gp} d\pi_s$. Project the latter in the direction of the propagating incident wave, and get:

$$F_R = E_{gp}\int_0^\pi (1-\cos\theta)\,d\Pi_s \qquad (6.3)$$

where θ is the angle between the direction of the incident and scattered waves.

According to [62], the effective differential cross-section is:

$$d\Pi_s = \frac{1}{9}\left(\frac{\omega}{c_g}\right)^4 r^6 \left(1-\frac{3}{2}\cos\theta\right)d\theta.$$

Substitute this expression into equation (6.3); integrate it, and obtain the following expression for the force in a traveling sound wave due to radiational drift of a sphere:*

$$F_R = \frac{11}{9}\pi\left(\frac{\omega}{c_g}\right)^4 r^6 \mu_g^2 \overline{E}. \qquad (6.4)$$

Maidanik [230] and, subsequently, L. P. Gor'kov [27], solved this problem for a more general case, including compressibility of a sphere and the refraction of the incident wave. This led to an identical expression for the case of aerosol particles. A comparison of derived equation (6.4) with equation (6.1) shows that they differed only by a numerical constant which was 2.7 times as great in King's equation. In both cases, the direction of force F_R was identical, i.e., in the direction of sound wave propagation. The radiational drift was many orders of magnitude higher in the standing wave field. To calculate this force, it is necessary to include the impulses of the direct and reflected waves, the magnitudes of which depended on the location of the sphere in the sound field. To sum up, the following expression is obtained for the radiation pressure force acting on a sphere in a standing sound wave:

$$F_R = \frac{8}{3}\pi\left(\frac{\omega}{c_g}\right) r^3 \mu_g^2 \overline{E}\sin 2kx_0 \qquad (6.5)$$

The above expression (without factor μ_g) was first obtained by Westervelt [286]. The same problem was recently solved for the general case by L. P. Gor'kov [27] who, however, obtained a 25% higher coefficient.

Comparison of equation (6.5) with King's equation (6.2) showed that they were identical. The only exception was a factor, 1.6 times greater than the factor in equation (6.2). This was verified experimentally by Rudnick [258], who used cork balls with radii $r \sim 1$ mm, suspended by threads in the standing wave field at frequencies between 400 and 2800 hz. Expression

---

* Instead of an expression for the drift force F, in all examined cases Westervelt [286] used the corrected specific pressure $F/\pi r^2 \overline{E}$, which he designated by an index d and called it the "drag coefficient." The index was partly useful in comparative estimates of different types of drift, although it proved insufficient for practical purposes, as it excluded μ_g.

(6.5) shows that the magnitude of radiational pressure force acting on aerosol particles in a standing sound wave was a function of their coordinates. At the nodes ($x_0 = 0$, $\lambda/2$, and λ) and antinodes ($x_0 = \lambda/4$ and $3\lambda/4$), the force $F_R = 0$. Moreover, the particle was stable at the nodes, and unstable at the antinodes. The maximum value of force F_R occurred at the midpoint between the node and antinode, i.e., at $x_0 = \lambda/8$, $3\lambda/8$, $5\lambda/8$, and $7\lambda/8$.

Find expressions for velocities of an aerosol particle due to radiational drift. Since the discussion centers on the progressive particle motion, the period of which is larger than the particle relaxation time, it can be assumed that the radiational pressure force F_R, expressed by equations (6.4) or (6.5), was balanced at every instant by the medium's drag expressed by Stokes' equation $F = 6\pi\eta r V_R$. Whence, in the case of a traveling wave:

$$V_R = \frac{11}{54\eta}\left(\frac{\omega}{c_g}\right)^4 r^5 \mu_g^2 \overline{E} \tag{6.6}$$

and in the case of a standing wave:

$$V_R = \frac{4}{9\eta}\left(\frac{\omega}{c_g}\right) r^2 \mu_g^2 \overline{E} \sin 2kx_0 \tag{6.7}$$

In the first case, the particle motion is uniform, and in the second it is nonuniform and is governed by the following equation:

$$\operatorname{tg} kx = e^{Bt} \operatorname{tg} kx_0. \tag{6.8}$$

where

$$B = \frac{8}{9\eta}(kr)^2 \mu_g^2 \overline{E}.$$

Equation (6.8), derived initially by St. Clair 179, 181 , may be obtained readily by integrating equation (6.7), the initial conditions being $x = x_0$ at $t = t_0$. The motion of aerosol particles in the sound field in the presence of radiational drift acquires singular character, best illustrated in Figure 21.

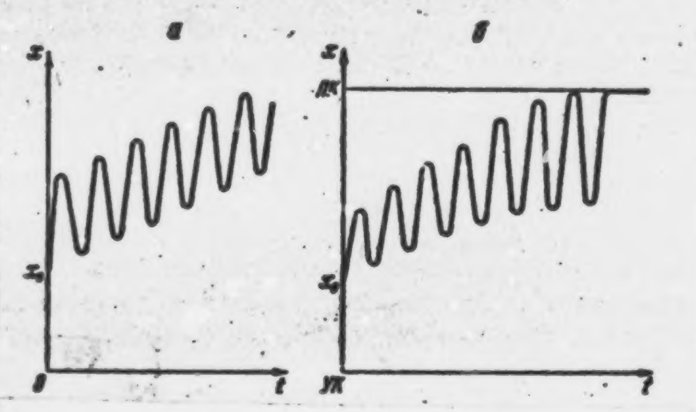

Fig. 21. Schematic presentation of aerosol particles drift phenomenon in a sound field (d)
a – in a flowing wave; b – in a static wave

All above equations are valid when the following two conditions are satisfied. Condition 1: medium's oscillation amplitude was small in comparison with the radius of the sphere, otherwise the motion of the medium loses its potentiality; Condition 2: the viscous losses of the acoustical energy in the boundary layer around the sphere are comparatively small, otherwise the sound wave fails to reach the sphere surface and remained unscattered by it. According to [61], the acoustical energy absorbed by the boundary layer of a small sphere ($kr \ll 1$) with 1 cm^2 cross section area is equal to $6\,v/c_g r$. Whence, Condition 2 is satisfied for the following inequalities:

$$\frac{11}{9}(kr)^4 > 6v/c_g r \tag{6.9а}$$

in the case of a traveling wave, and

$$\frac{8}{3}(kr) > 6v/c_g r \tag{6.9б}$$

in the case of a standing wave.

In air and at $f = 10$khz, this results in $r > 700\mu$ for a traveling wave, and $r > 25\mu$ for a standing wave. The dimensions are even larger at lower frequencies. Therefore, the incident energy is not so much scattered on the small-size primary aerosols, as it is absorbed by the viscous boundary layer around them. As a result, new types of drift arise and are examined below. However, the radiational drift occurred only due to highly enlarged aerosol particles in the standing wave field.

Drift induced by periodic variation in medium viscosity. The adiabatic compression and rarefaction of the medium in the sound field produce a periodical increase and decrease in the medium temperature. Using the adiabatic equation pv^γ = const. and the equation of state for an ideal gas $pv = R_g T$, it can be shown that in the case of sinusoidal sound pressure which varied according to $p = P_{st} + P_g \sin \omega t$ at a given point, the absolute temperature of the medium, within the first approximation, varied as follows:

$$T \approx T_0\left(1 + \frac{\gamma - 1}{\gamma}\frac{P_g}{P_{ст}}\sin \omega t\right), \tag{а}$$

where T_0 is the absolute temperature of the medium in the surrounding space at the static pressure P_{st}. When sound intensity was J = 0.1 - 1.0 w/cm^2, corresponding to P_g/P_{st} = 0.009 - 0.030 under normal conditions, the air temperature ($\gamma = 1.4$) in regions of compression or rarefaction changed by Δ = ± 0.75 - 2.5° C.

This substantial temperature variation of a gaseous medium induced a corresponding change in its viscosity. The viscosity and temperature of ideal gases, in the thermodynamic sense, were related as follows:

$$\eta \sim T^{1/2}. \tag{б}$$

This relationship may be derived readily from the following two equations [116]:

$$\eta = \frac{1}{3}\rho_g l_m v_m \tag{в}$$

$$\frac{m_m v_m^2}{2} = \frac{3}{2}k_B T \tag{г}$$

(m_m, v_m and l_m are the average mass, velocity, and the free path of the gas molecules respectively; k_B is the Boltzmann constant.

According to (b), an increase in the medium temperature during compression was accompanied by an increase in its viscosity, and a decrease in temperature during rarefaction was accompanied by a decrease in viscosity.

The difference in the medium viscosity during compression and rarefaction resulted in some difference in the magnitude of forces exerted, according to Stoke's law, on the suspended particles during forward and backward motions. This produced an appearance of an excess force, the drift force F_η, acting on the particle in the direction of the sound source in the case of a traveling wave, or in the direction of a node in the case of a standing wave. The drift force was predicted theoretically by Westervelt in [285], which dealt with the mean static pressure and velocity of gas particles in a plane sound wave. In this study the author accounted for the variation in the parameters of the oscillating medium caused by the variation of their coordinates for oscillations with finite amplitude. By means of a corresponding transformation of coordinates, the author obtained the following expressions for the instantaneous sound velocity c_g and the velocity of medium particles u_g in fixed (Euler's) coordinates:

$$c_g = c_{g0}\left[1 + \frac{\rho_{g0}}{c_{g0}}\frac{dc_g}{d\rho_g}(-\xi_x + \xi_x^2 + \xi\xi_{xx}) + \frac{\rho_{g0}^2}{2c_{g0}}\frac{d^2c_g}{d\rho_g^2}\xi_{xx}^2\right], \quad (6.10)$$

$$u_g = \xi_t - \xi\xi_{xt}, \quad (6.11)$$

where c_{g0} is the velocity of sound in the surrounding medium having a density of ρ_{g0}; ξ_x and ξ_{xx} are the first and second derivatives of displacement of the medium's particle at a point x; ξ_t and ξ_{xt} are Lagrangian velocities of the medium particle and its derivative at a point x, respectively. On the basis of expression (c), where the product of the first three terms, $\frac{1}{3}\rho_g l_g$, is independent of temperature, and the fourth term, v_g is proportional to the velocity of sound c_g as determined by (6.10), the following expression may apply to the medium instantaneous viscosity in the first approximation:

$$\eta = \frac{c_g}{c_{g0}}\eta_0 \approx \left(1 - \frac{\gamma - 1}{2}\xi_x\right)\eta_0, \quad (6.12)$$

where η_0 is the viscosity of the surrounding medium. The product of instantaneous values of u_g and η, which appear in the Stokes formula (4.3), is defined as follows:

$$u_g\eta = (\xi_t - \xi\xi_{xt})\left(1 - \frac{\gamma - 1}{2}\xi_x\right)\eta_0.$$

The mean value of which over one period of oscillations is:

$$(u_g\eta)_{cp} = \frac{\gamma - 3}{4}\eta_0\frac{U_g^2}{c_{g0}}. \quad (6.13)$$

Substitute expression (6.13) into Stokes' formula and take the degree of streamlike flow μ_g into consideration, and obtain the following expression for the drift force caused by the periodic variation of the medium:*

---

* In Westervelt's subsequent work [286] and also in the book by Hueter and Bolt [205], this force was referred to as the "Stokes-type force."

$$F_{\eta} = 3\pi(\gamma - 3)\frac{v_0}{c_{g0}} r\mu_g^2\overline{E}. \qquad (6.14)$$

In the case of a standing wave, the above expression must be multiplied by a factor sin 2 kx_0. The following equation may be obtained for the drift velocity by equating expressions for the drift force (6.14) and the drag force $F_{st} = 6\pi\eta r V_{\eta}$:

$$V_{\eta} = \frac{\gamma - 3}{2\rho_{g0}c_{g0}}\mu_g^2\overline{E}. \qquad (6.15)$$

It is implied that the instantaneous particle temperature follows the medium temperature.

Drift conditioned by waveform distortion (asymmetry). If the sound wave had a distorted, sawtooth, form similar to the one shown in Figure 7, it indicates that the medium's particles move non-sinusoidally (see Figure 8). In the compression phase, which indicated the forward motion, i.e., in the direction of wave propagation, medium's particles acquire velocity faster and lose it slower than in the sinusoidal motion. In the rarefaction phase, where the motion is reversed, the opposite occurs: medium's particles gain their velocity faster than they lose it. These factors clearly influénce the motion character of particles suspended in a medium. During slow velocity increase, accompanied by backward medium motion, the aerosol particle is entrained into its motion to a greater extent than during "normal" sinusoidal velocity increase, and as a consequence acquires greater velocity. Having acquired greater momentum, a particle "slips" by medium's particles somewhat further than normally during the subsequent decrease in medium's velocity. This becomes considerably enhanced by a more than usually abrupt decrease in medium's velocity. In the case of the medium's forward motion, the opposite occurred: the aerosol particle lags medium's particle motion by the same amount. As a result, the aerosol particle fails to return to its initial position at the end of a vibration cycle and moves to a point opposite to the flow direction.

Now find the expressions for the drift force due to waveform asymmetry. Use Stokes' equation, as Westervelt did [286, 205], in the form given by Oseen (second approximation):

$$F_{Oc} = 6\pi\eta r u_{gp}\left(1 + \frac{3}{16}\mathrm{Re}\right). \qquad (6.16)$$

The second term of the correction factor in this equation gives an additional force ΔF which, in contrast to the basic Stokes' force F_{st}, is related to the velocity of the streamlike flow around a sphere by a quadratic relationship:

$$\Delta F = \frac{9}{4}\pi r^2\rho_g\overline{u}_{gp}|u_{gp}|. \qquad (6.17)$$

where $\overline{u}_{gp}$ is the streamline velocity vector, and $|u_{gp}|$, its magnitude. In the case of a sinusoidal variation of streamline velocity, the mean value of this force over each half-period is zero, indicating that the sinusoidal variation failed to upset the periodicity of particle's motion. However, the situation changes in the case of an asymmetrically distorted waveform, which generated harmonics (see Section 1): averaging of the force ΔF resulted in a nonperiodic unidirectional force F_h. If the analysis is limited to the second harmonic, the vibrational streamlined velocity of a particle may be expressed as follows:

$$u_{gp} = \mu_g U_g [\sin \omega t + h_2 \sin (2\omega t + \psi), \tag{6.18}$$

where $h_2 = u_2/U_g$ is the relative amplitude of the second harmonic, and ψ is its phase shift angle (equal to $-\pi/2$ in Figure 7b).

Square the above expression and substitute into equation (6.17) and get:

$$\Delta F = \frac{9}{4} \pi r^2 \rho_g \mu_g^2 U_g^2 [\sin^2 \omega t + 2h_2 \sin \omega t \sin (2\omega t + \psi) + h_2^2 \sin^2 (2\omega t + \psi)]. \tag{6.19}$$

Average the terms in brackets over the first half- period and get the following:

$$\frac{1}{\pi} \int_0^\pi \sin^2 \omega t \, d(\omega t) = \frac{1}{2},$$

$$\frac{1}{\pi} \int_0^\pi 2h_2 \sin \omega t \sin (2\omega t + \psi) \, d(\omega t) = \frac{4h_2}{3\pi} \sin \psi,$$

$$\frac{1}{\pi} \int_0^\pi h_2^2 \sin^2 (2\omega t + \psi) \, d(\omega t) = \frac{h_2^2}{2}.$$

Averaging the same terms over the second half-period (from $\omega t = \pi$ to $\omega t = 2\pi$) characterizes the velocity vector in the reverse direction, yields identical results with the exception of the second term, which acquires a negative sign. The latter indicates that only the component of force ΔF related to this term was in opposition to the velocity vector, i.e., it preserved previous direction. As a result, a unidirectional drift force appeared:*

$$F_h = -6h_2 \sin \psi \, r^2 \mu_g^2 \overline{E}. \tag{6.20}$$

The direction of this force is coincident with the direction of the sound wave propagation, if the phase angle ψ of the second harmonic is negative, as in Figure 7b; direction is reversed, if the angle ψ is positive, as in the usual case (see Figure 8).

Equate expression for the drift force (6.20) with the one for the drag force $F_{st} = 6\pi\eta r V_h$ and get the following equation for drift velocity:

$$V_h = -\frac{h_2 \sin \psi}{\pi \eta} r \mu_g^2 \overline{E}. \tag{6.21}$$

It is, thus, seen that the drift velocity V_h is directly proportional to the degree of waveform distortion and to the sine of the second harmonic phase angle, i.e., to the waveform asymmetry. The mathematical solution of the particle drift problem in a standing wave presented serious difficulties which stemmed from the fact that in a case of finite amplitude vibrations, the waveform varied with time [133]. However, it may be concluded from graphs in [286] that the maximum values of force F_h and velocity V_h were of the same order of magnitude in the standing and traveling waves.

---

* Westervelt [285, 286] referred to this force as the "Oseen force."

Drift conditioned by asymmetry of vibrational motion in a standing wave. It is known that a distinct characteristic of standing sound waves is that the vibrational velocity, displacement, and sound pressure were functions not only of time, but also of space [see Figure 1 and equations (1.4) - (1.6)]. In each region between a node and antinode, the displacement amplitude and vibrational velocity rose sinusoidally with distance from the node. In the course of vibrational displacement in the direction of the node, medium's particles fell into a zone of increased vibration amplitudes, and upon return - into a zone of decreased vibration amplitudes, as compared with the initial vibration amplitude, which corresponded to the start of each displacement. In other words, medium's particles accelerated in the course of their vibrational displacement in the node direction, and, in comparison with the "normal" sinusiodal motion starting from each extremal position, they decelerated upon return. There exists direct evidence to the effect that the asymmetry of vibrational medium motion was related to the finite vibration amplitudes.

If a particle suspended in the above described vibrating medium possessed appreciable mass, then, by virtue of its inertia, it digressed to some extent from the described behavior of medium's particles. That is, in the course of displacement in direction of the node when the medium was accelerated, an aerosol particle lagged medium's particles more markedly than in the course of its sinusoidal motion. During the return travel, when the medium became decelerated, the aerosol particle leads medium's particles more notably than during its sinusoidal motion. As a result, the aerosol particles came closer to the node than the medium's particles vibrating with it in both cases. With each vibration cycle the indicated shift of an aerosol particle increased relative to the medium's particles. This might soon lead the aerosol particle to the node, if other, directly opposed, forces had not acted on it simultaneously. The described type of aerosol particle drift had been predicted theoretically by S. S. Dukhin. A simplified mathematical solution of the drift problem was offered by A. Barginovskii [4]. Recently, Dukhin obtained an exact solution of this problem [35]. Both these solutions will be presented and discussed.

In the first approximation, the equation of an aerosol particle motion in a standing wave field, including (6.2) was as follows:

$$m_p \frac{d^2 x_p}{dt^2} = 6\pi\eta r \left(U_g \sin kx \sin \omega t - \frac{dx_p}{dt} \right). \tag{6.22}$$

or

$$\tau \frac{d^2 x_p}{dt^2} + \frac{dx_p}{dt} = U_g \sin kx \sin \omega t. \tag{6.22'}$$

If the difficulties associated with exact integration of the above equations are averted by utilizing formulas for approximate integration,

$$\frac{dx_p}{dt} \approx \frac{x_{n+1} - x_n}{\Delta t}, \quad \frac{d^2x_p}{dt^2} \approx \frac{x_{n+1} - 2x_n + x_{n-1}}{\Delta t^2},$$

equation (6.22') yielded the following expression for the (n+1) -th ordinate:

$$x_{n+1} = \frac{x_n\left(\frac{2\tau}{\Delta t^2} + \frac{1}{\Delta t}\right) + U_g \sin kx_n \sin \omega t - x_{n-1}\frac{\tau}{\Delta t^2}}{\frac{\tau}{\Delta t^2} + \frac{1}{\Delta t}} \qquad (6.23)$$

With the aid of this equation and the initially assigned conditions for the motion of an aerosol particle, a graph of its drift, in the absence of other forward motion, may be constructed by the method of successive approximations. This type of graph is a mirror-image of the one shown in Figure 21b. To arrive at the exact solution of the aerosol drift problem, examine equation of the oscillating particle as the second approximation, as was done by Dukhin. Considering that the particle drift was anharmonic, avoid the general expression (4.2) for force F" acting in a viscous medium with an arbitrarily varying velocity. This leads to the following expression for the motion of an aerosol particle:

$$\left(m_p + \frac{m_g}{2}\right)\frac{d^2x_p}{dt^2} + 6\pi\eta r\left(\frac{dx_p}{dt} + \frac{r}{\sqrt{\pi\nu}}\int_{-\infty}^{t}\frac{d^2x_p}{dt_i^2}\frac{dt_i}{\sqrt{t-t_i}}\right) =$$

$$= \frac{3}{2} m_g \frac{d^2x_g}{dt^2} + 6\pi\eta r\left(\frac{dx_g}{dt} + \frac{r}{\sqrt{\pi\nu}}\int_{-\infty}^{t}\frac{d^2x_g}{dt_i^2}\frac{dt_i}{\sqrt{t-t_i}}\right). \qquad (6.24)$$

where x_g and x_p are distances from the node to the medium and the particle, respectively, and $dx_g/dt = U_g \sin kx_0 \sin \omega t$.

Equation (6.24) describes motion in a rapidly oscillating field, which allows to use P. Kapitsa's method [63] for its solution. Since the amplitude of oscillations A_g was much smaller than the wavelength, $|x_g|$ on the right-hand side of the equation may be considered constant during one cycle of oscillations, $x_g = x_0$. In this case, the solution of (6.24) is the following equation for the harmonic particle oscillation with respect to the point $x_p = x_0$, namely:

$$x_p - x_0 = \mu_p A_g \sin kx_0 \cos[\omega t + (\varphi - \theta)], \qquad (6.25)$$

where the degree of particle entrainment μ_p and the phase shift angle $(\varphi - \theta)$ were determined by the previously derived equations (5.9) and (5.10) respectively.

The right-hand side of equation (6.24) may be considered as a quasi-periodic force with a slowly varying amplitude of medium's oscillations causing the particle to oscillate and to be displaced simultaneously during each cycle. Therefore, it can be substituted by equation (5.2) derived by Stokes. Interest here centers around particle drift so that equation (5.2) can be averaged over one oscillation cycle. First expand $\sin kx_p$ into a series about point x_0:

$$\sin kx_p = \sin kx_0 + k\cos kx_0 (x_p - x_0). \qquad (6.26)$$

where $x_p - x_0$ is determined by equation (6.25).

Substitute the above series into the expressions for u_p and du_p/dt in equation (5.2), and average over one period of oscillations, in which the periodic motion component was zero, and obtain the following equation of motion of an aerosol particle:*

$$\left(m_p+\frac{m_g}{2}\right)\frac{d^2x_0}{dt^2}+6\pi\eta r\left(\frac{dx_0}{dt}+\frac{r}{\sqrt{\pi\nu}}\int\limits_{-\infty}^{t}\frac{d^2x_0}{dt_1^2}\frac{dt_1}{\sqrt{t-t_1}}\right)=$$

$$=\frac{k}{4}\mu_p U_g^2 m_g\left[\sin(\varphi-\theta)\cdot\frac{9}{4}(b^2+b)-\cos(\varphi-\theta)\left(\frac{3}{2}+\frac{9}{4}b\right)\right]\sin 2kx_0. \tag{6.27}$$

As was shown previously, the first and third terms on the left-hand side of this equation are small in relation to the second term (see Section 4). Therefore, equation (6.27) can be reduced to:

$$6\pi\eta r u_0=\frac{k}{4}\mu_p U_g^2\frac{4}{3}\pi r^3\rho_g\times$$

$$\times\left[\sin(\varphi-\theta)\frac{9}{4}(b^2+b)-\cos(\varphi-\theta)\left(\frac{3}{2}+\frac{9}{4}b\right)\right]\sin 2kx_0. \tag{6.28}$$

Consider relationships among (5.23), (5.18), and (4.4) and also the fact that the left-hand side of the given expression represented the force averaged over one period of vibrations, i.e., the drift force F_a, and obtain

$$F_a=\frac{\pi}{3}kr^3\mu_p\left[\frac{9}{2}(b^2+b)\mu_g-\left(3+\frac{9}{2}b\right)\mu_p\right]\overline{E}\sin 2kx_0. \tag{6.29}$$

Equate the above expression with the one for the drag forces $F_{st} = 6\eta\pi r V_a$, and get the following expression for drift velocity:

$$V_a=\frac{k}{13\pi}r^2\mu_p\left[\frac{9}{2}(b^2+b)\mu_g-\left(3+\frac{9}{2}b\right)\right]\overline{E}\sin 2kx_0. \tag{6.30}$$

Thus, it is seen that the force and velocity of a given particle type drifted in the node - antinode range, and varied in a manner identical to the variation of the force and velocity in the radiational drift. There were no other similarities. However, there was a characteristic detail: a "preferred" frequency of oscillations at which the drift velocity attained a maximum value (see Figure 23) corresponding to each particle size.

Table 5 presents a summary of formulas for the force and velocity of all the examined types of aerosol particle drift in a sound field. With reference to formulas for drift velocity, it can be seen that inasmuch as all had been derived from the expression for the drift force with the aid of Stokes' formula (4.3), they are valid only for the range in which the corresponding Reynolds number $R = 2rV/\nu$ did not exceed a unity. Otherwise, when particles were large and the sound intensity increased, the velocity should be corrected by Oseen's factor as follows:

---

* The equation in Dukhin's article [35] contained an error: m_p was shown instead of m_g. [Author]

$$V_{Oc} = -\frac{4v}{3r} + \sqrt{\left(\frac{4v}{3r}\right)^2 + \frac{8v}{3r} V_{Cr}}. \qquad (6.31)$$

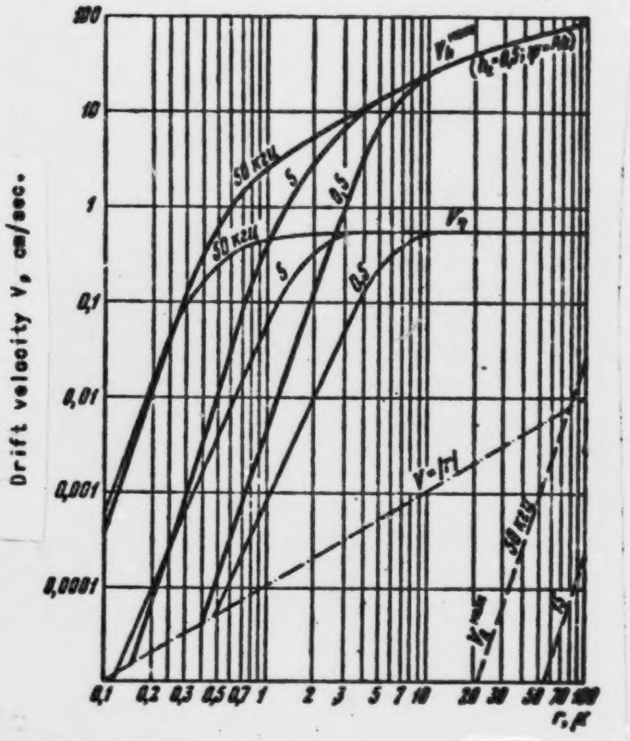

Fig. 22. Aerosol particles drift velocity in a flowing sound wave at J = 0.1 bm/cm^2
(ρ = i g/m^3, medium - air)
V_R-drift velocity resulting from sound radiation pressure; V_η - drift velocity conditioned by periodic medium velocity changes; V_h - drift velocity conditioned by wave form distortion
($\varphi = \pm \pi/2$; $h_0 = 0,5$).

The above equation is easily arrived at by comparing the right-hand side of the expression for the drag force of the the sphere in the normal form given by Stokes and in the refined form given by Oseen.

Below are shown absolute values of drift velocity of spherical aerosols with unit density ($p_p = 1$), computed by the above formulas in atmospheric air at J (or I) = 0.1 w/cm^2 for a traveling wave (Figure 22) and an undistorted standing wave (Figure 23). Curve analyses in Figures 22 and 23 yield the following important conclusions:

1. Drift caused by a periodical variation in medium's viscosity is predominated in an undistorted traveling wave, although its velocity was small (V_η^{max} = 0.55 cm/sec). Drift velocity caused by radiative sound pressure was insignificant and can be disregarded in all cases.

2. Drift caused by waveform distortion usually predominated in distorted traveling waves, and its velocity could attain high values (up to $V_\eta^{max} \approx$ 10 cm/sec and up) if the distortion degree and asymmetry were sufficiently large.

3. Drift caused by vibrational motion asymmetry predominated in undistorted standing waves in the case of small particles. In the case of medium-size and large particles, the predominating drift was due to periodic variations of the medium's viscosity and radiative sound pressure, respectively. Drift velocity in the first and second cases was small ($V_a^{max} \approx 0.17$ cm/sec; $V_\eta^{max} \approx 0.55$ cm/sec, respectively), and in the third case, could attain higher values (when r = 100μ, V_R^{max} = 7 - 40 cm/sec at f = 5 - 50 khz).

4. Drift caused by asymmetry in vibrational motion of the medium predominated in highly distorted standing waves when particles were small. When particles were larger, drift due to sound waveform distortion predominated. Drift velocity in the second case could attain high values (when r > 5μ, V_η^{max} > 10 cm/sec), higher than in the radiational particle drift. Drift

direction of this type depended on the phase shift of its harmonics.

5. Particle size and oscillation frequency highly affected aerosol drift velocity. High drift velocities were usually attained only for larger particles, or at elevated ultrasonic frequencies.

6. Velocity of all types of aerosol particle drift was directly proportional to sound energy density and, consequently, to sound intensity. At sound intensity increased up to J (or I) = 1 w/cm^2, particle drift velocity increased tenfold, if Reynolds number did not exceed unity. Otherwise, drift velocity increased more moderately.

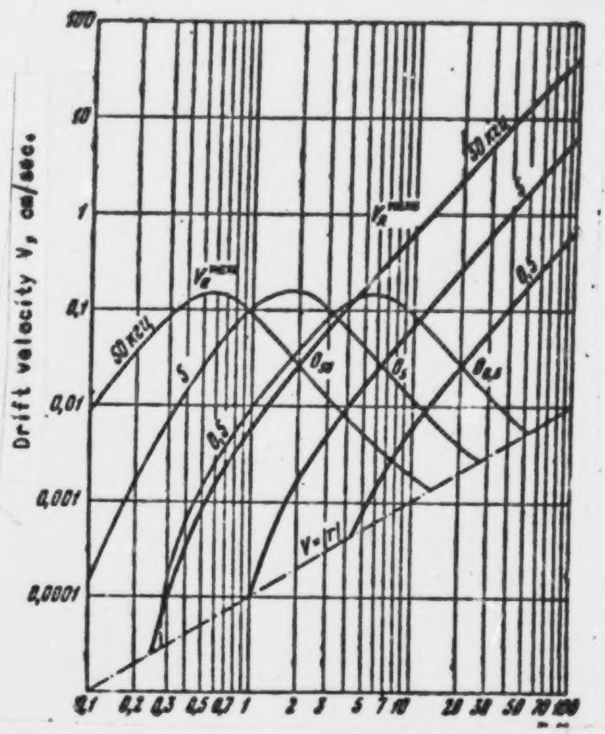

Fig. 23. Amplitude values of aerosol particules

Fig.- 23. Amplitude values of aerosol particules' drift velocities in a non-distorted static sound wave at J = 0.1bm/cm^2 ($\rho_p = 1$ г/см^3; $V_R^{\max}$ - drift velocity conditioned by intensity of sound radiation; $V_a^{\max}$ - drift velocity conditioned by asymetric oscillating medium movement drift velocity (values conditioned by periodic medium velocity changes $V^{\max}$, can be determined with the aid of Fig.22)

Table 3

Cause of particle drift	Force and velocity of drift particles	
	In migrating wave	In static wave
Sound radiation pressure (intensity)	$F_R = \frac{11\pi}{9}\left(\frac{\omega}{c_g}\right)^4 r^6 \mu_g^2 \overline{E}$ $V_R = \frac{11}{54\eta}\left(\frac{\omega}{c_g}\right)^4 r^5 \mu_g^2 \overline{E}$	$F_R = \frac{8\pi}{3}\left(\frac{\omega}{c_g}\right) r^4 \mu_g^2 \overline{E} \sin 2kx_0$ $V_R = \frac{4}{9\eta}\left(\frac{\omega}{c_g}\right) r^3 \mu_g^2 \overline{E} \sin 2kx_0$
Periodic changes in medium viscosity	$F_\eta = 3\pi \frac{(\gamma - 3)\nu}{c_g} r \mu_g^2 \overline{E}$ $V_\eta = \frac{\gamma - 3}{2\rho_g c_g} \mu_g^2 \overline{E}$	$F_\eta = 3\pi \frac{(\gamma - 3)\nu}{c_g} r \mu_g^2 \overline{E} \sin 2kx_0$ $V_\eta = \frac{\gamma - 3}{2\rho_g c_g} \mu_g^2 \overline{E} \sin 2kx_0$
Distortion in sound wave shape	$F_h = -6h_2 \sin\psi r^2 \mu_g^2 \overline{E}$ $V_h = -\frac{h_2 \sin\psi}{\pi\eta} r \mu_g^2 \overline{E}$	No analytical solution was found
Asymetrical oscillatory migration		$F_a = \frac{\pi}{3}\left(\frac{\omega}{c_g}\right) r^2 \mu_p \left[\frac{9}{2}(b^2 + b)\mu_g - \left(3 + \frac{9}{2}b\right)\mu_p\right] \overline{E} \sin 2kx_0$ $V_a = \frac{1}{18\eta}\left(\frac{\omega}{c_g}\right) r^2 \mu_p \left[\frac{9}{2}(b^2 + b)\mu_g - \left(3 + \frac{9}{2}b\right)\mu_p\right] \overline{E} \sin 2kx_0$

7. CIRCULATING AND FLUCTUATING AEROSOL PARTICLE MOTIONS

Aerosol particle motion executed under the effect of acoustical wind is referred to as circulating motion. The period during which acoustical wind velocity changed is greater than the relaxation time of aerosol particles. In view of that, as also in the case of drift, it is apropos to assume that the particles achieved velocity of the medium almost instantaneously, and, subsequently, follow it entirely. In order to make it more apparent, an equation will be considered for the motion of particles under the effect of a force acting from within the medium. If acoustical wind was w_a, and if, for the sake of simplicity, the second and third terms of equation (4.2) had been disregarded, the equation for the particle motion could be presented in the following form:

$$m_p \frac{dw_p}{dt} = 6\pi\eta r (w_a - w_p), \qquad (7.1)$$

or

$$\frac{dw_p}{dt} + \frac{w_p}{\tau} - \frac{w_a}{\tau} = 0. \qquad (7.1')$$

Assume that in a given time interval particle velocity was constant: w_a = const. In that case, solution of equation (7.1'), which is trivial for $t = 0$, is [39]:

$$w_p = w_a(1 - e^{-t/\tau}). \qquad (7.2)$$

According to this solution, velocity of an aerosol particle differed from the velocity of acoustical wind by 37% at $t = \tau$, by 0.6% at $t = 5\tau$, and by less than 0.005% at $t = 10\tau$. Therefore, aerosol particles almost fully achieved acoustical wind velocity for following time periods:

при $r = 0{,}1\ \mu$ $t \approx 10^{-6}$ сек
» $r = 1\ \mu$ $t \approx 10^{-4}$ »
» $r = 10\ \mu$ $t \approx 10^{-2}$ »
» $r = 100\ \mu$ $t \approx 1$ »

If the third integral term of equation (4.2) were taken into account, the correction factor would not exceed 4%, and the order of magnitude would be preserved.

It can be shown that an identical situation existed also when aerosol particles moved under the effect of any other slowly varying force, including the drift forces, discussed in the preceding paragraph. Aerosol particles are entrained with the same velocity also in the overall gas flow through the sonication chamber.

Now analyze the behavior of aerosol particles at the turn points of acoustical flow in a standing sound wave. Here, an additional centrifugal force acted on each aerosol particle, as a result of which the particle moved radially with a velocity which could be determined from the following formula [121]:

$$V_c = \frac{w_a^2 \tau}{R}, \qquad (7.3)$$

where R - radius of curvature at the turn of acoustical flow. The value of radial displacement at the turn with angle φ (radians) is:

$$\Delta R = V_c t_w, \tag{7.4}$$

where t_w - time of motion at the turn equal to $\varphi R/w_a$. Substituting the latter, and also (7.3) into (7.4) yields:

$$\Delta R = \varphi \tau w_a. \tag{7.5}$$

In the present author's work [73], this problem is discussed, the velocity curves computed according to Rayleigh's formulas (1.24 - 1.26), and the acoustical flow trajectories in the field of a standing wave with a frequency of 4.25 khz are presented. It can be seen, therefore, that the flow velocity at the turns had a reduced value, not exceeding w_a = 1 cm/sec at J (or I) = 1 w/cm^2. Accordingly, in the order of magnitude, the radial particle displacement at φ = π/2 did not exceed the value of relaxation time, which, as is known, lies within the range $\tau = 1.2 \cdot (10^{-7} - 10^{-3})$ sec for the initial sonicated aerosol particles (r = 0.1 - 10μ). Consequently, the radial displacement of aerosol particles at the turns can be disregarded safely if the particles failed to coagulate initially into larger ones. Thorough experimental investigations of the aerosol particle motion in a sound field had been conducted by Andrade [140], who obtained, by means of aerosols, satisfactory "prints" of the acoustical wind trajectories in the node - antinode region of a standing sound wave with λ = 56.5 and λ = 91.8 cm. Later, this phenomenon was observed by many investigators who worked in the field of the acoustical aerosol coagulation.

It would seem apropos to compare the direction of the circulating aerosol particle motion with the direction of their drift, discussed in the preceding paragraph. The direction of circulating motion of aerosol particles in an undistorted traveling wave, determined by the acoustical wind, is opposite to the direction of particle drift in the central part of the acoustical beam. Thus, the resultant particle velocity is an arithmetical difference between the acoustical wind and drift velocities at a given point. The directions of the above types of particle motion coincide at the beam periphery. Consequently, the value of the resultant particle velocity becomes equal to the sum of the acousticsl wind and particle drift velocities. If the waveform remained substantially undistorted, the acoustical wind velocity usually predominated over the drift velocity and, consequently, the particle motion was directed away from the sound source.

The direction of the resultant velocity of aerosol particles in a standing wave depended on their size. Small particles, the low-velocity drift of which was determined mainly by the asymmetry of the vibrating motion of the medium, moved along the central portion of the acoustical beam and on its periphery toward an antinode. This occurred with either a decreased or increased (by the value of V_a) velocity of acoustical flow at a given point. Large particles, the drift of which was determined mainly by the radial sound pressure moved towards an antinode in the central portion, and towards a node or antinode on the periphery, if V_λ was great. In the intermediate region of a sound field, where acoustical flow direction was mainly perpendicular to the direction of the particle drift, the magnitude and direction of particle motion was determined mainly by the magnitude and direction of drift velocity in the longitudinal direction, and by the acoustical flow velocity in the transverse direction. As a result, aerosol particles move at a certain angle to the direction of the sound wave. While participating in the vibrating and circulating motions of the medium, aerosol particles simultaneously participated in the acoustical flow fluctuations induced by acoustical turbulence. This has been observed visually by many investigations [167, 76, 30, 156, 231, 232].

The question can now be asked: what is the degree of enlargement of aerosol particles and turbulent fluctuations of the sonicated medium? Although this question has not been investigated experimentally thus far, nevertheless, its concept can be obtained if one proceeds from the theory of acoustical turbulence as developed in Section 1. If turbulent fluctuations are presented as harmonic vibrations with angular frequency w_1, as was done by N. A. Füchs [121], the extent of aerosol particle entrainment in these can be calculated clearly by using equation (5.9). Considering that frequency spectrum of turbulent fluctuations was in the low frequency range [see equations (1.38) and (1.39)] and, therefore, $w\tau \ll 1$, a simplified equation (5.16) can be used. In accordance with this equation, the degree of streamline flow of turbulent fluctuations with frequency w_1 around the aerosol particles was:

$$\mu_g^l = \omega_l \tau. \quad (7.6)$$

The mean square velocity of the relative particle and medium motions was:

$$v_{pg} = \mu_g^l v_l = \omega_l v_l \tau, \quad (7.7)$$

where v_1 - the mean square fluctuating velocity of the medium. Considering that the term $w_1 v_1$ represented acceleration of medium's fluctuations a_1, equation (7.7) could be written also in the following form:

$$v_{pg} = a_l \tau. \quad (7.8)$$

The relative motion of the particle and the medium is possible only in the case of fluctuations of the order of $l < l_0$, with the frequency, as indicated by (1.39), independent of the order. Fluctuations of the l_0 scale which, according to (1.36), have the highest fluctuating velocity, naturally have the highest acceleration

$$v_{l_0} \simeq \frac{1}{4}\left(\varepsilon \frac{b}{\rho_g}\right)^{1/4} \simeq \frac{1}{4} \frac{\xi^{1/4} b^{1/4}}{(\rho_g c_g)^{1/4}} J^{1/4} f^{1/2}. \quad (7.9)$$

In view of this, an equation for the maximum acceleration of fluctuations can be presented as follows:

$$(a_l)_{max} = \omega_{l_0} v_{l_0} \approx \frac{v_{l_0}^2}{l_0} \approx \frac{1}{15} \frac{\varepsilon^{3/4}}{(b/\rho_g)^{1/4}}. \quad (7.10)$$

In accordance with (7.8) and (7.10), the maximum value of relative fluctuating of particle and medium velocity is:

$$(v_{pg})_{\max} \simeq \frac{2}{135}\,\frac{\rho_p}{\eta}\,\frac{\varepsilon^{3/4}}{(b/\rho_g)^{1/4}}\,r^2 \approx \frac{2}{135}\,\frac{\xi^{3/4}\rho_p J^{3/4} f^{3/4}}{b^{1/4}\rho_g^{1/2}c_g^{3/4}\eta}\,r^2. \quad (7.11)$$

With Yaglom's calculations as the basis, V. G. Levich [68, 69] used $\sqrt{3}$ as the coefficient in (7.10) and converted equation (7.11) to the following:

$$(v_{pg})_{\max} \simeq \frac{2\sqrt{3}}{9}\cdot\frac{\rho_p}{\eta}\,\frac{\varepsilon^{3/4}}{(b/\rho_g)^{1/4}}\,r^2. \quad (7.11')$$

However, this equation, derived on the assumption that $v_{pg} << v_{1e}$, leads to exceedingly high values for relative velocity of the particle and medium, and, similarly, to highly elevated values of fluctuation velocity. The latter at times exceeded even the vibration velocity, a highly improbable condition; this can be shown by equating (7.11) and (7.7) and by finding the value of v_1. In view of this only equation (7.11) will be used hereafter. This action is reinforced by a simple experimental fact: particles suspended in a sound field, as a rule, trace coincident tracks and not a sine curve. The latter should be traced if velocity of fluctuations were much higher. Based on equations (7.6) and (7.11), Table 6 presents values of the extent of streamline flow around aerosol particles and the maximum relative fluctuating velocity of particles and medium in a sound field with frequencies f = 1 khz and 10 khz at the normal sound intensity of J (or I) = 0.1 w/cm² with numerator and denominator of each "fraction" corresponding to f = 1 khz and f = 10 khz respectively. Data in Table 6 show that relative fluctuating velocity of particles and medium in the 1 - 10 khz band is moderate and did not exceed 0.28 - 1.26 cm/sec for particles with r < 5μ. This constituted 0.2 - 1.1% of the medium vibrating velocity. The above values are accurate to within a factor ξ.

Table 6

r, μ	τ, sec	rad/sec	μ_g^l According to exact formula	μ_g^l As per simplified formula	cm/sec	max cm/sec
1	$1{,}2\cdot10^{-5}$	$\frac{370}{1200}$	$\frac{0{,}0017}{0{,}0055}$	$\frac{0{,}0017}{0{,}0055}$	$\frac{5{,}8}{10{,}4}$	$\frac{0{,}012}{0{,}067}$
3	$1{,}08\cdot10^{-4}$		$\frac{0{,}0151}{0{,}0497}$	$\frac{0{,}0151}{0{,}0497}$		$\frac{0{,}100}{0{,}567}$
5	$3{,}0\cdot10^{-4}$		$\frac{0{,}0420}{0{,}1366}$	$\frac{0{,}0420}{0{,}1380}$		$\frac{0{,}282}{1{,}680}$
10	$1{,}2\cdot10^{-3}$		$\frac{0{,}1655}{0{,}4830}$	$\frac{0{,}1680}{0{,}5520}$		$\frac{1{,}130}{5{,}850}$

8. SCATTERING AND ABSORPTION OF ACOUSTICAL ENERGY BY AEROSOL PARTICLES

Every aerosol particle, no matter how small, represented an obstacle to sound waves. A portion of the vibrating motion energy of a medium is used up in overcoming this obstacle. This is explained by the fact that the particle: 1) scattered incident sound waves in the surrounding space; 2) absorbed the energy of vibrating motions of the medium in its boundary layer; and 3) served as a source of irreversible heat loss, associated with periodical changes in its temperature. As a result, decrease in sound intensity during its passage through an aerosol was noticeably greater than during passage through an unpolluted gaseous medium. The theory of acoustical scattering on spherical and cylindrical obstacles was analyzed by Rayleigh [107] and was subsequently developed in the works of Lamb [61], Rzhevkin [105], and others. The theory indicated [62] that energy carried off per second by waves scattered on a spherical particle for which r << λ, was:

$$J_s = \frac{7\pi}{9}\frac{\omega^4}{c_g^4} r^6 E_{gp} \qquad (8.1)$$

In accordance with (1.22), total energy flux transferred per second by a sound wave through 1 cm of wavefront was:

$$J = \overline{E} c_g \qquad (8.2)$$

That portion of input energy lost in the aerosol layer due to scattering was, as also in the case of sound absorption by the medium, proportional to the layer thickness:

$$\frac{J_{sp}\, dx}{J} = \alpha_p^s dx, \qquad (8.3)$$

where α_p^s is the coefficient of acoustical energy scattering by aerosol particles. Substituting terms (8.1) and (8.2) and considering that $E_{gp} = \mu_g^2 \overline{E}$, get

$$\alpha_p^s = \frac{112\pi^5}{9}\frac{f^4 r^6 \mu_g^2}{c_g^4} n. \qquad (8.4)$$

It appears more practical to substitute the value of weight concentration of the particle instead of the numerical concentration; accordingly, taking into consideration (9.1), the following expression for the coefficient of acoustical energy scattering by aerosol particles is obtained:

$$\alpha_p^s = \frac{28}{3}\left(\frac{\pi f}{c_g}\right)^4 \frac{r^3}{\rho_p} \mu_g^2 k 10^{-6}. \qquad (8.5)$$

In the case of particles with unit density, suspended in air

$$\alpha_p^s \approx 0{,}68 \cdot 10^{-21} k r_\mu^3 \cdot \mu_g^2 f_{khz}^4 \qquad (8.5')$$

(r_μ - particle radius in μ; f_{khz} - frequency of vibrations in khz). Clearly, under normal conditions, α_p^s is of the order $\approx 10^{-20}$, which, for practical reasons, can be always disregarded. The theory of acoustical energy absorp- by station

The theory of acoustical energy absorption by stationary spherical and cylindrical obstacles was first developed by Sewell [265], who showed that the coefficient of acoustical energy absorption by spherical particles due to viscous losses, could be determined by the following formula, which took into account the extent of streamline flow around particles:

$$\alpha_p^v = \frac{6\pi\nu r n}{c_g}\mu_g^2\left(1 + r\sqrt{\frac{\omega}{2\nu}}\right). \qquad (8.6)$$

or by replacing n by k in formula (9.1)

$$\alpha_p^v = 4{,}5\frac{\nu k 10^{-6}}{c_g \rho_p r^2}\mu_g^2\left(1 + r\sqrt{\frac{\omega}{2\nu}}\right). \qquad (8.7)$$

The second term in parentheses in both equations is normally much smaller than 1 under the optimal coagulation conditions when, according to Section 16, small values of ω corresponded to large values of r, and could be disregarded. In such case, the following formulas can be obtained for the coefficient of acoustical energy absorption:

$$\alpha_p^v = \frac{6\pi\nu rn}{c_g}\mu_g^2, \quad (8.8)$$

$$\alpha_p^v = 4{,}5\frac{\nu k\, 10^{-9}}{c_g \rho_p r^2}\mu_g^2. \quad (8.9)$$

In the case of particles with unit density, suspended in air, the above formula becomes:

$$\alpha_p^v \simeq 1{,}73k\frac{\mu_g^2}{r_\mu^2}\ \text{дб/м} \quad (8.9')$$

(r_μ - particle radius in μ). The derivation of the above formulas is relatively simple, if the following elementary method suggested by Brandt, Freund and Heidemann is followed [162, 168].

The energy absorbed by the viscous medium during the streamline flow around aerosol particle is quantitatively equal to the work done by the reactive forces exerted by the particle against the motion of the medium. Assuming that instantaneous reactive force was determined by Stokes' formula (4.3), and that the relative velocity of the medium varied sinusoidally (5.22), it can be shown that energy absorbed by a particle in 1 sec was:

$$J_a = \int_0^1 F_{\text{Ст}} u_{gp}\, dt_1^* = 6\pi\eta r\mu_g^2 U_g^2 \int_0^1 \cos^2(\omega t - \varphi)\, dt = 3\pi\eta r\mu_g^2 U_g^2. \quad (8.10)$$

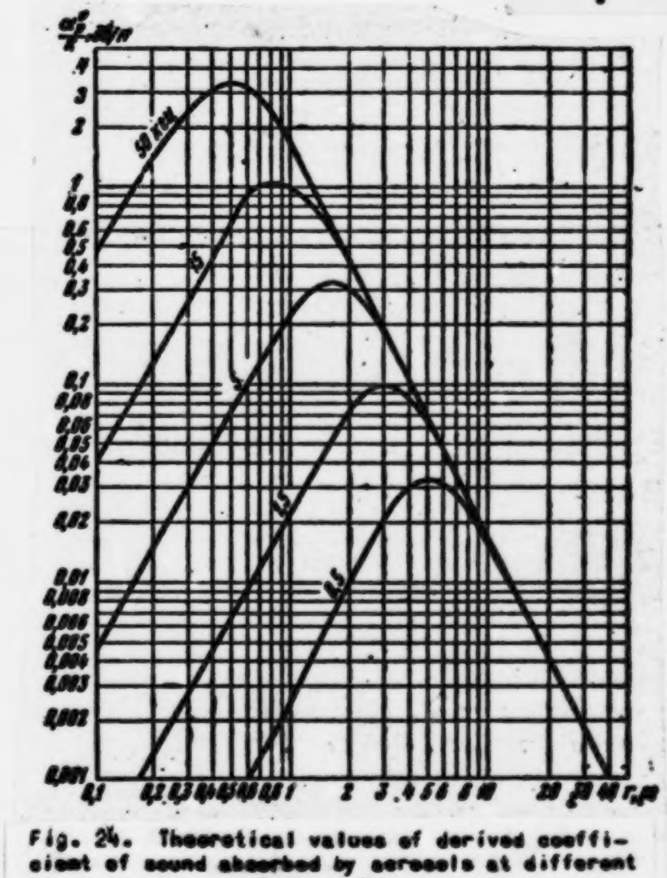

Fig. 24. Theoretical values of derived coefficient of sound absorbed by aerosols at different frequencies

The ratio of absorbed energy to total energy, which passed through an aerosol layer with thickness dx, and determined from (8.2), could be expressed by an equation identical to (8.3), so that after substitution of (8.10), equation (8.8) is obtained, and subsequently, allowing for (9.1), equation (8.9) is derived.

Based on calculations with the aid of (8.9), Figure 24 illustrates coefficient values of viscous sound absorption by unit-density aerosol particles in air as a function of their radius at k = 1 g/m³; in the case of particles with r < 1μ, Cunningham's correction factor for the medium was taken into consideration. As can be seen, each vibration frequency corresponded to a critical particle radius for which sound absorption was maximal. The value of the critical radius could be found readily by setting the derivative $d\alpha_p^v/dr$ to zero:

$$r_{\text{кр}} = \sqrt{\frac{9\eta}{4\pi\rho_p f}}. \qquad (8.11)$$

For air with $p_p = 1$, the formula becomes

$$r_{\text{кр}} = \frac{3{,}65}{\sqrt{f}}. \qquad (8.11')$$

At a critical radius $\mu_g = \sqrt{2}/2$. In view of this, and in accordance with (8. 9), the following equation can be written for the maximal coefficient of viscous absorption:

$$(\alpha_p^v)_{\text{макс}} = k\frac{f_{\text{кгц}}}{15{,}4}\ \text{дб/м}. \qquad (8.12)$$

In the 0.5 - 50 khz band, $(\alpha_p^v)_{max}$ amounts to 0.0325 - 3.25 db/m for 1 g of aerosol particles. Therefore, even at a comparatively low weight concentration of critical size particles, the coefficient of absorption α_p^v can far exceed the coefficient of sound absorption by the gaseous medium α_g, which attains enormous values at elevated frequencies. The value of α_p^v can be decreased only by changing the frequency of vibrations away from the critical frequency determined by the ratio (8.11) or (8.11'). The following expression was derived by Epstein and Carhart [188, 122] for the coefficient of sound absorption due to the periodic irreversible heat transfer between the particle and the medium, which leads to a corresponding increase in the medium's entropy and a decrease in free energy:

$$\alpha_p^\chi = \frac{4\pi\chi r n}{c_g}(\gamma - 1)\left(1 + r\sqrt{\frac{\omega}{2\nu}}\right)\mu_{g\chi}^2, \qquad (8.13)$$

where x - thermal conductivity of the medium, $\lambda g/p_g c_g$; μ_{gx} - degree of temperature compensation of the particle and medium, determined by an equation identical to the equation for the degree of streamline flow around particles, in which $b = 1/r\sqrt{2\nu/\omega}$ is replaced by $\theta = 1/r\sqrt{2x/\omega}$

$$\mu_{g\chi} = \sqrt{\frac{a^2}{a^2 + 3a\theta + \frac{9}{2}\theta^2 + \frac{9}{2}\theta^3 + \frac{9}{4}\theta^4}}. \qquad (8.14)$$

Substitute k for n in (8.13), and, considering that usually $r\sqrt{\omega/2\nu} << 1$, obtain the following expression:

$$\alpha_p^\chi = \frac{3\chi k\cdot 10^{-6}}{c_g\rho_p r^2}(\gamma - 1)\ \mu_{g\chi}^2. \qquad (8.15)$$

In the case of particles with unit density, suspended in air ($x = 0.2$; $\gamma = 1.4$), (8.15) becomes

$$\alpha_p^\chi \approx \frac{6\cdot 10^{3} k}{r_\mu^2}\ \mu_{g\chi}^2\ \text{дб/м} \qquad (8.15')$$

(r_μ - particle radius in μ).

In the case of large θ, values of particle and medium temperatures are nearly identical, the decrease in the free energy is negligible and, therefore, $\mu_{gx} \simeq 0$. In the case of very small θ the particle temperature is almost constant, the temperature drop and the decrease in free energy attain practically their maximum possible values and, therefore, $\mu_{gx} \simeq 1$. The total coefficient of sound absorption due to the presence of aerosol particles is:

$$\alpha_p = \alpha_p^s + \alpha_p^v + \alpha_p^T \simeq \alpha_p^v + \alpha_p^T. \tag{8.16}$$

All coefficients discussed above are additive up to the particle concentrations of $n < 10^8$ and provided that $(\gamma - 1)\omega x/c_g \ll 1$, which in the case of air yields $\omega \ll 4 \cdot 10^5$. In the case of water mist $|\alpha_p^T|$ is approximately 40% of $|\alpha_p^v|$. The total coefficient of sound absorption by aerosols, taking into account absorption by the medium, is expressed by the following sum:

$$\alpha' = \alpha_g' + \alpha_p. \tag{8.17}$$

Moreover, a variation in sound intensity with distance can be determined by the same exponential function (1.15') or (1.21) as for uncontaminated medium. In addition to the discussed phenomena occurring during propagation of sound waves through aerosols in the dispersed liquid phase, processes of evaporation and condensation of vapor droplets occurred periodically, as was shown by Ostwald. Evaporation was caused by a rise in the medium temperature during the compression phase, and condensation was caused by the temperature drop during the rarefaction phase.

Evaporation and condensation, which lagged medium temperature variations, constituted irreversible thermodynamic processes which lead to conversion of mechanical sound energy vibrations into heat, and, subsequently, to energy loss. In view of this, sound attenuation in mists was higher than the same in smoke and dust. This was established experimentally for low acoustical frequencies (33hz) by Mache and also by Shmaus [3].*

The coefficient of sound absorption, in a mist determined by the indicated processes of evaporation and condensation, greatly depended on: 1) frequency of acoustical vibrations; 2) presence of condensation nuclei; and 3) type of phase transitions sustained by mist during the propagation of sound waves (a transition from a humid region into dry one or from a humid region into water). In the case of a low number of condensation nuclei only water vapor diffusion to and from the nuclei should occur. In the case of a large number of nuclei, both condensation and evaporation occurred.

The theory of sound attenuation in mists was investigated in detail by Oswatitsch [245]. He postulated that the additional sound adsorption had a maximum in the band of several tens of hz. At lower frequencies, on the fringe of infrasound, temperature variation period of the medium was large, and, therefore, there was sufficient time for establishing a balance between droplets and vapor. At higher frequencies, however, that period was too small and, as a result, evaporation and condensation failed to develop, and the mist remained in an adiabatically dry state (a similar state was achieved also for a small number of condensation nuclei); the sound absorption coefficient was negligible. For better illustration of the above, the numerical results for the additional sound absorption coefficient $\Delta\beta$ for the water mist, containing droplets with mean radius $\bar{r} = 6.25\mu$ for $k = 2\ g/m^3$ [213] are presented:

---

* Reference [3] does not correspond to this author. [B.S.L.]

$f = 25$	50	100	500	гц
$\Delta\beta = 4$	3	2	0,2	дб·сек⁻¹.

According to Wei Chun-tseu [21, 22], results yielded by Oswatitsch's theory have been understated. Nevertheless, it can be assumed that at a frequency of 0.5 khz, additional attenuation was negligible as compared with the normal sound attenuation in a fog, computed from formulas for the solid phase (see Table 7 below). As a rule, higher frequencies had been used in practice for aerosol coagulation. Therefore, it can be considered that additional sound attenuation did not take place in coagulating fogs, and it was possible to use above formulas for aerosol with solid dispersed phases. The presence of suspended particles and increased sound attenuation induced some decrease in the sound propagation velocity. Zink and Delsasso [297] derived the following formula for the decrease in sound velocity Δc_g, due to the presence of aerosol particles:

$$\Delta c_g = \frac{1}{2} c_g \frac{M_p}{M_g} \left(\mu_p^2 + \gamma_{pg} \frac{\mu_{pg}^2}{C_{pg}} R_g \right), \qquad (8.18)$$

where M_p/M_g is the ratio of the dispersed phase masses and the medium; γ_{pg} - the ratio of their specific heats C_{vp}/C_v; C_{pg} - the gas molar heat capacity at constant pressure; R_g - the gas constant. The first term in the equation represents decrease in sound velocity caused by increase in the system's density. The second term determined decrease due to increase in the system's heat capacity. These factors have affected the sound velocity only when aerosol particles participated in the vibrating motion of the medium ($\mu^p > 0$), and when they absorbed and emitted heat ($\mu_{gz} > 0$). Therefore, sound absorption effect and decrease in the sound velocity were complementary.

It should be noted that the first purely qualitative experimental investigations of sound attenuation in aerosols (natural fogs) described by Tyndall [117] failed to reveal the negative effect of suspended particles on the transmission of sound. On the contrary, it was noticed that in a dense fog the sound propagated much further than in a transparent atmosphere. The reason for this, seemingly paradoxical, phenomenon was concealed, as was discovered later (see Section 1) by the fact that sound absorption depended on air humidity which changed considerably upon fog formation. In general, experimental sound attenuation measurements in natural fogs were highly unreliable, since under such conditions sound weakened due to wavefront expansion and to atmospheric density and humidity heterogeneities of the medium could not be taken into consideration. The first quantitative sound absorption measurements of aerosols were made by Altberg and Holtzmann [138]. Their experiments had been conducted at frequencies of 5 - 22 khz, and tobacco smoke was used as the aerosol. The size of its particles was not determined; moreover, tobacco smoke contained much carbon dioxide, which greatly increased the absorbing capacity of the medium. The results obtained by these authors were difficult to compare with the theory of sound wave attenuation in aerosols presented here.

Laidler and Richardson [220] experimentally investigated magnesium oxide and stearic acid absorption by smoke, and lycopodium spores at high ultrasonic frequencies (42, 98, and 695 khz). The first two aerosols were highly polydispersed, and the lycopodium spores were sufficiently homogeneous; their average radius was $r \approx 2.5\mu$, and their numerical concentration attained $n = 1.5 \cdot 10^6$. Degree of streamline flow around the particles was $\mu_g \approx 1$, i.e., and particles remained practically stationary. The following values were obtained for sound absorption coefficient α_p by the lycopodium spore aerosols: 0.029 and 0.031 at 42 and 98 khz, respectively. According to Füchs' calculations [121], theoretical values of α_p were 0.038 and 0.042, respectively, and discrepancy between the theoretical and experimental values was 30 - 35%, the causes of which will be discussed later.

The rate of sound attenuation in a resonant chamber filled with water or oil vapor, obtained by the mechanical atomization of the liquid, and also with ammonium chloride smoke, was measured experimentally by Kndsen Wilson, and Anderson [213]. These authors measured the sound attenuation coefficient β (db $\cdot$ sec^{-1}) which was related to α_p in the following manner:

$$\beta_p = 10 \lg e \cdot \alpha_p c_g. \tag{8.19}$$

In the case of water mist containing droplets ($\bar{r} = 6.25\mu$; $k = 2/g/m^3$), results obtained are shown in Table 7. In the case of mineral oil with ($r_{cp} = 5\mu$; $k = 1.17\ g/m^3$) and in ammonium chloride smoke with ($\bar{r} = 0.5 - 1.0\mu$, $k = 0.26 \div 1.03\ g/m^3$), results shown in Table 8 had been obtained.

Table 7

Oscil'n. frequency in kHerz	Absorption coefficient, β, db in sec^{-1}		
	Experiment'l.	Theoretical	
		According to Knudsen et al (213)	According to Epstein et al (186)
0,5	5	10,1	5,0
1,0	7	13,8	5,7
2,0	9,4	16,0	6,3
4,0	10,1	17,1	6,9
6,0	12,0	18,2	7,5
8,0	13,2	18,8	7,7

In addition to above mentioned experiments, sound attenuation measurements were also made in water mist at lower frequencies. Results of these experiments were as follows:

Oscillation frequency	Absorption coefficient β db, sec^{-1}
27,5	4,8
58,0	3,5
112,0	2,8
150,0	3,6
200,0	6,7
350,0	7,2

A decrease in sound attenuation in the 112 hz region was revealed.

Table 8

Oscillation frequency in kherz	Extinction coeff. β, db.sec^{-1}			
	First exptl. series	Second exptl series	Result averages	Calculated theoretical values
0,25	—	0,5	0,5	2,3
0,50	1,5	1,8	1,6	6,3
1,0	3,6	4,0	3,8	11,2
2,0	7,7	7,7	7,7	14,4
4,0	13,6	12,8	13,2	16,3
6,0	15,0	14,4	14,7	17,3
8,0	21,2	20,6	20,9	18,3

Table 9

Oscillation frequency	Extinction coeff. β, db.sec^{-1}					Computed coeff. at $k = 1.03 g/m^3$
	$k=0,36\ g/m^3$	$k=0,46\ g/m^3$	$k=0,53\ g/m^3$	$k=0,86\ g/m^3$	$k=1,03\ g/m^3$	
0,5	0,2	0,4	0,3	0,2	1,0	0,7
1,0	0,5	0,8	1,5	3,0	3,0	2,8
2,0	2,0	4,6	6,0	11,0	12,6	10,4
4,0	7,0	15,5	16,0	30,5	37,0	35,8
6,0	11,0	25,0	26,0	51,0	58,0	65,5

Data in Tables 7, 8, and 9 indicate that the discrepancy between Knudsen's et al theoretical calculations and those of the experiment was significantly great, which can be explained by the following: first, Knudsen et al in calculating theoretical values of the sound attenuation coefficient, failed to take into consideration attenuation resulting from irreversible heat losses of the medium caused by heating and cooling of aerosol particles, an occurrence which was investigated theoretically later. Secondly, as Fuchs [121] pointed out, the authors failed to account for the strong effect of aerosol polydispersion on the theoretically computed sound attenuation coefficient. The authors used the arithmetical mean $\bar{r}$ as the numerical value of the particle radius obtained from the relationship $\sum n_i r_i = n\bar{r}$, whereas they should have used the arithmetical mean ratio $\bar{r}$ to the cubic mean radius to the third power $\bar{r}/r_3^3$ instead of value $1/r^3$ in (8.9). Since r_3 was always greater than $\bar{r}$ in the case of polydispersed aerosols, failure to satisfy the above condition leads to highly elevated results.

Epstein and Carhart conducted theoretical calculations of sound attenuation coefficients, shown in the last column of Table 7, individually for the fractions, allowing for thermal conductivity of the medium according to equation (8.13). However, their results proved too low. This could be explained by the fact that the effects of evaporation and subsequent vapor condensation on the fog droplets were disregarded.

Wei Chun-tseu [22] measured the attenuation coefficient of 1 - f sound in an artificial water mist containing droplets of radius in the order of 5 - 9μ in an amount of $0.5 \cdot 10^4 - 1.5 \cdot 10^4$. Frequency of vibrations was varied in the 25 - 250 khz range. Measurements were conducted by the standing-wave method using a sound level recorder. Values of the attenuation coefficient were in the 8.8 - 20.8 db $\cdot$ sec^{-1} range (the highest absorption occurred at 35 - 50 hz). These values are much higher than those obtained using Oswatitch's theory. Exceptionally good agreement between the theoretical and experimental data on sound attenuation by aerosols at acoustical frequencies had been obtained by Zink and Delsasso [297]. Their method of measurements was based on comparison of acoustical pulses transmitted through aerosol and a pure gas. The attenuation coefficient was determined from the ratio of amplitudes and sound velocity in an aerosol - from a distance between sinusoids. Functional dependence of attenuation and sound velocity on vibration frequency was investigated for air, argon, oxygen and helium. Powdered aluminum oxide was used as aerosol particles ($n = 3 \cdot 10^4$) with radii from 2.5 to 7.5μ. For the purpose of theoretical sound attenuation coefficient computation, particles had been classed into four groups with radii of 2.5, 3.75, 5, and 7.5μ. Figure 25 shows the theoretical and experimental values of the sound attenuation coefficients in air obtained by the authors. Both data types are nearly coincidental. Identical degree of agreement was obtained for helium. Experimental data for argon and oxygen were slightly higher than the theoretical values (5 - 10%). At the same time, satisfactory agreement was obtained between the experimental data on the velocity of sound in aerosols and the theoretical calculations of the same, conducted using equation (8.18).

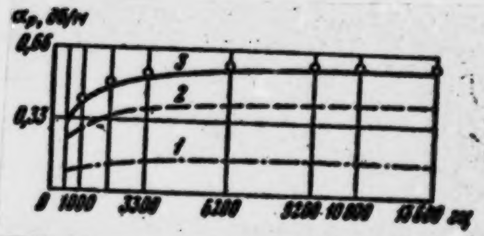

Fig. 25. Sound absorption by aerosol of aluminum oxide according to Zink and Delsasso.
1 - Theoretical sound absorbtion coeff resulting from total losses (a_p^v); 2 - Theoretical sound absorbtion coeff resulted from non-reversible heat transmission from particles to medium and *vice versa* (a_p^x); 3 - Total sound absorbtion coeff $a_p = a_p^v + a_p^x$;
Circles indicate exptl. values.

Zink's and Delsasso's experiments prove that the theory of sound attenuation in aerosols with a solid dispersed phase (smoke and dust) has been refined presently to a high degree and can serve as a dependable basis for practical calculations. Among other experimental investigations in the area of sound aerosol attenuation, the work of B. F. Podoshevnikov and B. D. Tartakovskii [97] should be mentioned. Podoshevnikov and Tartakovskii measured sound attenuation coefficients at 13 khz in a highly dispersed mist of dioctyl phthalate ($\bar{r} = 0.28\mu$) with particles strongly entrained into the vibrating motion of the medium (for details see Section 15). On the average, the attenuation coefficient was 2.7 db/m higher in this case than in the case of pure air. A substantial functional dependence of the results on the concentration of droplets could not be noticed, which undoubtedly should be attributed to inaccuracy of measurements.

CHAPTER 3

AEROSOL PARTICLE INTERACTION IN A SOUND FIELD

9. PRELIMINARY INFORMATION

Rules governing motion of individual aerosol particles exclusive of their mutual interaction had been examined in the preceding chapter. This situation is nonexistent under practical conditions. The average distance between coagulating aerosol particles was such that, any difference in their vibratory velocities may cause a mutual overtaking or interaction through the medium, thereby distorting the ideal picture of particle motion presented above. It has been known that different aerosols exhibited different physical characteristics; in particular, the dispersion state, density, and weight concentration. This created a wide variation in the following geometric parameters: number of aerosol particles per unit gas volume, average distance between particles, specific particle surface area, average particle radius, dispersed phase volume, etc. The above parameters substantially affected the kinetics of coagulation processes in general, and the acoustical aerosol coagulation in particular. Their influence, although less significant, was nevertheless quite apparent during evaporation, drying, desorption, and combustion of dispersed phase in the sound field.

Examine the geometry of an ideal aero-dispersive system, a mono-dispersed non-evaporating fog with strictly spherical droplets which upon coagulation formed spheres with larger radii of same density. The geometric parameters of poly-dispersed systems were easily deduced if the relationships derived for this case, and for the case of solid particle aggregates characterized by loosely packed primary particles, were used, and if the analysis had been conducted by parts.

If the weight concentration k(g/m^3), radius r, and density p_p of the mono-dispersed aerosol particles are generally known, the number of particles per 1 cm^3 - "numerical" particle concentration - can be determined by the following expression:

$$n=\frac{k\cdot 10^{-6}}{{}^4/_3\pi r^3\rho_p}\simeq 0{,}24\cdot 10^{-6}\frac{k}{r^3\rho_p}. \qquad (9.1)$$

In the case of small particle dimensions, numerical particle concentrations may attain values of the order of 10^{10} and higher. However, because of the primary particle coagulation brought about by intensive Brownian motion, even in the first few seconds after their appearance, the highly dispersed aerosol particles begin to aggregate, and their numerical particle concentration falls to 10^7 - 10^8. For example: assume radius of primary particles, formed by the condensation or sublimation of the substance, to be

$r = 0.02\mu = 2 \times 10^{-6}$ cm, and let the numerical particle concentration be $k = 10$ gm/m^3. According to equation (9.1), this corresponded to $n_0 \simeq 3.5 \times 10^{11}$. According to Smolunovskii [121], the rate of the Brownian coagulation of aerosols may be determined by the following quadratic relationship:

$$\frac{dn}{dt} = -K_{6p} n^2, \qquad (9.2)$$

which, upon integration, becomes:

$$n = \frac{n_0}{1 + K_{6p} n_0 t}, \qquad (9.3)$$

where K_{br} is the coagulation constant, equal to 1.8×10^{-9} cm^3/sec for particles under study.

Calculations made with the aid of this formula show that the numerical particle concentration decreased with time as follows:

when $t = 1$ sec $n = 5.5 \times 10^8$ (i.e., by a factor of 640)
when $t = 10$ sec $n = 5.5 \times 10^7$ (i.e., by a factor of 6,400)
when $t = 100$ sec $n = 5.5 \times 10^6$ (i.e., by a factor of 64,000)

The particle radius also increased to $r = 0.17$, 0.5, and 1.5μ, respectively (i.e., by a factor of 8.5, 25, and 75, respectively). It follows that highly dispersed industrial fogs only rarely contained droplets with radii less than $0.2 - 0.5\mu$, and a thinly dispersed smoke contained, as a rule, aggregates the dimensions of which were even greater.

Now, assume that n particles are uniformly distributed in 1 cm^3. Divide this volume into a series of cubes such that each cube contained one aerosol particle. In this case $\sqrt[3]{n}$ particles will be distributed on each side and, therefore, the average distance between particles s_m will be:

$$s_m = \frac{1}{\sqrt[3]{n}}. \qquad (9.4)$$

Substitute expression (9.1) into the above equation and perform a simple transformation, and obtain the following expression for the normalized distance $s_m = s_m/r$ [73, 74]:

$$s_m \simeq 160 \sqrt[3]{\frac{\rho_p}{k}}. \qquad (9.5)$$

This is the fundamental equation of aerosol geometry. Figure 26 presents values of calculated [using equation (9.5)] normalized distances s_m between particles as a function of gravimetric concentration k for different densities p_p. Thus, it is seen that the average normalized distance between particles varied only slightly with changes in the gravimetric concentration and particle density.

In the range of gravimetric concentrations $k = 1 - 100$ gm/cm^3, the average normalized distance for $p_p = 1$ lies in the range $s_m = 160 - 35$. Actually, equation (9.5) applied only to mono-dispersed aerosols. It demonstrates how the average distance varied as particles became larger during coagulation, provided they remained mono-dispersed. Factually, p_p and k remained constant during the coagulation of ideal aerosols, and as a consequence

$$s_m = \text{const}. \tag{9.6}$$

Whence, average distance between particles at each particle enlargement stage was linearly related to running radius r:

$$s_m = s_m r. \tag{9.7}$$

Radii of ideal aerosol droplets changed during their coagulation in the following manner. When two identical droplets with radius r_0 merged, the initial numerical concentration n_0 decreased to n. The mass remained conserved, i.e., $3/4\ \pi\ r_0^3\ \rho_p n_0 = 3/4\ \pi r^3\ \rho_p n$; therefore

$$r = r_0 \sqrt[3]{\frac{n_0}{n}}. \tag{9.8}$$

During total coagulation of n_2 small droplets with radii r_2, and n_1 large droplets with radii r_1, which acted as coagulation centers, the mass conservation principle postulated $3/4\pi r^3_2 \rho_p n_2 + 3/4\pi r^3_1 \rho_p n_1 = 3/4\pi r^3 \rho_p n_1$; therefore:

$$r = r_1 \sqrt[3]{\frac{n_2}{n_1} r^3_{2np} + 1}, \tag{9.9}$$

where $r_{2norm} = r_2 r_1$ is the "normalized" radius of small droplets. If the gravimetric concentration of small droplets k_2 is greater than the gravimetric concentration of large droplets k_1, formula (9.9) turns into formula (9.8), where $r_0 = r_2, n_0 = n_2$, and $n = n_1$. Solid particles form loose aggregates with lower density p'_p. If these were approximately spherical, equations (9.8) and (9.9) may be represented in the following form:

$$r = r_0 \sqrt[3]{\frac{n_2}{n} \frac{\rho_p}{\rho'_p}}, \tag{9.8'}$$

$$r = r_1 \sqrt[3]{\left(1 + \frac{n_2}{n_1} r^3_{2np}\right) \frac{\rho_p}{\rho'_p}}. \tag{9.9'}$$

Now, consider the theory of viscous streamline flow around spherical bodies. In the case of viscous streamline flow regime, a gas underwent considerable changes which remained unconstrained by the near field, but were propagated over distances exceeding the average distance between aerosol particles. Examine a velocity field developed in the region surrounding a spherical obstacle with radius r in the forward streamline gas flow, the nonturbulent relative velocity u_{gp} of which was directed parallel to x axis (see Figure 27). Assume that the center of coordinates was located at the center of the sphere, and that coordinates of the point in question were the polar ρ and angle θ between ρ and the x axis. Denote the radial component of the velocity vector by v [sic]* and the tangential component by v_θ. According to Oseen's theory [243, 244, 45, 111], which unlike Stokes' theory, partially accounted for the gas flow inertia incident on the sphere, the streamline flow velocity components can be determined from the following equations:

---

* Should read v_ρ. [B.S.L.]

$$v_{\rho} = \frac{3}{4}\frac{u_{gp} r}{m\rho^2}\{1 - [1 + m\rho(1 + \cos\theta)] e^{-m\rho(1-\cos\theta)}\} + u_{gp}\cos\theta, \quad (9.10)$$

$$v_{\theta} = \frac{3}{4}\frac{u_{gp} r}{\rho}\sin\theta e^{-m\rho(1-\cos\theta)} - u_{gp}\sin\theta, \quad (9.11)$$

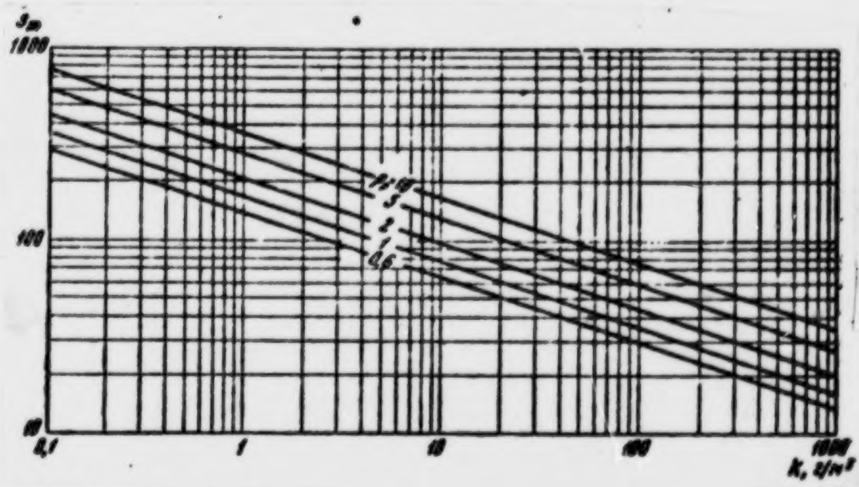

Fig. 26. Average derived distance between aerosol particles of different weight concentrations and density.

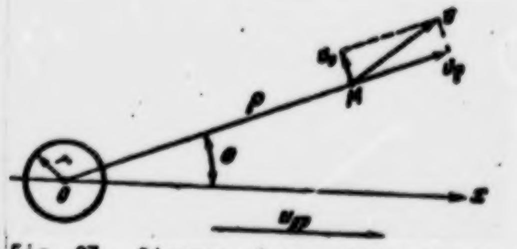

Fig. 27. Diagram of computed velocities in the field surrounding a particle.

where $m = u_{gp}/2\nu$. The last terms in these equations complement the equations cited in the literature above, insofar as the case considered was diametrically opposed to the case of a moving sphere in a stationary viscous medium (see [45], page 393).

Transform equations (9.10) and (9.11) by making $\rho_{norm} = \rho/r$ ("normalized" curve relative to the particle radius), and $m_{\rho} = \frac{1}{4}\mathrm{Re}\,\rho_{norm}$ by substituting equations (9.10) and (9.11), which will then assume the following "normalized," dimensionless form,

$$v_{\rho_{np}} = \frac{v_{\rho}}{u_{gp}} = \frac{3}{\mathrm{Re}\,\rho_{np}^2}\{1 - [1 + \frac{1}{4}\mathrm{Re}\,\rho_{np}(1 + \cos\theta)] e^{-\frac{1}{4}\mathrm{Re}\,\rho_{np}(1-\cos\theta)}\} + $$
$$+ \cos\theta, \quad (9.12)$$

$$v_{\theta_{np}} = \frac{v_{\theta}}{u_{gp}} = \frac{3}{4\rho_{np}}\sin\theta e^{-\frac{1}{4}\mathrm{Re}\,\rho_{np}(1-\cos\theta)} - \sin\theta. \quad (9.13)$$

making equations for the velocity components of streamline flow around a sphere more convenient for theoretical analysis. The resultant "normalized" streamline velocity can then be determined from a simple formula.

$$v_{np} = \sqrt{v_{\rho_{np}}^2 + v_{\theta_{np}}^2}. \quad (9.14)$$

Figure 28 shows the velocity field in the medium for the case (similar to ours) of a moving sphere with Re = 1, as calculated by Piercey and McHugh [251], who based their solutions on Oseen's equation refined by Goldstein [194]. The solid lines indicated the locus of all points in the medium with equal normalized velocities, i.e., maximum sphere velocities. The dotted lines indicate direction of normalized velocity at angles between sphere velocity and direction of its motion at infinity. Coordinate axes represent the "normalized" distances, i.e., distances with respect to the sphere radius. Important conclusions can be drawn by examining Figure 28. A cursory in-

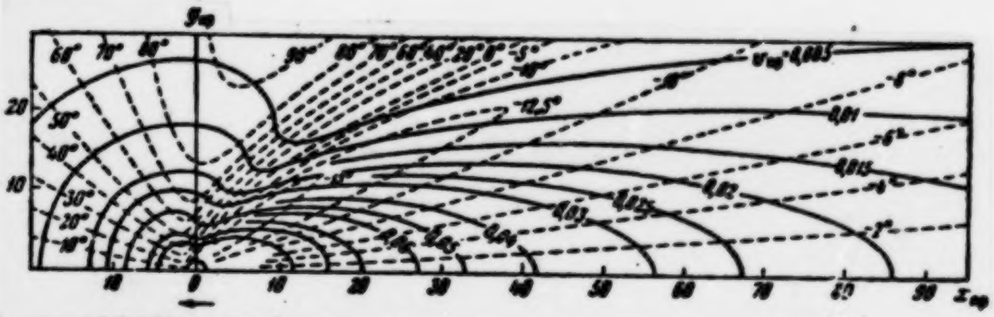

Fig. 28. Field of velocities surrounding a migrating spherical particle at great distances when Re = 1.

spection of the figure suggests first that the velocity field around the sphere was characterized by strong asymmetry in the direction of motion; a parabolic "trail," in this case a "stagnation" region, characterized by a reduced streamline velocity, appears behind the sphere, in the considered case - in front of it; secondly, the "boundary" layer around the sphere is unusually developed; the velocity differed perceptibly from that of infinity at distant point locations which exceeded the sphere radii tenfold, and in the "trail" region hundredfold. Figure 28 clearly indicates that the velocities which are 1% of the sphere velocity occurred at distances of about 20 r in front of and at the sides of the sphere, and at approximately 150 r behind the sphere in the "trail" region. The third conclusion following from analysis of the figure and equations (9.12) and (9.13) is: as Reynolds number decreased the boundary layer around the sphere increased accompanied by a decrease in asymmetry The asymmetry was apparent even at low Reynolds numbers, down to Re = 0, and at distances greater than those shown in the Figure.

This can be illustrated by supplementing the evidence with the following calculation: using equations [illegible]12) and (9.13), compute the normalized velocity of streamline flow around [illegible]here at low Re numbers in front of ($\theta = 180°$), on each side of (θ = 90 and 270°), and behind ($\theta = 0°$) the sphere at a distance of $\rho_{\text{norm}} = 75$, which corresponded to the average normalized distance s_n between aerosol particles when k = 10 gm/m^3. It should be noted that for large values of ρ_{norm} and fixed angles θ, equations (9.12) and (9.13) can be considerably simplified.*

At $\theta = 0°$

$$v_{x_{\text{пр}}} = 1 - \frac{3}{2x_{\text{пр}}} \quad v_{y_{\text{пр}}} = 0; \tag{9.15}$$

at θ = 90 and 270°

$$\begin{gathered} v_{y_{\text{пр}}} = 0, \quad v_{x_{\text{пр}}} = \frac{-3}{4y_{\text{пр}}} + 1 \ (\text{при Re} \to 0), \\ v_{y_{\text{пр}}} = \frac{3}{\text{Re}\, y^2_{\text{пр}}}, \quad v_{x_{\text{пр}}} = +1 \ \left(\text{при } \frac{1}{4}\text{Re}\,|y_{\text{пр}}| > 5\right); \end{gathered} \tag{9.16}$$

at $\theta = 180°$

$$\begin{gathered} v_{x_{\text{пр}}} = +1, \quad v_{y_{\text{пр}}} = 0 \ (\text{при Re} \to 0), \\ v_{x_{\text{пр}}} = \frac{-3}{\text{Re}\, x^2_{\text{пр}}} + 1, \quad v_{y_{\text{пр}}} = 0 \ \left(\text{при } \frac{1}{4}\text{Re}\,|x_{\text{пр}}| > 5\right). \end{gathered} \tag{9.17}$$

---

* In contrast to equations (9.12) and (9.13) the direction of the velocity component v_x is here considered to be coincident with the x axis.

It appears certain that the streamline velocity in front of and behind the sphere abated as $1/x_{norm}$ and $1/x^{3}_{norm}$, respectively. Calculation results are summarized in Table 10, which show that even when Re → 0, the difference in streamline velocities in front of and behind the sphere was only 2% of the flow velocity.

Table 10

Reynold number Re	Behind the sphere ($\theta = 180°$) $v_{x_{pr}}$	Behind the sphere ($\theta = 180°$) $v_{y_{pr}}$	Lateral to the sphere ($\theta = 90$ и $270°$) $v_{y_{pr}}$	Lateral to the sphere ($\theta = 90$ и $270°$) $v_{x_{pr}}$	In front of the sphere ($\theta = 0°$) $v_{x_{pr}}$	In front of the sphere ($\theta = 0°$) $v_{y_{pr}}$
0	1,00	0	0	0,99	0,98	0
0,25						
0,50						
0,75				1,00		
1,00						

The fourth conclusion, brought out be examining jointly Figure 28 and equations (9.12) and (9.13) is: the streamline flow in front of and in a narrow region behind the sphere was radial at large distances from the sphere, so that the tangential components may be practically disregarded when $\theta \to 0$ and $\theta \to 180°$; $v_{\theta} \approx 0$ and the radial components may be computed from simplified equations (9.15) and (9.17).

Now examine the trajectories of medium's particles moving around a sphere. This case was examined specifically by Tomotika and Aoi [280], who used Oseen's approximate solution, as refined by Goldstein, to derive the following expression for the normalized streamline function $\psi_{norm} = \psi/r^{2}u_{sp}$:

$$\psi_{np} = -\left\{\frac{3}{4}\left(\rho_{np} - \frac{1}{\rho_{np}}\right) - \frac{16+3Re}{32}\left(\rho^{2}_{np} - \frac{1}{\rho_{np}}\right) + \right.$$

$$\left. + \frac{3Re}{32}\left(\rho^{2}_{np} - \frac{1}{\rho^{2}_{np}}\right)\cos\theta\right\}\sin^{2}\theta. \qquad (9.18)$$

When Re → 0, the above equation reduces to the streamline function of Stokes' flow, which, in reality is an abstract concept:

$$\psi_{np} = \frac{1}{2}\left(1 - \frac{3}{2\rho_{np}} + \frac{1}{2\rho^{3}_{np}}\right)\rho^{2}_{np}\sin^{2}\theta. \qquad (9.19)$$

Figure 29 shows the streamlines for a case of a flow around a sphere at Re = 1 as calculated in [280]. Clearly, the streamlines exhibited apparent asymmetry even near the sphere. Ascertain whether relationships derived under the assumption of statior [illegible] streamline flow around bodies were perti [illegible] o the considered case, i.e., streamline flow of vibrating gas around particles. There are two special characteristics of streamline flow around aerosol particles in a high-intensity sound field. First, the particle dimensions are small as compared with thickness δ of the boundary layer ("depth of penetration" of the vortex motion) determined by equation (1.40), i.e., the following condition is satisfied:

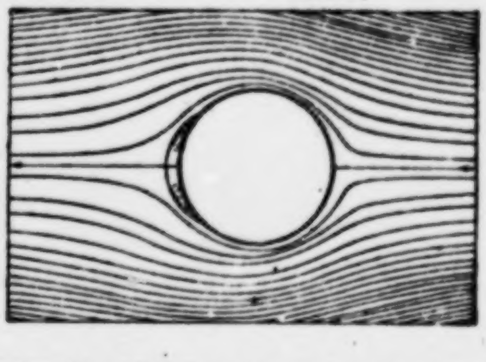

Fig. 29. Flow lines in the proximity of engulfed spherical particle at Re = 1 (φ_{pr} = 0.005; 0.05; 0.01; 0.2; 0.3; 0.4; 0.5, etc.)

$$(2r)^2 \omega \ll \nu. \tag{9.20}$$

Secondly, the Reynolds number is small: Re < 1, i.e., and the following condition is satisfied:

$$\frac{2r\omega A_{gr}}{\nu} \ll 1. \tag{9.21}$$

The case, as noted in [62], corresponded to low oscillation frequencies, in which the medium motion around obstacles could be considered stationary at each instant. In this case, equation (1.40) loses its effectiveness, and the boundary layer surrounding the sphere can be determined from the stationary streamline flow equations (9.12) and (9.13). These equations were independent of frequency of oscillations, a fact which has been overlooked occasionally by investigators, as in [12]. In the case of a multiple streamline gas flow around aerosol particles, there occur special new features which will be examined in Section 11. The difference in the vibratory velocities of aerosol particles, presence of wide streamline flow fields, and the general turbulence of a sonicated medium, all affected particle behavior. A complex hydrodynamic interaction develops between the aerosol particles. It may be analyzed only if subdivided into elementary types of interaction as follows: 1) orthokinetic interaction; 2) parakinetic interaction; 3) attractional interaction; 4) pulsation interaction.

All four interaction types are analyzed in the following paragraphs.

10. ORTHOKINETIC INTERACTION OF AEROSOL PARTICLES

If two adjacent particles differed in size or density and, consequently, had different velocities, they either converged on or diverged from one another in the course of their motion. This type of longitudinal convergence or divergence between particles is called the orthokinetic* particle interaction. It occurred during the drift and pulsating and vibratory particle motions. The most interesting is orthokinetic interaction which appeared in the course of vibratory particle motion. This type of interaction was the limiting case of all other types of orthokinetic interaction, since the velocity of vibratory motion was greater than the drift velocity and the velocity of pulsating particles. Examine the conditions under which two particles may converge on one another orthokinetically prior to actual contact, i.e., particle collision in the case of vibratory motion. It has been assumed normally [167] that orthokinetic collision between two vibrating particles was possible when the smaller particle fell into the "aggregate volume" of the larger particle. The latter was in the form of a cylinder, the radius of which was equal to the sum of radii of both particles $r_a = r_1 + r_2$, and its height was equal to twice the difference between the amplitude of vibratory particle displacements $h_a = 2(A_{p_2} - A_{p_1}) = 2(\mu_{p_2} - \mu_{p_1})A_g$, with two hemispherical ends. However, this model must be made more precise. In the first place it provided no allowance for phase differences in the interacting particle vibrations. Secondly, it disregarded the medium's streamline flow around the particles, as a result of which the converging particles deflected from one another.

---

* This term (in Greek, orthos - strait, kineticos - relating to motion) reflects the nature of the phenomenon much better than the term "kinematic" as proposed in [121] (in Greek, kinema - motion). This will be particularly apparent from the text in Section 11.

Now, examine both questions in that order. If the velocity of the medium's vibratory motion varied according to $u_g = U_g \sin \omega t$, the absolute difference in velocities of two spherical particles 1 and 2 having radii r_1 and r_2, respectively, at time t may be determined as follows:

$$\Delta u_p = u_{p_1} - u_{p_2} = \mu_{p_1} U_g \sin(\omega t - \varphi_1) - \mu_{p_2} U_g \sin(\omega t - \varphi_2), \quad (10.1)$$

where μ_{p1} and μ_{p2} are the degrees of entrainment of the first and second particles into the medium's vibratory motion, respectively, which are computed from (5.16), and φ_1 and φ_2 are the phase angles of the same particles calculated from (5.14). The maximum value (peak amplitude) of the difference in the vibratory particle velocities ΔU_p was attained at time t and phase angle φ_0. The time may be computed by taking derivative $d(\Delta u_p)/dt$ and equating it to zero:

$$\operatorname{tg} \omega t_0 = \operatorname{tg}\left(\frac{\pi}{2} + \varphi_0\right) = \frac{\mu_{p_2}^2 - \mu_{p_1}^2}{\mu_{p_1}\mu_{g_1} - \mu_{p_2}\mu_{g_2}}. \quad (10.2)$$

The ratio of amplitudes of difference in the particle velocity and the vibrating velocity U_g, i.e., degree of relative particle motion $\mu_{12} = \Delta U_p / U_g$, can be determined from the following expression:

$$\mu_{12} = \{\mu_{p_1}^2 + \mu_{p_2}^2 - 2\mu_{p_1}\mu_{p_2}(\mu_{p_1}\mu_{p_2} + \mu_{g_1}\mu_{g_2})\}^{1/2}. \quad (10.3)$$

Figure 30 shows values of μ_{12} as a function of 1) radius of the larger particle r_1, and 2) normalized radius of the smaller particle $r_{norm} = r_2/r_1$ at different frequencies. It can be seen that each particle pair had its own optimum sound frequency with μ_{12} as a maximum. To find this frequency, derivative $d\mu_{12}/d\omega$ should be taken and set to zero, obtaining the following expression:

$$\omega_{\text{опт}} = \frac{1}{r_{\text{пр}}\tau_1}^{\frac{1}{2}}. \quad (10.4)$$

or explicitly:

$$f_{\text{опт}} = \frac{9\eta}{4\pi\rho_p r_2^2} r_{\text{пр}}. \quad (10.5)$$

In the case of particles with unit density suspended in air, equation (10.5) had the following form provided r was expressed in μ and f in khz:

$$f_{\text{опт}} = \left(\frac{13{,}2}{r_2^2}\right) r_{\text{пр}} \text{ кгц}. \quad (10.5')$$

Parameters of the vibratory motion of the particle and medium at optimum frequency are given by the following expressions:

$$\mu_{p_1} = \mu_{g_2} = \cos\varphi_1 = \frac{r_{\text{экр}}}{\sqrt{1+r^2_{\text{экр}}}}, \tag{10.6}$$

$$\mu_{p_2} = \mu_{g_1} = \cos\varphi_2 = \frac{1}{\sqrt{1+r^2_{\text{экр}}}}, \tag{10.7}$$

$$\operatorname{tg}\varphi_1 = \frac{1}{r_{\text{экр}}}, \quad \operatorname{tg}\varphi_2 = r_{\text{экр}}. \tag{10.8}$$

$${}_{0} = \frac{\pi}{2}, \quad \varphi_0 = 0, \tag{10.9}$$

$$\mu_{12} = \frac{1-r^2_{\text{экр}}}{1+r^2_{\text{экр}}}. \tag{10.10}$$

At the instant the relative particle velocity attained its peak value, the entrainment coefficients become:

$$\mu^0_{g_1} = \mu^0_{g_2} = \frac{1}{1+r^2_{\text{экр}}}, \tag{10.11}$$

$$\mu^0_{g_2} = \mu^0_{g_1} = \frac{r^2_{\text{экр}}}{1+r^2_{\text{экр}}}. \tag{10.12}$$

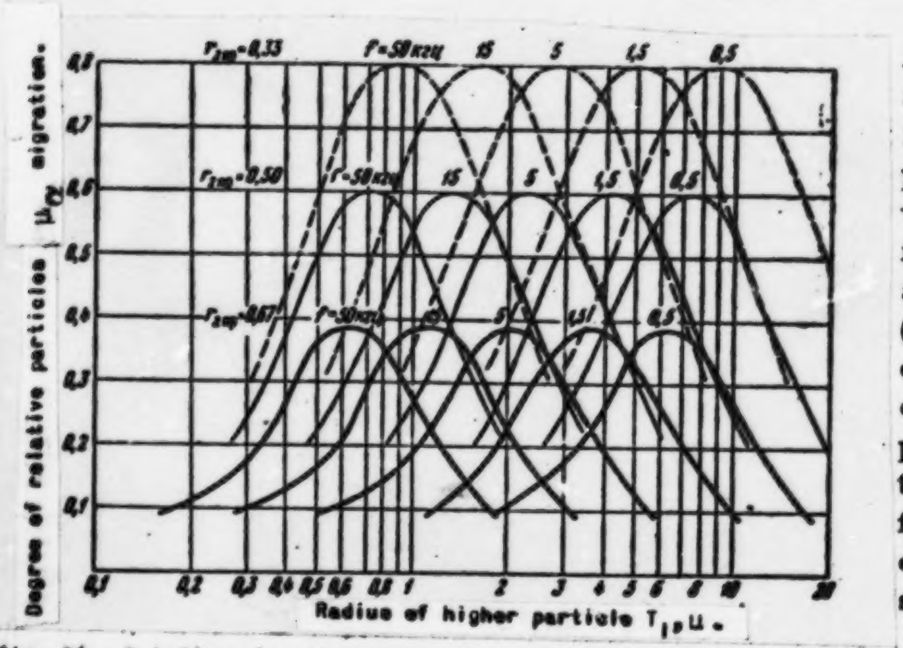

Fig. 30. Relative migration degree of two aerosol particles μ_{12} at different frequencies and size ratios.

Analogous expressions are obtained for the relative particle displacement, since both velocity and displacement were proportional, as shown in equation (1.11). Accordingly, it can be argued that the critical distance between particles, in the direction of vibratory flow, for which the orthokinetic collision is possible, was:

$$A_{12} = \mu_{12} A_g, \tag{10.13}$$

and consequently, height of the aggregate volume was:

$$h_a = 2\mu_{12} A_g. \tag{10.14}$$

Height of the aggregate volume computed from this formula exceeded twice the difference of the vibratory particle displacement amplitudes, if the fact that the particles were retarded by the presence of surrounding boundary layers were disregarded.

Examine the trajectory of a small particle as it converged on a large particle. If the size of the smaller particle were absolutely and relatively negligible, it "obediently" followed the gas motion along the original streamline, and the probability that it would be captured by a larger particle was nil, since all the streamlines bent around the larger particle without bisecting it, except for the center line. However, the size and mass of aerosol particles were finite and, consequently, the smaller particle diverged from the original streamline by virtue of its inertia as shown in Figure 31. The aggregate volume in this case had the shape indicated by the dotted lines.

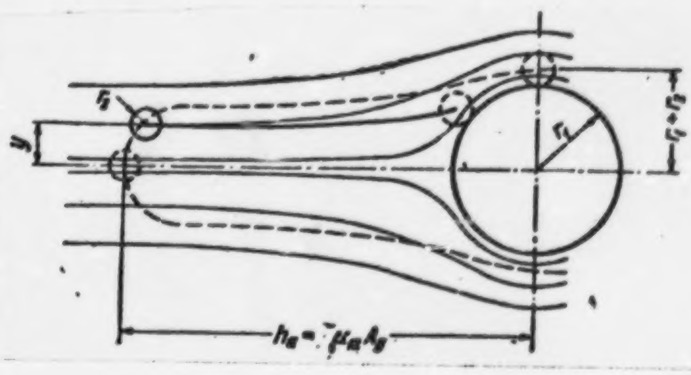

Fig. 31. Diagrams of orthokinetic impact between aerosol particles.
Dotted line indicates the "aggregate" volume involved in a single contact, or impact, between particles.

It had been shown in [66, 121, 122, 129] that the coefficient of particle entrainment was characterized by the following relationship:

$$Э = \left(\frac{y}{r_1}\right)^2 = y^2_{np}. \qquad (10.15)$$

Unfortunately, the existing formulas for calculating the coefficient of entrainment, Langmuir's formula [120] in particular, can not be applied here. In the first place, the formula pertained to cases where particle sizes were small in relation to the streamed sphere. In the case considered, both particles as a rule were commensurate with one another and the "engagement" effect [121] was significant. Secondly, it had been assumed that the particles moved uniformly, while in the case under consideration, they moved nonuniformly according to a sinusoidal, or a more complex, relationship and, moreover, they started from different initial positions. Thirdly, it had been assumed that the boundary layer surrounding the sphere was negligibly small in comparison with its size. In this case, the thickness of the boundary layer considerably exceeded the dimensions of interacting particles and, consequently, when a small particle converged on a large one, its motion became retarded.

The exact mathematical solution of the problem related to the coefficient of aerosol particle entrainment in the course of the particle's singular orthokinetic approach in the sound field was difficult. Fortunately, there appeared no need to surmount these difficulties, since in a sound field, where multiple orthokinetic convergence and divergence of particles prevailed, the concept of a coefficient of entrainment loses its conventional meaning, as will be shown later (Section 11). However, to complete the picture of the aggregate volume the approximate critical values of the "singular" coefficient of entrainment, which characterize the minimum and maximum values of the cross-section area of the volume, will be computed.

Inertial particle divergence from the original streamline occurred mainly in the case of close approaches to the streamed sphere, where the curvature of a streamline radius was very small (see Fig. 29). In the case of more remote portions of a streamline, the magnitude of the inertial particle displacement during the approach was small, since the streamlines here were bent considerably less. Therefore, the minimum value of the entrainment coefficient ε_{min} occurred when the particle was situated away from the sphere at the time when its relative velocity dropped to zero. Moreover, it can be assumed for rough calculations, that the particle moved along without diverging from its original streamline.

If the normalized particle radius was $r_{a\,norm}$, the radius vector at the instant the particle touched the sphere was $\rho_{norm} = 1 + r_{a\,norm}$. For the sake of simplicity assume that contact occurred when $\theta = 90°$ (actually $\theta \approx 98°$, but this affected the calculations only slightly). The streamline function through a point ($\rho_{norm} = 1 + r_{a\,norm}$, $\theta = 90°$) according to (9.22) is:

$$\psi_{\text{пр}} = \frac{r_{\text{зпр}}}{2(1 + r_{\text{зпр}})}\left[r^{2}_{\text{зпр}} + \frac{3}{2}r_{\text{зпр}} + \frac{3\mathrm{Re}}{16}(r^{2}_{\text{зпр}} + 3r_{\text{зпр}} + 3)\right]. \quad (10.16)$$

To compute ε_{min} using equation (9.18) it is necessary to find the ordinate of a point along the streamline at a distance of $\rho_{norm} = h_a = 2\mu_{12}A_z$. The terms $1/\rho^{2}_{norm}$ and $1/\rho_{norm}$ in equation (9.18) can be disregarded when the distance from the sphere was $\rho_{norm} > 10$. The streamline function was as follows:

$$\psi_{\text{пр}} = \left[\frac{1}{2}\rho^{2}_{\text{пр}} - \frac{3}{4}\rho_{\text{пр}} + \frac{3\mathrm{Re}}{32}(1 - \cos\theta)\rho^{2}_{\text{пр}}\right]\sin^{2}\theta. \quad (10.17)$$

Since the question concerns the streamline near the center line, it can be assumed that $\rho_{norm} \approx x_{norm}$ and $\sin^{2}\theta = (y_{norm}/\rho_{norm})^{2} \approx y_{norm}/x_{norm})^{2}$. In addition, angle θ between the radius vector and the center line was small under these conditions and, therefore, $\cos\theta \approx -1$ may be assumed for the left hand side branch of the streamline where $\theta \to \pi$, and $\cos\theta \approx +1$, for the right hand side, where $\theta \to 0$. As a result of these approximations, the streamline function assumed the following form:

$$\psi_{\text{пр}} = \left(\frac{1}{2} - \frac{3}{4}|x^{-1}_{\text{пр}}| + \frac{3\mathrm{Re}}{16}\right)y^{2}_{\text{пр}} \quad (\text{при } \theta \to \pi). \quad (10.18)$$

$$\psi_{\text{пр}} = \left(\frac{1}{2} - \frac{3}{4}|x^{-1}_{\text{пр}}|\right)y^{2}_{\text{пр}} \quad (\text{при } \theta \to 0). \quad (10.19)$$

In considering particle convergence, it is necessary to use equation (10.18); when their divergence is analyzed - (10.19). The latter is, incidentally, the Stokes' streamline function. Normally, distance x_{norm} was large enough to assume that $x^{-1}_{norm} \approx 0$; in that case, equations (10.18) and (10.19) can be simplified even further:

$$\psi_{\text{пр}} = \left(\frac{1}{2} + \frac{3}{16}\text{Re}\right) y^2_{\text{пр}\infty} \quad (\text{при } \theta \to \pi), \qquad (10.18')$$

$$\psi_{\text{пр}} = \frac{1}{2} y^2_{\text{пр}\infty} \quad (\text{при } \theta \to 0). \qquad (10.19')$$

Equate expressions (10.16) and (10.18'), take equation (10.15) into consideration, and get the following:

$$Э_{\text{мин}} = \frac{8r_{\text{зпр}}}{(1 + r_{\text{зпр}})(8 + 3\text{Re})} \left[r^2_{\text{зпр}} + \frac{3}{2} r_{\text{зпр}} + \frac{3\text{Re}}{16}(r^2_{\text{зпр}} + 3r_{\text{зпр}} + 3) \right]. \qquad (10.20)$$

The above expression has a minimum value when Re →0. Thus, to compute ϵ_{min}, use the following formula:

$$Э_{\text{мин}} = \frac{r_{\text{зпр}} + 1{,}5}{r_{\text{зпр}} + 1} r^2_{\text{зпр}} \simeq (1{,}25 \div 1{,}50) r^2_{\text{зпр}}. \qquad (10.20')$$

In deriving this formula the particle divergence from the original stream line due to inertia was disregarded, so that the formula yielded somewhat lower values. The maximum coefficient of entrainment ϵ_{max} was obtained in a case when a small particle was in the proximity of a sphere and reached it with a maximum relative velocity. The approximate value of ϵ_{max} can be computed in the following manner:

> Let the magnitude of entrainment coefficient ϵ_1 (excluding the effect of engagement), as calculated by Langmuir's formula, be known. According to (10.15) the ordinate of the initial point of the particule trajectory was

$$y^L_{\text{пр}} = \sqrt{Э_L}. \qquad (10.21)$$

In the case of a finite particle size, its trajectory partly changed its course and moved up. By examining figure 29, where the streamlines in the vicinity of the streamed sphere are shown, it may be concluded that if y_1 was not too small ($y_1 \geq 0.4$ - 0.5 or, $\epsilon_1 \geq 0.16$ - 0.25), an increase in the ordinate of the initial particle trajectory was roughly equal to particle radius r_{snorm}. Thus, the initial particle trajectory ordinate, include the engagement effect, is as follows:

$$y_{\text{пр}} \approx y^L_{\text{пр}} + r_{\text{зпр}} \approx \sqrt{Э_L} + r_{\text{зпр}}. \qquad (10.22)$$

and the coefficient of entrainment, accounting for (10.15) is:

$$Э_{\text{макс}} \approx (\sqrt{Э_L} + r_{\text{зпр}})^2. \qquad (10.23)$$

Langmuir's formula, which is normally used to compute the entrainment coefficient without allowing for "engagement" effect ϵ_1, has the following form [120, 121]:*

$$Э_L = \left(1 + \frac{0{,}75 \ln 2k}{k - k_{\text{кр}}}\right)^{-2}, \qquad (10.24)$$

---

*Shishkin's simplified formula [120] used under our conditions (comparatively large K) yielded elevated results.

where k is the inertia coefficient of a small particle:

$$k = \frac{u_{s1}\tau_s}{r_1} \qquad (10.25)$$

(u_{s1} and τ_s are the relative velocity and relaxation time of a small particle, respectively, and r_1 is the radius of a large particle); $k_{s\,r}$ is the critical coefficient of inertia which, according to L. M. Levin [66], can be determined for the Oseen streaming regime by the following formula:

$$k_{kp} = 1{,}49\sqrt{\frac{16-3\mathrm{Re}}{24+12\mathrm{Re}}}. \qquad (10.26)$$

Table 11 shows the computed (using the methods described) minimal and maximal coefficients of entrainment for the singular orthokinetic convergence of particles in a sound field of normal intensity (J (arI)= 0.1 w/cm^2, U_J = 220 cm/sec) at the optimum frequency for each particle pair. The relative velocity of a small particle u_{s1} may be calculated from the formual $u_{s1} = \mu_{1s}$ $v\theta_{norm}$ U_s, where $v\,\theta_{norm}$ is a correction factor for the retardation in the boundary layer which, according to (9.16), is equal to the normalized velocity at a point (y_{norm} = $1 + r_{s\,norm}$, $\theta = 90^o$) as follows:

$$v_{\theta np} = \frac{0{,}75}{1+r_{np}}e^{-\frac{1}{4}\mathrm{Re}(1+r_{np})} - 1. \qquad (10.27)$$

The Reynolds number Re was determined for the absolute value of the streamline flow velocity u_{sp} = μ^0_{s2} u_s, where μ^0_{s1} is the coefficient of streamline flow around a particle at an instant when the unperturbed oscillatory velocity attained its peak value expressed by the equation (10.11).

Table 11

r_1, μ	r_2, μ	amp.	sec,	μ^0_g	u_{gr} cm/sec	Re_1	k_{kp}	μ_{1s}	amp.	u_s, cm/sec	k	max.	min. max.	max.
1,0	0,25	0,25	$7{,}5\cdot10^{-7}$	0,94	207	0,276	1,110	0,88	0,496	96,0	0,72	- 0	0,09	0,09
	0,50	0,50	$3\cdot10^{-6}$	0,80	176	0,235	1,125	0,60	0,580	76,5	2,29	0,255	0,33	1,00
2,0	0,5	0,25	$3\cdot10^{-6}$	0,94	207	0,552	1,020	0,88	0,575	111,2	1,67	0,175	0,09	0,45
	1,0	0,50	$1{,}2\cdot10^{-6}$	0,80	176	0,470	1,045	0,60	0,650	85,8	5,15	0,492	0,33	1,45
	1,5	0,75	$2{,}7\cdot10^{-6}$	0,64	141	0,376	1,076	0,28	0,692	42,6	5,75	0,041	0,72	0,90
3,0	1,0	0,33	$1{,}2\cdot10^{-6}$	0,90	198	0,792	0,951	0,80	0,668	117,5	4,70	0,478	0,15	1,05
	1,5	0,50	$2{,}7\cdot10^{-6}$	0,80	176	0,705	0,976	0,60	0,705	93,0	8,37	0,607	0,33	1,65
	2,0	0,67	$4{,}8\cdot10^{-6}$	0,69	152	0,608	1,004	0,38	0,730	61,0	9,76	0,637	0,58	2,15
4,0	1,0	0,25	$1{,}2\cdot10^{-6}$	0,94	207	1,104	0,874	0,88	0,700	135,4	4,06	0,450	0,09	0,85
	2,0	0,50	$4{,}8\cdot10^{-6}$	0,80	176	0,940	0,912	0,60	0,753	99,4	11,93	0,678	0,33	1,75
	3,0	0,75	$1{,}08\cdot10^{-4}$	0,64	141	0,752	0,963	0,28	0,777	47,9	12,94	0,690	0,72	2,50
5,0	1,0	0,20	$1{,}2\cdot10^{-6}$	0,96	211	1,410	0,800	0,92	0,731	148,0	3,55	0,426	0,06	0,75
	2,0	0,40	$4{,}8\cdot10^{-6}$	0,86	189	1,260	0,835	0,72	0,778	123,2	11,82	0,676	0,22	1,50
	3,0	0,60	$1{,}08\cdot10^{-4}$	0,73	160	1,067	0,880	0,47	0,799	81,6	22,10	0,778	0,47	2,20
	4,0	0,80	$1{,}92\cdot10^{-4}$	0,61	134	0,893	0,925	0,22	0,814	39,4	15,12	0,719	0,82	2,70

The following conclusions may be derived from data in Table 11:

$\varepsilon = 0.3 - 0.7$ for particles with radii $r_1 = 0.5 - 1\mu$ and

$\varepsilon = 0.7 - 1.5$ for larger particles. Therefore, the aggregate volume of a large particle constituted a long cylinder with a cross section at each end of $\varepsilon_{min} \pi r_1^2$, increasing towards the middle and attaining $\varepsilon_{max} \pi r_1^2$ in the vicinity of the sphere. The cross section directly at the particle center line was even larger - $(1 + r_{2n \text{ or } n})^2 \pi r_1^2$.

Moreover, the magnitude of the aggregate volume in each case was considerably smaller than the volume of a cylinder with radius $r_1 + r_2$, for which the coefficient of entrainment would be $\varepsilon_{cyl} = (1 + r_{2n \text{ or } n})^2$. The orthokinetic interaction taking place during particle drift is characterized by small velocities. Therefore, the coefficient of particle entrainment may be considered here to be close to ε_{min}. The latter lies within the range of 0.09 and 0.82.

11. PARAKINETIC INTERACTION OF AEROSOL PARTICLES

If two aerosol particles of different size, or density, occupy positions in which their central axes did not coincide with the direction of oscillatory motion, they are subject to a transverse, or actually radially-transverse, interaction called the parakinetic* interaction. This type of interaction was first analyzed by the present author in [82]. The development of the interaction is the result on the one hand of the Oseen streamline asymmetry arising during a medium flow past the particles, and, on the other hand, by the particle inertia which enhanced a degree of particle divergence from a previous trajectory. Since an aerosol particle streaming in a sound field was of a multiple advancing-regressing nature, the initial particle divergence was followed by a second and third divergences - one cycle following another, As a result, the particles rapidly migrated with respect to one another in a short period of time. The parakinetic particle motion is a complex geometric process. Its understanding requires additional data on the theory of streaming which pertains to the stationary streamlines at large distances from the streamed sphere, the size of which was of the same order of magnitude as the average distance between natural aerosol particles. The simplified version (10.15) of the streamline function may be used in this case to draw the streamline. For the construction of streamlines passing near the center line (x-axis), it is possible to use even more simplified equations for the streamline function (10.18) and (10.19), provided the near field ($x_n < 10$) was disregarded; when solved for y_n they yielded the following equations:

---

*In Greek, para - beside, in the vicinity of, alongside of; kinetikos - relating to motion.

$$y_{np} = \left(\frac{\psi_{np}}{\frac{1}{2} + \frac{3}{4}x_{np}^{-1} + \frac{3Re}{16}}\right)^{1/3} \quad \text{at} \quad x < 0. \qquad (11.1)$$

$$y_{np} = \left(\frac{\psi_{np}}{\frac{1}{2} - \frac{3}{4}x_{np}^{-1}}\right)^{1/3} \quad \text{at} \quad x > 0. \qquad (11.2)$$

The second equation is the one of Stokes' streamline derived from the first equation by setting Re = 0. The ordinate origin of these, $y_{n\,-\infty}$, may be obtained by setting $x_{n\,-\infty}$.

Table 12

x_{np}	$-\infty$	-200	-100	-50	-25	-15	-10	0	$+10$	$+15$	$+25$	$+50$	$+100$	$+200$	$+\infty$
I. $\psi_{np} = 0{,}1$															
Re = 0 y_{np}	0,447	0,448	0,451	0,454	0,461	0,471	0,485		0,485	0,471	0,461	0,454	0,451	0,448	0,447
Re = 0 Δy_{np}	0	0,001	0,004	0,007	0,014	0,024	0,038		0,038	0,024	0,014	0,007	0,004	0,001	0
Re = 1 y_{np}	0,381	0,382	0,383	0,385	0,390	0,395	0,404								
Re = 1 Δy_{np}	0	0,001	0,002	0,004	0,009	0,014	0,023								
II. $\psi_{np} = 1$															
Re = 0 y_{np}	1,415	1,418	1,424	1,435	1,455	1,486	1,533		1,533	1,486	1,455	1,435	1,424	1,418	1,415
Re = 0 Δy_{np}	0	0,003	0,009	0,020	0,040	0,071	0,118		0,118	0,071	0,040	0,020	0,009	0,003	0
Re = 1 y_{np}	1,205	1,206	1,210	1,216	1,233	1,249	1,278								
Re = 1 Δy_{np}	0	0,001	0,005	0,011	0,028	0,044	0,073								

Table 12 shows calculated values of y_n and $\Delta y_n = y_n - y_{n\,-\infty}$ for ψ_n = 0.1 and ψ_n = 1 at Re = 0 and Re = 1 (using equation 11.1 and 11.2). Figure 32 shows exaggerated streamlines constructed by the use of experimental numerical values; (the increment (Δy_n) scale is 100 times the x-axis scale). These correspond to $\Delta y_{n\,-\infty}$ = 0.381 - 0.447 and $y_{n\,-\infty}$ = 1.206 - 1.415. Figure 32 also shows the normalized curvature radii $R_{1_n} = R_1 / r_1$ for streamlines calculated from the following formula (see, e.g., [11]:

$$R_{1np} = \frac{(1 + y_{np}'^{2})^{3/2}}{y_{np}''} = \frac{-\left(\frac{1}{2} + \frac{3}{4}x_{np}^{-1} + \frac{3Re}{16}\right)^{7/3} x_{np}^{3}}{\frac{3}{4}\psi_{np}^{1/3}\left[1 - \frac{9}{16}x_{np}^{-1}\left(\frac{1}{2} + \frac{3}{4}x_{np}^{-1} + \frac{3Re}{16}\right)^{-1}\right]} \qquad (11.3)$$

In this equation; (np = rt)

(y_n^1 and y_n'' are the first and second derivatives, of which the first may be disregarded as negligible .

The streamlines removed from the center line may be handled by equation (10.17). The solution of this for ρ_n yields the streamline equation in the explicit form; for higher values of ψ_n with a high degree of convergence, the equation is of the following form:

$$\rho_{np} = 12G^{-1} + \sqrt{32\psi_{np}}\,G^{-\frac{1}{3}}\sin^{-1}\theta, \qquad (11.4)$$

where G = 16 + 3 Re (1 - cos θ).

Figure 33 shows the exaggerated streamlines (the Δy_n increments scale is expanded 20 times) computed from equation (11.4) for ψ_n = 100 and ψ_n = 1000, in the case of two "cut-off" streaming regimes: a) Re = 0, and b) Re = 1 (dotted lines indicate backward flow streamlines). All the streamlines are situated at a considerable distance from the center line (x-axis). Their ordinates at the origin (at infinity), written above each line at the left, were derived in accordance with (11.4) from the following formula:

$$y_{np\_\infty} = \left(\frac{2\psi_{np}}{1 + 0{,}375\mathrm{Re}}\right)^{1/3} \qquad (11.5)$$

When ψ_n = 100, y_{n_∞} = 12-14, and when ψ_n = 1000, y_{n_∞} = 38-45. For the purpose of completeness, values of the normalized streamline curvature radii $R_{1_n} = R_1/r_1$ are given in figure (33a) and (33b). These were computed from the following well known formula [11]:

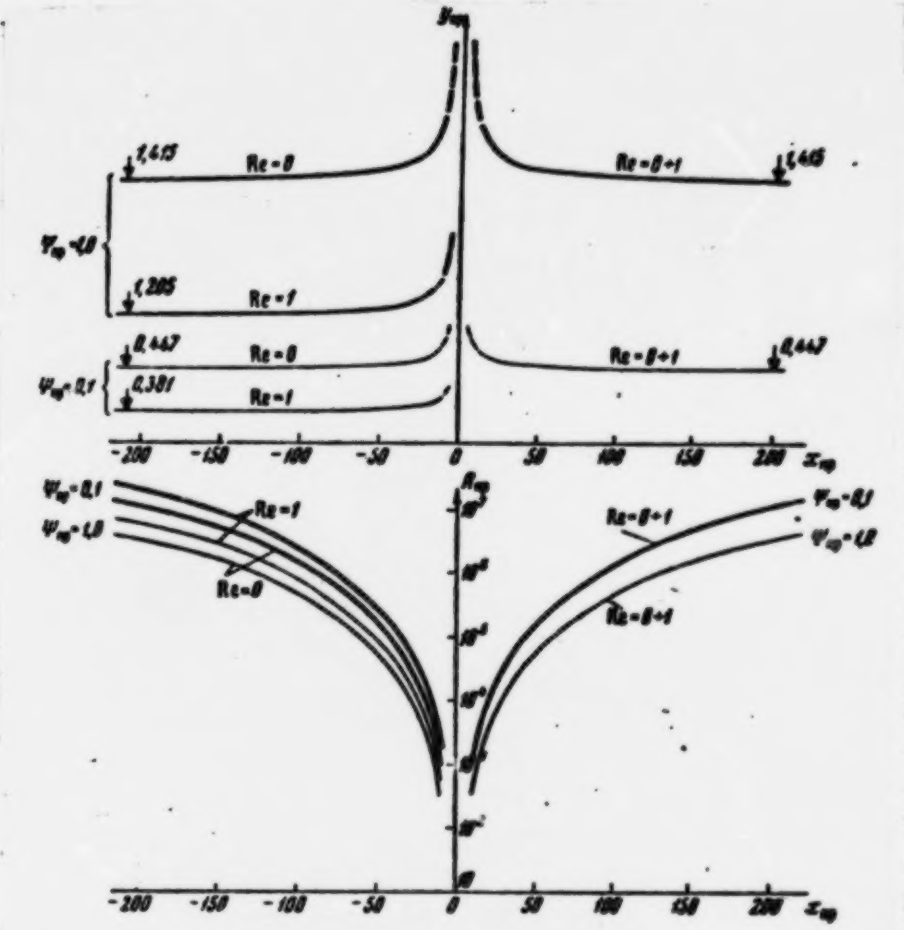

Fig. 32. Stationary current lines and their curvature radii in spherical particles in the proximity of central line (φ_{pr} = 0.1 and 1.0)

$$R_{1np} = \frac{(\rho_{np}^2 + \rho_{np}'^2)^{3/2}}{\rho_{np}^2 + 2\rho_{np}'^2 - \rho_{np}\rho_{np}''}, \qquad (11.6)$$

where p_n' and p_n'' are the first and second derivatives of the polar, derived by differentiating equation (11.4):

$$\rho_{np}' = -36\mathrm{Re}\sin\theta G^{-2} - \sqrt{32\psi_{np}}\,G^{-\frac{1}{2}}\left(\sin^{-2}\theta\cos\theta + \frac{3}{2}\mathrm{Re}\,G^{-1}\right),$$

$$\rho_{np}'' = 36\,\mathrm{Re}\,G^{-2}(6\mathrm{Re}G^{-1}\sin^2\theta - \cos\theta) +$$

$$+\sqrt{32\psi_{np}}\,G^{-\frac{1}{2}}\sin\theta\Big[2\sin^{-4}\theta - \sin^{-2}\theta + \qquad (11.6')$$

$$+\frac{3}{2}\mathrm{Re}\,G^{-1}\left(\sin^{-2}\theta\cos\theta + \frac{9}{2}\mathrm{Re}\,G^{-1}\right)\Big].$$

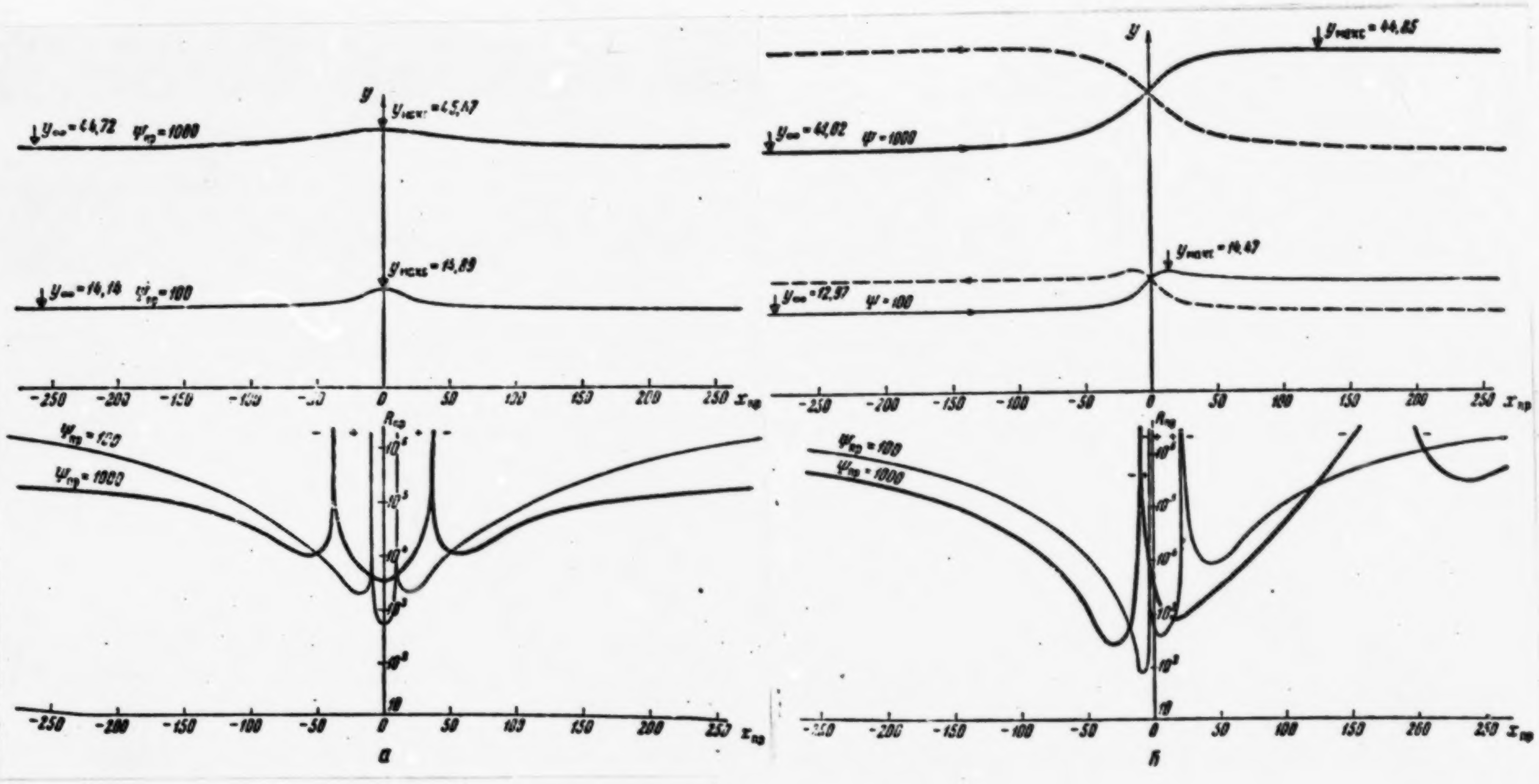

Fig. 33. Static current lines and their curvature radii for spherical particles at great distances from central line (φ_{rt} = 100 and φ_{rt} = 1000) a at Re = 0, b at Re = 1 (broken line indicates direction of reverse engulfment.

From the above stated it may be concluded that streamlines which passed near the center line were subjected to a relatively small deformation, excluding the near field, which may be disregarded in the case of singular streaming. However, the following is far more important .

a) streamlines originating in the case of Oseen's streaming regime ($Re > 0$) are obviously asymmetrical; moreover, the right branch is perceptibly steeper than the left branch. Thus, in the region $x_n = 10 - 50$ at $Re = 1$ an increase in the ordinate Δy_n is greater at the right than the left by $(0.003 - 0.015)\ r_1$ when $\psi_n = 0.1$ and by $(0.009 - 0.045)\ r_1$ when $\psi_n = 1$ (see, table 12);

b) curvature radius of a streamline, excluding the far regions, is small, and is predominantly found in the range $(10^3 - 10^5)\ r_1$ which even in the case of the "critical" radius $r = 3.5\mu$ yielded $R_1 = 0.35 - 35$ cm.

c) asymmetry, slope, streamline, and curvatures increased rapidly with the approach of streamed sphere, relatively speaking, it may be said that streamlines far from the center line were deformed more than those near the sphere (see figure 29).

The asymmetry of streamlines is very high here. The further from the center line the more the incident gas flow bent around the sphere with increases in retardation and curvature; moreover, after its rise, the streamline did not descend to its previous level, within the boundaries of the figure, as a result the right branch sloped more than the left branch. The curvature radius of a streamline, excluding the inflexion region, was approximately of the same order of magnitude as in the first case. This is the picture of a stationary aerosol particle streaming at large distances.

Assume, now, that a medium moved with an amplitude of vibration A, and analyze the behavior of the medium's vibrating particle:

1) near the center line at distant approaches to the streamed sphere, where the stationary flow lines exhibited form which can be described by equations (11.1) and (11.2) and figure 32.

2) far from the center line, symmetrically, with respect to the streamed sphere, where the stationary flow lines exhibited form which can be described by equation (11.4) and figure 33. These positions are notable because they illustrate two diametrically opposed tendencies of a viscous forward-backward flow around obstacles, which together manifested one facet of the parakinetic interaction of aerosol particles in a sound field.

In order to see immediately the essence and the functional state of these tendencies, assume first that the vibratory motion of the medium was subject to the right angle law in which absolute values of the incident and reverse gas flow velocity $|\vec{u}_s|$ and $|\overleftarrow{u}_s|$, respectively, were equal and constant, i.e., $|\vec{u}_s| = |\overleftarrow{u}_s| = \text{const}$. In this case, analyzing the forward motion of a medium particle, one can be guided by the stationary flow picture as characterized in Figs. 32 and 33, and in the case of a reverse flow, the mirror image with respect to the x-axis.

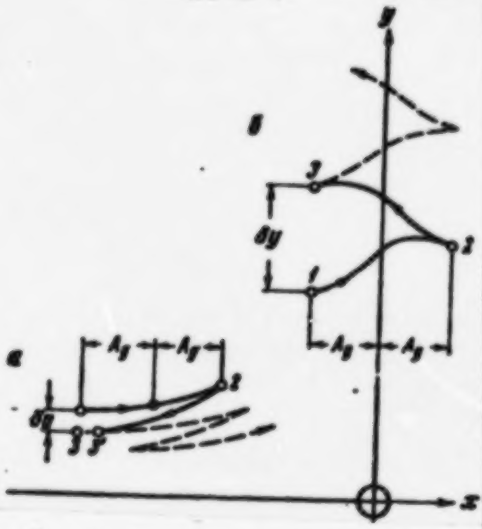

Fig. 34. Hysteresis of aerosol particles engulfment in a sound field. a – close to central line; b – away from central line

Now follow the behavior of medium's particle initially located at point 1 near the center line to the far left of the x-axis (Fig. 34a). If the magnitude of the vibration velocity and the Reynolds number Re were finite, the particle during the forward motion moved along a straight Oseen streamline as illustrated in Fig. 32. Moving along this line, the particle finally reaches point 2. The backward motion of the particle follows a line constituting the mirror immage of Stokes streamline, passing through symmetry point 2. It was mentioned earlier that this line was steeper than the Oseen line. This is the reason why a particle moved in the direction of point 3 during its backward motion below point 1 displaced by a somewhat smaller but finite distance δ_y. It has been known, however, that the velocity behind a streamed obstacle was lower than the velocity in front of it (see #9 and 12). Consequently, instead of reaching point 3, our particle reaches point 3' located somewhat closer to the center of the obstacle. During the succeeding vibration cycles the displacement process is repeated several times. As a result the particle approaches the center of the obstacle in a zig-zag manner.

When the observed particle of the medium is initially at point 1 far from the center line and left of the x-axis (see fig. 34b) the particle behaved differently. During the forward motion the medium's particle follows a straight Oseen streamline, as illustrated in figure 33b, coming to rest eventually at point 2. During its return motion the particle followed a streamline constituting a mirror image of Oseen's line through point 2. Toward the end of the return path, this line guides the particle to a higher point 3 displaced from the starting point by an amount δ_y. In the succeeding vibration cycles, this phenomenon occurred repeatedly; as a result, the observed particle zig-zags continuously away from the center line. The reason for this phenomenon [81] is the same as in the case of asymmetrical Oseen's streaming, namely, the medium's inertia; that the vibrating medium was predisposed to the streaming hysteresis appeared evident from the velocity field shown in Fig. 28: velocity angle inclination at a point on the right hand side always differed from the identical angle at the symmetrical point on the left hand side.

For practical purposes, the sonicated medium vibrational velocity was not constant, but varies sinusoidally, or in some other complex way. It can be easily seen, however, that even in those cases, the described phenomenon held even though same specific characteristics appeared. In the case of medium's vibration velocity where sinusoidal $u_g = U_g \sin \omega t$, these characteristics are reduced to the following:

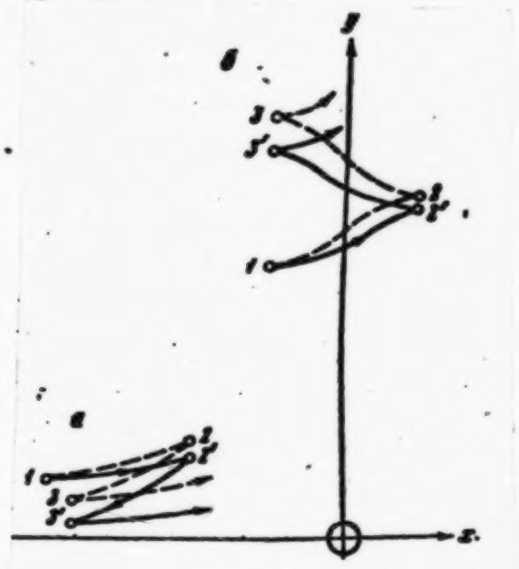

Fig. 35. Diagram illustrating the origin of autocentralization phenomenon of (a) and autodecentralization (b) of aerosol particles in a sound field.

Assume the particle oscillating near the center line to be at the same point to the left of x-axis at the starting moment (Fig. 35). During the initial displacement, when the vibration velocity and Reynolds number are negligible, the particle will, naturally, move along the stationary Stokes line. However, as the flow velocity and, consequently, the Reynolds number increased the particle motion followed increasingly greater slopes as it crossed into a more sharply defined Oseen's streamline. Having reached the peak velocity, at a point where the "peak" Oseen streamline passed, the trajectory slope increased in the reverse direction up to point 2, the medium's particle will glide into a new Stokes streamline. The medium's particle follows the entire new Stokes streamline during its reverse motion until it reaches point 3, located below point 1, the distance between the two being somewhat less than i in Fig. 34. The equation for the medium's particle trajectory in the above described "sinusoidally developing" Oseen's streaming of a sphere may be derived by disregarding the retarding effect of the boundary layer, i.e., far from the sphere, using equations (11.1) and (11.2) and by substituting $Re = \overline{Re} \sin \omega t$, and assuming that $\sin \omega t = \sqrt{1 - \cos^2 \omega t}$, where $\cos \omega t = (x_1 - A_g - x)/A_g = 1 - (x_n - x_{1n})/A_n$. Here $\overline{Re}$ is the peak Reynolds number, equal to $2r_1 U_g/\nu$; A_{gn} is the normalized amplitude of vibration equal to A_g/r_1.

Equation (11.1), which corresponds to the forward motion, assumes the following form:

$$y_{np} = \left\{ \frac{\Psi_{np}}{\frac{1}{2} + \frac{3}{4} x_{np}^{-1} + \frac{3Re}{16}\left[1 - \left(1 - \frac{x_{np} - x_{1np}}{A_{g_{np}}}\right)^2\right]} \right\}^{1/2}. \qquad (11.7)$$

Equation (11.2), which corresponds to the backward motion, remains unaltered.

The particle of a medium vibrating sinusoidally at some distance from the center line and to the left of the y-axis also begins to move along the Stokes streamline (Fig. 35). However, as the flow velocity and, consequently, Reynolds number increased, the particle assumed a progressively steeper trajectory as it crossed onto a more sharply defined Oseen's streamline. Then, having reached the peak velocity, at a point where the "peak" Oseen's streamline passed, the slope began to level off in the opposite direction and the particle glided onto a new Stokes streamline at point 2 to the right of the y-axis. The equation for the medium's particle trajectory in the above described "sinusoidally developing" Oseen's streaming of a sphere, if the flow retardation were disregarded, may be derived from equation (11.7) by substituting, as before, $\mathrm{Re} = \overline{\mathrm{Re}} \sin \omega t$ and assuming the following:

$$\cos \omega t = \frac{x_1 - A_g - \rho \cos \theta}{A_g} = 1 - \frac{\rho_{np} \cos \theta - x_{1np}}{A_{gnp}}, \qquad (11.7')$$

This resulted in the following:

$$\psi_{np} = \left\{ \frac{1}{2} \rho_{np}^3 - \frac{3}{4} \rho_{np} + \frac{3\,\mathrm{Re}}{32} \rho_{np}^2 (1 - \cos \theta) \left[2\, \frac{\rho_{np} \cos \theta - x_{1np}}{A_{gnp}} - \right.\right.$$
$$\left.\left. - \left(\frac{\rho_{np} \cos \theta - x_{1np}}{A_{gnp}} \right) \right]^2 \right\}^{1/2} \qquad (11.8)$$

At first the particle followed the same Stokes line in the reverse direction, changing over later to a progressively - defined and steeper reverse Oseen's line of the same type as shown by a dotted line in Fig. 33b. As a result, at the end of the return trip, having passed a new "peak" point, the particle assumes a higher point 3 through which a new Stokes line passes. Thus, tendency for a particle to move away from the center line of the sphere is also evidenced in this case.

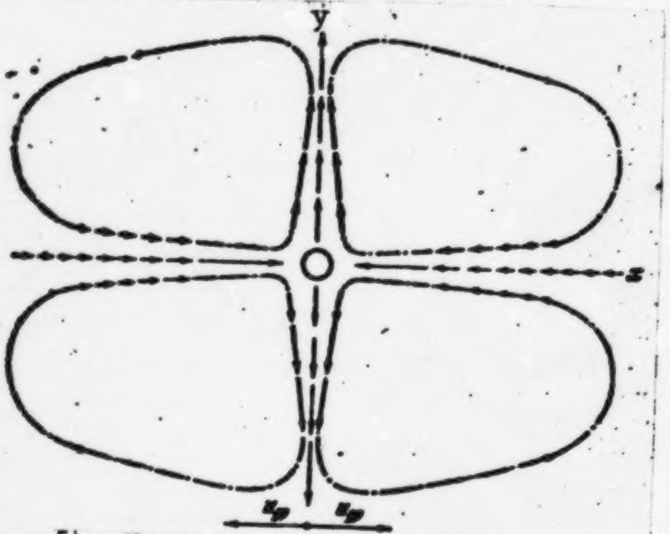

Fig. 36. Diagram of acoustical flow (current) around an aerosol particle suspended in a sound field

As a result of the streamline flow hysteresis around a sphere, a unique acoustical flow develops directed near the co-ordinate axes, shown by arrows in Fig. 36 with closed loops drawn arbitrarily. The flow is unique, because the size of its eddys was comparable to the vibration amplitude, while the eddy direction was directly opposite to that observed for $A_g << r$ by Andrade [140]. Andrade established that the condition for the formation of an eddy was $\mathrm{Re} > 5$. Subsequently, Schlichting [261] showed that under such conditions internal reverse flows must be generated near the obstacle surface as predicted by Carriere [173]. This hypothesis was verified experimentally by West [284] during tests conducted at Re > 40. Subsequent theoretical and experimental research conducted by Andres and Ingard [144], Holtsmark, et al. [201], Westervelt, et al. [225], and Lane [222] indicated that, as the transition to a viscous streaming had taken place, the scale of the internal eddys rapidly increased, displacing the outer eddys further away and, thereby, reducing them to zero, since the eddys were subsequently dispersed by the turbulent pulsations of the medium. The latter occurred, actually, in author's case, $A_s \gg r$, although it differed in the following:

a) Scale of eddys was independent of medium's vibration frequency which followed from the assumption that the flow was quasistationary;

b) eddy configuration depended on medium's vibration amplitude, which thus far, can be shown only geometrically, since the analytical solution of the problem of an acoustical flow around small obstacles for $A_s \gg r$ was handicapped by serious mathematical difficulties.

Now, assume that in the above field, existing around a streamed spherical particle, an aerosol particle with radius r_s was located at the point of the medium's particle. For the sake of simplicity, assume at first that the degree of entrainment into the vibratory motion was nearly unity for this particle, and, therefore, the particle was deprived of its own streaming field which could distort the indicated streaming pattern of a sphere. If the aerosol particle were negligibly small, its behavior would not differ practically from the behavior of the medium's particles; it would vibrate and zig-zag together with the latter, as shown earlier. However, if the particle had a perceptible inertia, its behavior in the streaming field might take on new features. Moving along curved portions of a streamline, the particle would be subject to some centrifugal forces which might displace it from the original streamline into the region of convexity. Therefore, in the first case, Fig. 35, an aerosol particle in a forward streaming would not assume point 2, but rather point 2' below, and this would be repeated with each succeeding cycle. Thus, it could be concluded that the particle inertia contributed to its hysteresis-like approach to the center line.

In the second case, shown in Fig. 35b, as a result of the centrifugal force, a particle would not assume point 2, but rather point 2' below. During the return motion, a particle would assume point 3' below point 3, and this would be repeated with each cycle. Thus, it may be condluded that the particle inertia restrained its motion away from the center line as a result of the streaming hysteresis. The zig-zag approach of an oscillating aerosol particle to the center line of a streamed particle caused, on the one hand, by the particle inertia, has been referred to as self-centering of a particle [82]. In contrast, particle motion away from the center line may have been referred to as self-decentering of a particle. Theoretically speaking the phenomenon of parakinetic counter-balance was also conceivable where moving particles assumed a position in which none of the above diametrically opposed tendencies predominated. All these phenomena characterized parakinetic interaction of aerosol particles in a sound field.

The question can now be asked:

What form did parakinetic particle interaction assume in each real case?

The answer to this depended upon the respective positions of aerosol particles, their size and density, and on the medium's viscosity and the mode of its sonification. Unfortunately, a general analytical solution of this problem necessitated the use of computers. However, velocities of the parakinetically interacting aerosol particles in a sound field could be estimated readily if observations were limited to the case of vibratory velocity which varied as $|\overrightarrow{u_g}| = |\overleftarrow{u_g}| = \text{const}$. In the case of sinusoidally varying vibratory velocity, all results should be correspondingly lower.

The hysteresis component of velocity of a parakinetically moving aerosol particle may be found from the following formula: $V_g = f\delta_g$ (11.9); where δy_g is the extent of hysteresis for the forward and backward streamline flow around a streamed particle for one period of vibrations. The inertial component of velocity of parakinetically moving aerosol particle may be determined from the following formula (7.3):

$$V_c = \frac{u_{p2}^2 \tau_2}{R_1} = \frac{\mu_{12}^2 U_g^2 \tau_2}{R_{1np} f_1}, \qquad (11.10)$$

where u_{p2} and τ_2 are the relative velocity and relaxation time of a small particle, respectively, and R_1 and R_{1n} are the absolute and normalized radii of curvature of streamlines, respectively, around the larger particle at a given point.

In the case of particle self-centering (Fig. 35a) the quantity V_g may be analytically estimated by the following equation:

$$\delta y_{np} = \sqrt{\frac{\vec{\psi}_{np}}{\frac{1}{2} + \frac{3\mathrm{Re}}{16}}} - \sqrt{\frac{\vec{\psi}_{np}\left(1 - \frac{3}{2} x_{2np}^{-1}\right)}{\frac{1}{2} - \frac{3}{4} x_{2np}^{-1} + \frac{3\mathrm{Re}}{16}}}, \qquad (11.11)$$

which may be derived readily from equations (11.1) and (11.2) by assuming that $x_{1n}^{-1} = 0$.

If Re = 1 and $x_{2n} = -10$ we get: for $\psi_n = 0.1$, $\delta y_{1s} = 0.0095\, r_1$,
for $\psi_n = 1$, $\delta y_{1s} = 0.030\, r_1$.

At frequencies of f = 1 - 10 kHz the following velocities are obtained for particles with "critical" radius of $r_1 = 3.5\,\mu$.

$$V_g^{\text{max.}} = 0{,}03 - 0{,}30 \text{ см/сек at } \psi_{np} = 0{,}1,$$
$$V_g^{\text{max.}} = 0{,}10 - 1{,}00 \text{ см/сек at } \psi_{np} = 1. \qquad (11.11')$$

The magnitude and sign of V_e are different at each point of the particle trajectory. In the case of a particle with normalized radius $r_{2n} = 0.33$ ($\mu_{12} = 0.8$) and $r_1 = 3.5\mu$ when $U_g = 220$ cm/sec ($J = 0.1$ w/cm^2) in the range $R_{1n} = 10^3 - 10^5$, the following values for the inertial velocities of particle divergence are derived:

$$V_e = 0.015 - 1.5 \text{ cm/sec}$$

In the second case, when particles diverged from one another (Fig. 35b), the magnitude of V_g may be estimated by graphical-analytical methods using Fig. 35b. If Re = 1 and $A_{gn} = 50$, we get: for $\psi_n = 100$, $\delta y_{gn} \approx 1$, and for $\psi_n = 1000$, $\delta y_{gn} \simeq 3$. In accordance with this, the following maximum velocities of hysteresis separation of particles are obtained for particles with the "critical" radius of $r_1 = 3.5\mu$ at a frequency ~~of~~ $f = 1 - 10$ khz;

$$V_g^{\text{max.}} \approx 0{,}35 - 3{,}5 \text{ см/сек at } \psi_{np} = 100,$$
$$V_g^{\text{max.}} \approx 1{,}05 - 10{,}5 \text{ см/сек at } \psi_{np} = 1000. \qquad (11.11'')$$

The order of magnitude of V_e is the same as in the first case, if the radii of curvature were identical.

A more graphic description of the parakinetically self-centering particle velocity calls for the introduction of a "normalized" interaction velocity concept defined as the ratio between the absolute velocity and the distance covered, i.e., $V_g/y_{-\infty}$. This parameter shows the number of times the covered distance may be traversed per second for a given absolute interaction velocity. The reciprocal quantity, $y_{-\infty}/V_g$, characterizes the times necessary to achieve complete coincidence of the particle center lines for the same absolute value of interaction velocity. The following formula may be derived for the normalized velocity of hysteresis-assisted self-centering, using equations (11.1), (11.2) and (11.5):

$$\frac{V_g}{y_{-\infty}} = \left[1 - \sqrt{\frac{\left(\frac{1}{2} + \frac{3\mathrm{Re}}{16}\right)\left(1 - \frac{3}{2} x_{2np}^{-1}\right)}{\frac{1}{2} - \frac{3}{4} x_{np}^{-1} + \frac{3\mathrm{Re}}{16}}}\right] f. \qquad (11.12)$$

Figure 37 shows normalized velocity of hysteresis-assisted particles self-centering as a function of Re for a constant $x_{2n} = 10$. It may be concluded from the graph that hysteresis-assisted coincidence of the center lines of both particles was achieved (if $\mathrm{Re} \neq 0$) in tenths or hundredths of a second (divergence occurred even quicker).

Assuming that parakinetic interaction occurred at an optimum vibration frequency for each particle pair, so that μ_{12} may be determined from (10.10), the normalized velocity of inertial self-centering $V_e/y_{-\infty}$, allowing for (11.10) and (11.5), may be found from the following formula:

$$\frac{V_e}{y_{-\infty}} = \frac{\sqrt{2}}{9}\frac{\rho_p}{\eta}\left(r_{2np}\frac{1 - r_{2np}^2}{1 + r_{2np}^2}\right)^3 \frac{U_g^2}{\sqrt{\psi_{np}}}\frac{\sqrt{1 + 0{,}375\mathrm{Re}}}{R_{1np}}. \qquad (11.13)$$

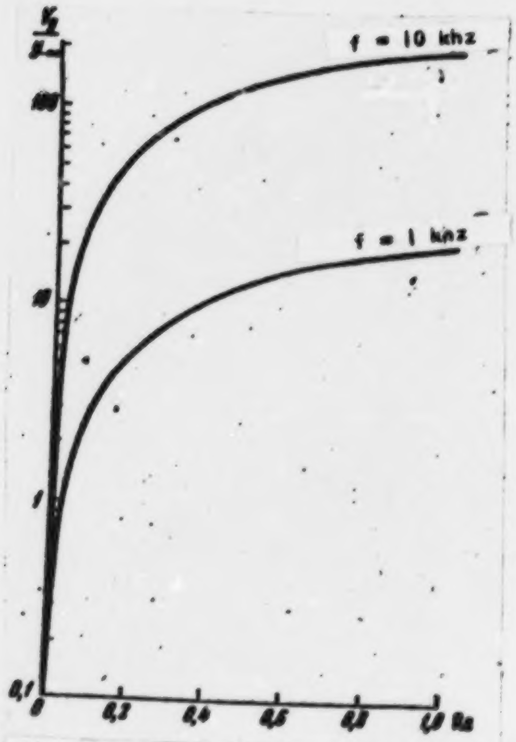

Fig. 37. Adjusted velocity, or rate, of hysteresis autoconcentration of aerosol particles in the sound field at I = 0.1bt/cm/2

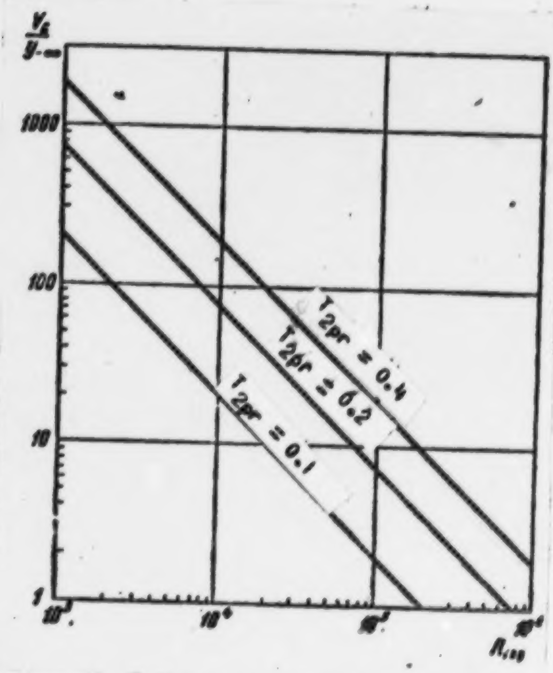

Fig. 38. Adjusted rate of inertia autoconcentration of aerosol particles in a sound field at J = 0.1 bt/cm^2

Figure 38 shows the normalized inertial self-centering velocity as a function of the normalized curvature radius of streamline R_{1s} for different values of normalized radii of a vibrating particle r_{ss} for a case when U_s = 220 cm/sec (J = 0.1 w/cm^2), $\psi = 1$, and Re = 0. It may be concluded from the graph that the inertial coincidence of the center lines occurred even faster, namely in hundredths and thousandths of a second, even though the absolute value of velocity V_s was comparatively small. The aforementioned indicated that the parakinetic interaction of aerosol particles was very intense. As a result, the concept of particle coefficient entrainment in a sound field loses its ordinary sense and meaning. Due to self-centering, orthokinetic collision was probable not only for vibrating particles which were initially in the aggregate volume of the streamed particle, but also for particles which were far beyond its boundaries. The value of the entrainment coefficient, if only this term may be applied to a given case, is primarily determined here by the duration of sonication; moreover, even for the shortest time, it is greater than the critical value of the coefficient of entrainment for the stationary streaming of objects, such as, the coefficient of entrainment of falling droplets estimated on the basis of Oseen's attractional forces, as done by Piercey and Hill [250].

No experimental data had been found on the parakinetic interaction of aerosol particles in a sound field, except for the work of O.K. Eknadiosyants and L. I. Buranov [12] in which the phenomenon of aerosol particles "counter-balance" was recorded by a high-speed camera. The aerosol particles in this case were an aluminum paint dust with a radius in the range of 1.5 and 15μ. The frequency of vibrations was 0.7 - 3.0 khz, and the camera speed was from 300 to 5000 frames per second. The investigators observed the manner in which spatial complexes consisting of 2, 3, 4, and more vibrating particles formed and moved together across the field of vision.

12. ATTRACTIONAL INTERACTION OF AEROSOL PARTICLES

By the attractional* interaction of aerosol particles in a sound field is meant their drawing together, brought about by the action of hydrodynamic forces created by the reciprocal interference of flow fields around the particles, and which are arbitrarily called forces of attraction. These include, respectively, the Bernoulli [2], Bjerkness [109], and Oseen [103] forces. The first two were assumed responsible for the acoustical aerosol coagulation without sufficient grounds; therefore, they have been merely mentioned at the end of the paragraph, and only because they have been mentioned in many previous publications.

The basis of attractional interaction of aerosol particles in a sound field consist, as S. V. Pshenay-Severin has shown [103], in the hydrodynamic forces of Oseen. These forces are generated by asymmetry in the velocity field which surrounded all interacting particles.

Unlike the previously mentioned types of aerosol particle interaction, attractional interaction required no gradient in particle size density. Therefore, the physical nature of this form of interaction between two equidimensional spherical particles will be mentioned for the sake of simplicity without taking into account differences in the phase oscillations of the interacting particles, as a rule, greatly complicated the understanding of the basic principle of the phenomenon.

In #9 it was shown that velocity fields created around each particle with a flow around it is asymmetrical in the direction of the acoustical motion. Back of the particle there was a wide parabola-like "stagnated" zone in which the velocity of the medium was appreciably lower at every point than at the symmetrical point of the weakly restrained "frontal" zone formed in front of the particle.

Now, assume that two aerosol particles, 1 and 2 (Fig. 39), were moving under the effect of an acoustical flow in a way that one of them, namely particle 2, moved along its path in the stagnated zone of particle 1; the latter, in this case, was in the slightly stagnated frontal zone of particle 2. It can be

---

*From the Latin attractio -- attraction. In the literature this type of interaction is often termed "hydrodynamic", which seems less appropriate, since this term is too all-embracing and vague.

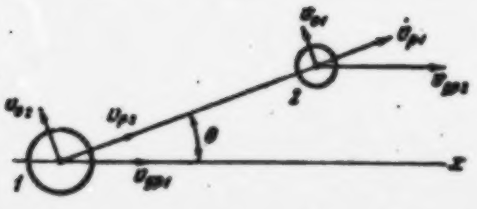

Fig. 39. Diagram illustrating superposition of velocity fields of two aerosol particles

seen that in this relative position of the particles, they retarded each other's movement. In such cases, the "head" particle (1) actually slowed its motion considerably less than "tail" particle (2), so that the particles converged somewhat, as if attracted to each other. In a reverse medium motion, the particles changed roles: the role of the "head" particle becomes transferred to particle 2, while particle 1 played the part of the "tail". The distance between them again diminished, and cycle after cycle of oscillatory medium motion is repeated.

Taking into account that Oseen's hydrodynamic equation is linear, it is possible, when studying the attractional interaction of the particles, to proceed from the assumption of the superposition of the flow fields around the particles. In this case, the magnitude of the force acting on the investigated particle in the direction of the acoustical flow can be estimated approximately by the formula:

$$F_x = 6\pi\eta r (u_{gp} - \Delta v_x), \qquad (12.1)$$

where, u_{gp} - unperturbed flow velocity of the investigated particle, determined from equation (5.22), and $\Delta \nu_x$ - perturbation of the flow velocity created by the presence of the second particle at the location point of this particle center; it is equal to the difference between the same unperturbed flow velocity of particle u_{gp} and flow velocity of the second particle ν_x at a given point determined on the basis of equations (9.10) and (9.11) or (9.12) and (9.13). Consequently, the expression in parentheses in (12.1) was merely the velocity of the flow around the second particle ν_x at the center of the investigated particle since $(u_{gp} - \nu_x) = u_{gp} - (u_{gp} - \nu_x) = \nu_x$. Accordingly, the force acting along the line of centers on "head" particle (1) can be expressed as follows:

$$F_\rho^{(1)} = 6\pi\eta r v_{\rho 2}^{(1)} \qquad (12.2)$$

and on "tail" particle 2 of the same radius:

$$F_\rho^{(2)} = 6\pi\eta r v_{\rho 1}^{(2)}, \qquad (12.3)$$

where $\nu^{(1)}_{\rho 2}$ - radical component of the flow velocity around particle 2 at the location point of particle center 1 determined from equation (9.10) when $\rho = \rho_{12}$ and $\theta = \theta_{12} + \pi$; $\nu^{(2)}_{\rho 1}$ - radical component of the flow velocity around particle 1 at the location point of particle 2 center determined from equation (9.10) when $\rho = \rho_{12}$ and $\theta = \theta_{12}$. The difference in the motion velocities of both particles is numerically equal to the difference in the flow velocities around them. Therefore, the following expressed the attractional convergence velocities of the particles:

$$V_{attp} = v_{\rho 1}^{(2)} - v_{\rho 2}^{(1)} = (v_{\rho 1np}^{(2)} - v_{\rho 2np}^{(1)}) u_{gp} \qquad (12.4)$$

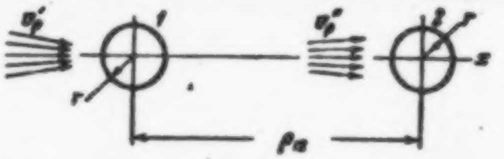

Fig. 40. Simplified diagramatic presentation of particles attraction interaction separated far apart.

If the particles are positioned one behind the other, so that $\theta \to 0$, then at great distances ρ_{12} velocities $v^2\rho_1$ and $v^1\rho_2$ assumed a directional position radially close to the x-axis, as shown in Fig. 40, and could be determined by expressions (9.15) and (9.17), respectively. In this case:

$$V^x_{\text{атр}} = \left(\frac{3}{2x_{\text{ср}}} - \frac{3}{\mathrm{Re}\, x^2_{\text{ср}}}\right) u_{\text{гр}}. \qquad (12.5)$$

According to this equation, velocity V_{attr}, with the particles directly touching ($x_a = 2$) at Re = 1, is equal to zero (since condition $V_{attr} < 0$, which occurred when $x_a < 2/\mathrm{Re}$, signified the absence of any interaction characteristic of the Stokes flow for $r_1 = r_2$).

It is known that in a sound field flow velocity around a particle varied in magnitude and direction, causing variation in the Reynolds number and with it, according to (12.5), also variation in the attractional convergence velocity of the particles. Compare the second term in parentheses in equation (12.5) with the first term at the beginning of the medium's oscillatory motion, when the Re number is small. Velocity V^x_{attr} is close to or greater than zero; as the oscillatory velocity increased, Re increased rapidly, and when it attained the peak value, velocity V^x_{attr} attained its maximum value. When the product Re $x_a >> 2$, the second term in parentheses in equation (12.5) (representing the velocity $v\rho_2$) can be disregarded, and the expression for the attractional convergence velocity of particles becomes simplified:

$$V_{\text{атр}} \simeq \frac{3}{2x_{\text{ср}}} u_{\text{гр}}. \qquad (12.6)$$

Moreover, the one-sided hydrodynamic effect of the "head" particle on the "tail" particle has been thereby, achieved.

Use equation (12.6) and estimate the order of magnitude of the instantaneous attractional convergence velocity of the particles at the mean and shortest distances between particles $x_a = 100$ and $x_a = 10$, respectively, for which the equation will still hold. Under such conditions:

when $x_a = 100$ $\qquad V^x_{attr} = 0.015\ u_{gp}$;

when $x_a = 10$ $\qquad V^x_{attr} = 0.15\ u_{gp}$.

Thus, the magnitude of the instantaneous attractional particle convergence velocity consisted of comparatively small part of the instantaneous velocity of their flow. In absolute values the figures are substantial. Thus, at a flow velocity of 100 cm/sec, the attractional particle convergence velocity V^x_{attr} is 1.5 and 15 cm/sec, respectively.

Now, compute the mean attractional particle convergence velocity for one half period of oscillation for the case shown in Fig. 36, i.e., when $\theta = 0$. The use of equation (12.5), where the variable Re is introduced for this purpose, leads to insurmountable difficulties in integrating the particle convergence equation due to the quadratic term in x. In order to avoid such difficulties, Pshenay-Severin [103] proposed the use of formula (12.6), assuming that particle convergence occurred at some instant t_1 when Re attained some sufficiently high value Re_{sr}.

Up to $t = t_1$, the flow velocity around both particles varied according to law (5.22), and for $t_1 < t < \frac{1}{2}T$, the flow velocity around "head" particle 1 continued to vary according to formula (5.22), and flow velocity around "tail" particle 2 varied according to the following:

$$v_x^{(2)} = (u_g - u_p) - \frac{3}{2x_{\text{пр}}} v_x^{(1)}. \tag{12.7}$$

Where the equations of particle motion were:

for "head" particle 1 -

$$m_p \frac{du_p^{(1)}}{dt} = 6\pi\eta r\,(u_g - u_p^{(1)}). \tag{12.8}$$

for "tail" particle 2 -

$$m_p \frac{du_p^{(2)}}{dt} = 6\,\pi\eta r\,(u_g - u_p^{(2)}). \tag{12.9}$$

Solving the second equation with the aid of the first and expressing the result in dimensionless variables $V_{attr} = V_{attr}/U_g$ and $t_n = t/\tau$, get:

$$\frac{d(V_{\text{аттр}}^{\text{пр}})}{dt_{\text{пр}}} + V_{\text{аттр}}^{\text{пр}} = \frac{3\mu_g}{2x_{\text{пр}}} \cos(\omega\tau t_{1\text{пр}} - \varphi). \tag{12.10}$$

The initial conditions are as follows: $V^n_{attr} = 0$ and $\Delta X_n = 0$ when $t_n = t_{1n}$. The integration of equation (12.10) yields displacement ΔX_{12} for time interval $\Delta t = 1/2\ T - t_1$, in the following form:

$$\begin{aligned}\frac{\Delta x_{12}}{A_g} = -1{,}5\frac{\mu_p\mu_g}{x_{\text{пр}}}\{[2\mu_p\mu_g\cos\omega\tau t_{\text{пр}1} - (\mu_p^2 - \mu\ )\sin\omega\tau t_{\text{пр}1}] - \\ -\frac{\mu_g}{\mu_p}\left[2\mu_p\mu_g\sin\omega\tau t_{\text{пр}1} + (\mu_p^2 - \mu_g^2)\cos\omega\tau t_{\text{пр}1}\right] e^{-\left(\frac{1}{2}T_1 - t\right)} + \\ + \left(\sin\omega\tau t_{\text{пр}1} - \frac{\mu_g}{\mu_p}\cos\omega\tau t_{\text{пр}1}\right)\}.\end{aligned} \tag{12.11}$$

Figure 41 presents the calculation results of ΔX_{12} carried out by Pshenay-Severin on the basis of equation (12.11) for water fog droplets, when $x_n = 100 =$ const. The critical Reynolds number was assumed to be very high, namely $\mathrm{Re}_{sr} = 1$, which forced the author to calculate the attractional particle convergence in a sound field at elevated sould intensities. The obtained values of the attractional displacement ΔX_{12} were related by the author to the particle radius r and were multiplied by the product fx_n to obtain comparable values at different frequencies. As a result, values of the normalized attractional particle convergence rate $V_{attr}/\Delta X_{12}$ were plotted along the ordinate, as shown in graph of Fig. 41.

Examining Fig. 41, it may be concluded that the attractional particle convergence velocity was high; even at the lowest sound intensities the displacement per second was ten times greater than the distance between particles. Therefore, the attractional particle convergence before they touched could be accomplished in tenths of seconds or less. The graph indicates that

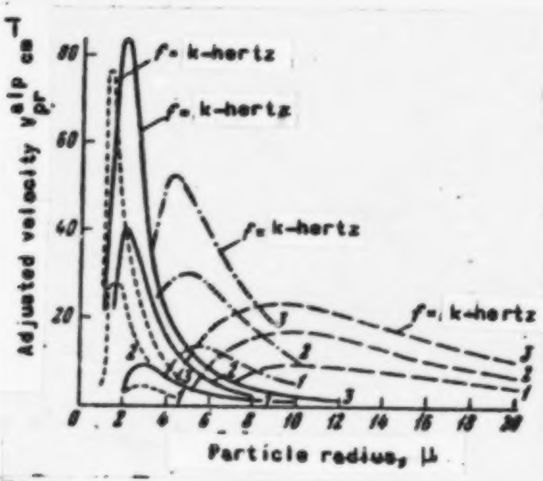

Fig. 41. Adjusted rate of mutual attraction approach of aerosol particles at high oscillating velocities

1 — at $U_g = 400$ см/сек ($J \approx 0{,}33$ вт/см²); 2 — at $U_g = 700$ см/сек ($J \approx 1.0$ vt/см²); 3 — при $U_g = 1000$ см/сек ($J \approx 2{,}1$ vt/см²)

the rate of attractional convergence of aerosol particles greatly depended upon oscillation frequency. For each particle size there was an optimal oscillation frequency at which the attractional particle convergence rate had a maximum value. The greater was the particle size, the higher was the value of the optimal oscillation frequency; for particles with radius r = 5 -- 15μ, low audio frequencies of the order of several hundred Hertz are effective, while for particles with a smaller radius r < 5μ, it is several khz. To compare these oscillation frequency values with the optimal frequency values observed in the experiment presented difficulties, due to the occurrence of industrial aerosols coagulation as a rule, at lower sound intensities than those chosen by the author.

The existence of an optimum frequency was directly indicated by equation (12.5) because the attractional particle convergence did not exist ($V_{attr} = 0$) in the following two cases:

a) during complete particle entrainment into the oscillatory motion of the medium when $u_{gp} = 0$ and Re = 0;

b) during the full medium flow around the particle when the particles were stationary.

It follows, accordingly, that particle convergence occurred only in the intermediate case when they had not been fully entrained, a condition which achieved only at certain oscillation frequency values.

Two more specifics of the presented curves deserved further attention: the curves' compression along the abscissa, i.e., compression of particle radius values with the increase of the particle size, and optimum displacement in the direction of the smaller particle radius with increase in sound intensity. Several limitations of the author's conclusions were pointed out by N. A. Füchs in his review [122]. It can be shown easily that the attractional particle convergence occurred even when θ → 90° ; however, here, the active principle was repulsion, which was of lesser interest. The attractional particle interaction also occurred when there was a difference in their sizes, but the particle contact here usually occurred orthokinetically, since its rate was considerably greater. Of particular interest was the case of attractional particle convergence which had full medium flow around it, while the second was fully entrained by the medium. It is understandable that the second particle, while oscillating, tended to approach the first particle at the acoustical medium flow rate described in #11. However, unfortunately this fact could not be used in determining the path of the eddys, a practice commonly used by investigators in a case of large obstacles: $r \gg A_g$ (see [140, 261] and others). The long particle tracks, comparable to the eddys' scale, impact mutually appearing as a solid background in the photograph. The problem of determining eddy paths in the case $r \ll A_g$ may be solved only by synchronizing the pulsed photography with the sound source.

Let us now proceed with a discussion of S. V. Gorbachev and A. B. Severny [26, 195] experiments in order to confirm the attractional particle interaction in a sound field as described above. The authors studied the elementry interaction process of two water droplets with radius $r = 100\mu$, each suspended on glass threads at a normalized distance of $\rho_{1g_2} = 26$ between them in a low-frequency sound field generated by an "Accord" - type loudspeaker. The oscillation velocity of the medium was actually very small, so that it could be maintained with certainty that a viscous flow regime around the droplets occurred. The authors established that at successive droplet distribution ($\theta = 0^\circ$) an attraction occurred, whereas, in the case of side by side distribution ($\theta = 90^\circ$) a repulsion occurred. Such particle interaction in a sound field was clearly characteristic of attractional interaction defined by Oseen's asymmetrical particle flow which the investigators and the interpreters did not perceive. Before concluding the present paragraph the hydrodynamic forces of Bernoulli and Bjerkness will be discussed at some length. The Bernoulli forces occurred between two bodies resulting from the constriction of the flow passing between them, and the attendant loss of a portion of the static pressure in the constricted space. When the viscous losses in the medium are negligible and this occurred at an eddy-less potential streaming, then, as is known, the following was equally maintained for the full duration of the flow:

$$\rho + \tfrac{1}{2}\,\rho_g u^3{}_g = \text{const.} \qquad (12.12)$$

The phenomenon is known as the Bernoulli law or integral, which represented a mathematical expression of the law of energy conservation for an ideal liquid.

According to equation (12.12), the pressure of the medium was somewhat lower than the pressure from outside in the space between the particles where the constriction of the flow pipe and the attendant increase in velocity occurred. As a result, forces are created between the two bodies which strive to bring them together. Based on Bjerkness' [146] hydrodynamic theory, Koenig derived the following equation for the force acting in a sound field between spherical bodies along the line of centers [215]:

$$F_p = \frac{3}{2}\,\frac{\pi\rho_g r_1^3 r_2^3}{R_{12}^4}\,U_{gp}^2\,(3\cos 2\theta_{12}' + 1), \qquad (12.13)$$

where, θ_{12} - is the angle between the line of centers and the direction of the oscillation velocity.*

This equation was satisfactorily confirmed by experiments in the early works of Thomas [279], who studied the interaction of spheres with a radius of 2.8 - 7.8 mm in a very low-frequency sound field generated as in [283] (see #5) the Zernov method. At the same time, considerable disagreement with the theoretical calculations has been observed in several experiments. On the basis of experimental study of spherical bodies streaming in a sound field, Andrade [141] concluded that the reason for this disagreement was the formation of eddys around the bodies generated when $u_{s,p}r>0.35$. Citing Cook's observations [182], the author noted, that in the case of shorter distances between the spheres the line of centers, which was perpendicular to the direction of the acoustical flow, at times repelling instead of attracting forces appeared.

Recently, Stashevskii [271], verified experimentally and refined this thesis using wax and glass spheres of diameters 0.34 - 5.45 mm. Experiments were conducted in a glass tube of 35 - 40 mm diameter, at frequencies of 184 - 533 nz, and different sound intensities. Later, Adamchik and Stashevskii [136] noted a similar phenomenon with the spheres arranged in a linear succession; the repulsion at certain small distances here, was replaced by an attraction. Doerr [185], established experimentally, that angular dependence of the attraction forces was expressed by the factor $(6 + 4 \sin^2 \theta)$ rather than by the factor in Koenig's formula (12.13). He used hollow glass spheres of 2.75 -- 4.95 mm diameter, suspended on fine threads at distances of 7 - 10 mm. The oscillation velocity amplitude could attain 40 cm/sec.

Andrade [2] tried unsuccessfully to use the Bernoulli forces in explaining the mechanism of acoustical aerosol coagulation. It had been previously indicated, that a viscous flow regime was characteristic for aerosol particles located in a sound field, which is remote from the ideal conditions, for which equation (12.13) was formulated. Viscous losses decreased and, with some reservations, may be disregarded only at high Re numbers, occurring at higher sound intensities and larger particle sizes. The latter may occur only in the case of highly coarse aerosol particles not required, as a rule, for additional particle coagulation, or as a result of prolonged finely dispersed particles coagulation. However, the appearance of Bernoulli attractional forces during the final aerosol coagulation stage has become of little use, since their magnitude in any given case was insignificant. To verify this thesis, Brandt, Freund, and Hiedemann [167], derived the following formula for the convergence time of two equidimensional spherical particles before contact at their optimal relative positions with respect to the acoustical flow ($\theta = \pi/2$) at a total streaming

---

*In [215] expressions are given for forces X and Y representing the projection of the resultant "radial" force $F\rho$ and of the "tangential" force $F\theta$ perpendicular to it on axis x and y.

(μ_s = 1):

$$t_{c\delta\pi} \approx \frac{2}{5}\frac{\eta}{\rho_g}\frac{(\rho_{1\text{snp}})^3}{U^2_{gp}}. \qquad (12.14)$$

The authors arrived at this formula by equating the attraction force F_ρ defined by formula (12.13) to the force of the medium's motion resistance which, according to Stokes, equalled to $F_{st} = 6 \pi n r (\frac{1}{2} \; d\rho_{12}/di)$, and integrating the obtained equation from ρ_{12} when t = 0 to ρ_{12} = 2r when t = t converge. Strictly speaking, such a procedure is irregular, for when Re >1, the resistance force, is not a linear function of the radius, as expressed by Stokes' formula, but a quadratic or nearly quadratic function. In this connection, determine what results formula (12.14) will yield, if it is assumed that Re was not too large. The mean normalized distance between aerosol particles lies within the limits S_s = 35 - 160. Accordingly, at a sound intensity J (or I) = 0.1 w/cm^2 (U = 250 cm/sec), following expression for $t_{s\,oz\,v}$ in air for particles with unit density; is obtained:

$$t_{s\,oz\,v} = 138 \text{ -- } 2.76 \times 10^5 \text{ sec.}$$

Thus, it can be seen that even at high particle concentrations (of the order of $\bar{k}$ = 100 g/m^3), the convergence time before contact is more than 2 minutes, while at low concentrations ($\bar{k}$ = 1 g/m^3 and lower), it is tens of hours. This suggests the conclusion that the existence of Bernoulli forces in aerosols undergoing coagulation in a sound field may be disregarded even during the final consolidation stage. Forces of attraction (or repulsion), called Bjerkness forces, originated between two bodies oscillating, or pulsating, under the effect of an external force. As Kelvin noted long ago, the oscillation velocity of a medium's particles behind a body located in a sound field always had been somewhat less than in front of it. This is governed by the scattering of a portion of the particles energy on the frontal surface of the body; it was true only in the case of an ideal medium. According to Bernoulli's principle, the pressure behind a body was somewhat higher than in front, and, consequently, in this case the body was acted upon by some force tending to make it approach the oscillating object. Another body which was oscillating or pulsating, or both simultaneously, can serve as such an object. In the latter case, both attractional and repulsive forces may occur between the bodies, depending on the oscillation phase.

The described ponderomotive forces of interaction arising during the oscillating or pulsating motion of bodies was theoretically studied by Bjerkness [146]. P. N. Lebedev [64] experimentally studied the nature of the ponderomotive forces in cases of electromagnetic, hydrodynamic, and acoustical oscillations; he came to the conclusion that the laws which govern these forces were identical, i.e., the forces were independent of the wave field character.

White studying the interaction arising between two water droplets in a sound field (109), A. B. Severngi came to the conclusion by taking Ollivier's observations into account [242], that the droplets were virtually in a state of pulsation; each ellipsoidal droplet, extended with respect to the two axes, became transformed into a compressed ellipsoid symmetrical with respect to the same axes. According to the author, the pulsating droplets acted on each other, creating attraction or repulsion between the droplets.

On the basis of an equation derived by Bjerkness for the forces of interaction of two radially pulsating spheres

$$F = \frac{1}{\rho_g} \frac{\Omega_1 \Omega_2}{4\pi\rho_{12}} \qquad (12.15)$$

Ω_1 and Ω_2 - mean quadratic values of the rate of change in volumes of the first and second spheres, respectively, and having transformed it to apply to virtual pulsations, Severngi derived, through complex calculations, the following expression for the force of interaction between equidimensional particles located in the plane of a sound wave ($\theta = 90^\circ$):

$$F = -K\frac{u_g^2}{\rho_{12}^2}, \qquad (12.16)$$

where $K = -6.19 \cdot 10^3 \frac{r^4}{p_\rho} C_g \frac{6+(kr)^2}{12+(kr)} \approx -(3.1 - 6.2)\, 10^3 C_g r^4$.

Here, $k = \frac{2\pi}{T_\rho}$, where T_ρ - period of ellipsoidal and symmetrical pulsations determined by Ollivier's [242] expression:

$$T_p = \sqrt{\frac{3\pi m}{8\sigma}} \qquad (12.17)$$

(m_p - droplet mass, ∂ - surface tension which for water at 20° C, is 73 dyn/cm.)

Using equation (12.17) and disregarding the medium resistance, Severngi derived the following equation for the convergence time of droplets before contact:

$$t_{\text{сбл}} = \frac{\rho_{12}}{u_{gp}} \sqrt{\frac{(1+\rho_{12})(2+\rho_{12})\, m_p}{2K\rho_{12}}} \approx \frac{1}{U_{gp}} \sqrt{\frac{\rho_{12} m_p}{2K}}. \qquad (12.18)$$

For droplets of radius $r = 10\mu$, the ratio $\frac{mp}{K} \approx 0.01$; hence, at a distance between the droplets of the order of $\rho_{12} \approx 1$ mm, and a sound intensity of $J = 0.1$ w/cm^2 ($u_{gp} \approx 150$ cm/sec), $t_{\text{сбл}} = 0.0014$ sec which corresponded to an average convergence velocity of $V_{\text{сбл}} = 70$ cm/sec. The results are more than favorable. However, they have been obtained with equations not usable in the case of real aerosol sonication, where viscous streaming of particles prevailed. Moreover, the adduced equations fail to hold even in the case of the final prolonged aerosol coagulation stage, when viscous streaming yielded to potential streaming.

Calculate the natural frequency of droplet pulsations of a real water fog, using formul (12.17), and verify that it is great as compared with oscillation frequencies of the sound field used in practice. In these, far-from-resonance, conditions, it is impossible to "swing" the droplet and cause it to execute virtual pulsations. A simple experimental fact proves the unsoundness of the theory: solid aerosol particles, not capable of virtual pulsations, undergo coagulation as successfully as liquid particles, provided they were not too coarse and, thus, adhered poorly. It follows from all that has been discussed that the Bjerkness and Bernoulli forces in the coagulating of aerosols in sound fields may be completely disregarded when studying the mechanism of acoustical aerosol coagulation. The same may also be said of the new forces of interaction related to the radiational particle drift forces studied by Embleton [302].

13. PULSATION INTERACTION OF AEROSOL PARTICLES

It was shown in #7, that medium size aerosol particles participated in some way, in the turbulent pulsations of a sonicated medium. As a result, it is possible for them to converge on each other at some finite velocity.

Two mechanisms for the convergence of colloidal particles were suggested by Levich [67, 68, 69], in his theory of turbulent coagulation of colloids:

1) the diffusion mechanism, according to which particles converged by purely diffusional means, as the result of their participation in different pulsations of the medium in different directions;

2) the orthokinetic mechanism created between different size particles resulting from the joint participation in pulsations of an amplitude not exceeding the internal amplitude of turbulence.

Now, examine both mechanisms as they apply to the conditions arising in the turbulization of a sound field:

The diffusion mechanism. Both equidimensional and particles of different sizes can thus converge. The convergence of equidimensional particles in the turbulized sound field was practically the same as in a convergence studied by Levich [67], in a normal turbulent flow in so far as all particles participated in completely the same way in the oscillatory motion of the medium. Place an aerosol particle of radius r at the origin of spherical coordinates and examine the diffusion flow to this particle occurring in a turbulent sound field. The equation of steady-state diffusion to the surface of an absorbing sphere of radius a = R, surrounding a particle of radius r<< R is of the following form:

$$j = D_э \left(\frac{\partial n}{\partial a}\right)_{a=R} \quad \left[\frac{1}{см^2 \cdot сек}\right], \tag{13.1}$$

where, D_{eff} - effective coefficient of particle diffusion equal to the sum of two coefficients: $D_{eff} = D_{turb} + D_{brownian}$.
The boundary conditions are the following:

$$\begin{aligned} n &= n_0 \quad \text{при} \quad a \to \infty, \\ n &= 0 \quad \text{при} \quad a \to R. \end{aligned} \tag{13.2}$$

Turbulent particle diffusion is prevalent when the sphere radius satisfies the following inequality [69]:

$$R > \left(\frac{D_{бр}}{\sigma_2}\sqrt{\frac{2\nu}{\varepsilon}}\right)^{1/3}. \qquad (13.3)$$

For aerosol particles this implies that r>0.1μ, whence it follows that the coefficient of Brownian particle diffusion D_{Brown} may be practically always disregarded in comparison with the turbulent particle diffusion coefficient; therefore, it may be assumed that $D_{eff} \approx D_{turb}$. Moreover, the coefficient of turbulent diffusion of aerosol particles may be assumed to be equal to the coefficient of the turbulent particle diffusion of the medium. For aerosol particles completely entrained in the turbulent pulsations, this supposition is self evident. However, for particles partially entrained in the turbulent pulsations, this assumption is not so evident, yet Chan [175] convincingly proved that even in this case the coefficients of the turbulent diffusion of the aerosol particles and the medium are equal [122].

On the basis of the general expression $D \approx l^2/t \approx v_l\, l$, (l - length of "step", and t - time expired in this step), the coefficient of turbulent diffusion due to pulsations of amplitude l, taking expressions (1.36) and (1.37) into consideration, may be expressed as follows:

$$D_{турб} \sim v_l l \sim \begin{cases} \frac{1}{4}\left(\frac{\varepsilon}{b/\rho_g}\right)^{1/2} l^2 \text{ при } l < l_0, & (13.4)\\ (\varepsilon l)^{1/3} l \text{ при } l > l_0. & (13.5)\end{cases}$$

Accordingly, rate of diffusional convergence of two particles rapidly decreased as the distance between them diminished. For concentration gradients $(\partial n/\partial a)$ a = R at the surface of the absorbing sphere when $t \gg R^2/D_{turb}$, the theory yields the following simple expression [121, 69]:

$$(\partial n/\partial a)a = R = 3n/R \qquad (13.\ 6)$$

where n - numerical aerosol concentration taken as equal to the mean particle concentration in 1 cm^3. Substituting this expression and also equation (13.4) into equation (13.1) and taking into account that $l = R + r \approx R$, obtain the following equation for the specific flow of aerosol particles to the sphere:

$$j \approx 3/4\ (\varepsilon/b/\rho_g)^{1/2}\ Rn \qquad (13.7)$$

The total particle flow on the surface of the sphere, if (1.32) and (9.1) are taken into account, is equal to:

$$N = 4\pi R^2 j = 9/4(R/p_p)^3\ k/r\ \xi^{1/2}\ J^{3/4}\ f^{1/2}/b^{1/2}\ p_g^{1/4}\ c^{5/4}\ .\ 10^{-6} \qquad (13.8)$$

At weight concentrations of diffusing particles equal to k = 10 g/m^3, and at normal acoustical parameters (J = 0.1 w/cm^2 and f = 1 - 10 KHz), the particle flow of density $\rho_\rho = 1$ precipitating on a particle of the same radius (R = 2r) will equal:

$$N \approx 0.18 \text{ -- } 0.60 \frac{1}{\text{sec}}$$

Therefore, this flow is very small, and can be disregarded. The diffusion interaction of different size particles is characterized by a greater intensity, in a turbulent sound field. All small particles which fall within the aggregate volume, shown in Fig. 42a by the dash line, forming a cylinder of height $2A_{12}$ rounded at the ends having a cross section $\varepsilon \pi r_1^2$, where A_{12} - the amplitude of the relative particle motion, and ε - the entrainment coefficient of small particles, may come in contact with each large particle. For the greater part of the cylinder length the entrainment coefficient magnitude was determined by equation (10.20). Therefore disregarding the slight thickening in the middle and the roundness at the ends, the study of the diffusion particle flow in a normal cylinder of height $2A_{12}$ with permeable walls of radius $R = \sqrt{\varepsilon}\, r_1$, can be substantially limited. For greater clarity the diagram of diffusional interaction can be presented in a way that the large particle oscillated with amplitude A_{12}, and the small particles diffusionally drifted into the aggregating cylinder, while the large particle continuously "emptied" the aggregating cylinder in front of the small particles which diffused into it.

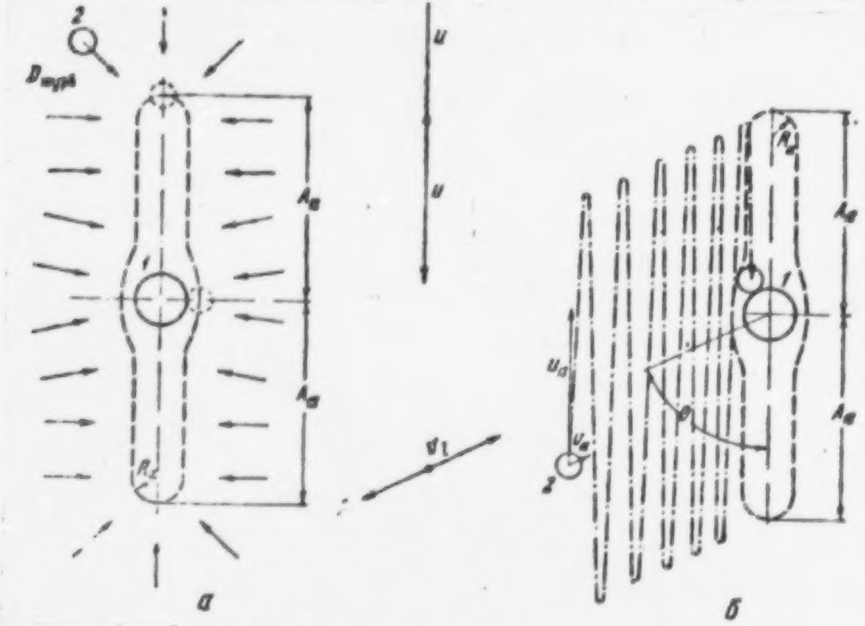

Fig. 42. Pulsation interaction between aerosol particles in a sound field
a - diffusion mechanism; b - orthokinetic mechanism.

The process of the small particles diffusion into the aggregating cylinder is accomplished in a series of short events, of duration t_D, a function of the diffusing particle ordinate and varied from 0 to T, where T, the period of oscillation, equals to 1/f. A study of curve x = F(t), shows that the mean length of the diffusional event equaled

$$(t_D)_{ср} = \frac{1}{2} T = \frac{1}{2f}.$$

The differential equation for small diffusion particles in the case of a cylinder is of the following form:

$$\frac{\partial n}{\partial t} = D_{турб}\left(\frac{\partial^2 n}{\partial a^2} + \frac{1}{a}\frac{\partial n}{\partial a}\right). \tag{13.9}$$

The initial and boundary conditions are:

$$\left.\begin{aligned} n(a, 0) &= 0 \quad \text{и} \quad \frac{\partial n}{\partial a}(0, t) = 0 \quad \text{при } a < R, \\ n(a, 0) &= n_2 \quad \text{и} \quad \frac{\partial n}{\partial \rho}(\infty, t) = 0 \quad \text{при } a > R. \end{aligned}\right\} \tag{13.10}$$

The thermal conductivity theory [70] postulates the following solution for an unbounded cylinder when a < R:

$$n = n_s\left[1 - \frac{4}{\pi^2}\int_0^\infty B_\mu J_0\left(\mu\frac{a}{R}\right) J_1(\mu) e^{-\mu^2 \mathrm{Fo}}\, d\mu\right], \qquad (13.11)$$

where
$$B_\mu = \frac{1}{\mu^2 [J_1(\mu) Y_0(\mu) - J_0(\mu) Y_1^2(\mu)]};$$

$J_0(\mu)$ and $J_1(\mu)$ - Bessel functions of the first kind of the zero and first orders, respectively; $Y_0(\mu)$ and $Y_1(\mu)$ - Bessel functions of the second kind of the zero and first orders, respectively; μ - variable of the characteristic equation $J_0(\mu) = 0$; Fo -- Fourier criterion $\frac{D_{turb}\, t_D}{R^2}$.

The obtained strict solution, containing non-elementary functions, is not very useful for practical computations, therefore, approximate solution must be found. An analysis of expression (13.11) shows that, at the risk of being slightly inexact, integration can be limited to $\mu_n = 0$ to 2.4 (the first root of the characteristic equation). Moreover, $B\mu$, which depended only slightly on the value of μ, can be assumed to be equal to $B\mu = \pi^2/4$, while functions $J_0(\mu \frac{a}{r})$, $J_1(\mu)$, and $e^{-\mu_n^2 \mathrm{Fo}}$ can be expanded into power series:

$$J_0\left(\mu\frac{a}{R}\right) = 1 - \frac{\mu^2}{2^2}\left(\frac{a}{R}\right)^2 + \frac{\mu^4}{2^2\cdot 4^2}\left(\frac{a}{R}\right)^4 - \frac{\mu^6}{2^2\cdot 4^2\cdot 6^2}\left(\frac{a}{R}\right)^6, \qquad (a)$$

$$J_1(\mu) = \frac{\mu}{2} - \frac{\mu^3}{2^2\cdot 4} + \frac{\mu^5}{2^2\cdot 4^2\cdot 6} - \frac{\mu^7}{2^2\cdot 4^2\cdot 6^2\cdot 8}. \qquad (b)$$

$$e^{-\mu_n^2 \mathrm{Fo}} = 1 - \mu_n^2 \mathrm{Fo} + \frac{\mu_n^4 \mathrm{Fo}^2}{1\cdot 2} - \frac{\mu_n^6 \mathrm{Fo}^3}{1\cdot 2\cdot 3} + \frac{\mu_n^8 \mathrm{Fo}^4}{1\cdot 2\cdot 3\cdot 4}. \qquad (c)$$

Substituting (a), (b), and (c) irto (13.11) and taking only the first four or five terms of each series, obtain:

$$n = (0.50 + 0.78\,\mathrm{Fo} - 0.99\,\mathrm{Fo}^2 + 1.03\,\mathrm{Fo}^3 - 0.99\,\mathrm{Fo}^4 + \ldots) n_s. \qquad (13.12)$$

The concentration gradient at the cylinder wall equals:

$$(\partial n/\partial a)_{a = R} = (0.78 - 2.52\,\mathrm{Fo} + 4.86\,\mathrm{Fo}^2 + \ldots)\frac{n_s}{R}. \qquad (13.13)$$

If the sound intensity is not too high ($J \leq 0.1$ w/cm²) and the frequency is not too low ($f > 1$ -- 2 KHz), only the first member in parentheses may be used as the first approximation.

The mean of Fo is: $$(\mathrm{Fo})_{\text{ср}} = \frac{D_{\text{турб}}(t_D)_{\text{ср}}}{R^2} = \frac{1}{8f}\left(\frac{\varepsilon}{b/\rho_g}\right)^{1/4} = \frac{1}{8}\,\frac{\xi^{1/4} J^{3/4}}{b^{1/4}\rho_g^{1/4} c_g^{1/4} f^{1/4}},$$

which, when $J = 0.1$ w/cm² for an air medium, yields:

$$(\mathrm{Fo})_s = \frac{4.67}{\sqrt{f}}.$$

In the frequency range f = 1 - 10 Khz; $(Fo)_{mean}$ = 0.148 -- 0.047, and consequently, the second term is 48 - 15% less than the magnitude of the first, and the third term is 6.1 - 0,7% less. Thus, in the first rough approximation:

$$(\partial n/\partial a)_{a=R} \approx 0.78 \frac{n_2}{R} . \qquad (13.14)$$

However, if the range is limited to f = 1 - 10 Khz a finer approximation (± 15%) can be achieved by the following formula:

$$(\partial n/\partial a)_{a=R} = 2/3\, n_2 /R. \qquad (13.14')$$

which will be used thereafter.

The diffusional particle flow onto 1 cm^2 of cylinder surface per second (considering that the mean diffusion time is one half of the total sonication time) is equal to:

$$j = \frac{1}{2} D_{турб} \left(\frac{\partial n}{\partial a}\right)_{a=R} = \frac{1}{12}\left(\frac{\varepsilon}{b/\rho_g}\right)^{1/4} R n_2, \qquad (13.15)$$

The total flow of particles onto the cylinder surface, if equations (1.32) and (9.1), are taken into account, equals:

$$N' = 4\pi R A_{12} j = \frac{10^{-6}}{4\pi \sqrt{2}} \frac{\mu_{12} k_2}{\rho_p f^3} \left(\frac{R}{r_2}\right)^3 \frac{\xi^{1/3}}{b^{1/4} \rho_g^{3/4} c_g^{1/6}} \frac{J^{3/4}}{f^{1/3}}. \qquad (13.16)$$

The relationship of this flow to the flow onto a sphere determined by formula (13.8), taking (10.20') into account, is as follows:

$$\frac{N'}{N} \simeq 0{,}1 \frac{A_{12}}{r_2}. \qquad (13.17)$$

Usually $A_{12}/r_2 > 50$ and, consequently, N'/N > 5. However, the absolute value of the flow of small particles diffusing into the aggregate volume of the large particle is small. Thus, under optimal conditions, when f is defined by formula (10.5), μ_{12} by formula (10.10), and ε by formula (10.20'), for a particle of radius r_1 = 3.5μ at normal sound intensity (J = 0.1 w/cm^2), the following is obtained:

at $r_{2_2} = 0.2$(f_{opt} = 5.4 KHz; $\mu_{12} = 0.92$; $\varepsilon_{s12} = 1.41$) N' = 0.8;

at $r_{2_2} = 0.5$(f_{opt} = 2.2 KHz; $\mu_{12} = 0.60$; $\varepsilon_{s12} = 1.33$) N' = 0.3;

Such a flow ensures only a partial filling of the aggregate volume by small particles during each diffusion event, since the average particle concentration inside a given volume is always considerably lower than the average particle concentration in the surrounding volume. Complete filling of the aggregate volume by the small particles is achieved at a much greater diffusion flow value, namely:

$$N'_{поля} = 2\,Э_{мин} \pi r_1^3 A_{12} f n_2 = \frac{075 \sqrt{2} \cdot 10^6}{\pi} \frac{\mu_{12} k_2}{\rho_g f^3} \frac{J^{1/2}}{(\rho_g c_g)^{1/2}}. \qquad (13.18)$$

According to this formula

at $r_{g_2} = 0.2$ $N' = 9.8$, at $r_{g_2} = 0.5$ $N' = 2.4$,

which is about one order of magnitude above the corresponding values of N'.

However, it is evident from equation (13.16) that the diffusional particle flow increased rapidly with an increase in the radius of the emptying cylinder. Determine what radius $R_{4\,1\,ff}$ will ensure complete filling of the cylinder volume by the small particles through diffusion. Equating expressions (13.16) and (13.18), get:

$$\frac{R_{эф\phi}}{r_1} = \sqrt{6}\,Э^{1/4}\left(\frac{b/\rho_g}{\varepsilon}\right)^{1/4} f^{1/4} = \sqrt{6}\left(\frac{1{,}5 + r_{amp}}{1 + r_{amp}}\right)^{1/4} r_{amp}\,\frac{b^{1/4}\rho_g^{1/4} c_g^{3/4}}{\xi^{1/4} f^{1/4} J^{3/4}}. \qquad (13.19)$$

Under the previous conditions, get the following:

at $r_{g_2} = 0.2$ $R_{4\,1\,ff}/r_1 = 0.81$ or $R_{4\,1\,ff}/(r_1 + r_g) = 0.68$

at $r_{g_2} = 0.5$ $R_{4\,1\,ff}/r_1 = 1.57$ or $R_{4\,1\,ff}/(r_1 + r_g) = 1.05$

i.e., usually $R_{4\,1\,ff} \leq r_1 + r_g$.

In these computations, the Brownian diffusion of particles was completely disregarded; it must be considered only when $r_g \lesssim 0.1$.

The orthokinetic mechanism. Particles, the distance between which is less than the internal turbulence amplitude ($l < l_0$), are being flowed around by each pulsation, and if these particles are not equidimensional, a difference in velocity develops between them, and they converge on each other, and diverge in a reverse motion. Taking (7.11) into consideration, the relative velocity of two particles with r_1 and r_g equals:

$$v_{12} = (\mu_{g1} - \mu_{g2})\,v_l = a_l(\tau_1 - \tau_2) = \frac{2}{135}\,\frac{\rho_p}{\eta}\,\frac{\varepsilon^{3/4}}{(b/\rho_g)^{1/4}}(r_1^2 - r_2^2) \qquad (13.20)$$

Since the particles are also simultaneously entrained into the oscillatory motion of the medium in different degrees, and the frequency of this motion is much higher than the pulsation frequency, particle convergence occurs sinusoidally, as shown in Fig. 42b.

The sinusoid "pace" is usually much smaller than the radius of a small particle: $(v_{1g}/4f) \ll r_g$. Therefore, it can be assumed that all small particles located in the circular parallelepiped of height $2A_{1g}$, length v_{1g} sinθ, where θ - the angle between the oscillation directions and the investigated pulse, $(\sin\theta)_s = 2/\pi$), and thickness $2\,\varepsilon^{\frac{1}{2}}_{s\,1\,2}$ r_1 can collide with the large particle in one second. Accordingly, the flow of small particles precipitating on the large particle under optimal conditions should be equal to

$$N'' = \frac{8}{\pi}A_{12}v_{12}Э^{1/4}_{max}r_1 n_2 \simeq 2\cdot 10^{-9}\,\frac{\xi^{3/4}k_2}{b^{1/4}\rho_g^{11/4}c_g^{10/4}\eta}\,\frac{1 - r^3_{2np}}{r^3_{2np}}\left(\frac{1{,}5 + r_{amp}}{1 + r_{amp}}\right)^{1/4}\frac{J^{10/4}}{f^{1/4}_{опт}}. \qquad (13.21)$$

In an air medium the following prevailed:

$$N'' \simeq 8\cdot 10^{-12} k_2 \frac{1-r^3_{зпр}}{r^3_{зпр}} \left(\frac{1{,}5+r_{зпр}}{1+r_{зпр}}\right)^{1/3} \frac{j^{13/9}}{f^{2/3}_{окт}}. \qquad (13.21')$$

The ratio of this flow to the flow onto a sphere in a normal turbulent field equals:

$$\frac{N''}{N} = \frac{8/\pi A_{12} v_{12} Э^{1/3}_{max} r_1 n_2}{\pi r_1^2 v_{12} n_2} \simeq \frac{A_{12}}{r_1}. \qquad (13.22)$$

usually A_{12}/r_1 and, consequently, $N''/N \geq 20$.

The absolute value of flow of small particles entering the aggregate volume of a large particle orthokinetically is also small. Thus, for a particle of radius $r_1 = 3.5\mu$ at normal sound intensity (in accordance with (13.21')), the following is true:

at $r_{2a} = 0.2$ $N'' = 1.5$,

at $r_{2a} = 0.5$ $N'' = 0.2$.

However, the presence of an orthokinetic flow markedly decreased radius R_{diff}, at which a diffusion particle flow, sufficient to completely fill an aggregate volume of radius R_a in the course of each diffusion event, is ensured.

At $r_{2a} = 0.2$ which corresponds to $R_a = 0.24\,(r_1 + r_2)$, $R_{diff} \simeq 0.40\,(r_1 + r_2)$; at $r_{2a} = 0.5$, which corresponds to $R_a = 0.58\,(r_1 + r_2)$, $R_{diff} \simeq 0.83\,(r_1 + r_2)$.

In both cases R_{diff}/R_a. Thus, it follows that at normal sound intensities there existed a thin "barrier" of thickness $\Delta R \simeq R_{diff} - R_a$ on the path of the particle to the aggregate volume; most of the particles cannot overcome this barrier by means of pulsation. This particle "barrier" is overcome by the phenomenon of particle self-centering examined in #11. At an elevated noise level, the need for this phenomenon actually vanishes, since, owing to the tendency toward an increase in orthokinetic flow [see formula (13.21)], the condition of $R_{diff} < R_a$ is achieved.

CHAPTER 4

MECHANISM AND GENERAL PRINCIPLES OF ACOUSTICAL AEROSOL COAGULATION

14. THE COURSE FOLLOWED BY ACOUSTICAL AEROSOL COAGULATION

It is apparent from the preceding chapters that the behavior of aerosol particles in a sound field differed essentially from their behavior in an unperturbed medium, or in a turbulent stream. Because of that the process of acoustic aerosol coagulation proceeded in an completely specific manner. This can be noted by simple macro-ocular observation of the process. When a sound source is switched on, the aerosol at first acquires a somewhat "tense" state, which is difficult to describe verbally, but is easily comprehended if it is remembered that at this instant the aerosol particles take on a vibrating motion, and begin to drift, and move forward under the action of an acoustical wind. A peculiar aerosol "orientation" occurred. Naturally, the behavior details of individual particles are not clear, since the initial particles, due to their minuteness, could not be seen with the naked eye, since the human eye perceives separate objects only when their sizes are of the order of 100μ. Subsequently, the aerosol becomes "bleached", and particles become visible, executing a random displacement, drifting, and circulating with the medium. Liquid particles form droplets, and dry hard particles form cotton-like and filiform structures which conglomerated with greater tightness than those in natural, Brownian, coagulation. The latter is illustrated by Fig. 43, which shows a carbon black aerosol deposited on a glass slide before and after sonication [272].

In a standing wave, local phenomena begin to appear at the instant of "bleaching". The "bleaching" proceeds in regularly alternating lateral bands, which gradually widen and encompass progressively larger areas. Particle aggregates emerging at that time accumulated and formed transverse "discs" or, more exactly, "rings", and sometimes longitudinal "sleeves" [277] at the antinodes. From there they speed away in the direction of vibration nodes near the walls of a vessel and settle in the shape of transverse ridges on the vessel's perimeter. The higher the vibration frequency, the smaller is the distance between the adjacent ridges. Occasionally, intermediate ridges can be distinguished on the walls which corresponded to harmonics of a sound wave. In a traveling wave, where the local phenomena are absent, the formed particle aggregates settle by gravity on the bottom of the sonication chamber and also partly on its walls. After the settling of particle aggregates, the sonication chamber looks practically aerosol free.

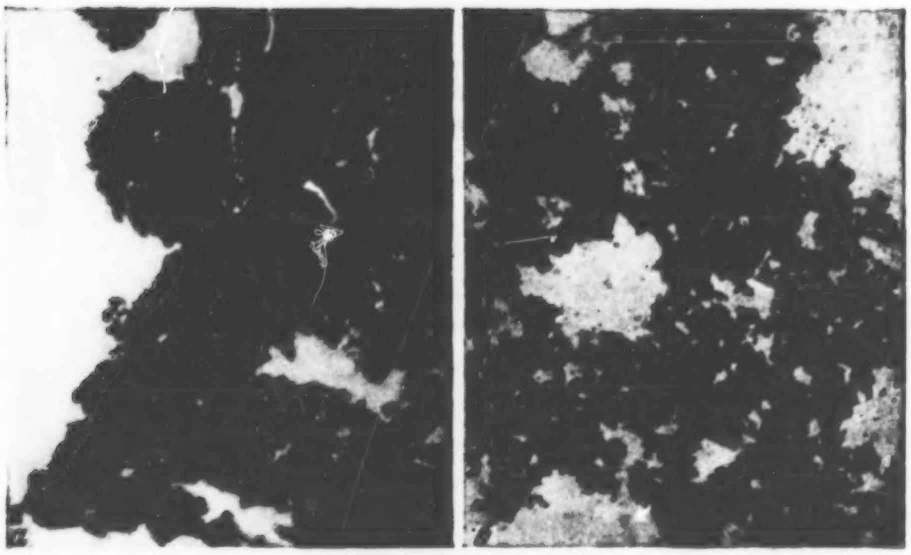

Fig. 43. Gas soot aerosol before sonication (a) and after sonication in the course of 4 sec. (b) x100

Such is the typical picture of highly dispersed aerosol coagulation, such as, ammonium chloride, magnesium oxide, titanium tetrachloride, carbon black, and others, which were sonicated in a stationary state at moderate sound intensities. Figure 44 shows photographs of four consecutive coagulation stages of ammonium chloride smoke, in the field of a 10-khz standing wave [179]. The first photograph shows an aerosol before sonication, the following two show aerosol during sonication, and the last one - shows coagulated and precipitated aerosol after sonication has been disconnected.

The coagulation process and subsequent precipitation of coagulated particles at moderate sound intensities lasts several second decades. At very high sound intensities coagulation is accomplished in several seconds; however, large flakes fail to form due to the instability of sound fields. Instead, whirling, fog-like clusters of smoke particles emerge at definite intervals along the chamber, and ridges* appear and disappear at the walls. When an aerosol is pumped through the sonication chamber, i.e., when it is in a flowing state, a spatial, rather than temporal, picture of aerosol "bleaching", and of the formation and random motion of particle aggregates is unfolded, i,e., along the course of aerosol's travel through the sonication chamber. The original aerosol can be seen at the inlet to the sonication chamber, the coagulated "bleached" aerosol, can be seen at the outlet. Moreover, all the described local phenomena are absent not only in a traveling wave, but also in a standing wave. This can be explained, in the first place by the short time it takes the aerosol to pass through the node-antinode region, and secondly, by the fact that the particle drift velocity vector and the

---

* Ridges can be easily "washed off" from the walls by changing frequency of vibrations.

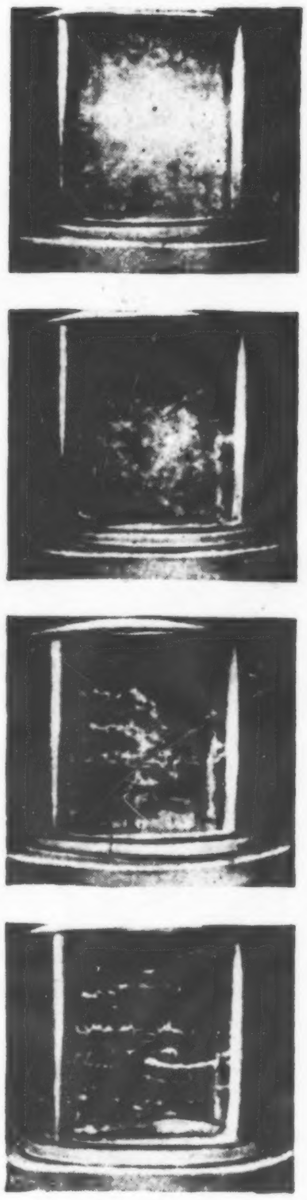

Fig. 44. Ammonium choride aerosol at different coagulation stages in a static sound wave (f = 10 khz)

acoustical flow vector alternately changed their signs during the transfer from one node-antinode region to another. A more detailed picture of the behavior of the particles can be secured by observing an aerosol coagulating in a sound field, through an ultramicroscope. It will be clearly seen that the particles participated in the vibrating motion of the medium, although this phenomenon is also hard to observe, since the particles rapidly pass through the field of vision. This difficulty can be somewhat avoided by observing the aerosol near the antinode, where the particle drift velocity approached zero. However, even then it is not possible to directly observe the elementary act of particle convergence and aggregation, due to the extreme speed and complexity of particle motion in a sound field, which the human eye is unable to follow.

Significant possibilities are offered in this respect by motion-picture filming of the process. This kind of investigation had been conducted by Brandt, Freund and Hiedemann [9, 170]. The speed of filming was 25 frames per second. Figure 45 shows eight consecutive microphotographs of acoustical tobacco smoke coagulation, selected by the authors from a series of photographs. The first picture (a) represents an aerosol before sonication. The second picture (b) was taken immediately after switching on the sound source - a magnetostrictive emitter, excited by a tube-type 10-khz oscillator; it can be seen that the particles just started their vibrating motion. The next four frames (c, d, e, and f) represent consecutive stages of acoustical aerosol coagulation; it can be seen distinctly that the particles participate in the circulating motion of the medium, and furthermore, execute some other undefined motion, indicated by the smudginess of the picture. The particles became progressively larger from picture to picture and scanned the increasingly greater areas of the field of vision. The last two pictures (g and h) were taken after the sound source was disconnected, and reflect the precipitation process of the coagulated particles under the effect of the gravitational force.

Based on results of conducted investigations the authors divided the process of acoustical aerosol coagulation into two stages. In the first stage the particles vibrated under the effect of sound and participated in the general circulation of a gas, increasing in size through colliding with each other. In the second stage, when the particles became enlarged so that their vibrations amplitudes decreased to small fractions of the gas vibrations' amplitudes, the particles suddenly ceased to vibrate and began to move along irregular, often sharply zig-zag trajectories, in the case of spherical particles, or spiral trajectories, in the case of particles with irregular shapes. At this stage, aerosol coagulation proceeded due to the convergence of non-vibrating particles, and also due to collisions between the non-vibrating and still vibrating particles.

The authors believe, that their investigations enabled them to fix the elementary aerosol coagulation processes in a sound field. It is difficult to agree with them, because in every frame there were about 400 vibration cycles which, naturally, prevented them from studying trajectories of interacting particles*. Nevertheless, the course of the process of acoustical coagulation of aerosols can be reproduced with a sufficient degree of accuracy, by basing it on the information of elementary interaction processes between aerosol particles and a sound field, obtained in the preceding chapter.

It can be concluded from the above mentioned information, that if the aerosols were monodispersed, sonication could have yielded insignificant effects. Actually, in this case only two forms of interaction occurred: attractional and diffusional. However, the velocity of attractional interaction in the immediate vicinity of a particle ($s = 2r$) equals zero and, consequently, the attractional interaction cannot be the cause of contact, and hence, the coagulation of particles. On the other hand, the velocity of diffusional particles interaction of the same size in a sound field is of the same order as the velocity of diffusional interaction of particles in an ordinary turbulent flow, i.e., negligible.

Fig. 45. Microphotographs of successive acoustical smoke coagulation stages (exposure time 0.04 sec)
a – before sonication; b – at the time of sound switching in; c – d – e – f – successive stages of increase in particles; g – h – falling out of increasing particles when sonication is discontinued

Meanwhile, experience indicated that aerosol particle coagulation proceeded with greater speed in a sound field than in a turbulent flow, at the same values of turbulent characteristics, which indicated that the intensifying effect of sound on the process of aerosol coagulation was conditioned largely by the fact that all aerosols were polydispersed and, consequently, there existed differences in the size of their particles, and also, differences in the velocity of vibrating motion. The following should be pointed out: regardless of minute differences in the size of two dissimilar particles, a difference in the velocities of their vibrating motions (if the particles are sufficiently entrained into the vibrating motion of the medium) developed during sonication. The following example will serve as an illustration: The most isodispersed aerosol, tested as an object of the coagulating sound effect, appears to be, the highly-dispersed vapor of dioctyl phthalate described in [94, 95]; the radius of its droplets ranged from 0.16 to 0.48μ, the mean radius being 0.28μ. The vibration frequency was 13 khz. Under these conditions, the degree of particle entrainment was very high amounting to $\mu\rho_1 = 1.0$, $\mu\rho_2 = 0.997$, and $\mu\rho_3 = 0.975$, for the smallest, medium, and the largest sizes, respectively. The arithmetical difference in the vibrations amplitudes of these particles did not exceed $\mu_{13} = 2.5\%$. For this reason, the author of [93] maintained, that there was practically no difference in the velocities of particle motion, and, consequently, no orthokinetic particle interaction. Meanwhile, calculation of particles, relative degree, according to formula (10.3), which took into account the difference in the phase displacement of particle vibrations, yielded different results: $\mu_{12} = 7.7\%$, $\mu_{23} = 15\%$, and $\mu_{13} = 22.4\%$ of the vibrational velocity of gas. These values are much greater, particularly, considering the fact, that the selected vibration frequency was far off from the optimal frequency values (296, 99 and 17 kHz) determined by formula (10.10).

---

* Recently, an attempt has been made at the Acoustical Institute of the Academy of Sciences, USSR, to obtain high-speed moving pictures of acoustical coagulation of aerosols with speeds up to 5,000 frames per second. However, the first experiments succeeded only in photographing the formation of spatial particle groups. This was already mentioned in #11.

All forms of the aerosol particle interaction in a sound field occurred in polydispersed aerosols, each playing a specific role. This can be understood better if it is noted that in order to form an aggregate with a radius r = 10 - 20μ from the initial particles, the latter must travel a distance of 500 - 1000μ, which follows from formula (9.5). This is a sizeable distance, and moreover, it is much larger than the average distance between the initial particles and the amplitude of the medium's vibrations. The convergence of particles located at considerable distances from the center of coagulation, can be accomplished only by the diffusional interaction due to turbulence of the sonicated medium. However, as the distance between particles decreased, their diffusional convergence velocity rapidly abated and, when a particle approached the volume of a large particle, its velocity became negligibly small. Here, the phenomenon of self-centering of small particles around a large particle occurred, sharply increasing the approach velocity of small particles towards the aggregate volume, with the exception of the middle portion of the aggregate volume, where the particles become first repelled and then drawn by the diffusion and acoustical flow to the outer regions of the volume. The self-centering velocity of small particles is such that the particles reach the aggregate volume within fractions of a second, especially as this is assisted by the attractional interaction of particles and the orthokinetic mechanism of the fluctuating interaction.

When a small particle entered an aggregate volume of large particles, its motion ends, (in one vibration cycle or less) following in an orthokinetic impact with a large particle. Evidently, charging of the aggregate volume was continuous, and its discharging - periodical.

The described course of acoustical aerosol coagulation as applied to a bidispersed aerosol model is shown in Fig. 46. Here, numeral 1 denotes a large particle, as the coagulation center, and the remaining numerals denote small equivalent particles located at different individual points of the surrounding space. The latter vibrates with respect to the large particle of amplitude A_{12}. The outline of a large particle aggregate volume is shown by a dotted line, and a broken line denotes an arbitrary outline of the pre-aggregate volume in which the self-centering phenomenon of the particles occurred, R_{diff} - mean volume radius. Zig-zag arrows, with index V_{sc}, denote small particles delivery by self-centering into the aggregate volume; identical arrows with index V_{sdc} denote the phenomenon of particles self-decentering. Straight arrows with index V_{attr} signify attractional delivery of small particles and the acoustical flow; arrows with index V_{ortho} signify delivery of particles by the orthokinetic fluctuating interaction mechanism. Arrows with index D_{turb} signify small particles diffusional delivery into the pre-aggregate volume. Such is the course of rapid aerosol coagulation observed in the optimal frequency range, when the difference between the velocities of vibrating particles is perceptible*.

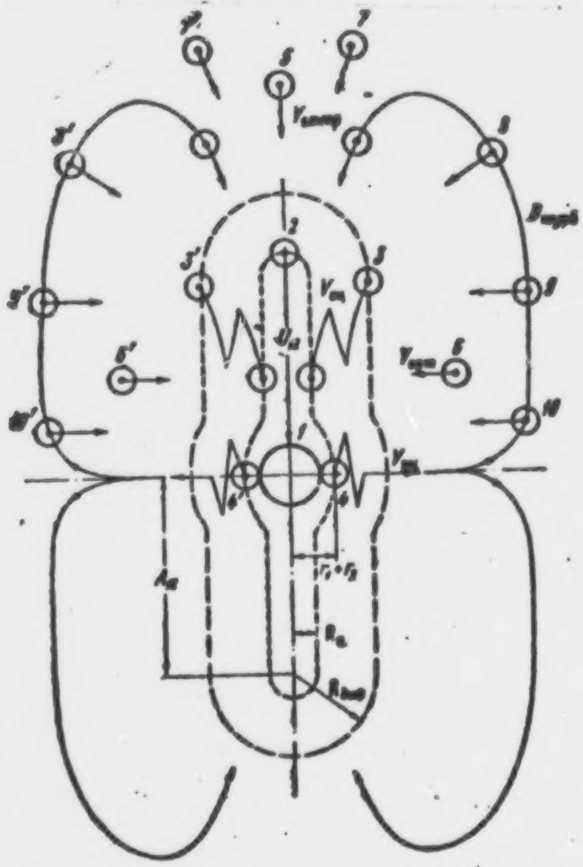

Fig. 46. Diagrammatic presentation of the course of acoustical aerosol coagulation

---

*Recently, A. I. Gulyaev and V. M. Kuznetsov [31] demonstrated that aerosol coagulation under the effect of recurrent shock waves, such as single shock wave, disclosed by E. Richardson [257], failed to produce any perceptible effect. Obviously, the aerosol coagulation mechanism in this case was the same as the one described above. This is witnessed by the fact, that the turbulence pressure amplitude intensity (0.3 atm), used by the authors, attained approximately the same values as in a sound field (4-6%) and, consequently, the effectiveness of coagulation with respect to a purely turbulent mechanism, described by V. G. Levich [68, 69], was inadequate to explain the high results obtained. It is not reasonable to maintain that the presence of oblique shock waves was a factor of any significance.

If no above-indicated difference exists, and this is unavoidable, in the sonication of coarsely dispersed and the coagulated finely-dispersed aerosols, aggregation of particles follows a different course. In that case, a definite difference is preserved only for the drift velocities of particles which aggregate with each other due to the orthokinetic mechanism and, at the same time, precipitate due to their own weight. In a standing wave, local accumulation of particles on the walls at the nodes takes place during the process. This is conditioned by the fact that a "dead" zone forms at these points between two opposing acoustical flows and the large particles, which rotate with them, fall into the indicated zone under the effect of the centrifugal force. Since the particle drift velocity is negligible in comparison with the vibration velocity, the described orthokinetic aerosol coagulation velocity is very small. Accordingly, this form of aerosol coagulation in a sound field shall be referred to as the slow aerosol coagulation. The same term will also be used for the coagulation of equivalent particles, where the aggregating processes proceeded at a slower rate.

15. KINETIC EQUATION OF THE PROCESS

Assume the interaction of dissimilar particles as the basic acoustical aerosols coagulation course, and establish that the rate of the process was a linear function of the particles numerical concentration. This can be illustrated by the following example of a bidispersed aerosol.

A bidispersed aerosol model is, indeed, not a complete equivalent of a polydispersed system; however, it exhibited its main distinguishing characteristic, namely, different particle size; generally, any aerosol can be represented as a combination of a similar kind of bidispersed system. Assuming that, our bidispersed aerosol contains n_{10} large particles and n_{20} small particles per unit volume at the initial moment. Assume also, that $n_{20} >> n_{10}$, otherwise any perceptible coagulation of particles was impossible (see #9). In accordance with what has been said in the preceding paragraph, it has been assumed that particles of equal sizes did not aggregate with each other, and that the reduction of numerical concentration during the process of coagulation has been achieved only due to adherence of small particles to large ones. To set up a kinetic equation of the acoustical aerosol coagulation, it is enough to turn to the formal kinetics of homogenous chemical reactions, which postulates the following [43]: the rate of reaction was proportional to the concentration product of reacting substances, during which each concentration participated to a degree, in the simplest cases, equal to the coefficient in front of the formula of a given substance in the reaction equation. The reaction mechanism of the substances, as is known, had not been mentioned there. Therefore, it is possible to extend the quoted rule to the case of the bidispersed aerosol, under present discussion, which, incidentally, is similar to the molecular reaction of two gaseous substances. Specific characteristics of the case under discussion, is the fact that concentration of one of the "substances", namely, the large particles, remained constant during the process: $n_1 = n_{10} =$ const. Taking this into account and also the fact that "coefficients in front of the formula of each substance" in the case under discussion, equal to 1, the rate of acoustical aerosol coagulation can be expressed by the following equation:

$$dn/dt = - K_a n \quad (15.1)$$

where n - particle concentration; taking into consideration that $n_s >> n_1$, it can be assumed that the total number of particles n and the number of small particles n_s were the same; t - sonication time; K_a - coefficient of acoustical aerosol coagulation, which is a function of the physical aerosol characteristics and of the sound field parameters. Thus, it can be seen that the equation of the process of acoustical aerosol coagulation agreed formwise with the equation of monomolecular chemical reaction.

It should be noted, that if the equidimensional particles interaction were the basis of the acoustical coagulation process, the rate of the process would not be a linear, but a quadratic function of the flowing particle concentration. The corresponding kinetics equation would then coincide with the equation of bimolecular chemical reaction, similar to one applicable to the Brownian aerosol coagulation, [see equation (9.2)]. This would contradict all experimental data on the kinetics of the acoustical aerosol coagulation process, which will be examined next. Before that, equation (15.1) will be integrated by first assuming that time t = 0 and the numerical concentration of particles $n = n_0$:

$$n = n_0 e - K_a t \quad (15.2)$$

The exponential dependence of numerical particles concentration on the coagulation coefficient and the sonication time established by this equation are in good agreement with the experimental data on the acoustical aerosols coagulation.

Relationship (15.2) was first demonstrated by Brandt [161] in experiments on the acoustical paraffin oil vapor coagulation, conducted at 10 khz frequency. The radii of the vapor droplets were in the range of 0.2 - 1.9μ (mainly 0.8 - 0.9μ), and their gravimetric concentration was 15 - 20 g/m³. Results of these experiments are shown in Fig. 47. According to the curves, the following values were obtained for the coagulation coefficient:

at $J = 0.0067$ w/cm² $K_a = 0.43$,

at $J = 0.06$ w/cm² $K_a = 0.92$,

at $J = 0.11$ w/cm² $K_a = 1.28$.

In comparing the coefficients of different aerosol coagulations, they will be henceforth related to normal sound intensity $J = 0.1$ w/cm²; such coefficient shall be referred to as "normal" coefficient of aerosol coagulation. In this case the normal coagulation coefficient was $K_a \simeq 1.25$.

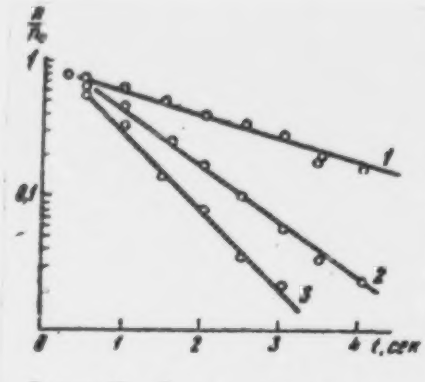

Fig. 47. Functional relation between rate of accoustical paraffin smog coagulation and particle count (f = 10 k-hertz). 1 - at I = 0.0066 bt/cm^2; 2 - at I = 0.06 bt/cm^2; 3 - at I = 0.10 bt/cm^2.

As a relationship confirmation (15.2), Inoue [37] quotes also the results of St. Clair's [179, 181] experiments conducted with ammonium chloride smoke, at a 10 - 20 khz frequency. It appears, however, that this was done irregularly, because in the experiments not the size of coagulating particles, but the change in the dispersed light intensity was controlled by them, which were far from being equivalent. Relationship (15.2) was demonstrated in a more conclusive manner by experiments on the acoustical coagulation of dioctylphthalate vapor, recently conducted by B. F. Podoshevnikov [94, 96]. The dioctylphthalate vapor was taken from LaMer's aerosol generator. The radius of vapor droplets was in the 0.16 - 0.48μ range (mainly 0.28μ). The gravimetric concentration was 1.8 - 2.1 g/m^3, and the acoustical vibration frequency, radiated with the St. Clair-type electrodynamic emitter, was -13 khz. The present author obtained the following experimental relationship between pt$_0$ (p - sound pressure in kilobars):

$$\frac{n}{n_0} = e^{-0.08pt_0 + 0.0002 (pt_0)^2} \cdot \qquad (15.3)$$

The second quadratic term of the exponent is extremely small in comparison with the first term at normal or even elevated sound intensities (J = 0.1 - 1.0 w/cm^2) and at moderate sonication times (t ≤ 15 - 20 sec). Therefore, the second term can be practically disregarded, and the equation will assume the form of (15.2). Moreover, the normal coagulation coefficient is K_a = 0.08 p= 0.08 · 6.4 = 0.5.

Changes of the dispersed composition during sonication, are characterized by particle size distribution curves according to their numbers, as shown in figure 48. It can be seen, that in the coagulation process the maximum shifted comparatively little, despite the fact that the large particle portions grew considerably. The exponential nature of the equation, which described the kinetics of acoustical aerosol coagulation is also supported by the results of many experiments at the semi-industrial scale on the acousto-inertial precipitation of different industrial aerosols, conducted by Oyama, Inoue, Savahata and Okada. Details of these experiments are presented in #20 (see Fig. 68 and table 18).

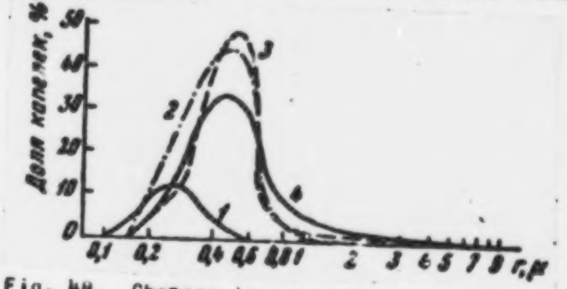

Fig. 48. Changes in composition of accoustical dioctylphthalate smog at sound intensity (f = 13 khz, p - [illegible]630 bar. 1 - Initial distribution of drop sizes (k = 1.82 g/m^3; 2 - after accoustical exposure for an interval t = 2.3 sec.; 3 - ditto - t = 8.75; 4 - ditto t = 14.8 sec.

Acoustic coagulability of cracking

gas vapor was investigated by the authors in great detail. Particle radii of this aerosol ranged between 0.5 - 5.0μ, mainly 3.0 - 3.5μ, and the weight concentration fluctuated in the range of 6 - 15 g/m^3. The optimum vibration frequency was 4 khz. According to the authors' calculations [259], normal coefficient of coagulation of a given aerosol in an industrial unit set up by them was $K_a = 0.35 - 0.37$.

Let us pause briefly on K_a, the physical content of the acoustical aerosol coagulation coefficient. Formal kinetics, enable us to establish only that the coefficient was proportional to the numerical concentration (n_0) of large particles, which are the coagulation centers:

$$K_a = K_{a1}\ n_{10} \qquad (15.4)$$

However, this concept can be supplemented on the basis of the earlier described behavior process, although it should be noted that due to the motion complexity of small particles the final analytical solution of the problem still presents a difficult problem.

It has been known that each large particle is a depository of those little particles which fall into its aggregate volume, outlined in Fig. 46 by a dotted line. This volume can be roughly visualized as a regular circular cylinder of cross section $E\pi r_1^2$, and the height - $2A_{12}$, so that its volume is $Q = 2E\pi r_1^2 A_{12}$. The small particles concentration n_a, filling the aggregate volume, is directly proportional to the average concentration of particles in the surrounding space: $n_a = \beta n$, where β - space factor, which thus has remained undetermined analytically ($\beta < 1$). The total number of small particles (Δn), entrained by the large particles during time (Δt) equals

$$\Delta n = -2Q_a\beta n n_{10} f\Delta t = -2\text{Э} n_{10} r_1^2 \mu_{12}\beta U_g n\Delta t. \qquad (15.5)$$

Whence, the rate of acoustical aerosol coagulation can be expressed by equation (15.1) if K_a is assumed equal to:

$$K_a = 2\varepsilon\beta\, n_{10}\, r_1^2\, \mu_{12}\, U_g\,. \qquad (15.6)$$

The foregoing indicates that the acoustical coagulation coefficient of bidispersed aersols represents a portion of small particles, entrained by all the large particles in unit time. The process of slow aerosol coagulation, which depended on different drift velocities, is also determined by equation (15.1), but in this case the acoustical coagulation coefficient is expressed as follows:

$$K_a = \Sigma\pi r_1^2 (V_1 - V_2)\, n_{10}\,. \qquad (15.7)$$

where V_1 and V_2 - drift velocities of large and small particles, respectively. It is not difficult to arrive at this equation, assuming that during drift each large particle entrained small particles in the cylinder, the cross section and height of which are $E\pi r_1^2$ and $(V_1 - V_2)$, respectively.

16. EFFECT OF AEROSOL AND ACOUSTICAL CHARACTERISTICS ON THE KINETICS OF THE PROCESS

Examine available experimental data relative to the effect of the physical characteristics of an aerosol and the parameters of a sound field on the kinetics of the discussed process, implementing these by the individual theoretical reasons pertaining to the present problem.

Aggregate state, density, and structure of aerosol particles. Solid particles grow somewhat faster than liquid particles of equal dispersion, density, and concentration. This may be due to the fact that solid particles gathered into more bulky, disorganized friable agglomerations in the shape of flakes, chains, etc., than droplets did. The ability of these to precipitate is higher than that of droplets of equal weight, dispite a sharp drop in their apparent density. This follows directly from the expression for the particle relaxation time (4.4), in which the particle sizes are expressed in the second power, and its density only in the first. However, dry aggregates of solid particles were less stable in an agitated stream and, consequently, they may become partially disintegrated upon entering a cyclone, or any other inertial precipitator [206], where the turbulence intensity is very high ($\epsilon = 10^9 - 10^{10}$). This pertains in particular to low-dispersion aerosol particles, which, according to the theoretical studies of B. V. Deryagin, stick to one another to a lesser degree than the highly dispersed particles.

In the case of high sound intensity where ($J > 1.0$ w/cm^2), the dry particle aggregates may break down partially also in the sound field; susceptible to this, however, are only the large conglomerates on the ends of which there builds up a sufficiently perceptible difference in the magnitude of sound pressure or turbulent pulsation velocity. However, the above mentioned, had little effect on the results of subsequent precipitation, since the "fragments" formed during the breaking up of an aggregate were still sufficiently large and precipitated with equal ease. This is confirmed by the fact that with increased sound intensity, the effectiveness of coagulated aerosols precipitation did not drop but invariably increased (compare, for example, the results of acousto-inertial precipitation of carbon black, at the sound intensities of 0.5 and 1.0 w/cm^2, quoted further in #20).

Apparently, the density of initial particles played no significant role, although there existed no experimental evidence in support of this fact. Of course, this can be explained by the fact that a change in density produced directly opposite phenomena. On the one hand, with the increased density, there was, according to (11.3), an increase in the rate of inertial self-centering of particles, due to that, an increase in the coagulation coefficient occurred; in addition, the optimal frequency value has been displaced toward lower frequencies at which the sound absorption by the medium was diminished. On the other hand, increased particle density indicated, according to (9.1), a decrease in the numerical particle concentration, which appeared in the kinetic equation of the process, directly and indirectly, as a multiplier in the expression for the coagulation coefficient. Likewise, no record existed of any specific effect of initial particles' shape on the rate of process. Spherical (fog droplets, carbon black), cubic (magnesium oxide), acircular (zinc oxide), etc., particles coagulated in the sound field, with approximately identical ease. It can be stated in general, that the physical characteristics of aerosol particles exerted comparatively little effect on the kinetics of the acoustical coagulation aerosol process.

Dispersion structure and the weight concentration of aerosol particles. Highly dispersed aerosol coagulated with greater intensity, than aerosols of medium or lower dispersion. This follows directly from the kinetic equation of the process (15.1), examined with regard to 1) findings on the acoustical coagulation coefficient, presented in the preceding paragraph, and 2) the relation (9.1) for the numerical particle concentrations. The acoustical coagulation coefficient changed comparatively little with the decrease on particle size, whereas the numerical particle concentration sharply increased, and this predetermined the process acceleration. Physically, this can be explained as follows: with the increased particle dispersion, the total area of the particle cross sections sharply increased; experimental evidence of this is the sharply decreased aerosol transparence; the volume, "combed" by the vibrating particles, increased sharply with it, and, as a result, the probability of particle collisions also increased. However, to enlarge particles of highly dispersed aerosols to sizes effectively precipitated by gravitational or inertial methods, an extremely large number of aggregation events is required. For instance, to enlarge droplets from a radius $r_0 = 0.1\mu$ to $r = 10\mu$, $(10^3/0.1) = 1,000,000$ events are required in accordance with (9.8). Such an operation necessitated a large sonication time, and, consequently, a greater power consumption. If the acoustical coagulation coefficient is known, the required sonication time can be found, with the aid of (15.2), and the following formulas:

for fogs: $t_0 = 3/K_a \ln(r/r_0)$ (16.1)

for smokes and dusts (which require correction to decrease the density of particle aggregates):

$$t_0 = \frac{3}{K_a} \ln\left[\left(\frac{\rho_p}{\rho_p'}\right)\frac{r}{r_0}\right]. \qquad (16.2)$$

It follows from these formulas that an increase in the particle dispersion entails a sharp increase in the required sonication time. For example, enlargement of highly dispersed dioctylphthalate vapor droplets ($r_0 = 2.28\mu$) to sizes $r = 5 - 6\mu$) which could be trapped in cyclones at a normal sound intensity $J = 0.1$ w/cm^2 when $K_a = 0.50$, in accordance required $t_0 \simeq 18 - 20$ sec according to (16.1). Sonication time can be reduced by increasing the sound intensity. Thus, according to (15.6), increase in sound intensity to $J = 1 w/cm^2$ the increased coagulation coefficient to $K_a = 1.6$, and reduced the sonication time to $t_0 \simeq 6$ sec. This value is acceptable to a degree for practical purposes; however, it increased the required energy consumption for the sonication of an aerosol unit volume more than three times [see formula (20.8)]. In connection with the above, optimal aerosols for industrial coagulation are of medium size, particularly the ones with particle radii in the order of $r = 2 - 4\mu$. Aerosols, which contained no particles with radii less than $5\text{-}7\mu$, coagulated poorly; this pertains in particular to solid state aerosols characterized by weak adherence between the particles. The following can serve as examples: fly ash, mineral dusts, atomized artificial fogs, and also suspended powders (which are "aggregated" aerosols).

The gravimetric particle concentration also strongly effected the course of acoustical aerosol coagulation. The greater the weight concentration the more intensively the aerosol coagulated, as equations (15.1) and (9.1) indicate. This is determined by the fact that at higher concentrations particles form aggregates from a smaller aerosol volume i.e., they overcome smaller distances to the center of coagulation.

It was established that the process effectiveness sharply decreased with concentrations below 2-5 g/m^3. In such cases injection of atomized water into a weakly concentrated aerosol - aerosol spraying - had a good effect. Moreover, the effectiveness of coagulation and subsequent particle precipitation sharply increased, as can be seen in Fig. 49, where the results of acousto-inertial carbon black aerosol precipitation in the natural and sprayed forms are shown [273].

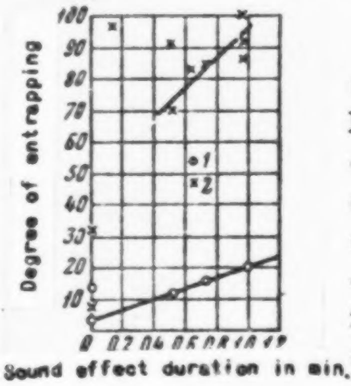

Fig. 49. Effect of added water fog on the effectiveness of carbon black acoustical coagulation. (P_c = 0.35 atm.; f = 2.1 kHz.)
1. Prior to water vapor introduction; 2. After water vapor introduction.

The intensifying effect of aerosol spraying is determined, in the first place, by the fact that during spraying an additional large number of coagulation centers is introduced into the aerosol which are completely captured in a precipitator, and only in the second place by the wetting of dry particle aggregates, (if such existed). A particle concentration above 100 g/m^3 is undesirable, since it weakened the sound intensity with distance and, as a result, lowered the rate of the acoustical aerosol coagulation.

Viscosity, temperature, and pressure of a gaseous medium. The higher the viscosity of the medium, the higher is the magnitude of optimal vibration frequency, as seen in equation (10.5), and the lower is the velocity of inertial particle self-centering, as shown by equation (11.13). Therefore, an increased gaseous medium viscosity is less favorable to acoustical aerosol coagulation. A temperature increase in a gaseous medium indicated an increase in its viscosity with all the resulting consequences, i.e, the rate of acoustical aerosol coagulation drops sharply, (see equation (b) on page 56). In other respects, the process proceeded normally; therefore, increased temperatures are not detrimental in using this process for purification of hot gases.

Cases of successful aerosol coagulation at temperatures of 300 - 500° C and higher are not new anymore. However, in such cases it is necessary to make certain that all the emitted acoustical energy was delivered to the aerosol, since strong sound waves reflection and dispersion occurred at the mixing interface between the cold air generated by a siren and hot aerosol. Increase in medium pressure indicated an increase in its density, and, similarly in its acoustical resistance, decreased the vibrational medium velocity according to equation (1.9), which, as will be shown later was directly proportional to the acoustical coagulation coefficient. The value of the latter decreased sharply, and the process rate slowed down with it. To maintain the coagulation coefficient at its former level, it is necessary to increase the sound intensity approximately by as many times as the pressure medium differed from the normal pressure. An experimental method of acoustical aerosol coagulation was tested at pressures of the order of 10 [86] and 50 [80] gage atmospheres. The viscosity, temperature, and gaseous medium pressure are approximately identical in the majority of aerosols, namely, close to atmospheric conditions; therefore, these characteristics, as a rule, did not determine the observed difference in the rate of acoustical aerosol coagulation.

Frequency of vibrations. It has been established experimentally that the vibration frequency had a highly significant effect on the acoustical coagulation process. This can be corroborated in the laboratory and also by large-scale acoustical method tests of fog dispersion, and the acousto-inertial method of industrial dust, smoke, and vapor precipitation, described in the next chapter.

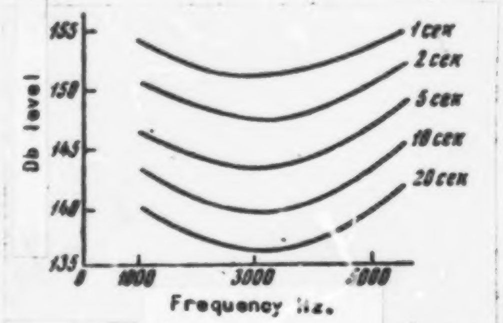

Fig. 50. Sound intensity level required to effect 50% clarification of artificial water vapor fog at different sound effect intervals and wave frequency.

Figure 50 shows sound level frequency dependence required for a 50% "bleaching" of the artificial water vapor. This dependence has been established by laboratory tests conducted by Horsley and Seavey at the Ultrasonics Corporation of USA [203]. Fig. 51 illustrates frequency dependence of degree of acousto-inertial precipitation of some industrial aerosols, obtained by Inoue and Oyama, and by Svahata and Okada [38].

The above graphs indicated that there existed an optimal vibration frequency for every aerosol at which acoustical coagulation proceeded most efficiently. Even a

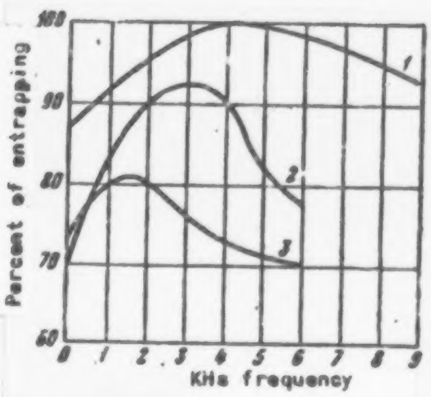

Fig. 51. Frequency relation between sound inertia precipitation of difent industrial aerosols.
1 – Coke gas tar; (r – 0.5 – 5.0 μ)
2 – Aggregated carbon black (r = 0.5 – 15 μ)
3 – Dilute sulfuric acid fog (r = 2.5 – 50 μ)

comparatively small frequency deviation from its optimum sharply affected the process effectiveness. Thus, in the first case (fig. 50), a 2-khz frequency shifted from its optimal value (3.0 - 3.5 khz) necessitated a 4-db increase in the sound level, or the doubling of the sonication time. In the second case (fig. 51), a similar frequency shift entailed a $1\frac{1}{2}$ - 2-fold increase in the residual concentration. It can be concluded from Fig. 50 that optimal frequency was independent of sound intensity and sonication time and, consequently, it was a function characteristic of the aerosol alone. Moreover, it should be pointed out that the gravimetric concentration of aerosol particles likewise had no effect on the magnitude of optimal vibration frequency. This was shown by Kawamura [210], who investigated the effect of acoustical characteristics on the acoustical coagulation process in tobacco and ammonium chloride smokes. Unfortunately, the frequency dependence of the process was determined in this investigation in degree of light dispersion by the aerosol particles, whereas the proof of the theoretical assumption required direct knowledge of coagulation rate dn/dt.

Table 13

Aerosol	Particle radii *r, μ	Optimal oscillating frequency ** f opt. kHz.	Autho.
I. Laboratory investigations			
Tobacco smoke	$\frac{0,2+2,5}{0,8}$	7—8	Kawamura [210]
Ammon. chloride vapor	$\frac{0,3\div2,6}{1,2}$	5—6	
Artificial water vapor fog.	—	5—6	H. P. Tserskey [115]
» » »	2,0	3—3,5	Kohrali and Syvp [156]
II. Plant investigations			
Gas furnace soot	0,03—0,07	3,5—4,0	Stokes [272]
Aggregated soot	0,5—15,0	3,0	Inoe et al [38, 246]
Zinc oxide vapor	$\frac{0,5+5,0}{2,5}$	3,0—3,5	
Coke gas fog	$\frac{0,5+5,0}{2,5}$	3,5—4,0	
Cracking gas fog	$\frac{0,5+5,0}{3,0}$	3,5+4,0	
Dilute sulfuric acid vapor	2,5—50	1,0—2,0	

* Numerator indicates limiting radius values, denominator indicates predominating values.

** Efficiency of aerosol coagulation in laboratory tests was evaluated on the basis of light clarification, and in the plant tests on the basis rate of inertia cyclone precipitation.

Table 13 shows composited data of the optimal frequency values of acoustical coagulation of different aerosols. Examination of these indicated that a lowering of the aerosol size lowered the optimal frequency vibrations. This conclusion has something in common with the conclusion related to the degree of aerosol particle entrainment into the vibrating motion of the medium, on the basis of which Hueter and Bolt [205] assumed that the following formula for determining optimal magnitude of vibration frequency in the atmospheric medium: (16.2) where r_s - predominant particle radius in μ. This equation was derived by the authors from the generalization which expressed the degree of particle entrainment (5.19), assuming that μ_p = 0.50, without any valid foundation. To verify this assertion examine the data on degree of particle entrainment and degree of the streamline particle flow into the vibrating motion of a gas for different aerosols coagulated in the sound field.

Table 14

Type of fog	Predominant droplet radius r, μ	Adjusted oscillation frequency f, kHz	Evaluation of results	Coefficient (%) of entrainment μ_p	Coefficient (%) of engulfment, μ_q
Artificial static fog (vertical flue ∅ 150 x 1000 mm)	4,0	0,5	Success	85,5	52,0
Artificial moving fog (horizontal flue ∅ 75 x 3,600 mm)	4,0	0,5	»	85,5	52,0
Artificial static fog (r, angle flue) (or chamber) 7,400 xm3 .)	2,0	3,5	»	68,8	72,9
Ditto, tunnel shaped (1,2x2, 1x30m)	4,5	0.6		73,6	67,8
Artificial Pimer test fog	7,5	8,5	Failure	2,8	99,9
Artificial static fog (swimming pool 5,600 m^3)	1,0	0,7	»	99,8	5,3
Artificial moving fog (chamber 12,8 x 14 x 18 m)	0,5	33	Success	84,7	52,9
Ditto	4,0	33	Failure	2,7	99,9
	0,5	9,5		98,4	17,9
Ditto, in a section of the chamber, (400 m^3	4,0	9,5	Slow clearing	8,7	99,6
Natural slow moving continental fog at USA Lunken Airport	6,0	0,44	Success	64,1	76,7
Natural continental fog at Arcata and Breice Cove, USA	15	3,5	Failure	1,7	99,98
Natural sea or ocean moving fog at Sndburg, USA	5,0	0,44	Success	77,0	64,0

Table 14 presents data on degree of entrainment and of streamline flow of natural and artificial fog droplets. These were used as objects for the acoustical dispersion method, examined in #18. The Table shows that in the successful experiments entrainment degree was usually higher than μ_p = 0.65 - 0.85. Boucher [156] interpreted this as indicating that orthokinetic interaction was the basis for the process of acoustical aerosol coagulation. Experiments with the acousto-inertial precipitation of industrial fogs, examined in #20 yielded other values for the entrainment coefficient and, consequently, of the droplets (Table 15) streamline flow coefficient. Thus, the degree of entrainment at optimal vibration frequency was in these experiments considerably below μ_p = 0.50, namely, μ_p = 0.15 - 0.27. The above indicates that the initial condition, assumed in the derivation of the proposed formula for the optimal vibration frequency was arbitrary; therefore, it is not surprising that a considerable discrepancy existed between the formula and results of the experiments.

A greater discrepancy existed between experimental results and Wyrzykowski's formula $f_{opt} = 7.64/\rho_p r^2 m$, derived on the basis of considerably simplified assumptions of acoustical aerosol coagulation [295]. Reference is implied in both cases to deviation from the results of laboratory investigations of the process. It will be shown later that this was due to the fact that the optimal vibration frequency for industrial installations was affected not only by the aerosol dispersion, but also by geometrical factors.

Now, analyze equation (15.6) for the bidispersed acoustical aerosol coagulation coefficient: the only frequency-dependent terms of this equation are degree of the respective particle motion μ_{1g} and, possibly, the space factor β. If it is assumed that the latter was remotely connected with the vibrations frequency, its optimal value could be determined from (10.5).

$$f_{\text{опт}} = \frac{9\eta}{4\pi\rho_p r_g^2} r_{g\,\text{пр}}, \qquad (16.3)$$

derived from the condition of maximal value μ_{1g}. For air as the medium, this formula has the following form:

$$f_{\text{опт}} = \frac{13{,}2}{\rho_p r_g^2 \mu} r_{g\,\text{пр}}. \qquad (16.3')$$

Table 15

Aerosol	Prevailing droplet radius, r, μ	Droplet density rho$_p$, g/m^3	Gas viscosity η g.cm^{-1} sec^{-1}	Optimal oscillation frequency, f optim. kHz	Theoretical involvement coeff. in % μ_p	Theoretical engulfment coeff. in % μ_g
Sulfuric acid fog	7,5	1,7	$1{,}8\cdot10^{-4}$	1,0	15	99,0
Cracking gas hydrocarbon fog	3	1,1	$1{,}0.10^{-4}$	4,0	18	98,0
Coke gas tar fog	2,5	1,2	$0{,}9\cdot10^{-4}$	3,5	27	96,5

However, the practical application of equation (16.3) encounters difficulties associated, first, with the fact that real aerosols are polydispersed. Even in cases in which particle size distribution curve was available, it becomes difficult to decide which figures are to be substituted in the formula for r_g and $r_{g\,pr}$, except most appropriate $r_g < r_m$, and $r_1 < r_{max}$. Moreover, it must be remembered that particle dimensions increased during coagulation and this, in accordance with (16.3), means a continuous decrease of the optimal vibration frequency. Therefore, the value of optimal vibration frequency depended not only on the initial, but also on the final particle dimensions. The experimentally observed optimal vibration frequency corresponded to a near average value between the instantaneous values at the beginning and the end of the process. In addition to the foregoing, it should be mentioned that in the case of industrial installations, geometrical factors, such as coagulation chamber length, begin to exert serious effects on the optimal vibration frequency. This becomes evident during the coagulation of highly dispersed aerosols, particularly, of carbon black. The theoretical value of the optimal vibration frequency at the initial stage of particle enlargement, derived from formula (16.3), can be as high as tens and even hundreds of khz. However, such high-frequency vibrations attenuate in gases with distance from their origin rapidly, so that an aerosol flowing through the chamber remained unsonicated most of the time. Therefore, in practice, low-frequency vibrations, of the order of 3 - 4 khz and lower, which attenuated much slower proved the most effective. Coagulation of the original particles which required much higher frequencies, was accomplished by harmonics, generated during the propagation of a sound wave, and partially present in the emission spectrum of the sound sources used. This opinion was confirmed by the intensifying effect of high-frequencies vibrations "addition" to the coagulator, noted by Boucher [150, 151] and other investigators. Geometrical factors are in strong evidence also in tests of acoustical dispersion of natural fogs, where the sonicated zone is especially large. Here, the value of optimal vibration frequency as a rule, is even lower than that in industrial coagulators. It is difficult to consolidate all above factors into a single function. Therefore, so far, the only reliable and available method of determining the optimal vibration frequency is direct experimentation with natural aerosols under working conditions. It is maintained in (33) that the rate of acoustical aerosol coagulation was generally independent of the applied frequency. Therefore, it is recommended, that the process be carried out at the lowest, and, consequently, at slow attenuating vibrations [89]. However, this is a misunderstanding, originating from the fact that an atomized powder of zinc white, in the place of zinc oxide aerosols was used in the tests. Aerosols, prepared in this way, contained adhesive, coagulated aggregates of original particles and, due to their coarse size, the aggregation of particles occurred in them in the form of slow coagulation (see #14), i.e., by means of orthokinetic collisions between unequal particles, dependent upon the difference in their drift velocity. This is confirmed by the function $p^2 t_0$ = const. derived by the authors. For any type of drift, the particle velocity $V \sim p^2$ (see table 5 in #6); whence, $p^2 t_0 \sim (V_1 - V_2)\, t_0 = L_{12}$ = const (L_{12} - length of path of large particles with respect to small particles).

Sound intensity. It has been established that the acoustical coagulation coefficient was a power function of sound intensity. At moderate sound intensity and sonication time, the following relationship holds:

$$K_a \sim J^{1/3} \qquad (16.4)$$

Inoue [37] was the first to stress this important relationship, which he based on the experimental data obtained by Brandt and Freund [161, 163], and Neumann and Norton [239].

By taking into consideration relations (1.9) and (1.10), the above relationship can be written thus:

$$K_a \sim p_s \sim u_s \qquad (16.4')$$

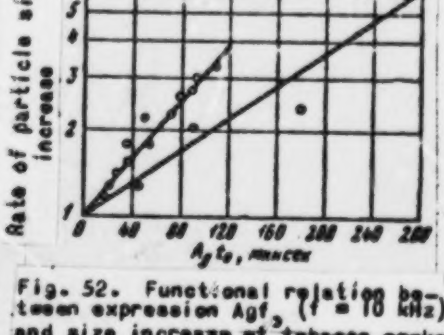

Fig. 52. Functional relation between expression Agf_3 (f = 10 kHz) and size increase of tobacco smoke particles

Fig. 52 illustrates the functional dependence of the numerical concentration of tobacco smoke particles on the product $A_s t_0$ which is proportional to $J^{1/2} t_0$ and $U_s t_0$. The data were taken from the experiments of Brandt and Freund. Fig. 53 shows the functional relationship between the degree of titanium chloride particles on consolidation and $J^{1/3}$, derived in the experiments of Neumann and

Norton. Since the graphs were plotted on the logarithmic scale, the relationship between the above quantities is linear.

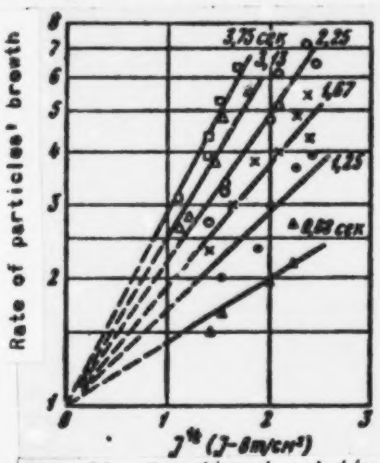

Fig. 53. Functional relation between growth rate of titanium titanium tetrachloride particles and expression

$J^{1/3}$(f − 1,6 кгц)

Existence of the above functional relationships is further confirmed by the results of tests conducted by B. F. Podoshevnikov with acoustical dioctylphthalate, and presented earlier as formula (15.4). In accordance with (15.4), the coefficient of acoustic coagulation increased progressively slower with an increase in the sonication exposure pt_0 above the 400 - 500 kiloparsec level. Moreover, it is known that sound absorption by the medium increased rapidly at the same time, (see #1). In view of this, application of very high sound intensities to industrial aerosol coagulation is economically unsound. The most frequent used sound intensities are of the order of 0.1 w/cm^2, and the most frequently used sound pressure is of the order of 6400 bar.

Structure of the sound field. The consolidation of aerosol particles proceeded faster in a standing wave field than in a traveling wave field. This may be due to the fact, that the vibrating motion amplitude was higher in a standing than in a traveling wave for the same output of the sound generator, and that a certain, even insignificant (see #17), increase in the numerical particle concentration took place. In addition, though not required in practice, considerable particle consolidation can be achieved in a standing wave field. The foregoing refers, naturally, only to the case of the acoustical coagulation of motionless aerosols, since (see #14), no local phenomena occurred otherwise. It can be asserted that where the sonication chamber was sufficiently long, better results were achieved with an aerosol moving against the sound source than away from it. This follows from the fact that aerosols are initially subjected to the effect of harmonics of the sound wave, in reversed motion, i.e., at higher frequencies. No experimental confirmation of this has been presented thus far. An attempt to solve this problem in [94] failed to produce differences in the results of "forward" and "reverse" aerosol sonication; this may be explained by the small length of the sonication chamber.

Geometrical dimensions of the sonication chamber, and of the sound field affected the rate of the acoustical aerosol coagulation process, not only when they had been reversed. In fact, the longer was the sonication chamber, the more harmonics were created in the sound wave, and the stronger was the attenuation of sound entering the chamber; consequently, the smaller was the average sound intensity inside the chamber with respect to its nominal intensity related, as a rule, to the exit cross section of the sound source. In accordance with (16.4), this means that under invariant conditions, the acoustical coagulation coefficient decreased with an increase in the length of the sonication chamber. Therefore, the findings of the acoustical aerosol coagulation coefficient, quoted in #15, should be examined from this point of view. It follow from the experiments of B. F. Podoshevnikov and other [30] that the coagulation coefficient depended also on the cross section of the sonication chamber. In those experiments, longitudinal partitions (d = 1 - 2 cm) were placed in the sonication chamber and some slowing down of the process rate had been observed (see fig. 57). However, it is not certain that this situation might exist in sonication chambers of large cross sections.

17. SOME EARLIER HYPOTHESES OF ACOUSTICAL AEROSOL COAGULATION

A general review of the acoustical aerosol coagulation presented in #3, showed that earlier attempts had been made to define the process itself or its mathematical theory. One need not dwell on the first two attempts to portray the process of acoustical aerosol coagulation, undertaken by Andrade [2] and A. B. Severnyy [109]; it was shown in #12, that the authors' theoretical calculations were based on fictitious effects and, therefore, their concepts were completely unsound. It shall be added only, that if the basis of the acoustical coagulation process rested on some attractional forces which required no difference in the particle dimensions, as assumed by individual present day investigators, the rate of the process would be in the nature of a quadratic function of the numerical particle concentration, which is contrary to experimental results.

The third attempt to portray the process was made by Brandt, Freund, and Hiedemann [167], and was based on correct premises; unfortunately the level of theortical knowledge of aerosol particles behavior in a sound field, available at the time was inadequate to permit the authors to bring their work to the point of finality.

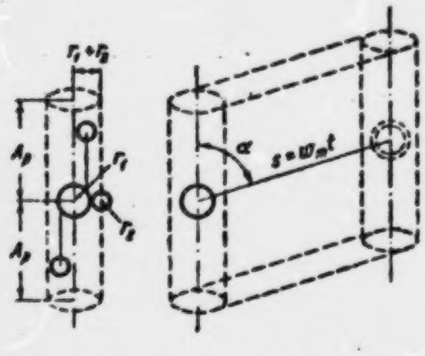

Fig. 54. Diagram of computed orthokinetic interaction between aerosol particles in a sound field according Brandt, Freund Hydeman.

As the base of their scheme, shown in Fig. 54, the authors used the orthokinetic interaction of aerosol particles in conjunction with a given disordered motion which the large particles executed with respect to the small ones. The broken line shows the contours of the aggregating volume of a large, practically non-vibrating particle; clearly, the authors represent it as a cylinder with a radius $r_1 + r_2$ and height $2A_2$. The lateral component of the random motion velocity of a large particle was designated there by ω_m. The total aggregating volume was presented as a rounded off parallelepiped of height equal to double the amplitude of small particle vibrations, and the length to the product $\omega_m t$. The authors' basic concept, that the acoustical aerosol coagulation process hinged on the interaction of unequal particles, is realistic and, as can be seen from #14 , it was used in constructing the general flow diagram of the process.

The fact that the orthokinetic particle interaction was considered by the authors in conjunction with the relative particle motion in the lateral direction deserved still greater approval. In the absence of the lateral motion of large and small particles ($w_s = 0$), the aggregating volume would be limited to a cylinder, as shown by the broken lines at the left of Fig. 54, which would be void of small particles, immediately after the first attempt at their orthokinetic convergence.

However, the diagram shown in Fig. 54, is a very primitive model appropriate only for visual demonstration of aggregating capabilities of the orthokinetic interaction of vibrating particles, taken in conjunction with their lateral motion with respect to each other. Introduction of a random motion of large particles was not well-founded theoretically, and any reference to the visual observation of this type of motion is not very convincing, since no proof was offered that this motion was executed by the large particles alone and not in association with the small particles. The elongated enlarged particles' tracks, seen in photographs (see Fig. 45), and fixed by the increased gravitational and drift forces, were distorted under the effect of turbulent pulsations which almost prevented the particles from converging, and were more apparent for the small particles at close distances.

Some investigators used to associate acoustical aerosol coagulation, partially or completely, with the particle drift in a standing wave. For instance, St. Clair [179, 181], attached great importance to the fact, that due to the radiational drift (the remaining forms of drift were unknown at that time) particle concentrations increased in the direction of an antinode where the vibrating velocities were higher. Using equation (6. 8) to illustrate his concepts the author plotted the distribution of particle concentration with $r = 1\mu$ in the node-antinode intervals of a sound wave for different periods of sonication time at a frequency of 10 khz (see Fig. 55). In addition, the author showed, that due to the occurrence of harmonics an increase of the particle concentration actually greater than shown in Fig. 55 should be achieved. However, the use of equation (6. 8) for the calculation of the finest aerosol particles drift was as shown in #6, absolutely incorrect. In fact, the author's statement pertained only to the case of a standing wave in stationary aerosols. Furthermore, the author's graph showed that even under these conditions the effect indicated by him played a small part. According to the graph, the antinode particle concentration doubled in 21 sec, (which is intolerably long), and trebled in

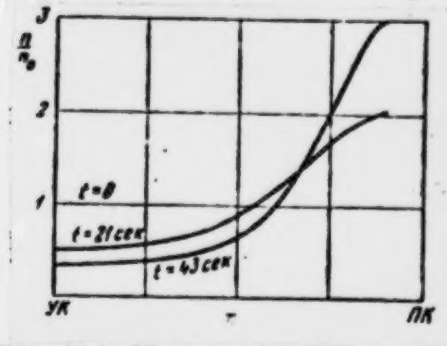

Fig. 55. Concentration distribution of particles of radii $r = 1\,\mu$ $\rho_p = 1$ cm^3) along section UK – PK according to St. Clair($\bar{E}$ 300 erg/cm^3; f = 10 kHz).

42 sec, which is not excessively long for the process of highly dispersed aerosol coagulation. Moreover, if the presence of drift due to the asymmetry of vibrating motion in a standing wave of reverse direction were taken into consideration, then the concentration increase will be smaller than the one shown in the graph.

Jahn [206] attempted to substantiate the advantage of using audio frequencies with the aid of local phenomena as follows: "In a 22 khz ultrasonic field, nodes, at which the dust agglomerated were 0.87 cm apart. In a sonication chamber with a volume of 1 m^3 and a height of 1 m there were 128 nodes with a total surface area of 128 m^2, over which the dust collected and coagulated. If the aerosol volumetric flow velocity through the chamber with a concentration of 8 g/m^2 was approximately 3 m^3/sec, then 24 g of dust will be distributed over a surface of 128 m^2. Under such conditions the resultant agglomerates will be of small sizes. However, if 1.5 khz vibrations were generated in the same chamber, then the distance between nodes for same dust concentrations in a gas, is approximately 12 cm. In such a case, 24 g of dust became distributed over eight nodal planes with a total area of 8 m^2. As a result, considerably larger dust agglomerates will result." This explanation can not be criticized adversely; since low frequencies were also more effective in the case of traveling waves, where local phenomena are absent.

A. D. Bagrinovskii [4] emphasized the orthokinetic interaction of particles in the drift path due to asymmetric vibration movement of the medium in a standing wave. The soundness of this point of view, can be evidenced by determing the maximum number of small particles entrained in the drift path by every large particle. The maximum length of the aggregating cylinder in a standing wave equals the length of the node - antinode interval i.e., λ/4. Now, assume that the entrained particles were small so that their their motion, in the same direction, could be neglected and, consequently, their average concentration could be considered constant along the entire drift path of a large particle.

Consider equations (15.1) and (15.7) for the maximum number of small particles entrained by every large particle and also equations (10.20) and (9.1), and derive the following equation:

$$N_{\text{макс}} = 3\pi r_1^2 \frac{\lambda}{4} n_2 = \frac{(2{,}3 \div 2{,}8)\, c_g h}{\rho_p r_1 f} \cdot 10^{-7}. \qquad (17.1)$$

The minimum time in which a large particle traveled across the node - antinode interval can be computed from the following formula:

$$t_{\text{мин}} = \frac{\lambda}{4V_d} = \frac{c_g}{4fV_d}, \qquad (17.2)$$

where V_d - resultant drift velocity of a large particle.

The preceding formulas used in conjunction with the graph in Fig. 23, yields the following values when f = 5000 hz at $\rho_p = 1$ and $\bar{k} = 10$ g/m^3:

at $r = 0.1\mu$ $N_{max} = 1.6 - 1.9$ in $t_{min} \rightarrow \infty$

at $r = 1\mu$ $N_{max} = 0.16 - 0.19$ in $t_{min} = 2$ min

at $r = 10\mu$ $N_{max} = 0.016 - 0.019$ in $t_{min} = 6.7$ min

It can be seen that even under more favorable conditions a large particle fails to entrain a single small particle in a short time. Admittedly, if it is considered that due to turbulent particle diffusion the entrainment coefficient E is considerably large than E_{min}, the resultant figures are higher by approximately one order of magnitude, however, this likewise fails to offer a satisfactory explanation of the intensive aerosol coagulation in a sound field.

* * *

Some investigators, particularly the ones who conducted aerosol coagulation tests in high-intensity sound fields, favored agitation of the sonicated gaseous medium. The most emphatic statement on the subject was made by Matula, who wrote in his dissertation [232]: "There is no doubt that sound field turbulence played a fundamental role in the aerosol coagulation process." Such conclusion was prompted by experimental findings, whereby a rapid coagulation of aerosols occurred only after the sound intensity attained a sufficiently high level, when the gaseous medium turbulence offered simultaneous relief. These findings were also confirmed by Boucher [156], who found strong similarity in the experimental data on aerosol coagulation in turbulent and acoustical fields, conducted earlier by E. Richardson [257]. Richardson's experiments were conducted in a 1-m^3 chamber, filled with ammonium chloride smoke ($r \approx 1\mu$). Turbulence was generated by a rotary fan, and the sound vibrations by a loudspeaker. The desired coagulation effect was determined from changes in the degree of light beam absorption when passing through the aerosol. Experimental results for the turbulent field are shown in Fig. 56a, where the relative change in the degree of absorption is presented as a function of time for different rates of gas pulsations (smoke concentration by weight - 0.25 g/m^3). Similar results are shown in Fig. 56b, for sound fields of different vibration frequencies (smoke concentration by weight - 0.50 g/m^3, $n = 9.2 \cdot 10^4$).

An even greater similarity in the results of the aerosol coagulation in the turbulent and sound fields was observed in the NIIOGAZ experiments, conducted for the purpose of investigating the dependence of aerosol coagulation rate in a turbulent gas washer (Venturi scrubber) and in an acoustical coagulator on the Reynolds number. In the first case, Reynolds numbers were used which represented progressive and oscillatory streams respectively. It was demonstrated that in both cases the coagulation rate was a linear

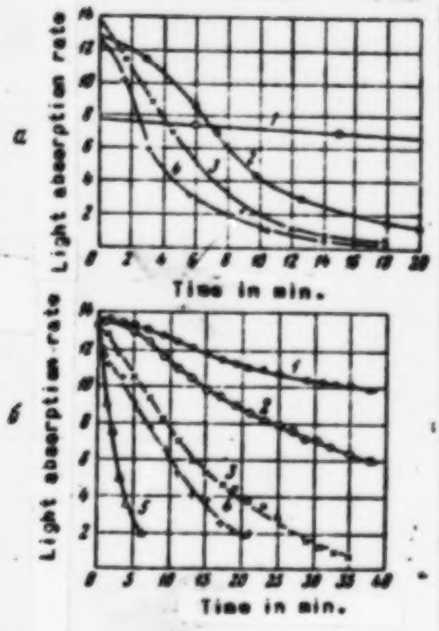

Fig. 56. Effectiveness of ammonium chloride aerosol coagulation according to. E. Richardson.
a – in turbulent field of different pulsation velocities μ' : 1, $\mu' = 0$; 2, $\mu' = 6$ cm/sec; 3, $\mu' = 8$ cm/sec; 4, $\mu' = 12$ cm/sec;
b – in acoustical field (1 – free of sound; 2 – at f = 0.5 kHz and μ_g = 0.5 cm/sec; 3 – f = 2.0 kHz and μ_g = 2 cm/sec; 4 – f = 7.0 kHz and μ_g = 2.0 cm/sec; 5 – f = kHz at static wave)

function of the corresponding Reynolds number, and, also of the gas stream velocity. However, the above similarity studies failed to provide acceptable grounds in support of the assumption that turbulence of a sonicated medium was the fundamental mechanism of acoustical aersol coagulation. These studies could only confirm the fact that in both processes the particle aggregation was initiated by the common orthokinetic mechanism. The only distinction, according to Levich [68, 69] and others [122], was that orthokinetic particle collisions in a turbulent field were due to a difference in the degree of particle entrainment into the turbulent pulsations of the medium, and, in the sound field, they were due to the difference in the degree of their entrainment into the vibrating motion of the medium, which, according to E. Richardson, exemplified a "monochromatic" turbulence of a medium.

Nevertheless, turbulence of the sonicated medium played an important role also in the acoustical aerosol coagulation process, since it offered means for the conveyance of remote particles into the aggregating zone. Any artificial suppression of turbulence degree of a sonicated medium should lead to a reduction in the coagulating effect of acoustical vibrations. This was confirmed by Podoshevnikov's et al experiments [30], which showed that installation of numerous longitudinal partitions in the chamber, which decrease the scale of vortices, brought about a significant decrease (1.8 times) in the effectiveness of aerolsol coagulation (dioctylphthalate vapor). The experimental results are illustrated by Fig. 57, in which parameter K denotes the ratio of the aerosol-scattered light intensity before and after coagulation. It seems that such striking results were possible because the spacings between the partitions were less than the wavelength λ of the primary vortices propagating from the nearby generator field.

Some authors, e.g., White [291] and, Müller [238] were of the opinion that it was necessary to include the electrical forces. However, since the presence of aerosol particles in a sound field did not entail the appearance of charges or dipoles on them, their mention would serve no pertinent purpose. None of the investigators discovered any bearing of the electrical characteristics of particles on the effectiveness of their coagulation in the sound field, which is understandable, since the acoustical aerosol coagulation is undisputably a purely hydrodynamic process.

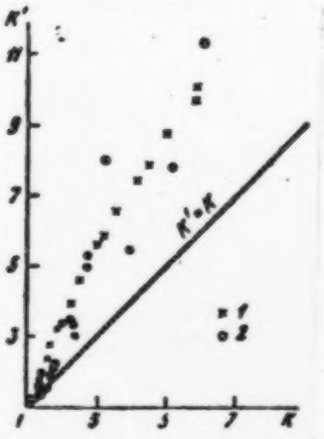

Fig. 57. Effectiveness of acoustical dioctylphthalate fog coagulation following the installation of longitudinal obstructions, according to B. F. Podoshevnikov *et al*.

K – Light intensity ratios in a flue having longitudinal obstructions;

K' – Ditto without the obstructions

k – 1.3 g/m³ and k = 2.5 g/m³

CHAPTER 5

PRACTICE OF ACOUSTICAL COAGULATION AND AEROSOLS PRECIPITATION

18. ACOUSTICAL DISPERSION OF NATURAL AND ARTIFICIAL FOGS

It has been known that natural fogs, formed as a result of spontaneous damp air cooling near the earth's surface, greatly decreased atmospheric transparency. This hampered, or completely excluded, visual communication and human orientation, performance of outdoor work, and general transportation, and particularly air transportation. Despite the use of radar, even at present, the landing of modern aircraft at airports in foggy weather is still risky; civil airports are often closed to incoming aircraft. This circumstance has forced scientists to seek ways of artificially dispersing fogs. The following methods of artificially dispersing supercooled fogs has been tested and used to a limited extent:

1) heating of the surface boundary layer up to a temperature at which the fog droplets evaporated; this so called thermal method of fog dispersion was conducted, for example, in the FIDO dispersal system with J-33, J-47, and other burner types;

2) fog seeding with hygroscopic substances, such as calcium chloride, aluminum sulfate, etc., which absorbed the air moisture and thus created conditions for fog droplets evaporation; this dispersal system, based on Langdon's proposal, was practiced at the San Diego airport in California, USA;

3) fog seeding with highly supercooled crystalline substances such as dry ice, propane, etc., which produced new condensation nuclei for the moisture, and, subsequently, water crystallization;

4) introduction into the fog of special smokes, such as silver iodide, lead iodide, etc., which are ready nuclei for the condensation of moisture and of water crystallization.

The last three methods are different physical-chemical methods of fog dispersion tested also on clouds [120]; they have been used in several countries.

Increase in atmospheric transparency can be achieved using the first two methods by eliminating the air suspended droplets, while on the other hand, in the remaining two methods, this can be achieved by consolidating* them with the aid of moisture condensation and crystallization.

Increase in atmospheric transparency by consolidating the fog droplets is believed to be the result of decrease in light scattering in the system. In natural fogs, the droplet size is usually considerably greater than the wave length of the optical spectrum ($\lambda_{light} = 0.40 - - 0.76\ \mu$), and, therefore, light is scattered here basically according to the law of geometrical optics. In this case, the coefficient of light scattering is given theoretically by the following expression [16]:

$$\alpha_c = \pi r^2 n = \frac{0{,}75 \cdot 10^{-6} k}{\rho_{ж} r}. \qquad (18.1)$$

From this formula it follows that the greater the weight concentration of the droplets and the smaller their radii, the greater will be the light scattering by the fog.

For more thinly dispersed fogs in which the geometrical scattering yields at first to diffusional and later so called, Rayleigh scattering, a factor is introduced into formula (18.1) which depended on the droplet radius and the radiation wavelength. In the critical case when $r \ll \lambda_{light}$, the light scattering coefficient is propotional to the product $kr^3/\lambda^4_{\text{light}}$, i.e., a direct inverse dependence of light scattering on droplet size is observed. The intensity of the radiative flux passing through the fog diminished with distance just as the intensity of sound, i.e., according to the following exponential law;

---

* In view of this, the definition of artificial fog and cloud dispersion methods for the elimination of fog droplets as given by many authors (see, for example BSE, v. 30, pg. 314) is inexact. Indeed, artificial fog dispersion is not intended to eliminate the droplets as such, but only to decrease their scattering ability, which can be achieved both by eliminating as well as consolidating the droplets.

$$J_c = J_{c_0} e^{-k_c x}, \tag{18.2}$$

where k_{light} - attemuation coefficient equals to $k_{\text{light}} = \alpha_{\text{light}}\,\beta_{\text{light}} \approx \alpha_{\text{light}}$ (β_{light} -- absorption coefficient whose magnitude in fogs can be ignored.)

The increase in atmospheric visability during fog dispersion, recorded in experiments photoelectrically, is characterized by a relative decrease in the light scattering coefficient $\Delta\alpha_{lt}/\alpha_{ot}$ in %, which is equivalent to a relative increase in the distance at which the former light intensity $\Delta X/X \cdot 100\%$ is maintained. Practice has shown that existing fog scattering methods possessed significant disadvantages which severely limited their use. Thus, the thermal method required unusually considerable heat which, to a great degree was due to the fact that while heating the atmospheric surface boundary layer, strong convective flows were generated which drew in masses of cold air. The method of fog dispersion by seeding with hygroscopic substances required very large amounts of these substances. Thus, about 25 g of calcium chloride was required per cubic meter of fog; moreover, overseeding induced a reverse phenomenon - a decrease in atmospheric transparency. Other fog dispersion methods also have shortcomings.

Discovery of sound intensifying effect on aerosol coagulation and also on the process of droplet evaporation raised new hope for the solution of fog dispersion problems. At first, it was proposed to limit efforts to the simple sonication of natural fogs for the coagulation of droplets, leading, as in the case of condensation, to their consolidation and, thereby, to a decrease in the degree of light scattering by the fog. This method was called the acoustical fog dispersion method. It was first proposed by Amy in 1931, and was registered under US Patent No. 1980171 in 1934. The author proposed fog dispersing by sonicating them with a huge sound generator moving along an airfield or other area, and according to the author, instantly, coagulating and cooling the fog droplets entering the sound beam. The sound generator described in Amy's patent consisted of an assembly of Hartman ultrasonic whistles mounted on a common panel which turned in all directions like a military searchlight.

This project, however, was not exploited in practice in the USA, evidently due to the absence of corresponding laboratory work to support the proposed principles. However, as Brandt [156] recently reported in a private talk in Germany, experimental tests in natural fog dispersion has been conducted in 1940 using Hartman ultrasonic whistles with a central core (a sevory? * whistle). A noticeable "bleaching" was observed at a radius of about 10 m a-

---

*Sp. not certain.

round the sound source. In 1943 -- 1944 La Mer and Sinclair [156] of the USA, conducted detailed acoustical method dispersal tests. The authors first conducted laboratory experiments on dispersion of artificial fogs created with an atomizer at Columbia University. The average droplet radius was 4μ, the concentration by weight 14 g/m^3 which is greater than the droplet concentration in natural fogs (0.2 -- 1 g/m^3). The experiments, conducted in a vertical tube of 150 mm diameter and about 1 m long with a loudspeaker operating on 0.5 khz frequency showed that at a mean sound intensity of 150 db, the sonicated volume was cleared with a standing wave in less than 15 sec. Experiments conducted in a horizontal tube of 75 mm diameter and a 3.6 m length using the same sound source showed that fog sonication in a state of flow also had a positive effect. Thus, at a flow rate in the order of 0.5 m/sec, with a corresponding sonication time of 70 sec., visibility in the fog rose by 30%. A similar type of laboratory experiment was subsequently conducted by the U. S. Ultrasonics Corporation, Taraba in Czechoslovakia, and others.

Experiments conducted by the U.S. Ultrasonics Corporation in 1948 were conducted in a 7400 cm^3 rectangular glass vessel equipped at the bottom with a U-1 type dynamic siren operating in the 1 -- 6 khz range. The siren was separated from the vessel by a thin rubber diaphragm about 25μ thick. The mean fog droplet radius was 2μ, and the weight concentration was about 4.5 g/m^3. As in all experiments on fog dispersion, control was accomplished by varying the brightness of a thin light beam passing through the aerosol and picked up by a photoelectric cell. Experimental results are shown in Fig. 50. From the figure it is seen that the optimal oscillation frequency was 3.5 khz; moreover, this did not account as Boucher indicated [156], for the fact that the power radiated by the siren fell at high frequencies. To achieve a 50% "bleaching" of the fog, 1 to 20 sec are needed, depending upon the sound intensity (137 -- 152 db).

Taraba [156*, 274] conducted experiments on artificial fog dispersion in a horizontal tube of 400 mm diameter and a 4.5 m length, equipped with a dynamic siren with a maximal power of about 11 kw. Two dust extractors, connected in parallel, were mounted aft of the tube to pick up the coagulated droplets. The fog droplet concentration by weight was 5 -- 10 g/m^3 and droplet size was not controlled. The fog was drawn in at the rate of 0.9 m/sec. Oscillation frequency varied between 4 -- 17 khz. It was possible to disperse and to collect up to 99% of the coagulated fog droplets, within a few seconds.

La Mer and Sinclair extended their experiments on artificial fog dispersion to large spaces, such as a tunnel and at the Columbia University swimming pool [156, 266]. The tunnel had a 1.2 x 2.1 cross section and a length of about 30 m. The fog was produced by a battery of 12 atomizers. The mean droplet radius was 4.5μ and the concentration by weight -3 -- 6 g/m^3. The light source was located at the midpoint of the tunnel at a height of 0.6 m from the floor. Observations were conducted from outside the tunnel through a glass window in a door at one end. The 120-w HOR-type siren operated at a frequency of 0.6 -- 0.7 khz and was located between the observer and the light source. With an intensity of sound near the siren in the order of 137 db, in one case a 75% improvement in visibility was observed, and in another case an improvement of 50%. The experiments in the swimming pool of more than 5600 m^3 capacity were fruitless. A dynamic siren of the US Federal Electric Company with a rated power of 2.4 kw was used in the experiments. At a 0.7 khz frequency no signs of fog dispersion were noticed, which is explained by the large fog dispersiveness ($r_s \sim 1\mu$); all the fog particles at the chosen frequency were completely entrained into the oscillatory motion of the medium and did not coagulate with one another (see #16.)

---

*Does not correspond to author [Tr]

Experiments on a similar scale were conducted by Boucher in France (Chatillon, 1956) [156]. The dimensions of the experimental chamber were 12.8 x 14 x 18 m. The sound source was the author's static "multiwhistle" siren system suspended from the chamber ceiling. Two types of fog underwent sonication; coarse-particle, similar to natural fog (radius $r = 2$ -- 10μ, concentration 1 -- 2 g/m^3), and fine-particle (radius $r_s = 0.5\mu$, concentration 1 -- 2 g/m^3). The siren operated on two frequencies: 9.5 and 32 -- 33 khz. The coarse-particle fog dispersed well (2 min) at the low frequency (9.5 khz); under high frequency sonication (32 -- 33 khz), no results had been noted even at a considerably greater power (600 w). On the other hand, the fine-particle fog dispersed well at the high frequency (32 -- 33 khz) and showed a negative effect at the low frequency (9.5 khz). This was in complete agreement with the conclusions arrived at regarding the dependence of optimal oscillation frequency on the degree of particle size as described in #16. Under a 1943 US Air Force contract, La Mer and Sinclair tested the acoustical fog dispersal method under field conditions [156, 266]. The best known tests were conducted at Lankin airfield (Cincinnati, Ohio) in March 1943. The natural fog consisted of droplets with a radius of 4 -- 16μ (mostly 6μ) of 1 g/m^3 concentration. The atmosphere was still. Four dynamic "Victory" sirens of the Chrysler-Bell Corporation, each of 35 kw, were used for the fog sonication. These tests are illustrated diagrammatically in Fig. 58. The sirens sonicated in an area more than 120 m long, 23 m wide, and about 15 m high. Results of the tests established that fog clearing began within 1 min and increased atmospheric visibility from 65 to 130 m.

In December 1943, La Mer, et al tested the acoustical fog dispersion method over the open sea near Sandburg, California. Fog droplet radius was 5μ. Eight Chrysler-Bell Corp. sirens of 35 kw each, were used, placed 30 m apart along 210 m long line at 10 -- 15° of the prevailing wind direction. The wind velocity reached 5 -- 6 m/sec. Despite unfavorable conditions, a 50% fog bleaching was achieved. However, it was felt that in windy weather the radiated acoustical power was insufficient, and the method could barely be used. The U.S. Ultrasonics Corp. repeated the natural fog dispersion tests in 1946,

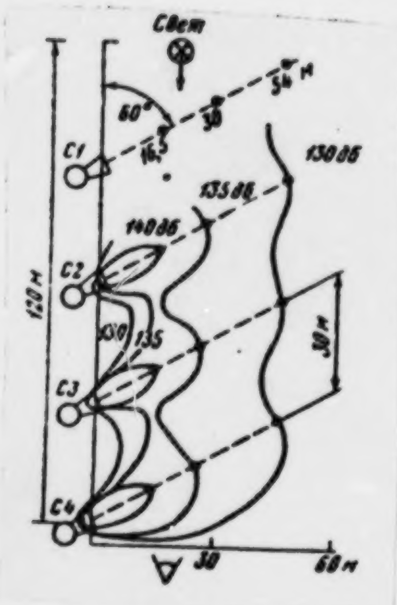

Fig. 58. Diagrammatic presentation of test conducted for the dispersion of fog at Lunken, USA aerodrome

using powerful U2 dynamic sirens and other types. Tests were conducted at first, in an open area near Arcata, and later near Bracey Grove. However, both attempts were unsuccessful. The fog had very coarse particles (mean radius 15μ), and at the frequency used (3.5 -- 4 khz), it did not coagulate, since it was not entrained in the oscillatory motion of the medium. Recently, fog dispersion experiments had been conducted in Denmark (Ingeniøren, 1959, 4).

Combined data of all different acoustical fog dispersion tests are summarized in Table 16. The general conclusions were as follows:

1). Coagulation, and resulting "bleaching" of artificial and natural fogs required some time. Even in small volumes and at high level sound the sonication time was at best several seconds; the required sonication time was 1 min or more for large volumes;

2). Appropriate choice of frequencies was of great importance for the effectiveness of acoustical fog dispersion. Coarse particle fogs required low sound frequencies, while fine-particle fogs required higher sound frequencies which usually did not exceed 0.5 -- 0.7 khz for natural fogs;

3). Sound damping in open spaces is considered limiting the distance of effective natural fog dispersion to 25 -- 30 m in the direction of the sound beam. Therefore, many sound sirens are required for large space sonication;

4). The last conclusion indicates that energy consumption in acoustical fog dispersion was rather high, although it did not exceed the energy consumed by the thermal fog dispersal method.

The unpleasant impact of sirens on the human ear constituted no impediment to the use of the method, due to the fact that beyond the limits of the dispersion zone the sound rapidly abated to the usual airfield level. However, many disadvantages of the acoustical fog dispersion method hampered its use under airport conditions, and attempts had been made to solve the problem by the process of intensified droplet evaporation (see Appendix 1).

Where tests were conducted	Average radius r, μ	Gravimetric concn. g/cm^3	Characteristics of purified volume
LABORATORY TESTS*			
Vertical flue Ø 150 x 1000 mm, Columbia Univ., US A	4	14	Nonmigrating mass, static waves
Horizontal flue Ø 75 x 3600 mm, Columbia Univ., USA	4	14	Continuous flow at the rate of 5 cm/sec
Right-angle chamber $7400\ cm^3$, Ultrasonic Corp., USA	2	4.5	Nonmigrating mass, static waves
Horizontal flue Ø 400 x 450 mm. No cyclone. Czechoslovakia	–	5–10	Continuous flow at 0.9 m/sec.
CHAMBER TESTS*			
Tunnel 1.2x2.1x30 m Columbia Univ., USA	4.5	3–6	$94\ m^3$; continuous flow; static waves
Swimming pool location, Columbia Univ. USA	1	–	$5600\ m^3$; nonmigrating mass
Experimental chamber 12.8x14x18 m. Chatillion, France	2–10 (predominating)	1–2	$400\ m^3$. continuous flow, static waves
Ditto	0,5	1–2	$100\ m^3$
"	2–10 (predominating)	1–2	$2600\ M^3$, static mass, unstable waves
"	0,5	1–2	$2600\ m^3$
NATURAL TESTS			
Lunken Aeroport, Cincinnati, Ohio, USA	4–16 (predominating)	1–2	$5100\ m^3$; quiet atmosphere; running waves
Open sea, Sandberg, Calif., USA	5	1	$100\ 000\ m^3$; wind 5–6 m/sec.
Open space near Acata and Bace Grove, USA	15	1	Running and stationary waves
Open space at Mining Height, Czechoslovakia	5	1	Still air; running waves
Elbrus High mountain Complex Expedition, AN, USSR Baxan Kenyon (See Paragr. 19)	–	–	Rain clouds; running waves.

*All artificial fogs were obtained by means of water spray vapor'n.

Table 15

Source and intensity of sound	Oscillation frequency kHz	Specific force bm/m^3, gas force	Dispersion time	Studies in the year of
Loud speaker (150 db)	0.5	–	15 sec	LaMair and Sinclair, 1943 (156,266)
Ditto	0.5	–	15 sec	Ditto (156)
Dynamic siren (132–137 db)	3.5	Several kvt/m^3	1–20 sec (See Fig. 50)	Horseley, and Sivi, 1948 (156)
Dynamic siren (11 kvt)	4–17	–	A few sec (90% sirens	Taraba 1956–1957 (156,274)
Dynamic siren (120 vt)	06,07	1,2	1 min. (brighten-up 50%)	LaMair and Sinclair, 1943 (156,266)
Dynamic siren (2.4 kvt)	0,7	–	No results	Ditto
Static siren (60–100 vt)	9,5	0,15	2 min	Boucher, 1956–1957 (156)
Static siren (60–100 vt)	32–33	4	2 min	Ditto
Static siren (60 vt)	9,6	0,02	15 min	"
Static siren (400 vt)	32–33	0,15	15 min	"
Four dynamic (35 kvt sirens)	0,44	2,35	1 min	LaMair and Sinclair, 1943 (156,266)
Eight dynamic 35 kvt. sirens)	0,44	–	slow clearing up to 50%	LaMair, Sinclair and Breishiz, 1943, 1944 (158)
Dynamic siren	3,5–4,0	–	No results	Ultrasonic Corp., U.S.A. 1946, (156)
Dynamic siren (11 kvt)	4–17	–	Undetermined	Taraba (Komsomol'skaya Pravda) 8 May 1957
Twenty-five kvt dynamic sirens	< 0.3	–	–	GeoPhILAN, USSR, 1960 (32)

19. ACOUSTO-GRAVITATIONAL PRECIPITATION OF INDUSTRIAL DUSTS, SMOKES, AND FOGS

Some industrial dusts and fogs contain very coarse particles, the precipitation of which from the air or gaseous medium for economic or sanitary hygienic reasons was usually attained through their own natural gravitational falling out process. On the other hand, some industrial smokes and fogs consist of highly dispersed particles, which under the effects of high pressure and temperature exploded easily, or they became highly adhesive, or highly reactive. In many cases the use of the highly effective precipitation devices as electrostatic precipitators or fabric dust catchers must be excluded, and only the gravitational precipitation of the aerosol particles should be applied. The gravitational precipitation rate of spherical particles, also referred to as "particle hovering" rate, is determined by the following known formula [11]:

$$V_g = \tau g = 2/9\ g\ p_p/\varkappa\ r^2 \tag{19.1}$$

which can be easily derived by equating the expression for the forces of particle gravity with the formula expressing the forces of the medium's resistance determined by the Stokes' formula.

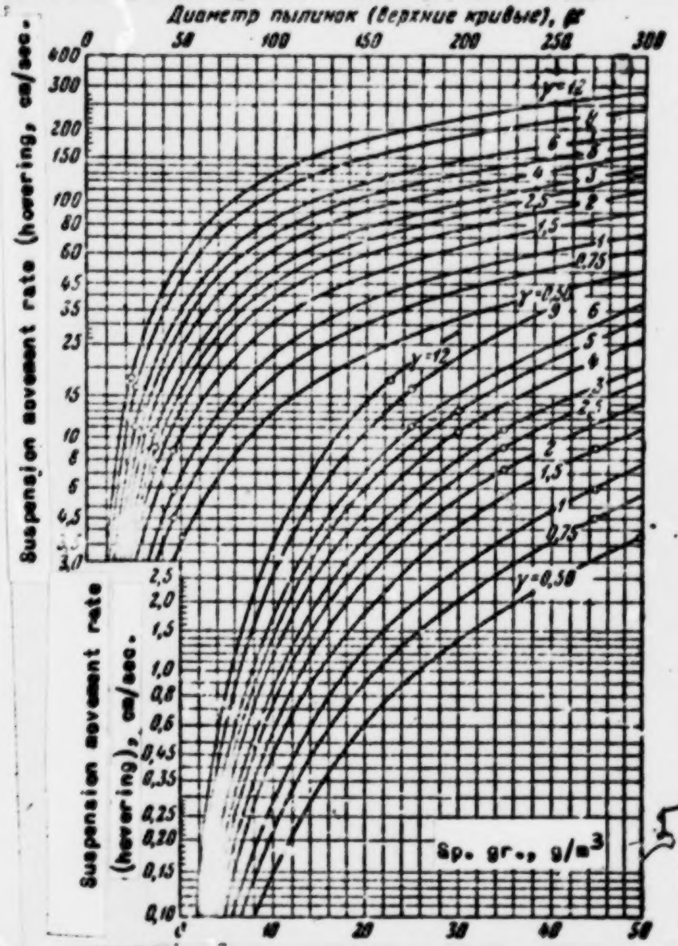

Fig. 59. Gravity settling rate of suspended spheroid particles

Figure 59 illustrates the values computed from equation (19.1) of gravitational precipitation rate as a ratio between the particle radius at different particle densities [119]. It may be concluded from the graph that the absolute magnitude of gravitational particle precipitation rate was sufficiently great only at particle radii greater than 25 -- 50μ. Finer particles, contained in all industrial aerosols to some degree, precipitated extremely slowly. This property has led investigators to sonicate precipitation chambers for the coagulation of high dispersion fractions for the purposes of increasing the rate of their gravitational precipitation.

The earliest experiments with acousto-gravitational industrial dust precipitation were conducted in 1950 by Tarnoczy and Greguss [275], who sonicated the gas ducts of an annealing cement furnace to increase the amount of the precipitated cement dust. This type of aerosol consisted of very coarse dust particles; the particle radii ranged from 5 -- 100μ and greater (15 -- 25μ particles predominate). A standard Hartman whistle mounted in a parabolic reflector was used as the source of sound in these experiments. Experimental results are listed in Table 17 and show that under sonication, dust precipitaion in the stove gas ducts was 1.6 -- 7.1 times greater than in simple gravitational deposition. However, these doubtlessly favorable results could be achieved by a simpler and more economical method, namely, by installing standard dust extractors aft of the gas ducts, which considerably reduced the residual dust concentration in the discharged gases.

Table 17

Place of particles settling	Oscillation frequency kHz	Dust collection plant	Collected dust amount		Increase in preciptd. dust amnt.
			Free from sound effect	During sound treatment	
First gas flow	4,6	Door No. 3	4	28,4	7,1
Second " "	1,2	Lower door	43	70,3	1,6
" "	3,0	» »	43	145,0	3,4
First " "	3,0	Door No. 1	2,00	5,75	
		» № 2	2,75	5,00	
		» № 3	3.50	2.40	
			8,25	13,15	1,6
» »	3,0	» № 1	2,00	7,50	
		» № 2	2,75	12,00	
		» № 3	3.50	2.30	
			8,25	21,80	2,7
» »	4,6 (Generator slanted downward)	» № 1	4,20	18,00	
		» № 2	5,60	12,00	
		» № 3	16,50	137,00	
			26,30	167,00	6,3
» »	5,5	» № 1	3,00	7,85	
		» № 2	3,80	2,75	
		» № 3	0,80	10,75	
			7,60	21,35	2,8
» »	3,9	» № 1	[illegible]	4,20	
		» № 2	[illegible]	2,90	
		» № 3	[illegible]	4,90	
			7,60	12,00	1,6
» »	4.0 (Generator slanted downward)	» № 1	3,00	10,30	
		» № 2	3,80	4,80	
		» № 3	0,80	4,40	
			7,60	19,50	2,6

Extensive experiments had been conducted in the Soviet Union on the Acousto-gravitational precipitation of boring dust formed during mining. P. Sh. Shkol'nikova [130, 131, 132] performed this type of experiment at the Leningrad "Gipronikel'" Institute. Laboratory acousto-gravitational precipitation of boring experiments with dust were conducted under static conditions in a 0.45 - m dust chamber. The dust generated by boring copperpyrite ore in the Urals contained up to 40% free silicon dioxide; it had the following particle composition: particle radius r = 2.5μ, 56.8%; r = 2.5 -- 5.0μ, 19.8%; r = 5 -- 26μ, 33.4%. Experiments lasted up to 60 min. Microscopic dust particle fraction concentrations were determined with SN-2 type counter, and the submicroscopic particles with a counter designed by Ye. A. Vigdorchik. The sound intensity generated by the Hartman whistle was about 0.1 w/cm^2. Experiments established that calculated dust particle concentrations decreased to 50 - 35% of the original due to sonication. The most favorable frequency was 7 khz; other frequencies -- 10 and 13.8 khz - yielded poorer results.

Laboratory experiments on the acousto-gravitational boring dust precipitation under dynamic conditions were conducted with a dust of the following particle profile: r = 0.5 - 2.5μ, 46.9%; r = 2.5 - 26μ, 10.5%, and r = 26 - 150μ, 42.7%. The gravimetric dust concentration ranged mainly between 66 to 1189 g/m^3. The air flow velocity varied from 0.004 to 0.016 m^3/sec. The following results were obtained during sonication:

at $\bar{k}_{in}$ = 66 g/m^3 $\bar{k}_{out}$ = 39.1 g/m^3 n_{precip} = 99.29%

at $\bar{k}_{in}$ = 453 g/m^3 $\bar{k}_{out}$ = 41.3 g/m^3 n_{precip} = 99.82%

at $\bar{k}_{in}$ = 753 g/m^3 $\bar{k}_{out}$ = 21.3 g/m^3 n_{precip} = 99.93%

Clearly, the degree of precipitation was high; however, the residue concentration, although about five times lower than without sonication, greatly exceeded standard sanitary MAC for dust in the air (10 mg/m^3). Research conducted under working conditions in the "III International" mine showed a 99.8% dust precipitation; however, the residual concentration reached $\bar{k}_{out}$ = 115.4 mg/m^3, which was considerably above the adopted standard MAC.

The experiments led investigators to conclude that acousto-inertial precipitation of boring and other mineral dusts may be used only in conjunction with subsequent filtration of the gas. After installation of a glass-wool filter with strands up to 40μ in diameter at a filter diameter of 190 mm and a height of 50 mm, pressure drop 40 - 50 mm hg, they succeeded in lowering the residual concentration to 2 - 6 mg/m^3.

In this case, the dust load on the filter was decreased considerably which resulted in an increased filtration rate, thereby, compensating for the cost in energy consumed by the sonication. This type of process combination represented a transitional stage in the acousto-inertial precipitation of aerosols examined in the next paragraph. Studies in boring dust precipitation are being conducted by this method at "Gipronikel'" [300].

It can be concluded from results of the described experiments that purely acousto-gravitational precipitation of industrial dusts, smokes, and fogs were acceptable and promising, in cases in which the gas volume to be purified was several hundred cubic meters per hour or less, or when the precipitated products were of special economic worth, or, the use of other precipitation methods were not feasible. Such cases occurred in modern industry, characterized by a great variety of conditions and demands, as for example, in the production of phthalic anhydride [88] and other similar substances.

If the volume of gas to be processed was not large, then the absolute magnitude of the energy consumed in the precipitation of products was small even when low-efficiency pneumatic sound radiators were used, and in the case of separation, precipitates from the volume of gas being sonicated by a dividing diaphragm which prevented gas rarefaction by the siren air. Neither a high gas temperature or pressure, nor explosion danger, or great reactivity of the dispersed phase in this case, constituted obstacles to the use of the acousto-gravitational aerosol precipitation method. This is a rare and significant quality which had no precedent in dust-droplet entrainment technology.

Promising possibilities are ahead for acousto-gravitational and acousto-inertial aerosol precipitation methods in separating condensates from by-product and natural gases. These gases have a high surplus pressure (100 - 200 atm) [112], part of which could be used for the generation of acoustical oscillations without loss in production efficiency. Therefore, the problem of the energy consumed in sonication is not important in this case. In the gaseous state are found not only light hydrocarbons, such as, methane and ethane, but even heavy hydrocarbons boiling at temperatures up to 300 - 400° C. The amount of such hydrocarbons has been estimated as up to 4 - 5% and higher.

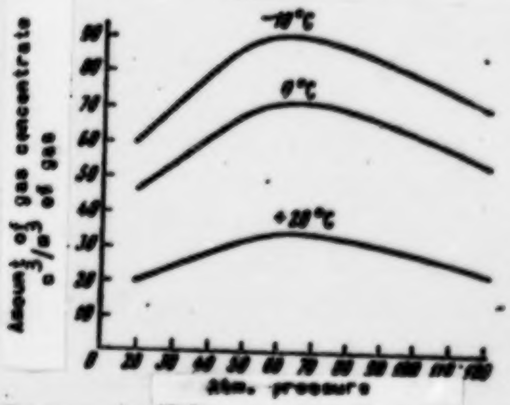

Fig. 60. Condensate content in the gas as a function of pressure at different throttling temperatures (Leningrad point of origin, Krasnodarsk region.)

Due to the drop in gas pressure and temperature during its travel along the borehole shaft, the gas contained a considerable amount of condensed heavy hydrocarbon and moisture - a "film" condensate. The entrainment of this condensate presented no particular problem. However, in avoiding the deposition of condensates and gaseous hydrates during subsequent transportation through gas ducts, the gas can be additionally throttled at the source, thereby sharply lowering the gas pressure (Joule-Thompson effect) and an additional condensation of hydrocarbon and moisture occurred, changing into fog, which immediately precipitated through gravity into residual, so called, "volume separators."

The condensation isotherms of natural gases, called reverse or retrograde condensations, are of the form shown in Fig. 60. The pressure at which the greatest number of hydrocarbons changed into a condensate has been referred to as the maximum condensation pressure, and is usually from 55 - 70 at gage. Due to the high degree of supersaturation at this pressure, it condensed into a fog in some cases up to 100 - 200 g per normal cubic meter of gas; when calculated in physical cubic meters at a pressure of 55 - 70 at gage, it yielded a value of the order of 5.5 - 14 kg/m³. Under such conditions the condensation process, isothermal distillation and hydrocarbon coagulation occurred very intensively (see Appendix I). However, to obtain a droplet consolidation up to the dimensions where the gravitational method of precipitation becomes effective ($r > 35$ to 50μ), the gas must remain in the separator for not less than 15 sec, which is a considerable length of time.

In order to intensify the condensation, distillation, and coagulation processes of the condensing hydrocarbons and moisture in the gas being throttled and to increase thereby the permeability and the entrainment ability of the separating unit, it was proposed that acoustical oscillation be used [80]. In contrast to the existing method, in which the natural gas is throttled by a standard cylindrical attachment ("sleeve") mounted in front of the separator, it was suggested [79] that the gas be throttled inside the separator with a special sleeve-whistle mounted in it (Fig. 61a)

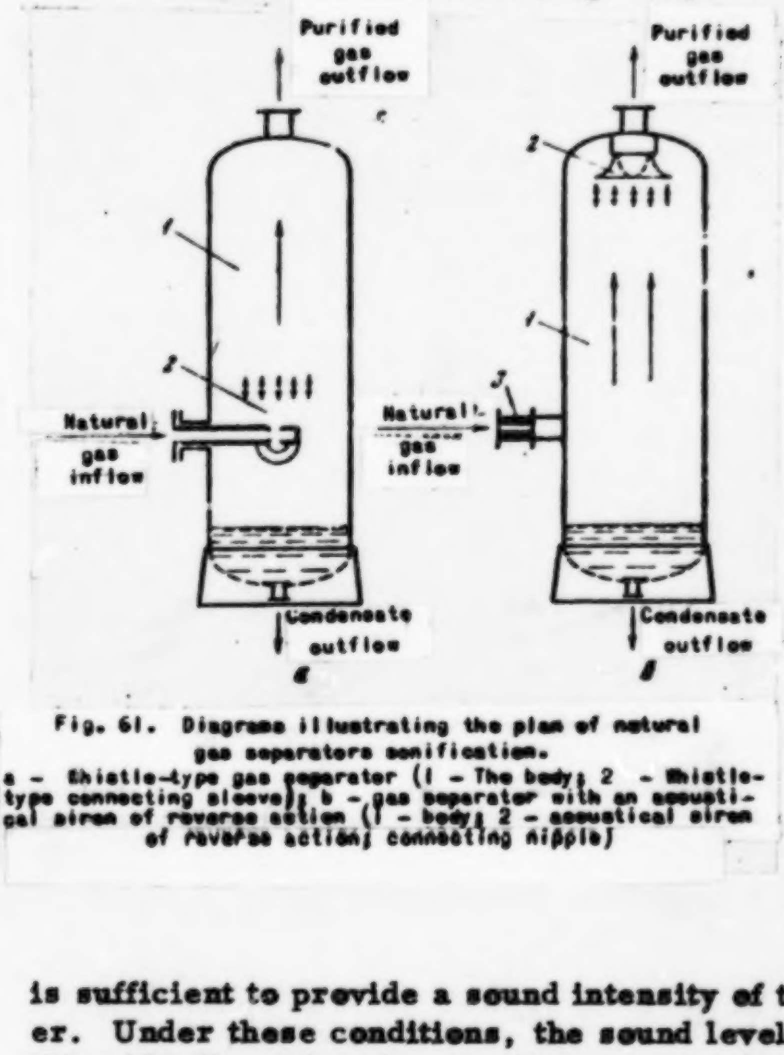

Fig. 61. Diagrams illustrating the plan of natural gas separators sonification.
a - Whistle-type gas separator (1 - The body; 2 - Whistle-type connecting sleeve); b - gas separator with an acoustical siren of reverse action (1 - body; 2 - acoustical siren of reverse action; connecting nipple)

In the presence of a large pressure drop and increase in the gas density, any predetermined acoustical intensity of up to 10 kw and higher may be obtained with a sleeve-whistle, which is also convenient, since the compressed gases had an increased acoustical resistance $p_g c_g$, caused essentially by an increase in gas density p_g, resulting in a decrease in the oscillatory gas velocity u_g [see equation (1.9)]. It is possible to maintain the oscillation velocity at the normal level only by correspondingly raising the sound intensity, as compared with its use under atmospheric conditions. Taking into account the small dimentions of the space being sonicated, and the increase in droplet concentration in the gas separators, for effective intensification of the process taking place in them, it is sufficient to provide a sound intensity of the order of 0.5 - 1.0 w/cm² or lower. Under these conditions, the sound level close to the separator wall reached 125 - 130 db, although, at a distance of 5-10m, it falls to permissible levels.*

---

*The permissible noise level depends on the frequency of the highest component of the sound spectrum f_0 and according to the adopted norms [110] has the following values:

Frequency	Permissible sound level L, db	Frequency	Permissible sound level L, db
350	90	3000-4000	70
800	85	5000	75
1600	80	6000	80
2000	75	10,000	85

In the second version of the sound-equipped gas separator (Fig. 61b, page 152), gas throttling is done by the usual method, while its self-sonication is done separately with a static siren mounted at the separator inlet; the gas discharged from the separator enters into the siren mouth. It can be shown that with reverse feeding of the siren, radiation of acoustical oscillations occurred in the usual proportion and direction, i.e., to the side of the widening of the mouth (the siren's radiation element is a pulsating gas jet which is an acoustical dipole radiating sound mainly in the direction of the mouth). As the experiment indicated, sonication of the gas caused the permeability of the gas separator to increase several times. However, in view of the strong turbination of the gas which develops because of this, thereby interferring with the droplets fall-out, it is more apropos that their precipitation be transferred to a separate settling chamber, or a direct-flow dust extractor, having lowered, at the same time, the frequency of the generated oscillations to the minimum.

Another variant of the sonication of gas separators was tested at the Korobkovskii deposits in the Volgograd oblast' [86]. A turbodynamic siren was used as a sound source; it was mounted between the flanges of the separator inlet pipe. The oscillation frequency was, according to the researchers, 6 khz (according to our calculation this figure was ten times overestimated!). The sound intensity remained constant; it was known only that the pressure drop used up in the rotation of the siren, the generation of sound, and the hydrodynamic losses were 1.5 - 2.0 atm. Tests were conducted in two separators for the by-product and for the natural gases, at a pressure of 10 at the gage. In the first case, the moisture content and condensate at the separator output were 0.2 and 0.1 cm^3/nm^3, respectively. Due to the sonication the remaining moisture content decreased by one half and the condensate, by 17 times. In the second case, the amount of condensate entrained in the separator increased from 19.5 to 25.6 cm^3/nm^3, i.e., by 30%.

Due to moisture in the gas, gaseous hydrate crystals were formed inside the separator in addition to condensate droplets, and massive gaseous hydrate growths developed on its walls hindering further normal use of the gas separator. To prevent the formation of hydrates on the gas separator walls and also to pre-stabilize and preheat the entrained condensate, the construction of a self-heating sound-equipped gas separator was proposed [84] in which the disadvantages of the separating devices noted above were eliminated (Fig. 62). The vortical whistle-tube 2 differed from the vortical whistle described in #2 by the fact that its internal chamber BK was somewhat more developed and equipped at its back end with an additional annular outlet, a regulating valve PK, as a Rank tube. Due to this, the gas eddy simultaneously excited the acoustical gas oscillations and separated the gas into cold and hot streams. The cold sonicated stream discharged from the upper opening OKhG, while the hot gas stream (10-20%) came from the lower end of the chamber through a reduction valve, it flowed under the hood, heated it and the space under it, came out into the annular space between the hood and wall in the form of a heat

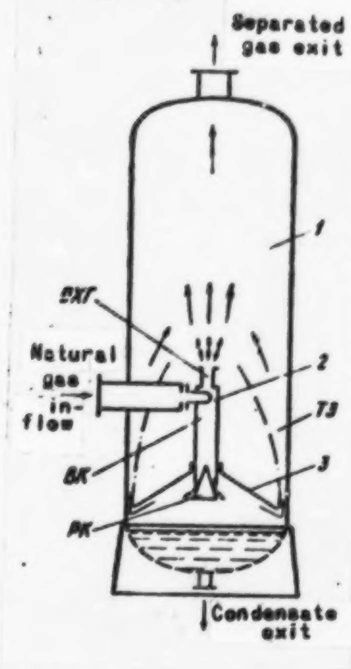

Fig. 62 - Schematic presentation of an automatically heating natural gas separator.
1 - Body; 2 - a whirle-type pipe wgustkel 3 - an umbrella hood; BK - whirle chamber of the pipe-type whistle; OXT - exit of sonified cold gas; PX - reducing valve of hot gas; TZ - a heated screen.

screen TZ, heating the wall and preventing the formation of gas hydrate growths on it. Rising still higher, the hot gas, which contained the main body of the condensing hydrocarbons, mixed with the sonicated cold stream coming from the whistle. The condensate droplets and the gaseous hydrate crystals precipitated on the heated hood, where the crystals melted, and the lighter hydrocarbons dissolved in the condensate, evaporated and left the separator with the gas.

In the above vertical gas separator, the need for constructing heating coils and insulation in the boiler device was eliminated in the above vertical gas separator. However, the fact could not be ruled out that the turbulization of the sonicated gas arrested precipitation of droplets also in this case, this being the case, another solution to the self-heating idea has to be found.

Original experiments in the acousto-gravitational precipitation of aerosols were recently carried out in Czechoslovakia by Slavik and Geyd [24]. The investigators tried to test the coagulating properties of sound for combating harmful gaseous impurities. For this purpose they proposed to introduce into the gas corresponding gaseous reagents, which, after chemically uniting with the harmful gas impurities, formed suspended solid or liquid particles. If, for instance, SO_3 was to be removed from the atmosphere, ammonia (NH_3) could be introduced as a reagent. In the presence of moisture, SO_3 might react with NH_3 in the following way:

$$SO_3 + H_2O + 2NH_3 = (NH_4)_2SO_3$$

forming a suspended ammonium sulfate solid.

The above method for the removal of SO_3 from the atmosphere was tested in a foundry casting the light alloy Electron. Upon completion of pouring, the mold was covered with a hood on which four Hartman whistles were mounted in series and were operating at a frequency of 8 - 11 khz. Small containers with ammonia were placed under the whistles. After several minutes the asphyxiating gas was eliminated from the mold and no longer poisoned the foundry atmosphere.

In conclusion, mention should be made of the experiments using the coagulating effect of sound for the artificial precipitation of clouds for the purposes of rainmaking, which are of definite interest to meteorologists and agricultural workers. The radius of the cloud water droplets varied over a wide range of 1 - 2 to 70 - 100 μ, with a mean radius of 10 - 20 μ [120]. Experiments with the artificial rain generation by sound were conducted by members of the El'brus Alpine Expedition of the Academy of Sciences USSR [32]. Powerful low-frequency acoustical sirens were installed on the slope of the Baksanskii Pass mountains. The radiated power of each siren was about 25 kw. Each siren was equipped with a mouth having an outlet cross section of up to 9 m^2. The sirens were directed toward rain clouds hanging above the pass. Under the effect of the sound the cloud droplets consolidated resulting in a rain.

20. ACOUSTO-INERTIAL PRECIPITATION OF INDUSTRIAL DUSTS, SMOKES, AND FOGS

The acousto-inertial method of aerosol precipitation differs from the acousto-gravitational method examined in the previous paragraphs; the precipitation process of coagulated particles operates in a separate inertial precipitator which is incomparably more effective than the sump; this precipitator is usually a cyclone. The precipitation rate of spherical particles under the effect of inertial forces developes in a cyclone with an inner curvature radius R and is determined by formula [121]:

$$V_c = \frac{w_t^2 \tau}{R} = \frac{2}{9} \frac{\rho_p}{\eta} \frac{w_t^2}{R} r^2, \qquad (20.1)$$

where w_t -- tangential velocity of the aerosol motion. The ratio of inertial particle precipitation rate to the rate of gravitational particle precipitation, determined by expression (19.1), is equal to:

$$\frac{V_c}{V_g} = \frac{w_t^2}{R}. \qquad (20.2)$$

Usually w_t = 15 - 25 m/sec, and R = 0.1 -- 1.0 m; thus, it is seen that the rate of inertial particle precipitation is 25-600 times greater than the rate of gravitational particle precipitation.

A diagram of a typical acousto-inertial industrial dust, smoke and fog precipitation installation is shown in Fig. 63. The dusty gas and aerosol first enter coagulation chamber 1; while passing through the chamber, the gas sustains the acoustical oscillations radiated by sound siren 2 operated by compressed air from compressor 5; the suspended particles consolidate, and a portion of these is precipitated. The gas then enters inertial precipitator 3, in which the consolidated particles are separated from the gas. The purified gas is then discharged into the atmosphere by blower 4, or removed as a processed gas. Finally, the entrained dust enters a dust collector. When lowering the gas temperature is required, cooler 6 is mounted in front of the coagulating chamber; when it is necessary to dampen the gas, the chamber is equipped with liquid spray nozzles (7) or steam nozzles. If the siren is activated by gas instead of air, filter (8) is mounted in front of the compressor.

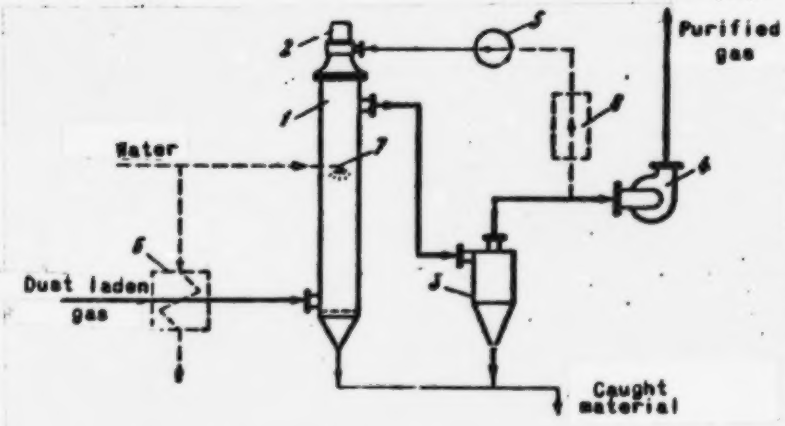

Fig. 63. Diagram of main characteristics of a sound-inertia dust-droplets catcher installation.
1 - Coagulation chamber; 2 - acoustical siren; 3 - inertia precipitators; 4 - ventilator; 5 - compressor; 6 - cooler device; 7 - spray nozzle; 8- filter.

The coagulation chamber, or simply the coagulator, is a vertical cylindrical tower lined with soundproofing material, such as glass wool, etc. [110]. The sound siren is usually located in the upper part of the chamber. To reflect the incident waves, the lower part of the chamber is flat or conical with a 45° tangent angle. The diameter of the coagulating chamber usually did not exceed 2.5m. The height of the cylindrical chamber part is in the 6-9 m range, sometimes reaching 11 m. The gas motion velocity w is related to the sonication chamber height H_s by the elementary function $w = H_s / t_s$, where t_s is the aerosol sonication time. Velocity, w for normal H_s and t_0 of industrial aerosols, is in the 1.5 -- 2.0 m/sec. range. This is considerably higher than the velocities encountered in electrofilters for the entrainment of fine particles and basically explains the smaller dimensions of the coagulation installation.

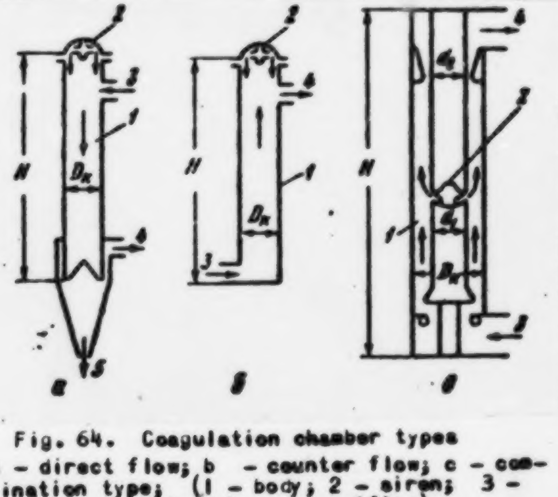

Fig. 64. Coagulation chamber types
a - direct flow; b - counter flow; c - combination type; (1 - body; 2 - siren; 3 - gas inflow; 4 - gas outflow).

Figure 64a shows a diagram of the coagulation chamber of the first experimental acousto-inertial installation designed to trap soot [272]. The dusty gas entered the chamber from above, and, after mixing with air fed from the siren, traveled to the chamber bottom, a system which may be called direct flow. The disadvantage of this system is, in the fact that upon entering the chamber the aerosol becomes diluted by the siren air. The fraction of siren air is 7 -- 10%, in industrial installations, while in laboratory-type installations the amount of air fed from the siren can exceed the aerosol amount.

The counterflow system (Fig. 64b) is more rational. Here, the aerosol is diluted by the siren air only upon completion of the particle coagulation. This system is normally used under production conditions. The gas dilution can be sharply decreased by discharging the siren air before mixing with the gas [73, 260, 225]. A combination system is also possible by mounting a radial siren inside the chamber, as shown in Fig. 64c. Dimentions of such a chamber are as follows: $D_{ch} = 2.4$ m; $d_1 = 1.17$ m; $d_2 = 1.3$ m; $H_s = 9.0$m

[269]. The gas purification level in an acousto-inertial installation depends on the degree of particle consolidation achieved in the coagulator, and on the precipitation effectiveness of the consolidated particles in the inertial precipitator. It was shown in [119] that the effectiveness of particle precipitation was characterized by the degree of entrainment, or purification, or indirectly by the residual weight concentration of particles k_{ext} (g/m^3) related by the simple function:

$$\eta = \left(1 - \frac{k_{вых}}{k_{вх}}\right) 100\ \% \qquad (20.3)$$

(k_{in} - input particle concentration in g/m^3).

Different devices have been tested as precipitators in acousto-inertial installations: simple cyclones, multicyclones, disintegrators, rotary cyclones, bubble baths, damp wire filters, cloth filters, etc.

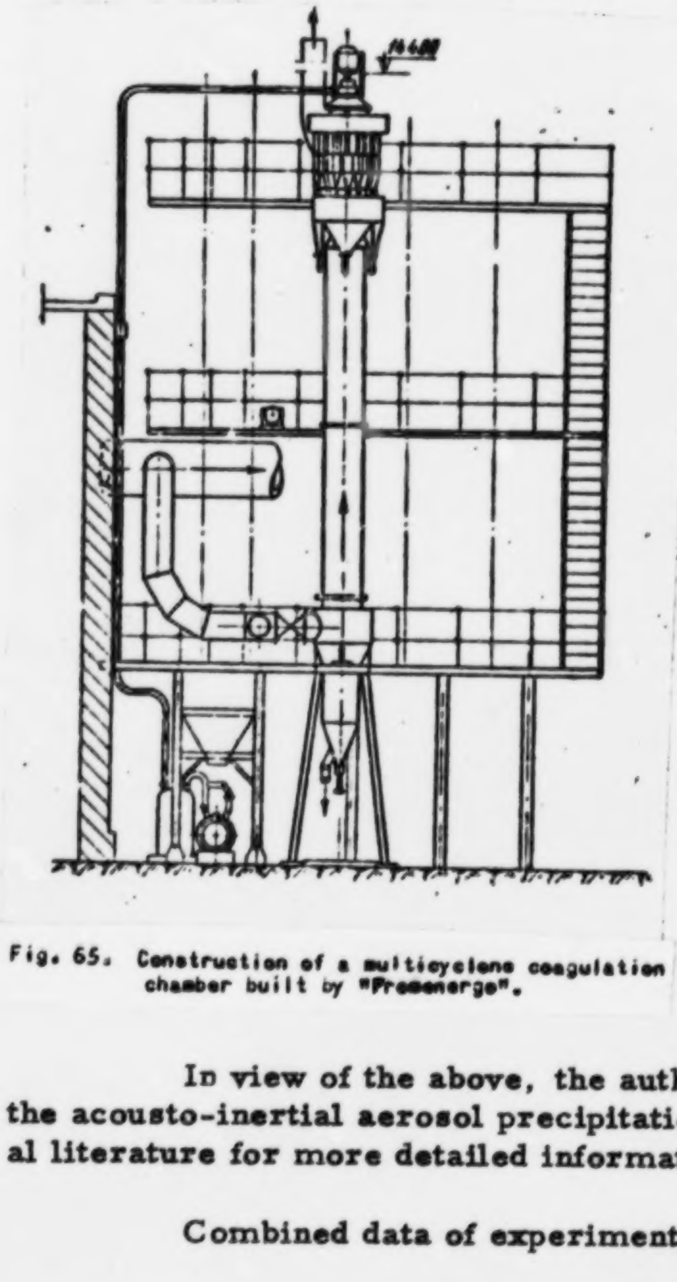

Fig. 65. Construction of a multicyclone coagulation chamber built by "Promenergo".

Fig. 65 shows a diagram of a coagulation chamber with multicyclones made by "Promenergo" for an acousto-inertial installation to trap zinc oxide dust from the discharging gases of a bronze-brass factory. Fig. 66 presents fractional efficiencies of several inertial precipitators at $\rho' = 1$. The graph shows that to obtain high acousto-inertial purification factors for industrial gases, it was necessary to consolidate the particles up to $r = 5$--$7\ \mu$, when using multicyclones, and not less than $\gamma = 10$--$15\ \mu$, when using simple cyclones. Results achieved in the acousto-inertial precipitation of industrial smokes, dusts, and fogs were published in the original articles and also in a series of review articles by the Soviet and foreign authors [7, 58, 78, 127, 150, 151, 157, 183, 184, 240, 241, 248, 269, 292,]. The most important of the foreign articles appeared in the collection of translations "The Acoustical Coagulation of Aerosols" [1] recently published by Goskhimizdat.

In view of the above, the author presented only a limited summary of the acousto-inertial aerosol precipitation. Readers are referred to the original literature for more detailed information.

Combined data of experiments with the acousto-inertial industrial

Name of substance	Aerosol				Nature of aerosol
	Particle radius, r, μ	Gravimetric concn. k, g/m^3	Temperature t, C°	Rate of acoustical treatment m^3/hr.	Type and dimensions, $(D_k \times H_k, m)$
Gas furnace soot	0.03–0.07	1.2–12.6	40	1 700–2 000	Experimental; direct flow Ø 1.1 x 6.6
" " "	0.03–0.07	1.2–2.1	40	1 700–2 000	Ditto plus humidification
Ditto, aggregated	0.5–45	0.5–2.5	–	600	Experimental, plus humidification Ø 0.5 x 9
Spray soot	0.1–0.2	26	82	45	Experimental, ascending flow Ø 0.29 x 1.9
Hard coal soot	0.5–1.0	0.5–2.4	80–90	90–100	Experimental, reverse flow Ø 0.2 x 2.5
Sulfuric acid fog	0.5–5.0	5–40	180	1 700	Ditto, Ø 0.4 x 4
Fog of natural sulfuric acid	0.25–2.5	1	50	40 000	Industrial; combined flow Ø 2.4 x 10.5 (2 compen.)
Dilute sulfuric acid fog	2.5–50 Predominated 7.5	0.5–1.2		1 800	Experimental; reverse flow Ø 0.64 x 11
Artificial oil fog	0.5–5.0	10–40	35–40	25	Laboratory, reverse flow Ø 0.125 x 2.5
Zinc oxide vapors, generated by roasting zinc ore	0.5–5.0 Predominated 2.5	1–2	40–100	1 600	Experimental, reverse flow Ø 0.75 x 10
Zinc oxide vapor generated during copper melting	0.5–40	0.5–20	50–350	300–2 100	Ditto, Ø 1.0 x 9
Zinc oxide vapor generated during brass smelting	0.4–0.6	10	400	7000	Ditto, Ø 0.7 x 10
Coke gas (tar)	0.5–5.0	30–70	40–60	1 300–2 100	Ditto, Ø 0.5/0.64x9
Cracking gas (condensate)	0.5–5.0	5–70	35	1 200	Ditto, Ø 0.5 x 9
" " "	0.5–5.0 (Predominated 3.0–3.5)	6–15	40	12 000	Industrial, reverse flow plus humidification Ø 1.16 x 11 (2 compen.)
Open hearth smoke	2.5 (55%)	2	150	5 000	Experimental, humified reverse flow)
Carbide furnace smoke	0.5–15 Predominated 0.5)	0.25–2.8	120	500	Experimental, reverse flow
" " "	Ditto	0.25 2–8	120	500	Ditto, humidified $(5g/m^3)$

*Without cloth filter

**Aerosol not sprayed

***Similar results were obtained under practical conditions

Table 18

Exptl. chamber				Precipitator			
Acoustical siren	Oscillation frequency f in kHz	Sound intensity I vt/cm^3	Sonification duration t_0 in sec.	Type	Trapping degree without sonification in % η_{u}	Trapping degree without sonification in % η_{zn}	Place and Year of investigation
Dynamic radial	4	0.5–1.0	4.5	2 cyclones ø 1.3m, consecutively	40	83–90	USA, 1947–49 (272, 273, 269, 183)
Ditto	2–4	0.5–1.0	1.2	Ditto	8–32	99	Ditto
Dynamic axial	3	0.1	10	1 or 4 parallel cyclones	68–72	95	Japan, 1950–54 38,246)
Statc with suction remover	4.6	1.0	7	2 cyclones and a glass-cloth filter consecutively	(30)*	(99,98(97)*	USSR, NIIGAS 1959 (54,57)
Dynamic axial	3.6	0.10–0.14	3–4	Cyclone ø 0.15m	68–74 (81)**	87(97)**	USSR, IGI, 1959 (85)
Ditto	2.15	0.1	3	Parallel type multi-cyclone	84	99.6–99.9	USA, 1949 (218, 241, 243)
Dynamic radial	2.25	0.1	4	2 parallel cyclones	–	90	USA, New York, 1948 (184)
Dynamic axial	1–2	0.1	7	4 parallel cyclones	69–72	78–12	Japan, 1950–54 (38,246)
Ditto	2 –4	0.1–0.2	2.4	Cyclone ø 0.15 m	93–95	99.0–99.8	USSR, MEI, 1954–5 (73,74)
"	3–3.5	0.1	10	Cyclone	84–87	94.98	Japan, 1950–54, (38,246)
Dynamic radial	3–9	0.13	10	Cyclone ø 1.35	70	90–95	Poland, Shepenitzy, 1954–5 (227,228)
Dynamic axial	0.7	0.6	2.5	Cyclone ø 0.15 0.30 m with filters, consecutively installed	–	99.8	USSR, Promenergo, 1958–61, (299)
Ditto	4	0.1	5–8.5	2 Parallel cyclones	88		Japan, 1960–64, (38,246)
"	4	0.1	5	Ditto	76–82	95.5–99.3	Japan, 1950–54 (38,246)
"	3.5	0.1	6	2 Parallel "puluzy" (Not familiar to me –BSL)	73	95	Japan, Tokio, 1954 (259)
Dynamic	2.2	–	–	Type ø wet rotoclone	45	90.7	USA, 1961 (281,269)
Static	7+10+26	–	4–6	Parallel multicyclones	11	94	France, 1964 (150,151)
"	10.5	–	4–6	"	–	86	

aerosol precipitation method conducted in the Soviet Union and abroad, are listed in Table 18. Data on the following materials, the acousto-inertial precipitation of which was insufficiently covered in the literature are not included in Table 18.

1. Soda ash in gases discharged by wasteheat boiler of a paper factory, being entrained in an industrial acousto-inertial installation of 85,000 m^3/hr capacity [184].

2. Molybdenum sulfide, satisfactorily entrained in dry form in an industrial-size acousto-inertial installation [269].

3. Cement dust from the gases of a cement annealing furnace, successfully entrained only when water dampened, which caused no dust, hardening in the precipitator [269].

4. Fly ash of smoke gases from boiler installations [186, 193 216, 254], which coagulated poorly in dry form, due to the small particle size.

5. Sulfur from gases discharged from a catalyst chamber in which sulfur dioxide and hydrogen sulfide formed elementary sulfur; the degree of sulfur entrainment reached 93% [183].

6. Iron oxide from gases formed in oxygen-blown steel converters, and also cobalt oxide, 90% - entrained in an experimental installation with a 3000 m^3/hr productivity, at 1 -- 3 khz frequency [206].

7. Antimony oxide showing, according to Bush, even better results [150, 151].

8. Lead oxide, 95 -- 98% - entrained in an industrial installation of 10,000 m^3/hr capacity in Czechoslovakia.

9. Different "aggregating" aerosols obtained by mechanical spraying of earlier precipitated powder-form products in a gas which yielded negative results with aggregated coal dust, ash [73], magnesium and aluminum oxides [262], etc.

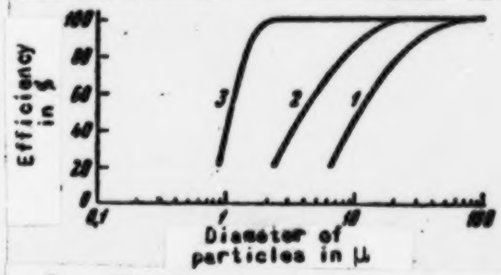

Fig. 66. Fractional efficiency coefficients of some inertia precipitators. 1 - Large diameter cyclone; 2 - small diameter cyclone; 3 - high impact laboratory precipitator

The table contains no information on materials, the acoustical coagulation of which was determined not by the degree of inertial precipitation but by other indices, and also on a laboratory scale, such as ferromanganese dust from blast furnace gases [171], cyclohexane oxime [87], flourides [15], etc. Data presented in Table 18 leads to the following conclusions:

Highly dispersed gaseous and lamp black aerosols consolidate sufficiently for effective precipitation in inertial precipitators only at an increased sound intensity, or sonication time of the order of

1 w/cm^2 and higher. Exhaustive precipitation can be achieved only using cloth filters as the final stage; due to particle consolidation and the decrease in dust concentration, cloth filters can operate at an increased gas filtration rate. Less highly dispersed aerosols, such as sublimates of zinc oxide, molybdenum sulfide, and others, are sufficiently consolidated at normal sound intensities (0.1 w/cm^2) and attain 90-96% entrainment levels. However, the residual 20-200 mg/m^3 particle concentration exceeded the standard MAC for toxic substances, necessitating, as in the previous case, the supplemental installation of cloth filters, justified only for entraining high-cost products or for small gas volumes.

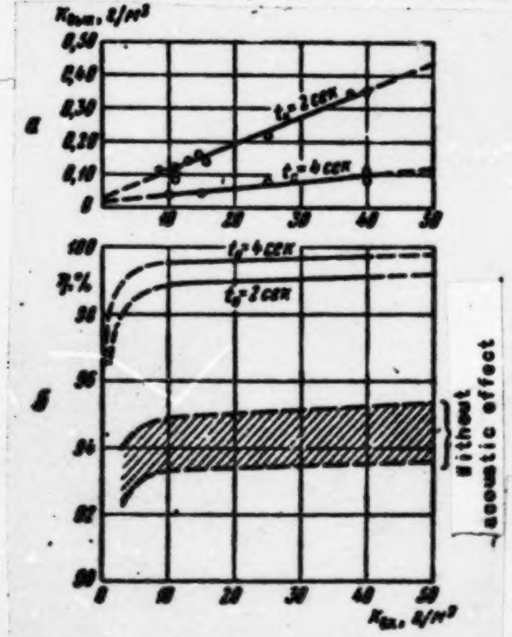

Fig. 67. Functional efficiency relation between acoustical inertia precipitation of colloidal oil (fog) and initial gravimetric concentration (f = 2.4 kHz; I = 0.1-0.2 vt cm^3) a - concentration of precipitate; b - trapping degree

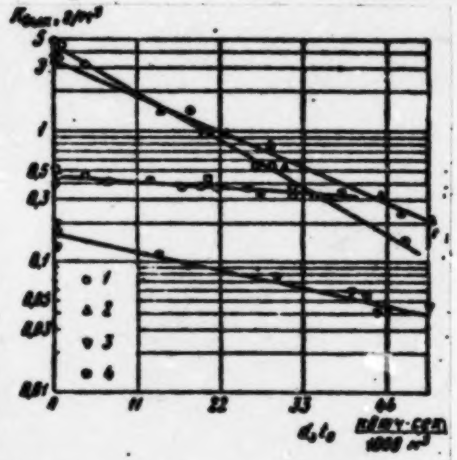

Fig. 68. Functional relationship between the concentration of residual sonified particles of some industrial aerosols and the product of $d_e t_0$ according to Oyama, Inoue, Savahata, and Okada. 1 - Coke gas tar with r = 0.5-5.0μ k_{inc} = 30-70 g/m^3; 2 - cracking gas condensate with r = 0.5-5.0μ k_{inc} = 5 - 70 g/m^3; 3 - aggregate soot with r = 0.5-15μ; k_{inc} = 0.5-2.4 g/m^3; 4 - dilute sulfuric acid fog with r = 2.5-50,0μ; k_{inc} = 0.5 - 1.2 g/m^3.

Different polydispersed dusts, such as dust from open-hearths, blast furnaces, furnaces for annealing cement, etc., of low weight concentrations of highly dispersed fractions, generally yield a high degree of entrainment only when 1) the gas is water dampened in the coagulating chamber followed by precipitation in a damp precipitator which assured a residual concentration of 100 mg/m^3, or 2) cloth filters are used as the final stage which assured a residual concentration of 5--10 mg/m^3 or less and increased permeability. Natural fogs such as coke gas, cracking gas, etc., were effectively precipitated by the acousto-inertial method (95--99.8%), if their concentration and dispersion degrees are moderate, in which case their residual droplet concentration did not exceed 30--300 mg/m^3.

In testing the acousto-inertial industrial aerosol precipitation method, several empirical relationships were derived. It was established that the residual particle weight concentration had a linear functional relationship to the initial particle concentration in the gas, as illustrated in Fig. 67a. Thus, the dependence of entrainment degree on the initial particle concentration was expressed by the typical curve shown in Fig. 67b. Thus, it can be concluded that the entrainment degree fell sharply at the "critical" concentration of 3 - 5 g/m^3, while at concentration above 10-15 g/m^3, it barely increased. The latter could be explained [see equation (20.31)] by the fact that with increasing $\bar{k}_{in}$ the ratio $\bar{k}_{out}/\bar{k}_{in}$ decreased (see Fig. 67a) progressively slower, as illustrated in Fig. 67a.

It has been established, in the case of acousto-inertial precipitation, that the residual particle concentration was an exponential function of the specific air compression energy consumed by the sound siren by the sonication time $\xi' = d_{energy} t_s$ [246]:

$$k_{\text{вых}} = k_{\text{вх}} e^{-m\xi'}, \qquad (20.4)$$

where m - constant depending on the form of the aerosol. This is illustrated in Fig. 68 in which are presented results obtained with acousto-inertial precipitation of different industrial aerosols by Oyama, Inoue, Sawahata, and Okada [246]. If m is a constant related to constant n - derived by the authors, through the relationship m = n/27.3, then the following values are obtained: coke gas -- 0.077; cracking gas -- 0.059: aggregated gas ashes -- 0.033; fog diluted by sulfric acid -- 0.009. The specific energy consumption is proportional to the product of the sound intensity, and the sonication time $d_{energy} \sim Jt_s$ [see equation (20.8)], since $\xi' \sim (\sqrt{Jt_s})^2$. By comparing equation (20.4) with equations (15.2) and (16.4) get the following relationship:

$$\frac{k_{\text{вых}}}{k_{\text{вх}}} = \left(\frac{n}{n_0}\right)^3. \qquad (20.5)$$

The above expression implies that weight concentration of coagulated particles decreased more rapidly after their precipitation in an inertial precipitator than the numerical particle concentration did in the course of acoustical coagulation. This is theoretically correct, since the heaviest of the coagulated particles precipitated in the inertial precipitator.

The following expression is obtained for the degree of entrainment, according to (20.4):

$$\eta_{\text{общ}} = 100 - (100 - \eta_{\text{и}}) e^{-m\xi'} \%, \qquad (20.6)$$

where $\chi_{inertial}$ -- efficiency of the inertial precipitator which can be attained in the purification of a non-sonicated aerosol. The equation holds for consolidated particles up to dimensions at which they become completely entrained by the precipitator, and for the unbroken consolidated particles therein, a phenomenon observed only in fogs.

On the basis of Stokes and Vivian's [273] experimental data, Kidoo [211] proposed another exponential equation for the gas black entrainment degree:

$$\eta_{\text{зв}} = 100 - e^{\frac{M}{K\sqrt{Jt_s}}} \%, \qquad (20.7)$$

where M -- coefficient depending on the form of gas black and the effectiveness of the coagulating and precipitating installations.

The question of energy consumption is important for a correct appraisal of the acousto-inertial aerosol precipitation method. Consumption consists of energy lost in the aerosol coagulation and precipitation. The specific energy consumption magnitude for the aerosol precipitation is well known for all existing precipitator types. For example, for cyclones, it is equal to an average of 0.5 Kwh per 1000 m^3 of gas; for rotary cyclones, it reaches several kilowatthours. If the required sound intensity radiated into a coagulation chamber of cross section S_{ch}, is J w/cm^2 and the sonication time is t_s sec, then, taking into account that the total amount of required sound energy equaled $W_{sound} = JS_{ch}$ and the amount of gas being processed equaled $Q_s = wS_{ch} = H_s/t_s\ S_{ch}$, the following expression for the specific energy consumption in aerosol coagulation [74] is derived:

$$d_э = \frac{Jt_э}{0{,}36\,\eta_c\,\eta_{к.у}\,\eta_{к.ж}\,H_э}\,\frac{\text{квт}\cdot\text{ч}}{1000\ \text{м}^3}, \tag{20.8}$$

where χ_{siren} - the acoustic siren efficiency, χ_{com} - the overall efficiency of the compressor operating the siren, $\chi_{ch\cdot osc}$ - utilization coefficient of the acoustical oscillations in the coagulating chamber; one must also take into consideration losses connected with the non-uniformity of the chamber's sound field, the absorption of the sound energy by the aerosol, leakage through the chamber openings and walls, the yield from the resonance state, etc., (determined experimentally); H_s -- amplitude of sonication of the coagulating chamber in meters. Thus, the measure of energy consumption in the process of aerosol coagulation is the product Jt_s of the sound intensity and the sonication time designated as the sonication factor.

Examining equations (15.2) and (20.8) and taking into account relationship (15.6), it can be concluded that an increase in J influenced the effectiveness of the process less perceptibly than an increase in t_s. However, J and t_s affect the specific energy consumption equally, from which it follows that the sound consumption was less at low values, while the capital expenditures for equipment are just the opposite, i.e., greater at small values of t_s since the permeability of the chamber increased with t_s. The optimal values of J and t_s are derived by technical and economic calculations based on experimental data.

Neuman Sodaburg, and Faul (Ultrasonics Corp., USA) indicated [240] the following limits for specific energy consumption: $d_{energy} = 0.65$ -- 2.0 Kwh per 1000 m^3 of gas. Other authors cited even higher values. Thus, in the course of semi-industrial experiments conducted by Oyama, Inoue, Sawahata, and Okada [246], the following values were obtained: consolidated carbon black and zinc oxide -- 4.2 Kwh;* diluted sulfuric acid -- 5.6 Kwh; coke gas -- 8.4 Kwh; and cracking gas -- 7.0 Kwh, calculated by the present author, hence x_{ees} = 0.65. Energy consumption in the acousto-inertial purification of cracking gas in an industrial installation designed by the same authors [259], was only 2.5 Kwh. The reason for the difference can be found in the fact that in the experimental installations non-economical sound sirens were used, the acoustical efficiency of which did not exceed 10 - 15%. For this reason, a value of 8 Kwh was obtained in the experiments on the acousto-inertial precipitation of zinc oxide sublimates conducted at the TsIOT(PNR) [227, 228], while in the precipitation of carbide furnace smoke [150, 151], values of 3.9 and 7.0 Kwh were obtained. In citing his experiments Schnizler [262] indicated a value of 10 Kwh, although he failed to mention the fact that it was obtained in the acousto-inertial precipitation of aggregates, i.e., poorly coagulated products. Generalizing on the accumulated experience in the acousto-inertial precipitation of industrial aerosols, it can be said that, generally the following factors may account for the increased specific energy consumption in the process.

---

* In reference [89] the value for the specific energy consumption in the sonication of zinc oxide equals only 0.6 Kwh, which, requires further checking.

1) poor acoustical coagulability of an aerosol, due to excessive particle sizes or their low weight concentration, etc.;

2) strong aerosol sound absorptivity due to the "critical" particle sizes, excessive particle concentration, etc.:

3) oscillations frequency deviation from the optimal value, due to a) limited sound generator capabilities, b) drive speed variations, c) variations in the aerosol dispersion composition;

4) low acoustical sound generator efficiency, due to improper design, manufacture, wear, etc.;

5) non-economical coagulating chamber operating conditions, due to the system's non-controlled resonance, unsatisfactory chamber height selection, heavy energy losses through the inlet and outlet ducts, gas temperature variability, etc.;

6) considerable aerosol dilution by the siren exhaust, which lowered aerosol coagulability and increased the energy consumed in thrusting;

7) decreased compressor efficiency, due to considerable deviations from the rated operating value, air throttling, and other factors;

8) poor choice of inertial precipitator type, or its operation below optimal conditions: reduced input velocities required increased degree of particle consolidation, and excessive velocity enhanced destruction of dry particle aggregates; according to Jahn [206], the critical velocity in cyclones was 10-12 m/sec.

Not all above factors can be completely eliminated. Therefore, 2--4 Kwh per 1000 m^3 of gas should be considered, thus far, as the practical total value of consumption for the acousto-inertial purification of gases. Only when it is necessary to dry the entrained products can the specific energy consumption reach higher values, as for example, for dust in an open-hearth gas d = 6.5 Kwh [269].

Measures making possible to increase the efficiency of acousto-inertial precipitation of industrial aerosols are listed below:

1) the introduction of water spray or condensed steam [189] into dry, or only slightly dusty gases, and, in the case of fogs, the introduction of entraining liquid droplets, such as fog recirculation in proper amounts. The introduction into the aerosol of charged water droplets, or some other liquid should be considered;

2) lowering the gas temperature to increase the actual particle concentration, thereby, stabilizing the condensation temperature of the input steam, and to decrease the gas volume leading to an increase in the coagulator permeability, or, conversely, the maintenance of a high gas temperature to sustain the liquid particle state;

3) an increase or reduction in the coagulation chamber height to achieve the most rational sonication conditions for a given aerosol;

4) the use of high-efficiency sound sirens, such as dynamic sirens with rectangular pressure pulses, also sirens with internal air circulation;

5) the use of purified gas to operate the sound sirens when it was under excessive pressure, as in blast furnace gas, or, if available, low-pressure steam, as exhaust steam from steam engines;

6) acoustical multifrequency aerosol processing, as in Boucher's [150, 151], demonstrated this as favorable measure;

7) special acoustical filter installation at the gas inlets and outlets from the coagulating chamber to backfeed acoustical energy into the chamber [180];

8) the use of more effective dust precipitators, in particular damp wire filters [184, 239, 240]; the use of electric filters also deserves attention.

A combination of a turbulent coagulator with an electric filter demonstrated experimentally, proved to be extremely useful in purifying blast furnace gas [119], the residual concentration of which was lowered to 5-10 mg/m^3 instead of 20 mg/m^3 and the permeability of the electric filter was increased by 50-100%.

Still better results may be expected from combining an acoustical coagulator with an electrical filter. The sonication time was fore-shortened, since electrical filters permit lesser particle consolidation than cyclones, and the permeability of electrical filters was increased. This reduced the capital outlay and the consumed sonication energy. An acoustical coagulator also has the important advantage over a turbulent coagulator in that coagulation can proceed in a dry form, with the exception of slightly dusty gases, since there is no danger that the aggregates coagulating in the electrical filters might disintegrate, since the gas velocity was small.

The acousto-inertial method of dust-droplet entrainment, like other methods, has its advantages and disadvantages. The advantages are these:

1) high degree of different industrial gas purification, primarily fogs, but also smokes, for which damp entrainment is possible;

2) infinitely small dimensions of the entrained particles of fogs, smokes, and dusts;

3) the independence of the effectiveness of gas purification from the electrical properties of the particles;

4) applicability to aggressive gases purification, and also gases with elevated temperature or pressure;

5) explosion and electrical safety of the acousto-inertial equipment;

6) simplicity of the coagulating devices, in particular when using static sirens and centrifugal compressors;

7) more moderate dimensions and capital expenditures as against electrical and cloth filters.

The disadvantages of the acousto-inertial method of dust-droplet entrainment are these:

1) higher specific energy consumption in the purification of gases, particularly smokes and dusts; the consumption is always higher than for electrical filters, but, as a rule, it is lower than for disintegrators, turbulent pipes - atomizers, and cloth filters;

2) the need to dampen certain smokes and dusts and to lower the gas temperature accordingly;

3) unsatisfactory residual particle concentration, not lower than 30 mg/m^3 for fogs and 100 mg/m^3 for dampened smokes and dusts, where cloth filters installations are suitable;

4) when using standard sound sirens, certain dilution of the contaminated gas by air, by the gas or the siren's steam;

5) the presence of rotary machines - the sound siren, if it is the dynamic type, and the compressor.

The most important disadvantage is the increase in the specific energy consumption most evident in the coagulation of highly dispersed aerosols, such as gas black, etc. In this connection, the two new systems for coagulating aerosols in a sound field proposed by the present author are of interest: the multifrequency multistage [77, 78] and the electro-acoustics [76, 78]. Consider briefly the physical nalture of these systems.

It was noted in #16, that for every coagulating aerosol there was an optimal oscillation frequency at which the coagulation process functioned more effectively. The coarser was the aerosol, i.e., the greater was its particle size, the lower was the optimal oscillation frequency value. This follows from the theoretical investigations reported in #10, 11, and 12 (see Figs. 30 and 41), and also general experimental investigations (see #16, Fig. 51 and Table 13).

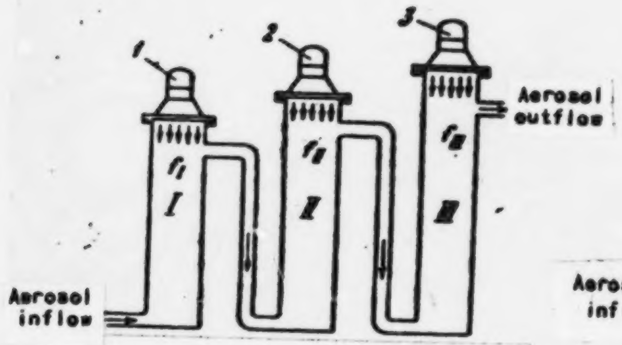

Fig. 69. Diagram of a step-shaped coagulation installation. I, II, III – Coagulation chambers I, 2, 3 – corresponding acoustical sirens ($f_I > f_{II} > f_{III}$)

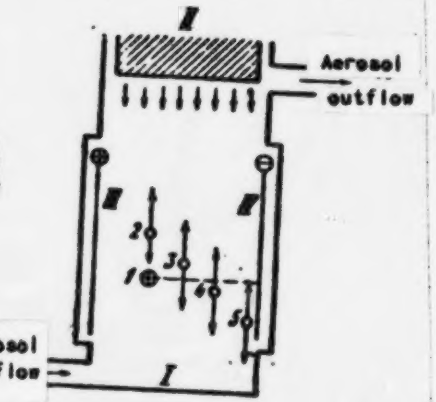

Fig. 70. Diagram of electro-acoustical method of aerosol coagulation and precipitation; I – Electroacoustical chamber; II – Sound receptor; III and IV – electrodes; I – a fog droplet; 2,3,4,5 – dust particles.

In the course of aerosol coagulation a gradual consolidation of particles occurred which implied that the oscillation frequency had to be decreased if it was desired to conduct the process under optimal conditions. This is a special requisite in the coagulation of highly dispersed particles requiring huge consolidations. Consequently, the existing methodology of conducting acoustical aerosol coagulation was a primitive one. In place of the existing system for the acoustical aerosol coagulation a more efficient system, shown in Fig. 69, was proposed. In this system, the aerosol passed through a series of chambers with step-down oscillation frequencies with respect to the change in the particle size. However, this did not imply an increase in capital expenditures and in energy consumption by the sirens, since the flow-through velocity in the chamber increased by a corresponding number of times, with three chambers three times, etc.

The nature of the electro-acoustical aerosol coagulation method lies in the fact that (Fig. 70) previously charged water droplets, or another liquid, mixed in with the sonicated aerosol as centers of coagulation, and the process of sonication occurred in an electrical chamber which outwardly appeared as an electrical filter without a corona. Having become charged, the particles moved toward the precipitating electrode and in the course of the movement had undergone a "bombardment" of oscillating polarized dust which penetrated into the droplets and moved with them to the precipitating electrode. Thus, the processes of aerosol precipitation and coagulation were combined here in one piece of equipment. However, the coagulation process proceeded according to a new method, since the longitudinal oscillatory particle motion was achieved acoustically, while the lateral motion was achieved electrically. In the case of an a-c current, the dust and droplets will undergo only coagulation and not precipitation on the electrode surface.

21. ACOUSTICAL AEROSOL SEPARATION AND FILTRATION

Acoustical oscillations intensify the aerosol precipitation by aerosol coagulation, and also directly. Direct intensification can be obtained primarily with the aid of drift forces, which prevent the aerosol particles from moving with the gaseous medium, thereby, allowing particles from becoming separated from the gas flow. Another possibility is presented by the use of the orthokinetic effect which makes possible the aerosol particles precipitation on large, rapidly-settling liquid droplets which then become separated from the dusty gas. Finally, a third possibility consists in using the gaseous medium movement generated at the boundary layer of obstacles (see #1) as a factor accelerating the turbulent diffusion and the inertial precipitation of aerosol particles on them.

Examine the proposed methods of excitation and use of the precipitating sound effect. A highly original method of acoustical aerosol separation was proposed by Westervelt and Sieck [290]. The basis for the method rests in Westervelt's theoretical work [286] cited in #6, in discussing aerosol particles drift forces in a sound field; the author described a new form of particle drfit resulting from a distortion in the sound waveform. It was shown in #6, that with great waveform distortion, the velocity of this drift type exceeded the velocity of all other drift types, and in particular, radiation drift. For the accelrated separation of the suspended particles from the dispersion medium, Westervelt and Sieck proposed sonicating the medium by means of an artificially distorted (asymmetric) waveform. This could be achieved in a gaseous medium by using a specially constructed dynamic siren, having rotor openings shaped according to one of the variants shown in Fig. 71.

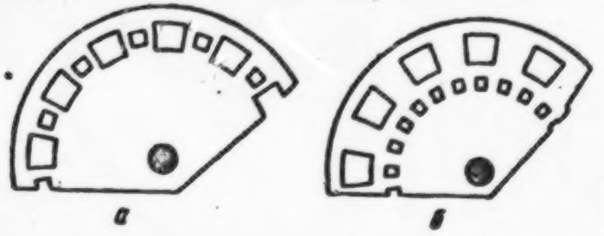

Fig. 71. Profile of dynamic siren rotor openings used in aerosol separation. (Westervelt and Syke).

The separation device is a vertical hollow chamber equipped at the bottom with a radiator, inside of which traveling sound waves were generated. The processed gas entered the chamber from below and moved upward, while the particles suspended in it were retarded by the drift forces, and then fell out by gravity. The rate at which the gas was drawn through the separator was determined by the minimal dimension of the particles expected to undergo precipitation. It can be concluded from Fig. 72, that precipitation of the smallest particles required a continuous low gas velocity. However, it can be as-

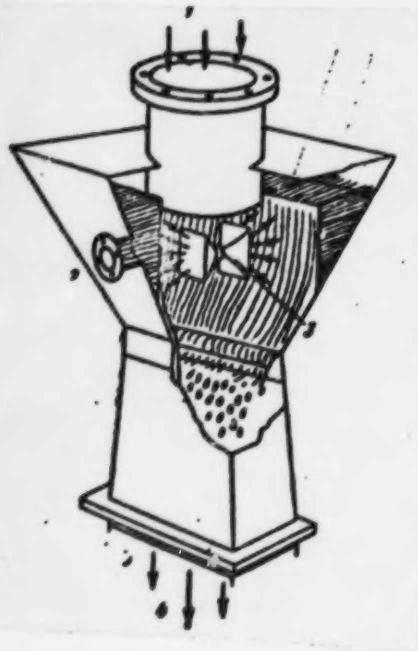

Fig. 72. Sonified Venturi scrubber proposed by Bouche.
1 - Gas inflow; 2 - water inflow; 3 - sound receptor; 4 - gas outflow

sumed that in the case of low concentration, the particles will create a suspended filtering layer which can support smaller particles at increased gas flow-through velocities. Unfortunately, no experimental data has been found in support of this assumption. It appears that the described aerosol separation method had prospects for use mainly in the removal of dust from small enclosed spaces which made possible prolonged sonication of the dusty gas. This situation occurred, for example, in the explosive work during the sinking of drift shafts and in mines.

Ten minutes was the time alloted for ventilating the drifts. Experience had shown that the usual sonication of mine workings provided for no actual shortening of the indicated time. For drift sonication, the use of special sirens with a distorted pressure pulse shape evidently permits considerable shortening of drift sonication time. Power loss was not expected to be great in this case, since sonication was episodical, and no sound suppressing measures were required in the surrounding space, since under the explosive safety conditions no people were present in the sonicated area. Boucher [157] proposed that the process of aerosol particle precipitation be intensified directly in existing dust-droplet entrainment devices by mounting compact gas-jet sound radiators at certain places in the devices. This idea has some merit, since its realization required small capital outlay, particularly when a compressed air supply was available.

Figure 72 shows that sound-equipped Venturi scrubber [149, 157] proposed by the present author. The liquid in it flowed downward along the inclined walls continously directed by diverting baffles through the pipe throat, and was scattered by the dusty gas moving at a great rate. The gas-jet whistle, mounted inside the pipe, sonicated the mixed aerosol and, due to increased orthokinetic interaction and turbulization, there followed a corresponding increase in the number of collisions with water droplets.

It is natural that sonication should have an appreciable effect only when the mixture remained in the sonication zone an appreciably long time. For this reason, different high-speed gas purifiers were not suitable for sonication, while, on the other hand, ordinary wet scrubbers and gas purifiers, in which the gas moved, relatively slowly, were suitable. This opinion was confirmed by the early experiments of Boucher and Weiner [159]. The authors studied the effect of an 11-Khz sound on the effectiveness of entraining the weakly concentrated aerosol triethyleneglycol ($r_s = 25\mu$; $k_{1s} = 79$--136 mg/m^3) in a 850-m^3 /hr gas purifier made by "Smig Industries".* The sound intensity level generated by the rod whistles was 150 db. On the basis of the conducted experiments the investigators stated that the sonication of water mist enhanced the efficiency of gas purifiers by 10-15%, even with a low concentration of aerosol particles.

---

* Not sure of spelling.

Figure 73 shows the sound-equipped conical cyclone proposed by Boucher [157]. The sound radiator in the form of a rod whistle, was installed in the rarefaction zone located under the outlet pipe of the cyclone. Due to the repelling action of the drift forces the sound waves created a sound barrier in the path of the small particles entrained by the gas. The size of this rarefaction zone was comparatively small; therefore, a high sound intensity was easily achieved with a moderate energy consumption. The volume of compressed air used by a whistle in large cyclones was small in comparison with the volume of the processed gases. It seems that a satisfactory effect could be achieved in a sound-equipped cyclone only when the sound radiator generated sound waves of sharply asymmetrical waveform, as in the previously mentioned Westervelt - Sieck separator. The method of acoustical fog filtration proposed by Asklöf [301], was based on a totally different physical principle. Figure 74 presents a schematic diagram of the filter-droplet trap designed by the author. The processed gas containing fog droplets, or dust mixed with them, entered the apparatus from below. After the large droplets had been separated in an internal cyclone, the gas entered through a porous nozzle sonicated from above by a rod whistle with a reflector. Under the action of the sound, an intensive gas purification from the particles occurred, and the purified gas was released from the top.

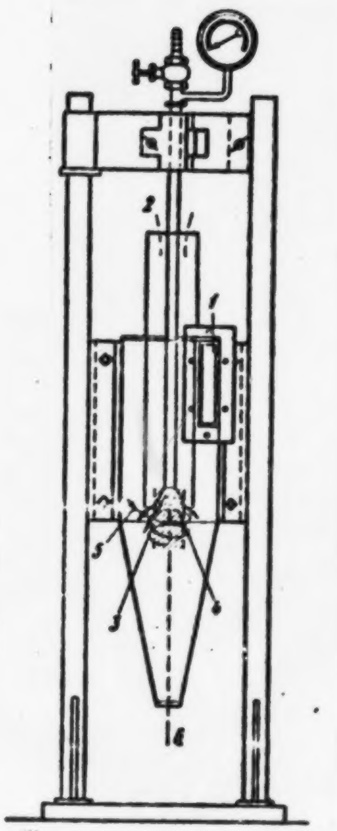

Fig. 73. Sonified cyclone proposed by Bouche. 1 - Tangential outflow nozzle; 2 - gas outflow; 3 - a straight flow rod-shaped whistle; 4 - acoustical field; 5 - trajectory of particles' movement; 6 - dust outflow.

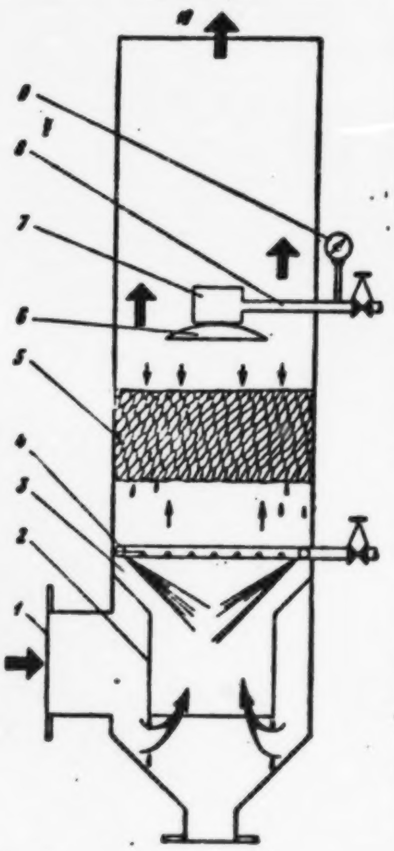

Fig. 74. Diagram of acoustical filter-coagulator proposed by by Askluphom
1 - Tangential inflow nipple; 2 - Inside cyclone outflow pipe; 3 - outflow into wet scrubber; 4 - ring sprayer; 5 - capping; 6 - sound generating reflector; 7 - sound generator; 8 - compressed air inflow; 9 - manometer; 10 - gas exit.

In describing this method in [157] Boucher discussed the nature of acoustical filtration as follows: "It had long ago been noted that during an intense sound radiaiion over a metallic grid, the latter acted as an acoustical lattice, transmiting and refracting the sound waves over a large area. By varying the ratio λ/D (ratio of the wavelength to the mean diameter of the grid openings), it is possible to amplify and concentrate the sound in any space, or transmit the radiated sound under a large solid angle. Each opening may thereby be considered as a point of sound source. The interference of sound waves may also take place.

When operating with a powerful sound generator, the grid transmitted a considerable amount of acoustical energy. For example, an ultrasonic gas-jet whistle of 80 w power located 0.3 m above a filtering nozzle of 5.4 cm diameter can purify the surface layer of tap water located 0.3 m below the openings. The radiational pressure is usually so great that the force fields transmitted through the openings were able to attract the suspended aerosol particles to the grid filaments or to repel them from the nozzle." Moreover, "when operating with a liquid aerosol, a high-intensity sound field repelled certain particles, impelled others to collide, resulting in orthokinetic coagulation, and generated a liquid film which covered the metallic grid filaments."

It appears to the present author that the main role in the proposed acoustical fog filtration process was played not by the radiation pressure, which was low for small particles, but by the gaseous medium eddy movement in the boundary layer of the filtering nozzle elements, which enhanced the turbulent diffusion and inertial precipitation of the aerosol particles they contained. Asklöf affirmed [301] that by filtering a thin hydrocarbon fog through a 100-mm thick gauze nozzle at a velocity of 3 m/sec, it was possible to lower the residual droplet concentration by sonication (f = 8 Khz; J = 0.05 c/cm^2) that 10 mg/m^3 to 0.5 mg/m^3 of gas, i.e., by twenty times. The author succeeded in lowering the residual concentration to the same degree in the acoustical filtration of radioactive aerosol uranium trioxide formed in the evaporation of a 0.5% solution of uranium nitrate, and the susequent drying of the droplets [301, 303]. The nozzle's capacity was 6000 m^3 of radioactive gas per hour with a pressure drop of 25--50 mm H_2O (at a nozzle height of 900 mm). The energy consumed in sonication (f = 19 Khz; J = 0.1 w/cm^2) and throttling of the gas totalled only 0.4 KWH per 1000 m^3 of gas; in other cases the energy consumption reached 1.2 KWH [157]. The acoustical aerosol filtration method deserves serious attention; it can attain fine purification of industrial gases, in particular, the ventilating of factory air at an accelerated filtration rate. The sound waves for cleaning filter bags of collected dust is of practical interest. According to the initial plan described in Abboud's patent [135], the sound generator was mounted inside the filter so as to irradiate the filter bag fibers from the clean side.

However, it seemed [157] that radiation of the dirty side of the fiber in the schematic shown in Fig. 75 was a more effective and cheaper method of filter cleaning. It is felt that the cleaning action of sound could be explained by the fact that the resonating plates inside each bag generated a standing wave, which induced a perceptible periodic gas pressure variation at nodes, forcing the fiber to vibrate, provided the oscillation frequency was not high.

In conclusion, a method will be briefly described, which was proposed by P. N. Kubanskii. The method was intended for the intensification of aerosol particle precipitation by a longitudinal screen mounted inside the coagulating chamber. The method is based on the author's mistaken conclusion [48, 49] that the eddy-like acoustical flows originating in the node-antinode intervals of standing waves supposedly enhanced the aerosol particle coagulation. Actually, the coagulating action of the acoustical flows was very slight, since their whirling velocity was small, and, therefore, the finer particles did not gravitate into the "dead" zones formed near the walls at the junction of two adjacent eddies at each node, as described in #7. Only small coagulated particle aggregates, or large primary particles, such as lycopodium powder particles [48] having radii exceeding 10μ, could possibly fall out in these zones. This fact was also noted by Brandt, Freund, and Hindemann [167] who pointed out that the local aerosol particle precipitation at the nodes was a secondary effect of sonication which followed the process of particle coagulation.

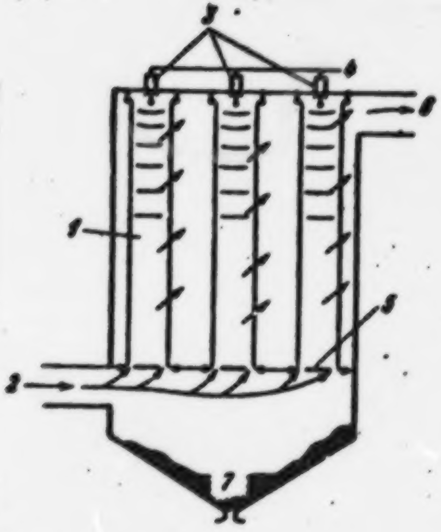

Fig. 75. Sonified sleeve-type filter proposed by Abbott
1 - Sleeve filter; 2 - dust laden gas inflow; 3 - sound generators; 4 - compressed air line, in the direction of sound generators; 5 - resonance plates; 6 - pure gas outflow; 7 - precipitated (settled down) dust.

It should be added in a supplemental way, that according to Rayleigh's equation (1.25), the acoustical flow velocity in the direction of the wall decreased linearly as the clearance between the walls decreased. For this reason the additional baffles failed to increase the amount, and even the coagulated particle aggregates precipitated at the nodes.

APPENDIX

#1. Evaporation and Condensation Droplet Growth During Fog Sonication

In fog sonication, in addition to the acceleration of the coagulation processes and droplet precipitation, phase transformations characteristic of these systems have also been observed to accelerate. If the gaseous medium were not fully saturated with the liquid vapors, then fog sonication could promote acceleration of droplet evaporation occurring in the system. However, if the gaseous medium were sufficiently supersaturated with liquid vapor, then the sonication could add to the acceleration of the attendant fog droplets' condensation growth, if the latter were not too great.*

Under certain conditions, the above processes suppressed coagulation and droplet precipitation, and came to the forefront, thus permitting the use of acoustical oscillation as a means of intensifying natural fog dispersion, the drying spray solutions, the separation of hydrocarbon gases, etc.

Examine the theoretical principles underlying the intensifying sound effect on evaporation and condensation growth of fog droplets. It has been known that the process of droplet evaporation consisted of two elementary processes [16]: a) separation of the molecules from the liquid surface and formation of a saturated vapor layer, and b) diffusion of molecules from the saturated layer into the surrounding medium. With these concepts in mind, Maxwell used the following equation to derive the rate of evaporation from the droplet surface in a stationary medium [16, 123]:

$$J_I = 4\pi Dr\,(c_s - c_\infty). \qquad \text{(AI.1)}$$

where D -- coefficient of vapor diffusion [128]: c_{sat} -- concentration of the saturated substance vapor: c_∞ -- vapor concentration in the surrounding medium. It can be assumed for a droplet system constituting a fog, with good approximation that each droplet evaporated at a rate as if it were in a vessel with non-absorbing walls of a volume equal to the mean volume of one droplet in the system. Based on this premise, the theory yields the following expression for the rate of fog droplet evaporation [123]:

$$J_I \simeq 4\pi Drc_s \exp\left[-\frac{3rD}{(b-r)^3}t\right], \qquad \text{(AI.2)}$$

where b -- radius of the vessel, and t -- time.

---

* Experiments of V. V. Bazilevich and N. P. Tverskii [5] showed that sonication also contributed to the freezing of supercooled fog droplets; however, since this phenomenon is of no great interest we shall not dwell upon it here.

Due to some "blow-off" of the diffusing boundary layer in a moving medium, the droplet evaporation rate is usually higher than in a stationary medium by f_v times, where f_v is, the so-called, "wind" factor:

$$f_w = 1 + \beta \, Sc^{1/3} Re^{1/2}. \qquad \text{(AI. 3)}$$

Here, β -- constant equal to about 0.276; Sc -- Schmidt number, which represented the ratio γ/D, equal to approximately 0.7 for water vapor in air under ordinary conditions; Re -- Reynolds number characteristic of the flow around the droplets: $Re = 2\ rug\rho/\gamma$. In this case, if K is defined as $k = \beta\ Sc^{\frac{1}{3}}$, the rate of droplet evaporation could be determined by the following Fressling equation:

$$J_f = 4\pi r D (c_s - c_\infty)(1 + K\sqrt{Re}), \qquad \text{(AI. 4)}$$

This equation leads to the conclusion that the droplet evaporation rate in a flow increased relatively slowly with increase in the Reynolds number. Moreover, Kinzer and Hahn's experiments [123] showed that when Re < 1, i.e., in the case of a viscous flow regime around the droplets, the rate of their evaporation generally did not depend on the rate of the relative motion of the medium, but on the Re number only. This is due to the fact that the concentration and temperature fields around the droplet in a viscous flow were distorted by the motion of the medium. The circulation inside the droplet generated by the droplet friction and the gaseous medium which promoted a temperature equalization in the droplet, also played no significant role at low Re numbers. In turn, as the Re number increased from 1 to 1.75, a rapid twofold increase in the evaporation rate took place, after which the evaporation rate rose more gradually (at Re = 3, f_v = 2.5, etc.).

Assume that the accelerating effect of the medium's motion on the droplet evaporation was apparent beginning with $Re_{cr} = 1$, then it could be concluded that the increase in evaporation rate began to appear only at the following critical value of the rate of the relative motion of the medium:

$$U_{cr} = \nu/2_r \qquad \text{(AI. 5)}$$

It follows that the critical motion velocity of the medium rapidly increased with the increase in particle dispersion, and was thereby, generally speaking, a significant figure. Thus, with particle radius r = 7.5μ, the critical velocity is 100 cm/sec, and for droplets with r = 1.5μ, it is 500 cm/sec. For comparison, it shall be noted that a three-fold rate of the same droplets was only 0.66 and 0.026 cm/sec, respectively. It is characteristic of acoustical oscillations that they aid in creating motion of a relatively high velocity of the gaseous medium in relation to all the fine particles suspended in the medium. In the critical case, which occurs at elevated oscillation frequency values, for which $\mu_g = 1$, the flow rate around the droplets becomes equal to the oscillatory gas velocity.

. The minimum water droplet radius is about r = 2μ, which assures a good flow of air around them ($\mu \approx 0.8$) oscillating with a critical frequency of 3.5 -- 4.0 KHz for large industrial installations.

The theory proves [123] that if the droplets were not too large, their evaporation under nonsteady-state can be regarded as a quasi-steady-state process. Hence, it can be concluded that equations (Al. 3) and (Al. 4)presented on the previous page, held even in an oscillatory motion of the medium, if the amplitude of the oscillations was great in comparison with the droplet radius $A_g \gg r$. The critical sound force level at which the intensifying action of acoustical oscillations began to appear in the process of droplet evaporation in an air medium is, according to (Al. 5), equal to:

$$L_{\text{кр}} = 164 - 20 \log (\mu_g r)\ \partial б. \qquad \text{(Al. 6)}$$

At such sound levels the gaseous medium could be agitated causing the droplets to flow around as turbulent pulsations of the medium. Moreover, as demonstrated in #11, around every particle suspended in a sound field, even at Re < 1, an acoustical flow was generated with an eddy scale comparable to the oscillation amplitudes.

The question can now be asked: what is the effect of these phenomena on the droplet evaporation process in a sound field?

It is possible that the two phenomena had practically no supplemental effect on the droplet's evaporation process, since the turbulent pulsation rates and acoustical flows were, as a rule, considerably lower than the critical velocities determined by equation (Al. 5). R. S. Tyul'panov [118] attempted to determine, approximately, the variation in droplet radii in the course of their evaporation in a pulsating flow, assuming the following idealized model of the process. The author assumed that during the first half of the half-period of the medium's oscillation, vapors accumulated in the droplet boundary layer and only partial evaporation from its outside surface occurred. For the next half of the oscillation half-period, part of the boundary layer "blows-off", and a corresponding molar discharge of the vapor accumulated near the droplet surface. Stating with these assumptions, the author obtained the following expression for the droplet radius:

$$r = \sqrt{0{,}326\frac{D}{l} + \left(r_0^2 -- 0{,}328\frac{D}{l}\right)e^{-\frac{lc_n}{\rho_p}t}} \qquad \text{(Al. 7)}$$

(or -- initial droplet radius). However, only very large particles may be computed with this formula.

It has been known that the droplet size decreased, and the flow rate decreased, in the course of evaporation resulting in a decrease in the Re number. As a result, the droplet evaporation rate gradually decreased, and, with Re less than 1, the intensifying action ceased. Only the parallel particle coagulation process could retard the onset of this moment; however, droplet coagulation had a high efficiency only at a sufficiently high particle weight concentration. In this connection, it seems that coarse-particle fog sonication was more effective than the sonication of less dispersed fogs. Actually, this is not the case. The total amount of moisture evaporated by all particles, allowing for (9.1) and (Al.4) equals:

$$G = J_l n \cdot 10^6 \doteq \frac{3kD}{\rho_{ж} r^2}(c_н - c_\infty)(1 + K\sqrt{Re})\frac{г}{м^3 \cdot сек}, \quad (Al.8)$$

where n - computed concentration, and k -- is the droplets' weight concentration.

Taking into consideration that the second multiple in parentheses increased with increasing r more slowly than $1/r^2$, it can be seen that the coarser the fog particles, the lower was the total amount of evaporated moisture at the same particle weight concentration, and, under the condition Re > 1, and $\mu_g \rightarrow 1$. The intensifying sound action on the evaporation rate was first proposed for use in solving problems of natural fog dispersion.

It was brought out in #18, that the acoustical method of fog dispersion had a limited dispersion range due to its high energy consumption, and several other disadvantages. In this connection, the idea arose of using sonication in connection with fog heating and, thus, solving the fog scattering problem by droplet evaporation in a sound field. Rodebush suggested this first in 1943, in his report on tests with the acoustical fog scattering method.

The new combination fog-dispersion method has been rapidly developed in recent years by Boucher [156] under the name of the thermo-acoustical method. It has been previously indicated that the thermal fog dispersion method necessitated great heat quantities, due to the fact that strong convection air flows were generated during the atmosphere heating; the warmer air rose while the surrounding cooler air, which replaced it, also contained fog droplets. As a result, quantities of fuel were consumed not only in air heating and in droplets' evaporating in the sector where the fog was being dispersed, but also in heating the additional surrounding air. It follows that fog droplets must be evaporated as rapidly as possible to avoid influx of large cold air masses. This, according to the author, must be done by fog sonication.

The first experiments in thermo-acoustical fog dispersion conducted in Arcata (USA) in 1950 had been encouraging. A J-33 turbojet engine with an afterburner ($3 \cdot 10^8$ BTU/hr) was used as the air heater, and U-2 and U3A-1 type dynamic sirens generating about 5 kw acoustical energy at a 3.5 Khz frequency were used as the sound source. The fog was scattered from a distance of 300 m and a height of 90--150 m. On the basis of the obtained results Downey and Smith estimated that ten J-47 type turbojet engines together with sonication could perform the work done by the FIDO installation (10^9 BTU/hr) in five minutes, which is equivalent to a heat output of 50 J-47 type engines. Thus, a five-fold decrease can be obtained in heat consumption as compared with the thermal method.

It is highly significant that much acoustical energy was generated as a side product of the turbojet stream itself. It was assumed that the J-47 engine radiated from 10 to 25 kw of acoustical energy, the main part of which was in the low frequency region of the order of 0.3 -- 0.6 Khz, for small engines -- 0.15 Khz, which was useful for the process. This suggested to Boucher the idea of completely eliminating the sirens from the installation and using the jet burners with which the air was heated as sound generators. It is calculated that at least 1% of the jet energy was transformed into acoustical oscillation energy, however, by installing resonators mounted in the paths of the jets, this figure can be increased by 5 -- 10%. In this case, the exhaust pipe will be similar to a Hartman-type shock-jet whistle. In place of the jet burners designed in the above-described manner, vortex whistles described by Greguss may also be used. Sonication combined with radiant heating of the fog is even more effective. In fact, the hot gases exhausted by the FIDO heating installation, similar to those of the jet engines, contain a considerable amount of water vapor which raises the moisture content of the fog air and thereby makes fog droplet evaporation more difficult, especially in still weather. Where heating is alternately turned on and off for economy, it happened that the content of the water vapors at times, exceeded the initial moisture content of the atmosphere. This may have occurred, for example, in 1953 in Los Angeles with the LAX-FIDO installation with which they could not raise the visability in excess of 180 m, (actually the heat output here was small).

The use of infrared heat bodies emission to evaporate fog, which is a rather good absorber of this type of energy, can exclude such unusual cases. It has been experimentally proven that atmospheric fog mixed with water vapor absorbed about 50% of the energy radiated by a black body with a temperature of 300 -- 1100° C at a distance of 90 m. However, all assertions require positive proof, since the noted presence of the critical flow velocity around the droplets as shown by [equation (Al.5)], was not taken into account in formulating the propositions. Boucher had also proposed to combine sonication with atomized hygroscopic and other chemical substances indicated at the beginning of the section. This fog dispersion method which henceforth shall be regarded as the acousto-chemical method was described in journal "Interavia" [152].

The purpose of sonication in the case of atomized hygroscopic substances is to speed up the water vapor condensation on the introduced condensation nuclei and the evaporation of the fog droplets. The scheme for carrying out this method for landing strips is shown in Fig. 76. Thus, it is seen that in this method the sprayers and sound sirens are positioned alternately along both sides of the runway and directed upward vertically. The hygroscopic nuclei entered the area affected by the sound field following the convection flow of air. In this case, it is assumed that the height to which the hygroscopic nuclei were lifted, an operation, which previously required large amounts of energy, can be reduced. In place of the hygroscopic substances,

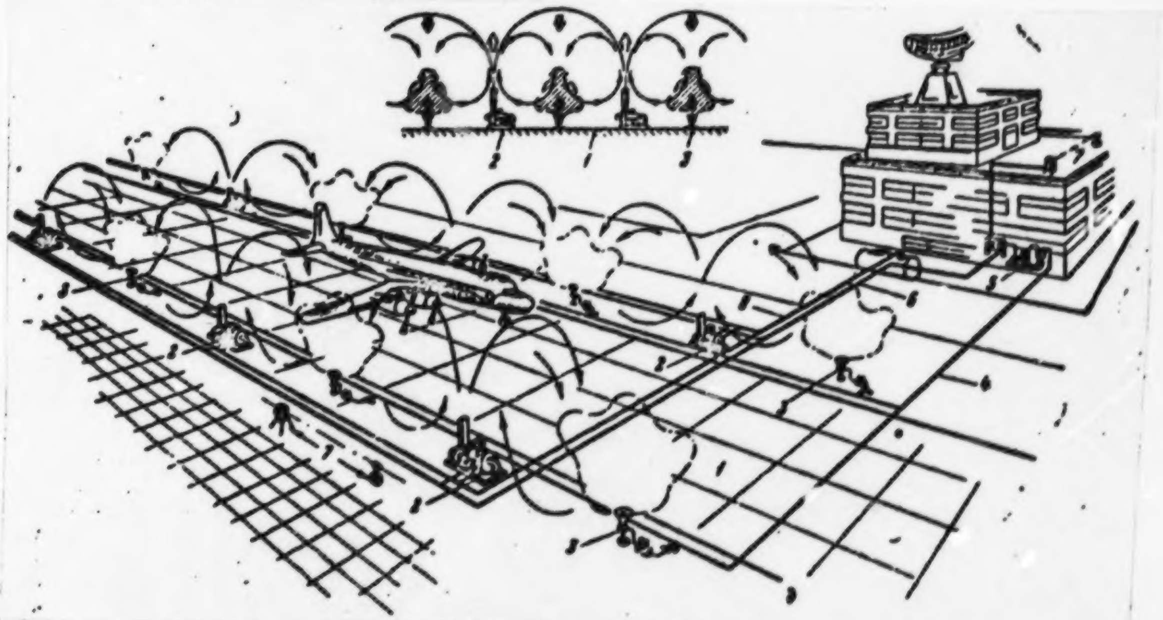

Fig. 76. Diagram of a thereacoustical method for aerodrome "fog lifting" according to Bouche.
1 - Path leading to ticket office; 2 - Thermic spraying generator; 3 - acoustical siren; 4 - compressed air conduit; 5 - compressor; 6 - electrical line; 7 - visibility recorder; 8 - fuel line.

such substances as silver iodide and others may be blown into the fog by the cold air.

According to reports by the "French Society for the Use of Ultrasound", 30 spray nozzles and 30 static sirens of the Boucher system proved sufficient for a runway 1000 m long. Such an installation was less costly than the FIDO installation. Each spray nozzle, including the burner and blower, requires about 7 kw, making a total of 210 kw. The air compressor for powering the sound siren required about 250 kw. This is more economical than the FIDO thermal fog dispersion system. It has been reported that the acoustochemical fog dispersion method, patented by Boucher, had been tried in several foreign countries: in France, by the Society for the Use of Ultrasound, in England by the Aerojet Company of London, in Sweden by the Aerojet Venturi Company of Vekso, and in the USA by Halton Industries Co., of Matachun, N. J.

In addition to natural fogs. there were many industrial aerosols, which, when being prepared or used, required accelerated liquid evaporation from the surface of the dispersion phase. This was the case in spray drying viscous solutions in the production of soap, dried milk, and other similar products; in cooling hot gases by water spray in scrubbers and other installations; in igniting vaporized liquid fuel in internal combustion engines, in liquid jet engines, and in industrial furnaces, etc. Several of the enumerated proposals have been patented [202, 207].

Horsley and Danser of the US Ultrasonics Corp., obtained a patent in 1951 for an acoustical damp products dispersion method [202] of the following characteristics:

1. The method of processing damp substances included the injection of different size particles of damp substances into a hot gas to form aerosols and to bombard the resultant aerosol with high-intensity sound waves with a sound intensity level of at least 150 db at a frequency of 3.5 Khz; in consequence, the sound waves not only promoted the moisture evaporation, but also formed dry particle aggregates.

2. The method of processing damp substances entailed the injection of different size particles of the damp substance into a hot dry gas stream and the generation of sound waves with a sound intensity of at least 150 db at a frequency of about 3.5 Khz in order to impart to the particles a velocity which varied according to the particle dimensions, and then separated the substance from the gas. This proposal was to be used in drying soap solutions, and for other similar purposes; however, no published information on its realization had been presented. Evidently, the energy consumed in the sonication of the drying chamber required to obtain good drying results was too great for such an enterprise as soap manufacturing. However, there were other enterprises in which sonication drying by atomization could be successful.

Turning to the intensifying effect of sound on condensation growth of fog droplets, the following is observed:

The first indication of possible condensation intensification with vibrations appeared in the little known work of Karlström (Svensk Tandlak Tskr, 1950, 43, 285), who proposed to use this effect in the production of dentistry amalgams. Of great practical interest was an attempt made by the present author in association with technicians of the Kuban Gas Industry to intensify droplet condensation and coagulation growth during natural gas separation. The sonicating gas separators proposed for this purpose had been previously described in #19 [79, 84, 80]. Therefore, here, only a brief discussion will be presented of the theoretical bases underlying the intensifying action of sound on the condensation growth of hydrocarbon fog droplets in the described gas separators.

It has been demonstrated [123] that the process of condensation droplet growth proceeded according to the laws of their evaporation. Accordingly, it follows that all equations and arguments previously presented by the present author also hold for this case. However, conditions in the gas separators were such that greater success could be expected from fog sonication than from other cases. The hydrocarbon vapor formed in the gas separators was under excess pressure (p = 50 -- 55 at gage), indicating that the Reynolds number characterizing the velocity of the gas flow around the droplet was about p times greater than under atmospheric conditions, since

η practically did not vary and ρ_g increased p times. At oscillatory velocity of u_g = 100 cm/sec the Reynolds number for condensate droplets of radius r = 1 -- 100 μ was in the range Re = 7 -- 700, and the Schmidt number Sc remained within the usual limits. Accordingly, the wind factor characterizing acceleration of the condensation droplet growth was in the range of f_v = 2 -- 10, which is significant.

It should be noted in conclusion that the discussion presented earlier on the kinetics of droplet evaporation in a sound field also held in relation to the heat transfer from the droplet to the medium and *vice versa*. In this case, when Re < 100 the following equality prevailed [123]:

$$Nu = 2(1 + \beta Pr^{1/3} Re^{1/2}), \qquad (A1.9)$$

where Nu - Nusselt number, $Qf/2\pi \gamma \lambda_g (T_\infty - T_0)$, and Pr - Prandtle number; γ/λ_g equal in air under normal conditions to about 0.8, Q_f -- amount of heat transferred from the droplet to the medium per unit of time; λ_g - heat transfer coefficient of the medium; $T_\infty - T_0$ -- temperature difference between the body and the medium: $\beta \approx 0.3$.

Studies discussed in [223, 289] are of interest in this connection.

#2. Sound Effect on the Processes of Combustion and Degasification of Fuel Droplets

It has been known that liquid fuel effectively ignited only in atomized form, i.e., in the aerosol state. Gaseous hydrocarbons were liberated in a similar form from crude oil solution. The sonication of such aerodispersed systems induced an actual acceleration of the processes operating in them, i.e., the combustion and degasification processes, while the coagulating sound action had practically no effect on coarsely dispersed droplets. The physicochemical relationships between combustion and degasification of liquid fuel droplets had little in common; therefore, they will be examined separately.

Liquid fuel droplets combustion in a burner induced evaporation of the individual droplets and the burning out of the vapors near the droplets and in the space surrounding them, which is according to the law of gaseous fuel combustion.

It has been known that acoustical oscillations enhanced the process of droplet evaporation, which offered the first explanation to the intensifying effect of sound on the process of droplet combustion. In addition, acoustical oscillation evidently affected even the combustion of liquid fuel vapors, since a strong turbulization of the gaseous medium had been generated. In any case, the data presented by Boucher [157] on the acoustical intensification of solid rocket fuel combustion leads to such a conclusion. Experimental research on the intensifying effect of sound on the combustion of an atomized liquid fuel was confined only to the work of Greguss [28, 196]. The author studied the effect of acoustical oscillation on the combustion of oil in a revolving furnace for the smelting of cast iron in a casting-mechanical factory in Budapest.

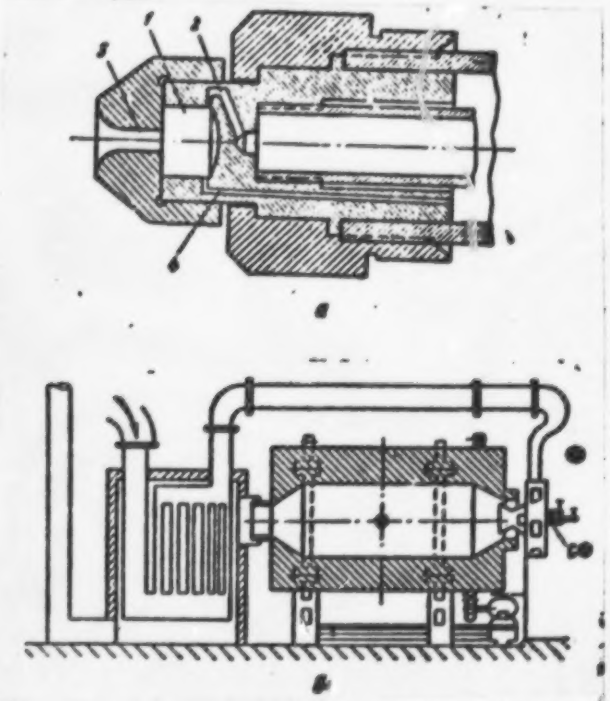

Fig. 77. Greguss. experiments in the intensification of sprayed liquid fuel combustion in a furnace (hearth) for smelting coke pig iron
a - construction of a whirle whistle spray generator (1 - whirle chamber; 2 - tangential air inflow; 3 - outflow; 4 - fuel delivery; b - Diagram of hearth with built-in whirle type whistle type spray generator.

Failure of Tarnoczy and Somhegyi's experiments [276] conducted on the intensification of a gas flame combustion by external sonication, led Greguss to sonicate the burning mixture from within. For this purpose, the author constructed a special "acoustical burner nozzle" out of a standard vortex whistle which was provided only with an additional opening for the injection of liquid fuel (Fig. 77a). Acoustical oscillations were thereby generated directly in the burning mixture; in this way the reflection of the sound waves from the boundary by the flames, which occurred in the Tarnoczy - Somhegyi experiments, had been avoided. Moreover, the revolving flame stabilized the combustion process.

Figure 77b shows the whistle-burner arrangement in a furnace. The oscillation frequency generated by the whistle-burner was 4 Khz, while the sound intensity level reached 150 db. According to the author, the acoustical efficiency of the whistle was 10 -- 15%. With the aid of sonication, the temperature required for smelting was reached after 40 -- 50 min. instead of one hour; fuel consumption dropped 10%. Moreover, metallurgists confirmed that the casting obtained after this was of a better structure and more suitable for thermal treatment. Greguss explained the increase in efficiency of atomized liquid fuel combustion by the following:

1) a higher degree of liquid fuel atomization;

2) intensification of liquid fuel droplet evaporation;

3) increased probability of liquid fuel droplets and molecules collision with the oxidizer molecules, which ensures a better approximation to stoichiometric ratios;

4) greater uniformity of temperature distribution around the revolving flame, ensuring a more homogeneous diffusion factor;

5) increase in the flame front boundary stability which increased the completeness of fuel droplet combustion.

The quantitative relationships characterizing sonication of atomized liquid fuel combustion have not been derived.

There seemed no doubt that acoustical oscillation intensified the combustion suspended solid fuel particles; however, appropriate data have as yet to be published.

It should be noted in conclusion, that the possibilities of acoustical oscillation in the intensification of liquid fuel combustion have not been exhausted in the reports.

Self-oscillating processes often arose in fuel combustion, including atomized liquid fuels, due to the interaction between flame and air. They originated from the pulsating character of fuel combustion. This form of combustion, called *vibrational*, or sometimes *pulsating*, arises in nearly all heating and thermal-powered installations, and, in most cases, it played a negative role in hindering the normal course of combustion; it generated noise, vibrations, and sometimes damaged the furnace and the combustion chamber. In addition, this form of combustion differed by its increased velocity, and its use assured considerable gains in increasing the heat load of pulverized coal furnaces, of liquid rocket engines, and of industrial furnaces in which the fuel was ignited in an atomized form. However, the principles underlying vibrational combustion are not connected with the fuel aerosol state; therefore, an examination of this process was regarded as beyond the scope of the book. It is suggested that students interested in this problem familiarize themselves with reports in [106] and [71] and with B. V. Rauchenbach's monograph *Vibrational Combustion*.

The degasification effect of sound on a liquid located in a gaseous medium is based on the same principle as the vacuum dryer. The latter is based on the fact that as pressure in the medium decreased, the amount of liquid being evaporated increased. This follows from Dalton's law which established that the rate of evaporation was connected with the vapor pressure in the surrounding medium by the following relationship [128]:

$$J_p = kS\ \rho_s - \rho_\infty / H \qquad \text{(AII.1)}$$

where ρ_s -- saturated vapor pressure of the liquid temperature; ρ_∞ -- vapor pressure in the surrounding space; H -- barometric gas pressure; S -- area of evaporation surface; k -- coefficient dependent on the character of the flow around the surface of the medium.

During the propagation of the sound wave at the moment of compression, no changes take place on the surface of the liquid droplet, since the medium is not saturated by the liquid vapors. Then, at the moment of rarefaction, when the pressure in the medium drops, an additional separation, i.e., desorption, of the gas from the liquid occurs. A small amount of rarefaction is thereby generated at the droplet surface which is compensated for by the instaneneous repetition of the process. An important experimental confirmation of the degasification effect of sound on atomized liquids was recently obtained with a by-product gas from oil at the Korobkovskii deposits in the Volgograd oblast'. The gaseous by-products are light hydrocarbons which are dissolved in large amounts in oil and are separated from it by a pressure drop which occurred in the course of the oil's passage along the borehold shaft and then in a special separator serving as a trap.

A turbodynamic siren was mounted in the trap inlet pipe for the investigation of sonication effect on the process of degasification of atomized oil. The oil-gas mixture was fed through the siren which began to turn it, generated the sound, and liberated the atomized oil together with the gas into the trap.

Experimental results established that separation of gaseous by-products from oil increased by 13 -- 32% during sonication as compared with standard means of atomizing oil. However, it has not been ruled out that the improved oil siren atomization played a role in these experiments. Should further investigation confirm these results, then sonicating traps will come into wide use in the oil-gas industry. Naturally, a more reliable, nonrotating sound generator, like the vortex whistle-burner, should be used instead of a turbodynamic siren.

#3. Behavior of Precipitated Solid Particles in a Sound Field of an "Acoustical Dryer"

Substances passing from the suspended state into a powder generally are not aerodispersed systems, expecially if their pores are filled with moisture. However, taking into consideration that many powders and pastes are products of aerosol precipitation and that they contain a coagulated dispersed phase, it is of interest to examine their behavior in a sound field. Dry powders reacted to sonication only with a periodically "muddying" of the layer in resonance with the pulsation of the static gas pressure over its surface, or by forming peaks at the oscillation nodes. This has been observed not only in parallel sonication of a powder layer, as in a Kundt pipe [218], but also in perpendicular sonication when transverse oscillation nodes were generated. The cause of local powder accumulation in both cases was the acoustical flow generated in the node-antinode intervals. They attracted the precipitated particles from both sides to the node line, and the lightest particles became separated from the layer, forming small dust clouds. Damp powders are dried in a sound field, without any perceptible temperature rise, which drew particular attention to the acoustical drying method.

Examine the existing hypotheses on the mechanism of acoustical drying of materials. It is known that the drying of damp porous materials consisted of two stages: the evaporation of the liquid from the surface, and its transfer from the internal pores to the surface. Boucher [154, 155] assumed that acoustical oscillations acted only in the first stage, i.e., they increased the liquid evaporation rate. He cited Dalton's Law (AII.1), considering that when the sound waves passed along the damp surface, no variations occurred in the compression areas; whereas in rarefaction areas, an acceleration of the liquid evaporation occurred similar to the one which took place in the degasification of droplets, described above. According to Boucher, turbulization of the sonicated medium facilitated moisture evaporation.

Greguss, accepting the described mechanism in the initial drying stage, assumed, on the basis of experiments with the drying of products with little moisture, that the sound wave also aided in transferring moisture from the internal pores to the surface [197]. It is known that as far as drying was concerned, the rate dropped due to decrease in the material moisture conductivity medium surface. Acoustical oscillations, according to Greguss, increased the material moisture conductivity owing to:

a) decrease in the liquid viscosity achieved, according to Altenburg's data, during sonication, and aiding the acceleration of liquid diffusion from the pores;

b) the pulsations of bubbles held in the pores and capillaries during the periodic variations of the medium's pressure and temperature aiding the liquid separation from the pores and capillaries:

c) the radiational pressure directed into the pores and capillaries from the liquid into the gas which moved the liquid column outward.

Both investigators, as well as their successors, ruled out the effect of temperature rise in the surface capillaries on the drying process, which occurred due to capillaries absorbtion of the incident sound waves energy (see formula [1.18]); they cited the fact that acoustial drying occurred in a "cold" method. On the basis of initial drying studies conducted in cooperation with N. M. Gynkina [8] (see also Acoust. Zh., 1962, 8, no. 1), Yu. Ya. Borisov suggested that the deciding effect on drying acceleration was the acoustical flow generated in the sonicated gaseous medium. His conclusion was based on the experiments which showed that the beginning of the intensifying action of the sound nearly coincided with the suspension of the dry powders at the nodes of standing wave. This, as is known, was due to the effect of the acoustical flows along the node-antinode intervals. However, this hypothesis, like previous ones, had not been confirmed.

Experiments conducted in the Ultrasonics Laboratory of the Acoustical Institute AS USSR demonstrated that greatest drying acceleration occurred at the anti-nodes of the oscillatory velocity; where the acoustical flow velocity was finite, drying has not been accelerated. Sonic pressure was minimal at the acoustical velocity nodes (theoretically it equals zero), indicating that the acoustical drying of materials occurred not according to the principle of vacuum drying, as Boucher supposed, but according to the principle of convective drying. Experiments also established that the drying effect in a sound field was almost equivalent to the effect of convective drying, achieved at an air flow rate equal to the oscillatory velocity. This conclusion has something in common with the conclusions relating to atomization drying in a sound field (see Appendix I) which is completely natural. The experimentally established fact that the rate of acoustical drying depended little on the employed oscillation frequency becomes understandable in the light of this observation.

The first experiments with the acoustical drying of materials had been conducted in 1955 by Greguss, who, with the use of a dynamic siren, obtained almost a ten-fold acceleration of raw cotton fibers drying at a frequency of 25 Khz. The drying of powdered products was investigated in detail by Boucher. The following hard-to-dry-products were used: carboxylmethylcellulose, titanium dioxide paste, colloidal zirconium hydroxide, and also silica gel, enzymes, and hormones. Figure 78 shows the results obtained in the drying of the first three products; it is seen that the sonication ensured a 6 -- 8-fold drying acceleration.

Silica gel, with a 25% initial moisture content was fully dried in 15 min. at a sound intensity of 152 db and at a frequency of 8 Khz; in the vacuum drying method and in thermal drying by heating up to 92° C with air, only 10 -- 15% of the moisture content could be removed in such a short time. Enzymes, which cannot endure heating above 40° C, were dried in 14 min., while the drying rate of thermal sensitive hormones was increased 3 -- 4 times as compared with the vacuum method.

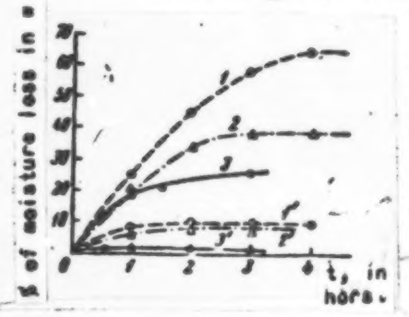

Fig. 78. Results of acoustical drying of some powdered materials according to Bouche.
1 - Colloidal zirconium hydroxide at f = 10 kHz; 2 - carboxymethylcellulose at f = 34 kHz; 3 - titanium peroxide at f = 9.5 kHz; 1', 2', 3' same materials dried naturally.

Boucher also investigated a series of cotton materials, blotting paper, asbestos cartons, and others [154, 155, 157]; results of these experiments will be discussed at some other time.

Experiments with the drying of ethylcellulose were conducted at the Acoustical Institute AS USSR [8]. This material was selected for the first experiments because it oxidized easily and could not be dried at high temperature. At 80° C it dried only in several hours. Due to the high dispersion of ethylcellulose, the material became sonicated in a layer strewn over the bottom of a small bath tub.

Figure 79 shows the results obtained. Thus, at a sound intensity of 152 db the material completely dried in 60 min. at normal temperature (20° C), and in 45 min. at 32° C. A change in the sound pressure of 3 db, equivalent to doubling the sound energy density, accelerated the drying by a factor of 1.5.

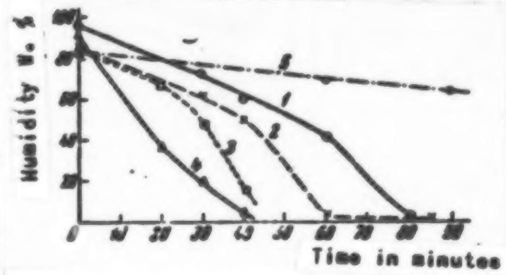

Fig. 79. Results of artificial drying ethylcellulose by the Acoustical Institute, Academy of Sciences, USSR.

1 - at f = 6.7 kHz; L = 152 db; temp. = 20°C; 2 - at f = 2.8 kHz; L = 152 db; temp. = 20°C; 3 - at f = 2.5 kHz; L = 152 db; temp. = 32°C; 4 - at f = 2.8 kHz; L = 156 db; temp. = 20°C; 5 - in the absence of sound at temp. = 20°C.

On the basis of the experimental data, it can be stated that the following had an effect on the acoustical drying rate: initial moisture, the form of moisture adhesion to the material, the thickness and structure of the layer, the presence of material agitation, and sound intensity. Moreover, the threshold sound intensity, below which the drying process failed to become accelerated, was 140 -- 145 db.

It has been established that in the propagation of sound waves along the surface of the material being dried, the drying process was only half as fast as when the waves strike directly. In the present author's opinion, this could be explained by the following: when striking directly; the sound wave partially penetrated into the material layer and easily flowed around its individual elements; the distance between the elements was slightly greater than their dimensions; this is obvious, even though the porosity of many materials reached 80 -- 85% and higher. It is also confirmed that the drying rate depended only partially on the oscillation frequency, even though at lower frequencies the process was somewhat more active, evidently due to the weaker absorption of sound by the medium. This was contrary to Boucher's initial assertion [172], which postulated that the drying process proceeded smoothly only at frequencies above 10 Khz, and that 9 Khz was the lower limit at which there was still a noticeable drying acceleration. He later established that even the lower frequencies enhanced the acceleration of drying, and that the most effective frequencies were in the 6 -- 10 Khz range [155].

According to data accumulated by the Acoustical Institute AS USSR, where the drying process had been studied in the 3 -- 15 Khz frequency range, the results obtained at 2.8 Khz were better than at 6.7 Khz (see Fig. 79).

The most promising area for the acoustical drying method application, which is distinguished by its high energy losses, is the drying of easily-oxidized, low-melting, thermol-sensitive, and explosive materials for which other methods were not feasible, or which yielded poor results in the final drying stage. The most expedient use was in the acoustical drying of powder-form products not in a stationary layer but rather in barrel dryers, or in the suspended state.